

NUMERICAL MODELING OF SOLUTE
TRANSPORT IN TIDAL CANAL NETWORKS

BY

RAYMOND WALTON

A DISSERTATION PRESENTED TO THE GRADUATE COUNCIL OF
THE UNIVERSITY OF FLORIDA
IN PARTIAL FULFILLMENT OF THE REQUIREMENTS FOR THE
DEGREE OF DOCTOR OF PHILOSOPHY

UNIVERSITY OF FLORIDA

1978

Engineering

ACKNOWLEDGEMENTS

The completion of a study of this magnitude necessarily involves the combined efforts of a large number of people. The author wishes to acknowledge collectively the assistance of the many people who have contributed substantially to this dissertation.

The author would like to express his appreciation to his committee chairman, Dr. B. A. Christensen, for his guidance and support during the course of this study. He would also like to thank other committee members, Dr. Wayne C. Huber of the Environmental Engineering Sciences, and Dr. Z. R. Pop-Stojanovic of the Mathematics Department for their assistance and input to the project.

Robert Snyder, of Snyder Oceanography Services in Jupiter, Florida, deserves special recognition for his many fundamental contributions to the canal research project. Bob and his wife, Bea, shared the author's enthusiasm for canal work and provided support and encouragement many times during the course of the investigation.

Jon Lee, presently with USGS in Bay St. Louis, Mississippi, contributed substantially to both the field surveys and the mathematical part of the modeling.

Rachel Christensen prepared the computer graphics for concentration displays and contributed substantially to the success of several field surveys. Among the many other students who volunteered to participate in field work, were Ho-Shong Hou, Clark Clement, Ron Chernik, and Jim Dlubac.

61-00-79

A special mention for assistance far beyond that which any reasonable person would ask is due for the drafting accomplished by Carol Dillard and Dave Bloomquist in the last few weeks of preparation of this dissertation. Without their good nature and highly professional skill this dissertation would have taken much longer to prepare.

The Northeast Regional Data Center (NERDC) computer was used for the development of the model and all of the canal design simulations. The author particularly appreciates and wishes to acknowledge the friendly assistance provided by the NERDC operators, when computer work extended late into the night and early morning hours.

The author wishes to thank Alice Moreau, Ilona Weber, and Adele Koehler for all the typing, retyping, and many hours of tedious proof-reading.

Finally, and most importantly, the author would like to acknowledge the love and encouragement of family and friends, particularly Pat who got him here, Rysie who got him through his qualifying examinations, and Sue who carried him through the late night programming and writing. In this category, he would also like to thank Dr. Roland K. Price of the Hydraulics Research Station, England (formerly a visiting Assistant Professor at the University of Florida) and Dr. P. Novak of the University of Newcastle-Upon-Tyne, England, for their support in applying for a graduate position in the United States.

The work described was funded by the Office of Sea Grant, National Oceanic and Atmospheric Administration under Project No. R/OE-4, through the State University System of Florida Sea Grant College Program, the Board of Regents of the State University System, and the Board of Commissioners of Palm Beach County.

TABLE OF CONTENTS

	<u>Page</u>
ACKNOWLEDGEMENTS.	ii
LIST OF TABLES.	vii
LIST OF FIGURES	viii
NOTATION.	xiv
ABSTRACT.	xx
CHAPTER	
1 INTRODUCTION.	1
1.1 Background Information	1
1.2 Research Aim	3
1.3 Philosophy of Numerical Modeling	4
1.4 Scope of Report.	6
2 ANALYSIS OF NUMERICAL MODELING TECHNIQUES	15
2.1 Development of One-Dimensional Model	15
2.1.1 Classification and Definitions of Canal Network Geometry.	15
2.1.2 Model Canal Network Geometry.	17
2.1.3 Hydrodynamics of One-Dimensional System	18
2.1.4 Transport Equation and Dispersion Coefficient	23
2.1.5 Boundary Conditions	27
2.2 Finite-Difference and Finite-Element Approaches.	29
2.3 Method-of-Characteristics Approach	32
2.4 Hybrid Computer Approach	34
2.5 Second Upwind Differencing Method.	39
2.6 Method of Second Moments	42
2.7 Comparison of Techniques	46
2.8 Effect of Varying Model Parameters on One-Dimensional Mass Transport	49
3 FIELD MEASUREMENTS.	98
3.1 Introduction and Site Descriptions	98
3.2 Geometry and Tides	100
3.3 Velocity and Wind.	101
3.4 Salinity and Temperature	102
3.5 Dye Dispersion Studies	103

	<u>Page</u>
✓ 4 THREE-DIMENSIONAL HYDRODYNAMICS IN CANAL NETWORKS.	133
4.1 Introduction.	133
4.2 Tidal Velocities.	137
4.3 Wind Induced Circulation.	138
4.4 Secondary Currents.	146
4.5 Density Induced Currents.	154
✓ 5 THREE-DIMENSIONAL MASS-TRANSPORT EQUATION.	175
5.1 Transport Mechanisms.	175
5.2 Longitudinal and Lateral Diffusion Coefficients	180
5.3 Vertical Diffusion Coefficient.	184
6 DEVELOPMENT OF THREE DIMENSIONAL NUMERICAL MODEL	191
6.1 Layout of Geometry.	193
6.2 Treatment of the Velocity Field	199
6.2.1 Tidal Velocities	199
6.2.2 Wind Induced Circulation	204
6.2.3 Secondary Currents	206
6.2.4 Density Currents	208
6.3 Treatment of Dispersive Terms of the Transport Equation.	210
6.3.1 Longitudinal Dispersion Term	212
6.3.2 Lateral and Vertical Dispersion Terms.	213
6.4 Lateral Inflows	215
6.5 Decay Coefficients.	217
6.6 Boundary Conditions	220
6.7 Results Presentation.	222
7 MODEL STABILITY AND CONVERGENCE CRITERIA	231
7.1 Conservative Property, Order of Accuracy, and Transportiveness.	231
7.2 Stability Criteria.	233
7.2.1 Velocity Criteria.	235
7.2.2 Dispersion Criteria.	239
7.3 Convergence Criteria.	242
8 MODEL TESTS AND RESULTS.	251
8.1 Introduction.	251
8.2 Case History #1: Results of Big Pine Key Canal III Runs.	252
8.3 Case History #2: Results of 57 Acres Model Runs. . . .	256
8.4 Case History #3: Results of Loxahatchee River Runs . .	262
8.5 Effect of Varying Model Parameters on Three- Dimensional Mass Transport.	264
8.5.1 Effect of Wind Induced Circulation	265
8.5.2 Effect of Density Current.	269

	<u>Page</u>
9 SUMMARY OF NUMERICAL MODELING	301
9.1 Summary of One-Dimensional Modeling.	301
9.2 Summary of Three-Dimensional Modeling.	306
9.3 Future Research.	310
9.4 The Numerical Model as a Design Tool	312
 APPENDIX	
A USER'S MANUAL	314
B FLOW CHART FOR THE COMPUTER PROGRAM	323
C PROGRAM LISTING	366
D COMPUTER RESULTS FOR 57 ACRES OCTOBER CASE HISTORY.	416
REFERENCES.	468
BIOGRAPHICAL SKETCH	476

LIST OF TABLES

<u>Table</u>	<u>Page</u>
2.1 Typical Measured Canal Parameters.	93
2.2 Comparison Between Horizontal Water Surface Assumption and Harleman and Lee's Hydrodynamic Model.	94
2.3 Standard Data Set for First Test Canal	95
2.4 Standard Data Set for Second Test Canal.	96
2.5 Comparison of Numerical Techniques	97
3.1 Field Surveys Conducted by Hydraulic Laboratory During the Canal Design Research Project.	129
3.2 Summary of Data for South Loop, 57 Acres	131
3.3 Summary of Data for Loxahatchee River North Canal.	132
7.1 Constant Parameters for Three-Dimensional Model Test Canal.	250
8.1 Parameters for Big Pine Key Canal III Case History	295
8.2 Parameters for 57 Acres Case History	296
8.3 Parameters for Loxahatchee North Canal Case History.	298
8.4 Parameters for Three-Dimensional Model Test Canal.	299
8.5 Variability Studies Using Three-Dimensional Model.	300

LIST OF FIGURES

<u>Figure</u>	<u>Page</u>
1.1 Undeveloped Canal Network in Florida.	9
1.2 Developed Canal Network Takeover of Natural System in Florida.	10
1.3 Example of Polluted Canal Network in Florida.	11
1.4 Example of Polluted Canal Network in Florida.	12
1.5 Criteria for Canal Design Without Consideration of the Environment (after Snyder, 1976).	13
1.6 Suggested Criteria for Canal Design With Consideration of the Environment (after Snyder, 1976)	14
2.1 Definition Drawing of Canal Network	54
2.2 Schematic Drawing of Trapezoidal Cross-Section.	55
2.3 First Test Canal Network.	56
2.4 Second Test Canal Network	57
2.5 Typical Atlantic Coast Tide Curve	58
2.6 Typical Gulf of Mexico Tide Curve	59
2.7 Typical Logarithmic Velocity Profile.	60
2.8 Schematic Drawing of Horizontal Water Surface Assumption.	61
2.9 Schematic Representation of Effect of Numerical Dis- persion	62
2.10 Low Tide Concentration Profiles for Various Δx and Δt -- Finite-Difference Method.	63
2.11 Schematic Representation of Convective Steps of Method of Characteristic Methods	64
2.12 Comparison of Concentration Profiles for Fixed Grid and Movable Grid Method-of-Characteristics.	65

<u>Figure</u>	<u>Page</u>
2.13 Low Tide Concentration Profile for Various Δx --Fixed Grid Method-of-Characteristics.	66
2.14 Schematic Drawing of Hybrid Method Test Canal	67
2.15 Generalized Analog Diagram of Single Node of Hybrid Model	68
2.16 Typical Analog Output	69
2.17 Low Tide Concentration Profiles for Various Analog Methods	70
2.18 Schematic Representation of Second Upwind Difference Method.	71
2.19 Low Tide Concentration Profiles for Various Δx and Δt --Second Upwind Difference Method	72
2.20 Rectangular Distribution Approximation to Actual Distribution.	73
2.21 Schematic Representation of Conservation of First Moment.	74
2.22 Low Tide Concentration Profiles for Various Δx and Δt --Method of Second Moments.	75
2.23 Comparison of Techniques' Accuracy in Modeling Pure Convection.	76
2.24 Comparison of Techniques' Accuracy in Conserving Mass	77
2.25 Concentration Profiles for Second Test Canal Network--Second Upwind Difference Method	78
2.26 Concentration Profiles for Second Test Canal Network--Method of Second Moments.	79
2.27 Variability of Tidal Entrance Time Decay Coefficient, τ	80
2.28 Variability of Tidal Amplitude, a	81
2.29 Variability of Canal Length, L	82
2.30 Variability of Dimensionless Canal Length	83
2.31 Variability of Bottom Width, b	84
2.32 Variability of Inverse Side Slope, s	85
2.33 Variability of Lateral Inflow Rate, q_1	86

<u>Figure</u>	<u>Page</u>
2.34 Variability of Lateral Inflow Concentration, c_I	87
2.35 Variability of Mean Tidal Depth, d_0	88
2.36 Variability of Nikuradse's Equivalent Sand Roughness, k	89
2.37 Variability of Dimensionless Dispersion Coefficient, K	90
2.38 Variability of Low Tide Concentration Profiles for Various Branch Canal Locations.	91
2.39 Variability of High Tide Concentration Profiles for Various Branch Canal Locations.	92
3.1 Location Map for Canal Studies.	105
3.2 57 Acres Site Plan Showing Measurement Stations	106
3.3 Topographic (7 1/2" quadrangle) Map for Loxahatchee River Canals.	107
3.4 Center Line Depths in 57 Acres System	108
3.5 Cross-Sections at K and Y in 57 Acres System.	109
3.6 Cross-Sections and Plan View of Loxahatchee North Canal, June 1977	110
3.7 Electromagnetic Velocity Meter Set-Up	111
3.8 Typical Vertical Velocity Profile in 57 Acres System.	112
3.9 Typical Vertical Velocity Profile in Loxahatchee River System, 13 June, 1977	113
3.10 Wind Recorder Set-Up.	114
3.11 Strip Chart Recording of Wind Data--57 Acres System, October, 1977	115
3.12 Measured Wind Velocity, 57 Acres Canal System, October, 1977	116
3.13 Station Salinities Versus Time in 57 Acres System	117
3.14 Station Salinities Versus Time in 57 Acres System	118
3.15 Salinity Versus Time at Station 3--57 Acres System, October, 1977	119
3.16 Salinity Profiles--Loxahatchee River System, June 1977.	120

<u>Figure</u>	<u>Page</u>
3.17 Photograph of Fluorometer and Recorder Set-Up.	121
3.18 Longitudinal Dye Concentration Profiles--57 Acres System, October, 1977.	122
3.19 Longitudinal Dye Concentration Profiles--57 Acres System, October, 1977.	123
3.20 Longitudinal Dye Concentration Profiles--57 Acres System, October, 1977.	124
3.21 Longitudinal Dye Concentration Profiles--57 Acres System, October, 1977.	125
3.22 Longitudinal Dye Concentration Profiles--57 Acres System, October, 1977.	126
3.23 Longitudinal Dye Concentration Profiles--57 Acres System, October, 1977.	127
3.24 Longitudinal Dye Concentration Profiles--57 Acres System, October, 1977.	128
4.1 Example of Typical Non-Gaussian Concentration Profile.	165
4.2 Definition of Coordinate System.	166
4.3 Schematic Drawing of Mean Depths in Lateral Cells of a Vertical Layer	167
4.4 Theoretical-Wind-Induced Vertical Velocity Profile	168
4.5 Comparison Between Observed and Theoretical Vertical Velocity, Profiles, With and Without Width Correction ($N_z = 0.002 \text{ ft}^2/\text{sec}$)--57 Acres	169
4.6 Schematic Drawing of Helical Current Induced by a Bend.	170
4.7 Comparison Between Observed and Computed Lateral Veloci- ties Induced by Bend in South Loop of 57 Acres System.	171
4.8 Schematic Drawing of a Salt Wedge Entering a Canal Showing Definitions.	172
4.9 Typical Salinity Profile in Loxahatchee River North Canal, Showing Presence of a Saltwater Wedge.	173
4.10 Comparison of Observed and Computed Velocity Profiles for Loxahatchee River Site	174
5.1 Lateral Variation of Velocity.	189

<u>Figure</u>	<u>Page</u>
5.2 Comparison of Saltwater Interface Stability Functions. . .	190
6.1a Astronomical Tides Meeting at Null Point	225
6.1b Astronomical Tides Recombining at Upstream Junction. . . .	225
6.2 Schematic Layout of Canal Network Showing Features	226
6.3 Cell Structure in Reach.	227
6.4 Cell Structure in Junction	228
6.5 Buffer Cell Structure.	229
6.6 Schematic Layout of Bend	230
7.1 Schematic Canal for Three-Dimensional Model Tests.	246
7.2 Variation of Δx and Δt after 50 Tidal Cycles	247
7.3 Variation of NLAYZ (NLAYY = 1)	248
7.4 Variation of NLAYY (NLAYZ = 3)	249
8.1 Model Layout of Reaches and Junctions in 57 Acres System .	273
8.2 Typical Longitudinal Sections and Cross-Sections, Big Pine Key III, Florida [EPA, May, 1975]	274
8.3 Observed and Predicted Concentration Profiles for Big Pine Key Canal III Case History.	275
8.4 Observed and Predicted Concentration Profiles for 57 Acres July, 1977, Case History	276
8.5 Observed and Predicted Concentration Profiles for 57 Acres October, 1977, Case History.	277
8.6 Variation of Vertical Dispersion Coefficient With Time and Wind Speed at Mid Point of Reach 1 (Figure 8.1), 57 Acres October, 1977, Case History	278
8.7 Comparison Between Observed and Computed Concentrations for Loxahatchee River North Canal, June, 1977.	279
8.8 Case 1W: Initial Concentrations, $c_i = 100$ ppm, Back- ground Concentration, $c_{RW} = 5$ ppm--Ten Tidal Cycles. . . .	280
8.9 Case 1W: Initial Concentrations, $c_i = 100$ ppm, Back- ground Concentration, $c_{RW} = 5$ ppm--Fifty Tidal Cycles. . .	281

<u>Figure</u>	<u>Page</u>
8.10 Case 2W: Initial Concentrations, $c_i = 5$ ppm, Background Concentration, $c_{RW} = 100$ ppm--Ten Tidal Cycles. . .	282
8.11 Case 2W: Initial Concentrations, $c_i = 5$ ppm, Background Concentration, $c_{RW} = 100$ ppm--Fifty Tidal Cycles. . .	283
8.12 Case 3W: Lateral Inflow Distribution Along Length of Canal--Ten Tidal Cycles.	284
8.13 Case 3W: Lateral Inflow Distribution Along Length of Canal--Fifty Tidal Cycles.	285
8.14 Case 4W: Lateral Inflow Distribution Along Upper 1/2 of Canal--Ten Tidal Cycles	286
8.15 Case 4W: Lateral Inflow Distribution Along Upper 1/2 of Canal--Fifty Tidal Cycles	287
8.16 Case 5W: Lateral Inflow at Dead-End--Ten Tidal Cycles	288
8.17 Case 5W: Lateral Inflow at Dead-End--Fifty Tidal Cycles	289
8.18 Case 1S: Effect of Salt Wedge With Initial Concentrations, $c_i = 100$ ppm, Background Concentration, $c_{RW} = 5$ ppm--Fifty Tidal Cycles	290
8.19 Case 2S: Effects of Salt Wedge With Initial Concentrations, $c_i = 5$ ppm, Background Concentration, $c_{RW} = 100$ ppm--Fifty Tidal Cycles	291
8.20 Case 3S: Effect of Salt Wedge With Lateral Inflow Distribution Along Length of Canal--Fifty Tidal Cycles	292
8.21 Case 4S: Effect of Salt Wedge With Lateral Inflow Distribution Along Upper 1/2 of Canal--Fifty Tidal Cycles	293
8.22 Case 5S: Effect of Salt Wedge With Lateral Inflow Distribution at Dead-End--Fifty Tidal Cycles	294

NOTATION

a	tidal amplitude (L)
$a_0 - a_4$	constants of integration
A	cross-sectional area (L^2)
A_{ws}	area of water surface upstream of section (L^2)
$\bar{A}(k)$	function defined by Equation (4.31)
b	bottom width (L)
B	top width (L)
$\bar{B}(z)$	function defined by Equation (4.29)
c_I	concentration of lateral inflow (dimensionless)
c_{RW}	background concentration in receiving waterbody (dimensionless)
c_m	concentration of rectangular distribution (dimensionless)
\bar{c}	turbulent time mean concentration (dimensionless)
c'	fluctuation from turbulent time mean concentration (dimensionless)
c_0	initial concentration (dimensionless)
C	Chezy coefficient ($L^{1/2}/T$)
d	depth (L)
d_0	mean tidal depth (L)
e	exponential constant = 2.718
e_{ijk}	error in cell ijk
E	dispersion coefficient (L^2/T)
E_k	layer averaged vertical dispersion coefficient (L^2/T)
\bar{E}_k	layer averaged, Richardson number dependent, vertical dispersion coefficient (L^2/T)

E_l	longitudinal dispersion coefficient (L^2/T)
E_n	numerical dispersion coefficient (L^2/T)
E_x	longitudinal diffusion/dispersion coefficient (L^2/T)
E_y	lateral diffusion/dispersion coefficient (L^2/T)
E_z	vertical diffusion/dispersion coefficient (L^2/T)
E_0	background dispersion coefficient (L^2/T)
f	Coriolis parameter ($1/T$)
$F()$	exact solution of partial differential equation
$\tilde{F}()$	numerical approximation to partial differential equation
F_m	dimensionless location of center of mass in cell
$F_1(\eta)$	function defined by Equation (4.38)
$F_2(\eta)$	smooth bed form of $F_4(\eta)$
$F_4(\eta)$	function defined by Equation (4.39)
$F_1(k)$	layer averaged form of $F_1(\eta)$
$F_4(k)$	layer averaged form of $F_4(\eta)$
g	acceleration due to gravity (L/T^2)
i	number of reach (Chapter 2) number of segment
j	number of reach (Chapter 2) number of lateral layer
k	Nikuradse's equivalent sand roughness (L) constant of proportionality (Equation (5.7)) number of vertical layer
K	dimensionless dispersion coefficient (Chapter 2) decay coefficient ($1/T$)
K_R	reach uniform decay coefficient ($1/T$)
K_w	wind drag coefficient (dimensionless)

ℓ	length scale of turbulent eddy (L)
	a characteristic length of the cross-section of a canal (L)
L	length of reach (L)
	length scale of convective period (Section 4.1) (L)
L_d	length of decay of secondary current (L)
L_w	length of saltwater wedge (L)
N_i	number of concentration distributions in cell (Section 2.6)
Nu	number of upstream reaches (Equation (2.9))
N_z	vertical momentum transfer coefficient (L^2/T)
\tilde{N}_z	constant defined by Equation (4.33)
p	variable used in Section 4.4
	permissible deviation from background velocity (Equation (4.51))
P_a	atmospheric pressure (M/LT^2)
q_I	lateral inflow per unit length (L^2/T)
Q	discharge (L^3/T)
Q_u	discharge at upstream section of reach (L^3/T)
\bar{Q}	discharge defined by Equation (6.3) (L^3/T)
r	radius of bend (L)
r_p	rate of production or loss of substance (1/T)
R	hydraulic radius (L)
Ri	Richardson number (dimensionless)
R_m	dimensionless width of distribution in cell
s	inverse side slope (dimensionless)
s_L	inverse side slope of left bank (dimensionless)
s_R	inverse side slope of right bank (dimensionless)
S_f	slope of energy grade line (dimensionless)
t	time (T)

t'	time since low tide (T)
T	tidal period (T)
u	cross-sectional mean velocity (L/T)
u_{D_x}	dispersion velocity in x-direction (L/T)
u_{D_y}	dispersion velocity in y-direction (L/T)
u_{D_z}	dispersion velocity in z-direction (L/T)
u_F	velocity of front of saltwater wedge (L/T)
u_0	cross-sectional mean velocity at upstream section of reach (L/T)
u^*	bed shear velocity (L/T)
u'	turbulent fluctuation from time mean velocity in x-direction (L/T)
u_{Δ}	densimetric velocity (dimensionless)
u_1	constant defined by Equation (4.54)
u_2	constant defined by Equation (4.56)
u_3	constant defined by Equation (4.59)
u_4	constant defined by Equation (4.64)
v	lateral velocity component (L/T)
V	volume of tidal prism upstream of section (L^3)
V_w	transfer volume due to wind (L^3)
w	vertical velocity component (L/T)
w_s	wind speed (L/T)
w'	turbulent fluctuation from time mean velocity in z-direction (L/T)
x	longitudinal distance from upstream section of reach (L)
x'	distance from tidal entrance (L)
y	lateral coordinate direction
z	vertical coordinate direction

Greek Letters

∂	partial derivative operator
Δ	dimensionless distance traveled by characteristic velocity to reach node (Equation (2.34))
ΔA	increase in cross-sectional area (L^2)
$\tilde{F}(\)$	truncation terms of numerical approximation
ΔH	head loss (L)
ΔQ	change in discharge along length of reach (L^3/T)
Δt	time increment (T)
ΔV	increase in volume (L^3)
Δx	longitudinal spatial increment (L)
Δy	lateral spatial increment (L)
Δz	vertical spatial increment (L)
$\Delta \rho, \Delta \rho_0$	incremental density (M/LT^2)
ϵ	small number (Equation (7.11))
η	elevation of water surface from the mean depth (L)
θ	angle between wind and positive x-direction or reach (degrees)
κ	von Karman's constant = 0.4
ν	kinematic viscosity (L^2/T)
ξ	dimensionless longitudinal variable
π	universal constant = 3.141593
ρ, ρ_0	density (M/L^3)
τ	time decay coefficient at tidal entrance (1/T)
τ_{xx}	shear stress in x-direction with respect to x-direction (M/LT^2)
τ_{xy}	shear stress in y-direction with respect to x-direction (M/LT^2)
τ_{xz}	shear stress in z-direction with respect to x-direction (M/LT^2)
ϕ	angle between interface and positive x-direction (degrees)

$\phi(Ri)$ function of Richardson number (dimensionless)
 ω tidal frequency (1/T)

Subscripts

av average over two time layers
b bottom layer
c center of cell
f variables in freshwater layer above saltwater wedge
 l vertical layer
LT low tide
m spatial mean value
max maximum value
p previous time level
s variables in saltwater wedge
t tidal variables
TE tidal entrance
w wind variables
0 node at upstream section of reach
1 node adjacent to upstream node of reach
2 node, two away from upstream node of reach

Superscripts

n time level
- turbulent time mean value
~ value of variable at intermediate step

Abstract of Dissertation Presented to the Graduate Council
of the University of Florida in Partial Fulfillment
of the Requirements for the Degree
of Doctor of Philosophy

NUMERICAL MODELING OF SOLUTE
TRANSPORT IN TIDAL CANAL NETWORKS

By

Raymond Walton

June 1977

Chairman: B. A. Christensen
Major Department: Civil Engineering

Florida's population is growing at a rate of twice that of the world and three times that of the United States. This rapid growth has been accompanied by a large demand for residential dwellings in the state's coastal zones. As a result, many finger canal networks have been dredged.

In the early days of canal development, there were few regulations or design criteria, construction was often indiscriminate and frequently led to ecosystem degradation. Recently, public opinion has created a demand for research into environmentally acceptable canal design.

A three year study has recently been completed by the Hydraulic Laboratory, University of Florida, to develop a manual for the evaluation and design of canal networks. The study included field measurements and physical and numerical modeling of the transport processes.

Low energy canals are commonly found along the majority of the Gulf of Mexico and the Eastern Atlantic seaboard. They are typified by small tidal amplitudes and small water surface slopes. Measured maximum water surface slopes are such that in most practical cases a horizontal water surface slope can be assumed. This allows the tidal velocity field and the dispersion coefficients to be calculated as closed form functions of the longitudinal displacement from the upstream section of a canal.

Traditional numerical analysis of proposed or existing canal networks used one-dimensional digital models to study the transport mechanism. Such models can only simulate net flux through any cross-section of the flow, such as that produced by the tide or by lateral inflow within the network. Field measurements indicate that these mechanisms are often of minor importance when compared with wind-induced circulation, or density currents.

A further drawback to these models has often been the severe damping of longitudinal concentration profiles due to the numerical dispersion inherent in the approximation schemes used. A number of solution techniques are compared to determine their effectiveness in reducing this error, while still producing an economic model. The effect of varying a canal network's geometric parameters is investigated, and a solution technique selected for an extension to a three-dimensional model.

A three-dimensional mass-transport model is presented based on a modified method of second moments technique. The model incorporates the horizontal water surface assumption to simplify the tidal component

to produce a composite velocity field. Again, dispersion coefficients are explicitly determined.

The model has been used to simulate the results measured from dye dispersion studies on the East Coast of Florida, and can explain the well-documented inability of one-dimensional models to simulate observed conditions in this type of canal network. Furthermore, in calibrating the model on a variety of canal networks operating under widely differing conditions, the parameters were remarkably uniform, indicating that the transport mechanism is well formed.

CHAPTER 1
INTRODUCTION

1.1 Background Information

Florida's population is growing at a rate of about twice that of the world and three times that of the United States. This rapid growth, caused mainly by people moving into the state, has been accompanied by a large demand for residential dwellings in the coastal zone. In particular, the demand for waterfront property has led to the dredging of many finger canal networks (Figures 1.1 and 1.2).

The state has 9,000 miles of coastline [Carter, 1974, p. 59], with over 3,000 miles along the Atlantic Ocean, and over 5,000 miles on the Gulf of Mexico (these figures include estuaries, bays, islands, and sounds). This far exceeds all the other states with the single exception of Alaska. Today, most of the residential finger canal development is on the southwest and southeast coasts, but as the demand continues, development sites are chosen ever further northward.

In the early days of canal development, there were few regulations or design criteria. Construction was often indiscriminate and frequently led to ecosystem degradation, as evidenced by poor water quality and loss of marine life and vegetation due to loss of a varied habitat (Figures 1.3-1.4).

Within the last few years the public has increasingly focused its attention on environmental issues, a point reflected in the President of

the United States' opening message in the First Annual Report of the Council on Environmental Quality presented to Congress in August, 1970 [Council on Environmental Quality, 1970, p. v]

The recent upsurge of public concern over environmental questions reflects a belated recognition that man has been too cavalier in his relations with nature. Unless we arrest the depredations that have been inflicted so carelessly on our nature systems--which exist in an intricate set of balances--we face the prospect of ecological disaster.

The hopeful side is that such a prospect can be avoided. Although recognition of the danger has come late, it has come forcefully. There are large gaps in our environmental knowledge, but a great deal of what needs to be done can be identified. Much of this has already been begun, and much more can be started quickly if we act now.

In Florida this "awareness" has focussed on the coastal finger canal networks. The demand is now for environmentally compatible designs which either maintain the original diversity of the ecosystem, or if possible, improve upon it. To achieve this, the need has arisen for a comprehensive study of the hydrodynamic and transport properties of these canal networks to develop realistic design criteria. Such criteria should be based on providing a varied habitat within the canal network for the natural wildlife, and on ensuring optimum mixing and dispersion in these low energy systems. Snyder [1976] examined present design criteria (Figure 1.5) and suggested improvements to the procedure (Figure 1.6) that might lead to environmentally acceptable designs. The work of this report is intended to aid the canal designer and research scientist to better analyze existing and proposed network to determine if such criteria are, or will be, met.

1.2 Research Aim

The current research effort is a three year program sponsored by the Office of Sea Grant, National Oceanic and Atmospheric Administration (NOAA), and the Board of Regents (BOR) of the State of Florida University System to study the hydrodynamics and transport properties of residential finger canal networks in the coastal zone. The research has been divided into three major areas:

- a) Physical modeling
- b) Numerical and analog modeling
- c) Field measurements.

The aim of the research effort is to produce a canal design manual which will assist engineers, planners, and research scientists analyze existing or proposed canal networks with a view to meeting a reformed set of design criteria. To this end a number of related reports and hydrodynamic surveys have already been published [Walton, Morris, and Christensen, 1975; Walton, Morris, Evans, and Christensen, 1975; Morris and Christensen, 1976; Morris, Walton, Dlubac, and Christensen, 1977; Morris, Walton, and Christensen, 1978]. The canal design manual will be a summary of all the work undertaken on this project.

The material presented in this dissertation is really the first half of a two-part publication. The first half of the work is an examination of numerical methods and modeling techniques to predict the hydrodynamics and transport phenomenon of canal networks. From this study a predictive three-dimensional model has been developed and will be outlined in the proceeding chapters. The second half of the work [Morris, 1978] is to take this model and, together with knowledge obtained from the physical modeling research and field measurements, develop a design procedure.

1.3 Philosophy of Numerical Modeling

Today, there is an abundance of numerical models to predict hydrodynamics, transport phenomenon, and water quality for almost every conceivable type of waterbody imaginable. A number of these models have been used so often that the results obtained from them are considered to be reliable; that is to say no obvious discontinuities appear in the solution, and computer operation does not uncover faculty programming. In fact, there are so many models that some research effort is frequently spent in either cataloging them or making comparisons between them [Lombardo, 1973; Grimsrud et al., 1976; Graham, 1977].

Unfortunately, however, there is some tendency to accept a model as proven and almost blindly, as it were, apply it to one's own, and frequently very different, situation. Added to this, there has also been some tendency to develop oversimplified models, or at the other extreme, elaborate models in which complex techniques are used to approximate terms which have only a small effect on the results, and which can usually be neglected when one considers the quality of the input data or of the other approximations and assumptions made.

In a recent final draft report from the Vertex Corporation, Virginia [Horowitz and Bazel, 1977], a study was made of the investigative and legislative procedures used in the development of what the U.S. Environmental Protection Agency (U.S. EPA) considered to be the six best examples of Advanced Wastewater Treatment (AWT) plants in the United States. Their report not only criticized the legal aspects as embedded in the Federal Water Pollution Control Act Amendments of 1972 and the local laws of many states, but also the data sampling procedures and the numerical analysis procedures,

WATER-QUALITY SURVEYS are generally suspect on technical grounds, beset with irregularities in sampling and analysis, and naive in matters pertaining to hydraulics, sediments, and water chemistry.

MATHEMATICAL MODELS are oversimplified and filled with elaborate guesswork. They are intricate, abstruse fictions. They rarely account for the principle feature of the waterways they claim to represent, and they are usually built from inadequate data on hydrodynamics and water quality. [Horowitz and Bazel, 1977, p. 1-2]

Now, this view may be somewhat overstated, but it seems that many people are not aware of the old adage G.I.G.O.--garbage in, garbage out, or as it could be modified, garbage in initially, always garbage out. This statement can be looked at from another point of view. Snyder [1977] examined the potential accuracy of a certain water quality model. He assumed that if each constant-- "to be read in"-- was known to be within 95 percent confidence limits, and that the reaeration coefficient can vary over two orders of magnitude, then the results from the model, reflecting the combined additive and multiplicative effects of errors in the constants would be accurate to within less than 0.04 percent confidence limits--not a very reassuring prospect!

The problem may be, for example, as it certainly is in some models, that the water quality module is well defined but that the hydrodynamic module is oversimplified, or else too elaborate to be physically meaningful. A frequent oversimplification is to assume that the hydrodynamics can be simulated with a one-dimensional model. This is fatal when used for the analysis of coastal finger canal networks in Florida because they are low energy systems with small velocities and dispersion coefficients. In these low energy systems, external influences such as the wind and salinity gradients give rise to multi-layered flows with flow reversals.

Similarly the elaborate hydrodynamic models tend to concentrate on accurate solutions of a complex set of equations, the complexity of which becomes redundant when one looks at how such models handle averaging processes over confined reaches with highly variable roughness and input data.

The aim of this research is to develop a predictive three-dimensional model which incorporates the physically important factors in canal hydrodynamics and transport. Simple closed form solutions for the velocity field are used instead of the full governing equations by simplifying the latter equations based on available field data and by considering the relative importance of terms when compared with the probable effect of unknowns, accuracy of input data, and discretization techniques.

1.4 Scope of Report

Florida's canal networks are low energy systems, that is low velocities are commonly measured and the energy available for mixing processes is small. Because the diffusion and dispersion coefficients associated with the mixing processes are small, the numerical dispersion produced by the discretization techniques, used in many models for the convection and time derivative terms of the mass transport equation, frequently dominates the natural dispersion being modeled. The result is that concentration profiles can be underestimated unless extremely small time and spatial increments are used, which is computationally and economically unrealistic.

The accuracy and stability of various types of models and numerical techniques are examined in Chapter 2 to determine their applicability in

modeling the hydrodynamics of Florida's coastal finger canal systems. A one-dimensional mass transport model is developed, using the assumption that the water surface in the system is horizontal to derive closed form expressions for the velocity field and dispersion coefficients. The most favorable scheme was chosen as a basis for extending the model to three-dimensions.

The velocity field in coastal finger canal networks is rarely one-dimensional. In fact observations, discussed in Chapter 3, often show multi-layered systems in which flow reversals occur due to wind circulation, density gradients, and secondary currents. However, approximate solutions of the full governing equations of momentum and continuity are unrealistic because of the averaging procedures used in determining roughness effects, wind circulation, and the effects of density gradients. In Chapter 4, the governing equations are examined and simplifying assumptions made consistent with the expected accuracy of input data and model results. Closed form solutions of the time and spatial variables for the various component parts of the hydrodynamics of a canal network are derived, which may be superimposed to determine the velocity field.

The three-dimensional mass-transport equation, developed in Chapter 5, describes the transport of a substance in a canal network under the influence of the velocity field and dispersion processes. Knowing the velocity field as closed form functions of the time increment and spatial variables, the dispersion coefficients are developed from classical relationships giving similar functions. These coefficients are modified, however, to take into account the fact that mixing still occurs during periods of slack tide when the tidal velocities are theoretically zero.

Using the form of the hydrodynamics and transport processes discussed in the preceeding two chapters, a predictive three-dimensional mass transport model is developed in Chapter 6 using a mass-in-cell technique. The model forms of the boundary conditions at solid boundaries, tidal entrances, and of the lateral inflows are presented, and are shown to be realistic using a comparison with the one-dimensional mass transport model developed in Chapter 2, and a simple two-dimensional finite element model of flow in the receiving waterbody.

In Chapter 7, the stability criteria for the model are developed and analyzed using a series of test runs which vary the time and spatial increments. The model is transportive, conservative, and is shown to be stable and accurate. In calibrating the model, field data, obtained on a canal network in southeast Florida, were simulated numerically by varying the model parameters. The model was then run to determine its accuracy by comparing the results with a second set of data in the same canal network. These comparisons are presented in Chapter 8. A summary and conclusions are given in Chapter 9.

Appendix A is a users' manual for the model. A flow chart of the program is given in Appendix B, and Appendix C is a program listing. Appendix D presents a typical model output for one of the simulations discussed in Chapter 8.

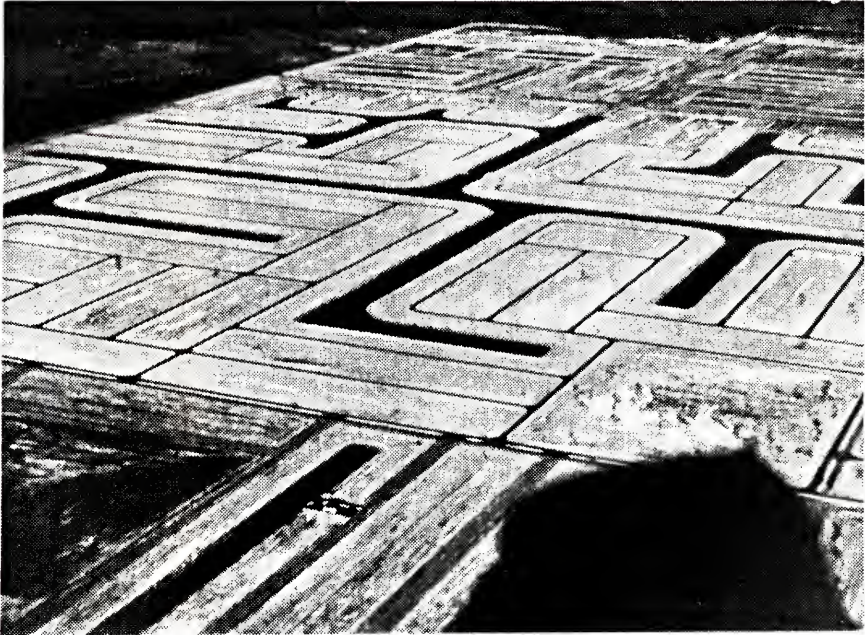


Figure 1.1 - Undeveloped Canal Network in Florida.



Figure 1.2 - Developed Canal Network Takeover of Natural System in Florida.



Figure 1.3 - Example of Polluted Canal Network in Florida.

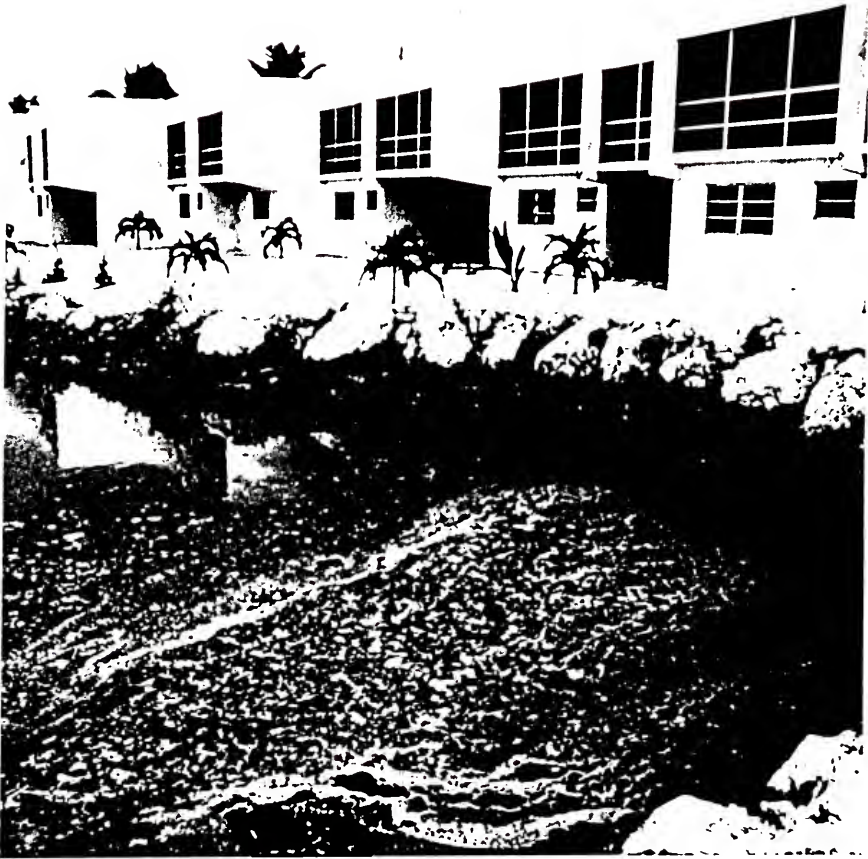


Figure 1.4 - Example of Polluted Canal Network in Florida.

GOAL	REQUIREMENTS	ENGINEERING CRITERIA	RESULTING DEVELOPMENT	ENVIRONMENTAL IMPACT
RESIDENTIAL UTILIZATION OF WATERFRONT WITHOUT ENVIRONMENTAL DEGRADATION	OFFSITE SEWAGE TREATMENT OR PACKAGE PLANT	ELIMINATE DOMESTIC WASTE SEEPAGE	BALANCE SALT INFLUXION WITH FRESHWATER HEAD	ELIMINATION OF POLLUTANTS
	OFFSITE WATER SUPPLY	ELIMINATE DIRECT STORMWATER DISCHARGE	VEGETATION FOR NUTRIENT UPTAKE	NATURAL WATER TREATMENT
WATERFRONT	RETENTION OF SOME SHALLOWS	RECHARGE GROUND WATER ON SITE	VARIED HABITAT SPECIES & NURSERY GROUNDS FOR NERITIC SPECIES	GROUNDWATER RECHARGE
	HABITAT DIVERSITY	NO DRAWDOWN OF WATER TABLE	NATURAL LOOKING NATURAL SHORES	COUNTERACTING SALT WATER INTRUSION
WITHOUT ENVIRONMENTAL DEGRADATION	INCREASE CIRCULATION	USE COMBINATION OF STABLE SLOPES, RIP RAP & VERTICAL BULKHEADS	NATURAL PRESERVES FOR BIRDS AND SHORE CRITTERS	GOOD MIXING
	PROMOTE MIXING	INCREASE UPLAND WATER TABLE FOR NATURAL ORAINAGE SLOUGHS		REDUCED DEBRIS COLLECTION
ELIMINATE SPECIFIED CONDITIONS		ELIMINATE NARROW DEAD ENDS		REDUCED SHOALING & EROSION
		"NATURAL" LAYOUT WITH GENTLE BENDS		BETTER FLUSHING
	BALANCE DEPTHS WITH WIDTHS & SHALLOWS	PROVIDE ROUGHNESS (BANKS & BOTTOMS)		AMENITIES OF NATURAL AND WATER SCAPING
	PROVIDE STABLE SECTIONS			
THE RATIONAL APPROACH TO CANAL DESIGN				
SNYDER OCEANOGRAPHY SERVICES				

Figure 1.5 - Criteria for Canal Design Without Consideration of the Environment (after Snyder, 1976).

CHAPTER 2
ANALYSIS OF NUMERICAL MODELING TECHNIQUES

2.1 Development of One-Dimensional Model

Before the development of a three-dimensional model was begun, it was decided to develop a one-dimensional mass-transport model to predict the transient concentration profiles of a passive, conservative substance in a simple canal network. A number of numerical techniques were tested and the results analyzed for accuracy, stability, and transportiveness. The various techniques used are discussed in the next five sections of this chapter. In Section 2.7 the techniques are compared, their results analyzed, and a method selected for extension to a three-dimensional model.

In the remainder of this section, the geometry, hydrodynamics, transport equation and dispersion coefficients, and boundary conditions for the one-dimensional model are developed.

2.1.1 Classification and Definitions of Canal Network Geometry

The majority of coastal finger canal networks in Florida consist of straight, prismatic reaches with trapezoidal cross-sections and relatively uniform depths, separated by junctions (see Figures 1.1 and 1.2). At the *tidal entrances*, a canal network has one or more hydraulic connections with a receiving waterbody, usually either the Intracoastal Waterway (ICW) or the ocean, or in some cases (particularly on the Gulf Coast) to an estuary. From the tidal entrances, a canal network

consists of an upward branching system of canals, possibly with loops, culminating in what will be called dead-ends. The *dead-ends* of a canal network are the upward limits of the system at which there is either an impervious boundary, a freshwater flow over a salinity control structure, or else at a distance sufficiently far up a river that the hydrodynamic effects of tides are negligible. A *loop* is defined as that part of a canal network in which a closed continuous line can be drawn along the longitudinal center lines of component reaches. The area of the water surface associated with each loop includes not only the surface areas of the reaches and junctions joined by the continuous line, but also the surface areas of canals and junctions which are hydraulically further away from that point of the continuous line which has the shortest hydraulic connection to a tidal entrance, and which have hydraulic connections to reaches and junctions along the continuous line (see Figure 2.1).

In this report, the positive x-axis for each component reach will be defined from the point of the reach which is hydraulically farthest away from the tidal entrances, along the longitudinal center line in the direction of the ebb tide (or towards the point closest to the tidal entrances). This will also be termed the *downstream direction*. Similarly the *upstream direction* will be defined along the negative x-axis. Facing downstream, the *left bank* will be the bank to the left of the longitudinal center line of the reach, and the *right bank* will be the bank to the right.

At a junction, which is the meeting point of two to four distinct reaches, the *downstream reach* for that junction is defined as the reach which lies hydraulically closer to the tidal entrance.

One of the remaining reaches coming together at the junction is then defined to be the *upstream reach* for that junction. When four reaches meet at a junction, this is the middle of the three upstream reaches. When only three reaches meet, the upstream reach is designated as that which is a more continuous extension of the downstream reach in the modeler's judgement. Once the upstream and downstream reaches are defined, the positive x-axis through the junction is from the former to the latter. Facing in this direction, a canal joining the junction from the left is termed the *left branch* for that junction, and a canal joining from the right is called the *right branch*.

All the above definitions are embodied in Figure 2.1.

2.1.2 Model Canal Network Geometry

To analyze some of the various numerical solution techniques available, two simple canal networks were defined. Each reach of the two networks was assumed to be trapezoidal in cross-section with bottom width, b , and with the same inverse side slope, s , on each side of the canal (Figure 2.2). The cross-sectional area, A , for any depth of water, d , is then given by,

$$A = d(b + sd) \quad (2.1)$$

The first network (Figure 2.3) consisted of a single straight prismatic canal of length, L , with a dead-end at the upstream end and a tidal entrance downstream. The second network (Figure 2.4) consisted of two canals meeting at a junction with a single tidal entrance at the downstream end, dividing the system into three reaches of lengths L_i , where i refers to the number of the reach. In Figures 2.3 and 2.4 the reach number is the uncircled number and the junction number

the circled number. For computational purposes, it was easier to refer to each dead-end as junction number 1, to number interior junctions consecutively from 2 to $(NJUNC + 1)$, where $NJUNC$ is the number of interior junctions, and to number tidal entrances consecutively from $(NJUNC + 2)$ upward.

2.1.3 Hydrodynamics of One-Dimensional System

There are several mechanisms which contribute to the hydrodynamics of canal networks, and these can be classified into two groups which have an internal or an external effect on the system. The internal mechanisms are those which cause a variation within the canal network by acting directly on the interior of the system. The external mechanisms are those which operate on the receiving waterbody, and which transfer their effects through the tidal entrances.

Examples of internal mechanisms are lateral inflow, secondary currents, wind induced circulation and density driven currents, induced by a saline wedge entering the canal network during the flood tide and retreating during the ebb tide, or by thermal gradients. However, all these effects except lateral inflow, produce circulation patterns whose net mass flux through a cross-section is zero at any time, and hence which cannot be modeled using a one-dimensional numerical scheme. To compensate, many modelers try to reproduce the three-dimensional effects by adjusting the one-dimensional model's coefficients, but the results are rarely satisfactory as the circulation pattern is not followed accurately enough. Only the lateral inflow, of the above list, can be thus modeled, because it has positive net flux in the system.

The main external influences are the astronomical tides, baroclinically induced tides and wind tides. All these phenomena have the effect of raising or lowering the water elevation at the tidal entrances to the canal network, and thus directly inducing a response within the system. In the one-dimensional model, these effects can be modeled in one of two ways. If the record of tidal elevations at the tidal entrances to the canal network follows a simple harmonic function, then the amplitude and frequency (or period) of this distribution can be read into the model, and the tidal elevations generated. Otherwise, the record can be digitized and read directly into the model as an input tidal entrance boundary condition.

Most hydrodynamic models are based on the de Saint-Venant Equations of continuity and momentum (or the dynamic equation as it is frequently termed). In one such model [Harleman and Lee, 1969], which will be used as a comparison with the hydrodynamic model presented in this section, the equations are written as follows, continuity,

$$\frac{\partial A}{\partial t} + \frac{\partial Q}{\partial x} - q_I = 0 \quad (2.2)$$

and momentum,

$$\frac{\partial Q}{\partial t} + u \frac{\partial Q}{\partial x} + Q \frac{\partial u}{\partial x} + g \frac{\partial d}{\partial x} A + g \frac{Q|Q|}{AC^2R} = 0 \quad (2.3)$$

where

t = time (T)

Q = discharge (L^3/T)

x = longitudinal displacement (L)

q_I = lateral inflow per unit length of reach (L^2/T)

u = cross-sectional mean velocity (L/T)

g = acceleration due to gravity (L/T^2)

C = Chezy coefficient ($L^{1/2}/T$)

R = hydraulic radius (L)

This model was used to study the hydrodynamics of a single canal with a variety of end boundary conditions. However, a number of investigators have used similar models to study canal networks with multiple branches, tidal entrances, and loops [Vreugdenhil, 1973; Abbott et al., 1975].

A study of the hydrodynamic variables measured in some of Florida's coastal finger canal networks indicates that it is usually not necessary to develop a one-dimensional hydrodynamic model based on the full set of equations. Canal networks in Florida are mostly fairly short, less than 10,000 ft long for example. They usually consist of straight prismatic reaches with negligible bed slopes separated by junctions. Typically, tidal ranges on the Atlantic coast are about 2 to 4 ft (Figure 2.5), and along the Gulf coast are 2 to 3 ft (Figure 2.6) [NOAA, 1974]. These small tidal ranges induce very small velocities in the networks (Figure 2.7), and is not uncommon to measure maximum velocities of less than 0.5 ft/sec at the tidal entrances (Figure 2.7). These and other typically measured hydrodynamic parameters are listed in Table 2.1. As can be seen from this table, maximum measured water surface slopes have been found to be between 10^{-5} and 10^{-6} .

This last observation in particular led Christensen [1975] to suggest that the acceleration terms in the momentum Equation (2.3) might be negligible in this case, and that a good approximation to the flow would be to consider a horizontal water surface rising and falling

with the tidal frequency and amplitude. Thus, the continuity equation alone would be sufficient to uniquely determine the velocity field [Walton, 1976a]. To test this assumption, a simple hydrodynamic model based on the conservation of mass principle was developed for the first test canal network (Figure 2.3), and the results compared with those obtained from Harleman and Lee's model for the same system.

For all the one-dimensional modeling, it was assumed that the depth varied sinusoidally with the tidal amplitude, a , and frequency, ω (Figure 2.8). Thus the depth, d_i , in any reach, i , of the canal network, is given by,

$$d_i = d_{0_i} + a \cos \omega t \quad (2.4)$$

where

$$d_{0_i} = \text{mean tidal depth in reach } i, (L)$$

and

$$\omega = \frac{2\pi}{T} \quad (2.5)$$

where

$$T = \text{tidal period} = 12.42 \text{ hrs.}$$

Such a representation is consistent with tides on the Atlantic coast Figure (2.5).

As the discharge for reach i , Q_i , can be written,

$$Q_i = A_i u_i \quad (2.6)$$

where the area A_i is not a function of x , Equation (2.2) becomes,

$$\frac{dA_i}{dt} + A_i \frac{du_i}{dx} - q_{I_i} = 0 \quad (2.7)$$

Integrating with respect to x_i from the upstream section of the reach,

$$u_i(x,t) = \left(\int_0^{x_i} q_{I_i} dx - x_i \frac{dA_i}{dt} \right) / A_i + u_{0_i} \quad (2.8)$$

where

u_{0_i} = velocity at upstream section of the reach (L/T).

The velocity, u_{0_i} , can be calculated in a similar manner in the upward branches of the reach considered, giving,

$$u_i(x,t) = \left[\sum_j^{Nu} \left(\int_0^{L_j} q_{I_j} dx - L_j \frac{dA_j}{dt} \right) + \int_0^{x_i} q_{I_i} dx - x_i \frac{dA_i}{dt} \right] / A_i \quad (2.9)$$

where

Nu = number of upstream reaches.

Now

$$\frac{dA_i}{dt} = B \frac{dd}{dt} \quad (2.10)$$

and

$$A_{ws} = B L$$

where

A_{ws} = area of water surface in canal network upstream of a section (L^2),

and

B = top width of cross-section (L),

thus Equation (2.9) can be simplified to,

$$u_i(x,t) = \left[\sum_j^{Nu} \int_0^{L_j} q_{I_j} dx + \int_0^{x_i} q_{I_i} dx \right] / A_i - \frac{A_{ws_i}}{A_i} \frac{dd}{dt} \quad (2.12)$$

Equations (2.4) and (2.12) are then sufficient to determine the depth of flow, and the velocity field at any point in the model one-dimensional canal network as a closed function of x and t .

To test the accuracy of this model, the depths and velocities were computed at various points inside the first test canal, the single prismatic canal (Figure 2.3), and the results compared with the results obtained from Harleman and Lee's model for the same system. Many of the parameters were varied, in particular, the canal length up to 11,000 ft. In all cases the depths and velocities calculated from the two models were within 2 percent of each other. A typical set of comparative results for a 9,500 ft canal is listed in Table 2.2. This was considered to be sufficiently accurate considering the errors inherent in numerical modeling and in the practical measurement of field data. Equations (2.4) and (2.12) were therefore used to describe the hydrodynamics in a one-dimensional canal network.

2.1.4 Transport Equation and Dispersion Coefficient

The three-dimensional mass-transport equation is developed by considering the conservation of a substance in an elemental volume of the flow. Using Fick's first law for molecular diffusion and an analogy for turbulent diffusion, the equation can be written [Harleman, 1966, pp. 576-578; Pritchard, 1971, p. 16],

$$\begin{aligned} \frac{\partial C}{\partial t} + \frac{\partial}{\partial x} (cu) + \frac{\partial}{\partial y} (cv) + \frac{\partial}{\partial z} (cw) = \frac{\partial}{\partial x} (E_x \frac{\partial C}{\partial x}) \\ + \frac{\partial}{\partial y} (E_y \frac{\partial C}{\partial y}) + \frac{\partial}{\partial z} (E_z \frac{\partial C}{\partial z}) + r_p \end{aligned} \quad (2.13)$$

where

x, y, z = coordinate directions (L)

u, v, w = velocities in x, y, z directions respectively
(L/T)

E_x, E_y, E_z = turbulent diffusion coefficients in x, y, z
directions respectively (L^2/T)

c = concentration (dimensionless)

r_p = rate of production or loss of substance (1/T).

The one-dimensional mass transport equation can then be obtained by cross-sectionally averaging Equation (2.13) [Harleman, 1971, pp. 37-38] and by using a Fick's first law analogy for longitudinal dispersion [Taylor, 1954; Aris, 1956],

$$\frac{\partial}{\partial t} (Ac) + \frac{\partial}{\partial x} (Auc) = \frac{\partial}{\partial x} (A(E_x + E_\ell) \frac{\partial c}{\partial x}) + Ar_p \quad (2.14)$$

where

E_ℓ = longitudinal dispersion coefficient (L^2/T).

Elder [1959] examined the orders of magnitude of the longitudinal turbulent diffusion coefficient, E_x , and the longitudinal dispersion coefficient, E_ℓ , and found that the latter was about ten times the former. Thus, Equation (2.14) is often written,

$$\frac{\partial}{\partial t} (Ac) + \frac{\partial}{\partial x} (Auc) = \frac{\partial}{\partial x} (AE \frac{\partial c}{\partial x}) + Ar_p \quad (2.15)$$

although measurement techniques for the longitudinal dispersion coefficient are integral methods and thus automatically include the effect of the longitudinal diffusion coefficient.

As the substance being modeled was considered to be passive and conservative, and as there were no sinks for the flow except at the tidal entrances, the rate of production term, r_p , includes only the lateral inflow, q_I . If the concentration of the lateral inflow is c_I , then the rate of production is given by,

$$r_p = q_I c_I / A \quad (2.16)$$

and Equation (2.15) becomes

$$\frac{\partial}{\partial t} (Ac) + \frac{\partial}{\partial x} (Auc) = \frac{\partial}{\partial x} (AE_x \frac{\partial c}{\partial x}) + q_I c_I \quad (2.17)$$

The above equation is called the conservative form of the one-dimensional mass-transport equation. The term *conservative* is used to imply that a finite difference approximation of the equation preserves the integral relationship of the continuity equation [Roache, 1972, pp. 28-33]. A *non-conservative* form of the equation does not have this property. Roache states that a conservative formulation does not always give more accurate results, but that the experience of many researchers has indicated that such formulations generally are more accurate. A non-conservative form of Equation (2.17), using the continuity Equation (2.3) and the fact that the area, A, is not a function of the longitudinal displacement, is,

$$\frac{\partial c}{\partial t} + u \frac{\partial c}{\partial x} = \frac{\partial}{\partial x} (E_x \frac{\partial c}{\partial x}) + q_I (c_I - c) / A \quad (2.18)$$

It will be seen later that it is sometimes necessary to use this form of the equation.

Classically, the longitudinal dispersion coefficient, E_L , is written [Taylor, 1954; Elder, 1959],

$$E_L = KRu^* \quad (2.19)$$

where

K = dimensionless dispersion coefficient

R = hydraulic radius (L)

u^* = bed shear velocity (L/T).

The dimensionless dispersion coefficient, K , is a function of the geometry of the system, depending on radii of bends, bottom roughness, wall Reynolds' number, etc. Although classically considered to be about twenty (based on the hydraulic radius), many researchers have measured values of K in various types of waterbodies, from less than ten to the order of several hundreds.

In many Floridian canals, logarithmic velocity profiles have been observed when the effects of wind induced circulation and density driven currents have been small (Figure 2.7). Such a profile gives a unique relationship between the spatial mean velocity, u , and the bed shear velocity, u^* [Nikuradse, 1933],

$$u = 2.5u^* \ln(10.9d/k) \quad (2.20)$$

where

k = Nikuradse's equivalent sand roughness (L).

Thus, from Equation (2.19)

$$E_L = \frac{0.4KRu}{\ln(10.9d/k)} \quad (2.21)$$

As the spatial mean velocity, u , is a closed form function of the longitudinal displacement and time, the longitudinal dispersion coefficient is also a closed form function of x and t . Therefore,

the only remaining unknown in the one-dimensional mass-transport Equation (2.17) or (2.18) is the concentration, c .

2.1.5 Boundary Conditions

The one-dimensional mass-transport Equation (2.17) or (2.18) is a second-order parabolic equation, being second-order in the spatial variable, x , and first-order in the time variable, t . Thus, to close the system, two spatial boundary conditions and a set of initial conditions are required.

For both the test canal networks, the initial conditions were that the concentrations at time $t = 0$ in the canal either equaled the background concentration, c_{RW} , or else that they were read in.

At the dead-ends of the canal system, a zero-flux condition was initially used in the form,

$$\frac{\partial c}{\partial x} = 0 \quad (2.22)$$

However, it soon became apparent that simple numerical approximations to Equation (2.22), such as a forward difference operator,

$$\frac{c_1 - c_0}{\Delta x} = 0 \quad (2.23)$$

where

c_0 = concentration at dead-end (dimensionless)

c_1 = concentration at adjacent node (dimensionless)

implied that the gradient of the concentration profile in the segment of the reach adjacent to the dead-end is zero, which led to erroneous results. Higher-order schemes were discounted because it was felt that they used information which was too far away from the dead-end to be meaningful.

To overcome this problem, a simple mass balance expression was developed based on the mean velocity between the two nodes at the dead-end. However, this condition was eventually simplified when it was observed that the concentration profiles resulting from this model were linear at low tide, and that the mass balance condition maintained this linearity all the way to the dead-end. Thus, the final form of the dead-end boundary condition for this test model was that the concentration at the dead-end was a linear extrapolation of the concentrations at the two-adjacent nodes,

$$c_0 = 2c_1 - c_2 \quad (2.24)$$

At the tidal entrances to the system, a dual condition was established. During the ebb tide a "floating" type boundary condition was used in which the concentration at the entrance was calculated using a backward difference operator. Dispersion was neglected at this point because the concentration would either be convected out of the system at the next time step, or else would be lost in the description of the flood tide boundary condition. Thus during the ebb tide, the concentration at the tidal entrance, c_{TE}^{n+1} , was given from the equation

$$\frac{c_{TE}^{n+1} - c_{TE}^n}{\Delta t} = \frac{u_{TE}^n c_{TE}^n - u_{TE-1}^n c_{TE-1}^n}{\Delta x} \quad (2.25)$$

where

Δt = time increment (T)

Δx = spatial increment (L)

n = time level

Assuming that the concentration at the tidal entrance reaches a values of c_{LT} at low tide, a first order decay was used to describe the time history of the concentration at the tidal entrance during the flood tide,

$$c_{TE} = c_{RW} + (c_{LT} - c_{RW}) \exp(-3t'/\tau) \quad (2.26)$$

where

t' = time since low tide (T)

τ = time decay coefficient (1/T).

The form of this boundary condition results in the concentration at the tidal entrance being within 2 percent of the background concentration, c_{RW} , after τ units of time after low tide.

To test the accuracy of this assumption, a simple two-dimensional finite-element model was developed to describe the transport in a receiving waterbody such as the ICW under a point source/sink loading. Results indicated that a first order decay type condition was a fair approximation to the resulting flood tide concentration profile at the tidal entrance. Furthermore, as will be seen later in Section 2.8, variation of the time decay coefficient, τ , does not dramatically alter the resulting concentration profiles in the canal network.

2.2 Finite-Difference and Finite-Element Approaches

Measured longitudinal dispersion coefficients in Floridian canals are usually very small, less than $5 \text{ ft}^2/\text{sec}$ being common. This means that the dispersion term in the one-dimensional mass transport Equation (2.17) or (2.18) is small. If this term is dropped altogether,

then the remaining first-order hyperbolic equation is the one-dimensional convection equation,

$$\frac{\partial c}{\partial t} + u \frac{\partial c}{\partial x} = 0 \quad (2.27)$$

A number of people have studied this equation [von Neumann and Richtmyer, 1950; Stone and Brian, 1963], and have concluded that model studies of this equation using the more common low order finite-difference approximations usually lead to inaccurate results, and possibly instabilities, depending on the scheme used. A survey of the more common finite-difference schemes such as the forward, backward, central explicit or implicit schemes, will not be given here as they are extensively covered in the literature [Ames, 1969; Milne, 1970; Roache, 1972; Smith, 1975].

The problem, termed numerical dispersion, arises out of a Taylor series approximation to the terms of Equation (2.27). If, for example, a constant velocity, u , is assumed in the positive x -direction and a backward difference scheme is used to approximate the equation to the second order [Molenkamp, 1968],

$$\frac{\partial c}{\partial t} + u \frac{\partial c}{\partial x} = \frac{1}{2} |u| \left(1 - |u| \frac{\Delta t}{\Delta x}\right) \Delta x \frac{\partial^2 c}{\partial x^2} \quad (2.28)$$

the term on the right hand side of Equation (2.28) is the numerical dispersion term with an associated numerical dispersion coefficient

$$E_n = \frac{1}{2} |u| \left(1 - |u| \frac{\Delta t}{\Delta x}\right) \Delta x \quad (2.29)$$

The effect of this pseudodispersion is to smooth the profile for positive values of E_n , and to produce instabilities in the results for negative values. This same problem can be shown diagrammatically (Figure 2.9)

for the case [Pedersen and Prahm, 1973],

$$u = \frac{1}{2} \frac{\Delta x}{\Delta t} \quad (2.30)$$

which gives a positive numerical dispersion coefficient.

From Equation (2.28), it can be seen that one way of reducing the error is to decrease the spatial increment. However, this tends to increase computer costs to astronomical levels as the time interval, Δt , usually has to be reduced also to meet stability criteria.

A second method would be to choose Δx and Δt such that

$$u = \frac{\Delta x}{\Delta t} \quad (2.31)$$

and this has been done successfully for some steady, uniform flow problems. In the tidal canal problem, however, the flow is unsteady and nonuniform, and the condition of Equation (2.31) cannot be met everywhere. In fact unless this condition is met at the tidal entrance, E_n will be negative somewhere in the canal network in this example.

The above analysis was based on the backward difference scheme, but serves to illustrate the problem. Similar numerical dispersion expressions can be developed for other schemes for idealized flow conditions. The aim of this study then, is to develop a scheme in which the inherent numerical dispersion present in the numerical solution is much smaller than the natural dispersion being modeled, and also one which does not require excessive computer time because of the smallness of the spatial and time increments, Δx and Δt , respectively.

A number of schemes were developed by this author [Walton, 1976a], forward, backward and central explicit, and backward and central

implicit, as well as by Langley [1976] who used an explicit central-difference scheme to model flow in a canal with a boat basin. For the first test canal network (Figure 2.3), using the standard data set listed in Table 2.3, it was found in every case that the only way to improve the accuracy of the schemes was to reduce Δx , and therefore Δt (Figure 2.10). For the 1,000 ft canal (Table 2.3), it was necessary to make $\Delta x = 25$ ft and $\Delta t = 100$ secs.

In conclusion it was decided that this type of restriction on the size of the spatial and time increments would serve to produce an uneconomic model for much larger canal networks and for a three-dimensional model. A similar finite-element model developed by Leimkuhler et al. [1975] was also tested, and was found to suffer from the same drawbacks as the finite-difference models. This latter method was therefore also discounted.

2.3 Method-of-Characteristics Approach

As was seen in Section 2.2, the numerical dispersion inherent in the more common low order finite-difference and finite-elements schemes is sufficiently large to swamp the natural dispersion being modeled, for economic choices of the spatial and time increments. The problem is then to model the convective part, Equation (2.27), of the one-dimension mass-transport equation economically and accurately, and minimize the numerical dispersion produced.

Equation (2.27) is a first-order hyperbolic equation. A traditional way to solve this equation is the Method-of-Characteristics. If the one-dimension mass-transport equation in its nonconservative form, Equation (2.18), is considered, the left hand side of the

equation can be expressed as a material derivative,

$$\frac{Dc}{Dt} = \frac{\partial c}{\partial t} + u \frac{\partial c}{\partial x} = \frac{\partial}{\partial x} (E_x \frac{\partial c}{\partial x}) + q_I (c_I - c)/A \quad (2.32)$$

A two step solution scheme can then be developed by firstly convecting the concentration field along the characteristic lines of the velocity forming new nodal concentrations \bar{c}_i^{n+1} , where i represents a spatial node and $n+1$ is the new time level. Equation (2.32) is now a second-order parabolic equation with no dominating first-order hyperbolic term, and can readily be approximated by a central-difference scheme, in which the time derivatives are approximated along the characteristic line of the velocity, and the spatial derivatives are estimated by averaging between the two time levels,

$$\begin{aligned} c_i^{n+1} = & \bar{c}_i^{n+1} + \frac{\Delta t}{2\Delta x^2} [(E_{i+1} + E_i)(c_{av_{i+1}}^{n+1} - c_{av_i}^{n+1}) \\ & - (E_i + E_{i-1})(c_{av_i}^{n+1} - c_{av_{i-1}}^{n+1})] \\ & + \Delta t q_I (c_I - c_{av_i}^{n+1})/A^{n+1} \end{aligned} \quad (2.33)$$

where

$$c_{av_i}^{n+1} = \frac{1}{2} (\bar{c}_i^{n+1} + c_{i+\Delta}^n) \quad (2.34)$$

in which

Δ = dimensionless distance traveled by characteristic velocity to reach node i .

The convective step can be performed in two ways as illustrated in Figure 2.11. The first method is to convect the concentrations at the existing nodes to form a new nodal grid at the next time level.

This is called the movable grid formulation. The second method is to interpolate between nodal values using the velocity characteristic lines to estimate where new nodal concentrations originated. This is called the fixed grid formulation.

The two variations were run with the standard data set of Table 2.3 for a variety of spatial and time increments. The results shown in Figures 2.12 and 2.13, and others, are analysed in Section 2.7.

2.4 Hybrid Computer Approach

If the convective Equation (2.27) is again considered, a function $F(x,t)$ is defined as follows,

$$F(x,t) = \frac{\partial c}{\partial t} + u \frac{\partial c}{\partial x} = 0 \quad (2.35)$$

for a uniform velocity field, u , and $\tilde{F}(x,t)$ is defined to be the finite-difference approximation to $F(x,t)$, then

$$F(x,t) = \tilde{F}(x,t) + \Delta\tilde{F}(x,t) \quad (2.36)$$

where

$$\Delta\tilde{F}(x,t) = \text{truncation terms of finite-difference series expansion.}$$

For a central difference scheme of the spatial derivative, and a forward difference scheme for the time derivate, using Taylor series expansions up to the second order,

$$\Delta\tilde{F}(x,t) = \frac{-\Delta t}{2} \frac{\partial^2 c}{\partial t^2} \quad (2.37)$$

as the central difference scheme is second order accurate. Differentiating Equation (2.35) with respect to t and noting that the differentiation is commutative,

$$\frac{\partial^2 c}{\partial t^2} = -u \frac{\partial}{\partial x} \left(\frac{\partial c}{\partial t} \right) \quad (2.38)$$

Using Equation (2.35) again,

$$\frac{\partial^2 c}{\partial t^2} = u^2 \frac{\partial^2 c}{\partial x^2} \quad (2.39)$$

and substituting into Equation (2.37)

$$\tilde{\Delta F}(x,t) = -\frac{\Delta t}{2} u^2 \frac{\partial^2 c}{\partial t^2} \quad (2.40)$$

Thus, for a central difference scheme, an expression has been derived for the numerical dispersion coefficient,

$$E_n = \frac{-\Delta t}{2} u^2 \quad (2.41)$$

This form of the numerical dispersion coefficient illustrates an intriguing possibility. If the time increment could be decreased to zero then the numerical dispersion would vanish irrespective of the spatial increment, Δx . Although Equation (2.41) does not accurately represent the numerical error present in modeling a nonuniform velocity field, it does at least suggest its basic form.

One way to decrease the time interval to zero, or make time continuous, is to use an analog or hybrid computer. This consists of a digital computer controlling the potentiometer settings of an analog computer. A project was initiated with the Hybrid Computations Laboratory at Martin-Marietta Aerospace in Orlando, Florida [Morris, Walton, and Christensen, 1977; Sorondo and Baldwin, 1977], to study the feasibility of applying analog modeling techniques to the transport in a one-dimensional canal network. A finite-difference model was also designed for the same system to verify the model.

An analog model has several advantages over the digital models which at that time were being considered for canal networks. Firstly, analog solutions are obtained very quickly, and many hundreds of tidal cycles could be simulated in less than a minute. On a digital computer this would take several minutes of central processing unit (CPU) time, plus a much longer time to print out the results. Secondly, because of the hybrid capability, many test runs can be run in a very short time, allowing a much more complete look at the effects of varying each parameter alone.

The objectives of the hybrid model study were

- a) To determine whether the hybrid approach and the Martin-Marietta facilities were capable of implementing a two-dimensional simulation of pollution transport in a tidal canal network.
- b) To evaluate the hybrid model by comparison with digital models being developed by the Hydraulic Laboratory.
- c) To determine whether the nonconservative or the conservative formulation of the mass-transport equation was preferred.
- d) To determine the most consistent finite-differencing techniques.
- e) To determine which of the boundary conditions provides the most realistic results consistent with other models using difference techniques.
- f) To assess the relative influence or significance of variations in the independent variables of the analog model.

The analog model was set up as the first test canal (Figure 2.3) with five segments in the canal and a sixth segment in the receiving water to control the tidal entrance boundary condition (Figure 2.14). The model, which included the capability of switching between four different explicit finite-difference techniques, the forward, backward, central, and first upwind differencing schemes (the latter being simply a backward-difference scheme for the ebb tide, and a forward-difference for the flood tide), required a large percentage of an analog patch-panel, sometimes called a *hybrid terminal*. An example of a circuit diagram for one node of the canal is given in Figure 2.15. It was estimated that a total of twenty nodes could be programmed onto one panel. The output was in hard copy form on an eight channel strip chart recorder, the eighth channel giving the velocity at the tidal entrance (Figure 2.16). The results for the first test canal case for each of the four different finite-difference techniques are given in Figure 2.17.

After the work was completed a more detailed report was written [Morris, Walton, and Christensen, 1977] and submitted to the Office of Sea Grant. The value of this modeling technique and its possible extension to three-dimensional modeling will be covered in a comparative discussion of all the techniques investigated in Section 2.7. The conclusions are given below.

1. The central difference form of the nonconservative equation appears to give the most consistent results, both in the analog and the digital models. The capability of obtaining a set of concentration plots over a thousand tidal cycles in a matter of seconds (after the model has been initialized) is very convenient.

2. The conservative form of the equation has potential, but its results were obscured by an unrealistic boundary condition and some instabilities. Further testing of this form would be required before a choice between them can be made.
3. The boundary condition at the open-end of the canal is satisfactory.
4. The zero-flux ($\partial c/\partial x = 0$) boundary condition at the closed-end of the canal appears to distort the results. However, the linear boundary condition gives results which are in very good agreement with other models developed.
5. The mass balance boundary condition at the dead-end was not functioning properly, although it has been shown to operate properly in digital models developed by the Hydraulic Laboratory. Further testing of this formulation would be desirable.
6. The five-segment model is somewhat coarse spatially, but better than was initially expected. A ten or twenty-segment model would be useful for verifying the results of the five-segment model, but could not be expected to provide much additional information.
7. Flushing time, the time for the model to reduce concentrations at all sections to "steady-state" values from some initial, nonequilibrium condition, cannot be inferred from the present model results due to inconsistencies in the variability portion of the study. However, these inconsistencies may be due in part to difficulty in accurately reading plotted results.
8. Expansion of the model to about twenty sections is possible using one analog programming board on the hybrid computer. A two-dimensional model incorporating three nodes in the vertical direction would therefore require three analog consoles. Multiple-board simulations are difficult to schedule and expensive to run. Therefore, it is concluded that for canal networks and two-dimensional models the analog/hybrid approach is extremely limited by hardware availability, not generally practical, and quite expensive.
9. It typically would take several days to a week to have a specific set of analog or digital computer runs completed and mailed to the Hydraulic Laboratory, although it is possible to greatly reduce this time if expense is secondary.

10. Numerous refinements, as outlined in the initial proposal were not tested as they required more hardware and would have obscured the basic evaluation. These refinements included variable canal geometry and additional water quality parameters. Incorporation of these additional variables, which would ultimately be required for a complete canal design capability, would be prohibitive from an analog hardware standpoint.
11. The basic canal *network* formulation was not tested due to lack of a good closed-end boundary condition and lack of time. A single canal junction in one-dimension could be implemented without much difficulty on the analog computer, but extension to a full canal network is definitely limited by analog hardware availability.

2.5 Second Upwind Differencing Method

The "Second Upwind Differencing" method, as termed by Roache [1972] and used by Bella and Dobbins [1968], or "the Donor Cell" method as it was called by Gentry, Martin, and Daly [1966], is a finite-difference technique used by Lee [1977] to solve the one-dimensional mass-transport Equation (2.17). Written in its conservative form in terms of the discharge, Q , rather than the cross-sectional mean velocity, u ,

$$\frac{\partial}{\partial t} (Ac) + \frac{\partial}{\partial x} (Qc) = \frac{\partial}{\partial x} (AE_x \frac{\partial c}{\partial x}) + q_I c_I \quad (2.42)$$

Using the schematic canal of Figure 2.18 as a guide, the method uses a backward finite-difference expression for the convective term $\frac{\partial}{\partial x} (Qc)$ during the flood tide, and a forward finite-difference term during the ebb tide.

The Second Upwind Differencing method has several advantages over other finite-differencing techniques. Firstly, it is conservative, that is the net accumulation of mass in a region equals the net flux across the boundaries of the region during the convective process.

Secondly, it is transportive during the convective phase, that is "the effect of a perturbation in a transportive property is advected only in the direction of the velocity" [Roache, 1972, pp. 67-72]. No stationary finite-difference formulation of the oscillatory convective process possesses this property.

The method suffered originally from the major disadvantage that numerical dispersion was large, as mentioned by Roberts and Weiss [1966]. This problem was examined for the First Upwind Differencing method by Noh and Protter [1963] who derived an expression for the numerical dispersion present in the solution. The theory was extended here to the Second Upwind Differencing method by Lee [1977]. Bella and Dobbins [1968] had suggested that the numerical dispersion might be subtracted from the natural dispersion to give a composite dispersion term that accurately modeled prototype conditions. However, in their studies on rivers and estuaries, the natural dispersion was much larger than the numerical dispersion, giving positive values for the composite dispersion. The problem is that this is not the case in Floridian canals, in which the resulting composite dispersion is negative for reasonable choices of Δx , giving rise to unstable solutions. As mentioned previously, a negative dispersion term has the effect of augmenting instabilities present in the numerical scheme rather than smoothing them as positive dispersion does.

Recently, Boris and Book [1973, 1976] and Book, Boris, and Hain [1975] developed a correction technique termed "flux-corrected transport." This technique extended the idea of Bella and Dobbins in subtracting the numerical dispersion to include the extra condition that the antidiffusion stage should generate no new maxima or minima in the

solution, nor should it accentuate already existing extrema. To accomplish this, the antidispersion flux terms are corrected or limited so that no antidispersion transfer of mass can push the concentration at any grid point beyond the concentration value at neighboring points.

Using the schematic canal of Figure 2.18 as a guide, the Second Upwind Differencing model with flux-corrected transport may be described as operating as follows during one time step:

1. addition of pollutant through lateral inflow,
2. net tidal convection of pollutant into the segment from adjacent segment with values of concentration, c , defined at the center of the segment, and values of the discharge, Q , defined at boundaries of the segment,
3. limited antidispersion to correct for the numerical dispersion errors introduced in the convective step but controlled by the flux-corrected transport criterion,
4. net transport of pollutant into the segment by natural longitudinal dispersion.

This method is essentially second-order accurate, as it has been corrected for the second-order error, the numerical dispersion. Even with the correction term, the method remains both conservative in all steps and transportive in the convection step, properties which cannot be claimed in all cases by the other finite-difference and finite-element models so far considered. These properties alone do not ensure that the desired solution will be obtained. The stability and convergence of the solution must also be considered.

Although there is no universally accepted definition of stability, this term is generally used to refer to the damping with time of small perturbations (or errors) introduced into the finite-difference solution. It can readily be seen from Figure 2.19 that the solution shows no visible instabilities to be present. One is also concerned about convergence, or whether the solution approaches the solution of the partial differential Equation (2.17) as Δx and Δt approach zero.

For equations such as the one-dimensional mass-transport Equation (2.17), with variable coefficients, necessary and sufficient stability and convergence conditions are not available. However, conditions such as

$$|u_{\max}| < \frac{\Delta x}{\Delta t} \quad (2.43)$$

and

$$E_{\text{max}} < \frac{\Delta x^2}{2\Delta t} \quad (2.44)$$

make sense physically and provide guidelines for choosing Δx and Δt .

In the final analysis, comparisons of the numerical solutions of the difference models must be relied on in attempting to assess the accuracy and, considering computing costs, the economics of any one model. This comparison is made in Section 2.7.

2.6 Method of Second Moments

The Method of Second Moments is essentially an upwind finite-difference scheme. However, instead of considering a concentration represented at a single point, or node, the concentration is considered to be a block with the height being the magnitude of the concentration

and the width being the width of the cell, Δx , the spatial increment. Thus, like the nodal finite-difference representation, this method suffers equally from numerical dispersion.

The advantage of this way of representing the concentration is that it conserves the mass, or the zeroth moment of the mass. One method that has been used in meteorology to reduce the numerical dispersion present in finite-difference schemes, is to also conserve higher order moments of the distribution [Egan and Mahoney, 1972; Pedersen and Prahm, 1973]. Any number of moments could be chosen to represent the distribution, but commonly the first and second moments are used. These physically represent the center of the mass, and the width of mass with respect to its center. Higher order moments, such as third order moments which represent the skew of the distribution, do not have the same intuitive feel, but could be used if the lower order moments fail to represent the distribution accurately.

Consider the concentration distribution, $c(\xi)$, shown in Figure 2.20 in a cell of unit width, represented by a rectangle having the same mass, c_m , the same center of mass, F_m , and the same second moment squared, R_m^2 [Pedersen and Prahm, 1973], then,

$$c_m = \int_{-0.5}^{0.5} c(\xi) d\xi \quad (2.45)$$

where

$$\xi = \frac{x - (i - 1)\Delta x}{\Delta x} \quad (2.46)$$

and

$$F_m = \int_{-0.5}^{0.5} c(\xi) \xi d\xi / c_m \quad (2.47)$$

$$R_m^2 = 12 \int_{-0.5}^{0.5} c(\varepsilon)(\varepsilon - F_m)^2 d\varepsilon/c_m \quad (2.48)$$

Figure 2.9 illustrates what happens if only the convection of a square wave as defined by Equations (2.27) and (2.30) is considered. This form conserves the zeroth moment of the distribution, or its mass. If the first moment of the distribution is also conserved (Figure 2.21), it can be seen that the analytic distribution is much more closely approximated. Inclusion of the second moment for this particular problem reproduces the square wave exactly, and is another reason for considering only moments up to the second order.

The problem defined in Equations (2.27) and (2.30) is a uniform flow case. For an oscillatory flow in canals the method has to be amended. A closed form solution for the velocity at any point in the canal was developed in Section 2.1.3 (Equation (2.9)). Assuming that the lateral inflow entering each cell has a uniform longitudinal variation in that cell, then the velocity variation over the length of the cell is linear in x and represents the distortion the cell undergoes as the tidal elevation changes from the old cross-sectional area, A_p , to the new area, A . As each reach of the canal network is prismatic, the ratio A_p/A represents the amount of expansion or contraction of each cell in the reach. Thus, the first step in the solution procedure is to distort the cell,

$$c_m = c_{mp} A_p/A \quad (2.49)$$

$$F_m = F_{mp} \quad (2.50)$$

$$R_m = R_{mp} A_p/A \quad (2.51)$$

where

p = previous time level.

The second step is to move this new distribution in the direction of the flow a distance equal to the distance moved by the center of mass in the time interval, Δt

$$x = \Delta x(1/2 + F_m) - V/A \quad (2.52)$$

where

V = incremental volume of tidal prism upstream of cell (V is defined as positive for a flood tide). (L^3).

The new distribution and the lateral inflow are then allocated to the various cells into which they fall, where for each cell the square of the second moment, $R_{C_i}^2$ of each composite distribution is calculated about the center, c , of cell i ,

$$R_{C_i}^2 = 12 \sum_{j=1}^{N_i} \int_{-0.5}^{0.5} c_j(\xi) \xi^2 d\xi / c_{m_i} \quad (2.53)$$

where

N_i = number of distributions that lie inside cell i .

When all the cells of each reach have been readjusted, the square of the second moment of the resulting distribution about the new center of mass, F_{m_i} , is found using the parallel axis theorem for each cell,

$$R_{m_i}^2 = R_{C_i}^2 - 12 F_{m_i}^2 \quad (2.54)$$

Finally, dispersion is modeled at the new time level using the central finite-difference scheme as before,

$$c_i^{n+1} = c_i^{n+1} + \frac{\Delta t}{2\Delta x^2} [(E_{j+1} + E_j)(c_{i+1}^{n+1} - c_i^{n+1}) - (E_j + E_{j-1})(c_i^{n+1} - c_{i-1}^{n+1})] \quad (2.55)$$

where

\tilde{c}_i = is the concentration value at node i after the convective step.

As this method is an upwind differencing method, the method also possesses the properties of being conservative and transportive as defined in Section 2.5. Similarly, the same stability and convergence conditions must be expected to apply to this method. The results of varying the spatial and time variables, Δx and Δt , for the first test canal (Figure 2.3) using the standard data set of Table 2.3 are shown in Figure 2.22. A comparative analysis of this and the other methods described in the preceding sections follows.

2.7 Comparison of Techniques

In Sections 2.2 through 2.6, several numerical techniques to evaluate the one-dimensional mass-transport Equations (2.17) or (2.18) were discussed, and the results shown for the simulation of the first test canal, Figure 2.3, using the standard data set in Table 2.3.

Several methods are immediately discounted. The finite-element and finite-difference methods up to second order were discounted because of the restrictive choice of the spatial and time increments, Δx and Δt , respectively, to achieve comparable results with the other models investigated. An extension to a complex canal network would require an excessive amount of computer time. Higher order methods

were not considered in this analysis because they require small Δx and Δt increments so that the information being used to model conditions at one node is not spread out over too great a distance. The movable-grid method-of-characteristics approach was also discounted because it was found that the net convection out of system due to the lateral inflow, also convected the grid out of the system over time.

The other four methods, the hybrid method, the fixed grid method-of-characteristics, the second upwind differencing method, and the method of second moments, produced very similar results for the first test canal with the standard data set. In obtaining this result, the hybrid model used seven nodes. At the Martin-Marietta facility, it was estimated that twenty nodes could be used on one patch-panel and that three patch-panels could be linked together in series. However, this would tie up the laboratory and provide only sixty nodes which are clearly not enough for a model of any complexity. Several ideas were considered in which the solution domain could be divided up, using the digital computer to control the operation, and the solution matched at boundary nodes. These ideas were dropped when it became apparent that the complexity of such a set-up would be unrealistic. Also, once a patch-panel is set up, the geometry becomes fairly rigid, and it is not easy to program for varying spatial increments and numbers of nodes per reach. For all these reasons, it was decided that the disadvantages outweighed the primary advantage of speed, and further research was discontinued.

The three remaining models are cheap to run and gave very similar results for the first test canal. Therefore, a second run

was designed in which there was initially a square wave of a substance of concentration twenty units located for x in $[400, 600]$ at low tide. The background concentration was five units. After ten tidal cycles, the resulting profiles are shown in Figure 2.23. From this figure, two things can be seen. Firstly, the effect of the limited antidispersion is shown for the two runs of the second upwind differencing scheme. Secondly, the profile for the method-of-characteristics is severely attenuated and dispersed. The reason for this is that the interpolation procedure for redefining nodal values cannot handle the steep gradients of the leading edge found in the square wave.

This can be shown again if another test is performed with the first test canal in which convection only is modeled. The initial concentrations in the canal are background, and a constant lateral inflow load is applied uniformly along the length of the canal. The resulting profiles after 290 tidal cycles are shown in Figure 2.24. Once again, it is clear that the interpolation procedure cannot handle the sharp gradients of the distribution at the tidal entrance, and thus the method-of-characteristics solution technique was also discounted here. It can also be seen from Figure 2.24 that the method of second moments is the most successful method in conserving mass.

From Figure 2.23, and theoretically also, as explained in Section 2.6, the method of second moments convects the square wave very accurately. Added to this, the second upwind differencing method's limited antidispersion step is somewhat artificial and has a fairly complex form in junctions. To examine the effect of junctions, a second data set, Table 2.4 was developed for the second test canal, Figure 2.4. The results are shown in Figures 2.25 and 2.26. The

results show that the junction in the second upwind differencing model is causing a change in the gradients of the profile at that point.

Taking all the above factors into account (Table 2.5), it was decided that the method of second moments, because of its extreme accuracy in modeling the square wave, its superior ability to conserve mass, its intuitive relations to physical properties of the distribution, its ease of computation, and its relative economy, was ideally suited for an extension to a three-dimensional mass-transport model of a coastal finger canal network.

2.8 Effect of Varying Model Parameters on One-Dimensional Mass Transport

In the previous sections, a one-dimensional mass-transport model has been presented. After an extensive investigation of some of the numerical solution techniques available, it was decided that the method of second moments gave the most accurate results, was stable, convergent, transportive, and was also fairly economical to run.

It has been pointed out in the introductory chapter that the physical phenomena associated with mass transport in a coastal finger canal network are fully three-dimensional processes under the influence of wind, salinity gradients, tides, secondary currents, and lateral inflows. Their features have been incorporated into a three-dimensional model and the results generated using the numerical scheme selected in this chapter.

However, a study of the variability of the one-dimensional model's parameters is useful here because the effects will be similar in a three-dimensional model, the only difference being the actions

of all the other effects modeled. These may be studied independently using the latter model. The variation of these parameters, then, will give a qualitative guide to design engineer as to the relative effects of design elements. Once a canal network is designed, its quantitative functioning can be evaluated using the three-dimensional model. All the variability runs unless otherwise stated used the first test canal network (Figure 2.3) and varied the standard data set (Table 2.3).

The parameters may be divided into two groups called non-controllable and controllable parameters. The first category includes the tidal amplitude, and the decay coefficient, τ , associated with the flood tide, tidal entrance boundary condition. From Figure 2.27, it can be seen that the decay coefficient, τ , has a surprisingly small effect on the equilibrium concentration profile in the canal over the range of half a tidal period. This means that the inaccuracies inherent in the selection of such a flood tide boundary condition do not have a significant effect of the mass transport in the canal network. On the other hand, the results from varying the tidal amplitude, a (Figure 2.28), show a much more dramatic effect as would be expected from a simple volumetric tidal prism analysis. Areas with low tidal ranges, and thus automatically low energies, could expect severe pollution problems at the dead-ends of canal systems, unless either suitable flow-through systems can be designed, or other sources of energy, such as the wind, can be utilized to improve flushing.

The second category, called the controllable parameters, includes the geometric parameters of length, width, mean tidal depth, and inverse side slope, as well as the lateral inflow rate and its

concentration, Nikuradse's equivalent sand roughness, and the dimensionless dispersion coefficient. The geometric parameters, with the exception of the mean tidal depth, give results that would appear to be intuitively obvious. The effect of increasing the length of the canal, L , was simply to linearly increase the concentration at the dead-end (Figures 2.29 and 2.30), whereas the effect of increase of the bottom width, b (Figure 2.31), or the inverse side slope, s (Figure 2.32), for constant lateral inflow and concentration, was to proportionally decrease the equilibrium profile as a greater volume of water is presented to dilute the inflow. Conversely, the effects of increasing the lateral inflow, q_I , while holding its concentration constant (Figure 2.33) or holding the inflow rate constant and increasing its concentration, c_I (Figure 2.34), for fixed canal geometry, proportionally increased the resulting equilibrium profile.

The effect of increasing the mean tidal depth, d_0 , has a different effect (Figure 2.35). The other geometric parameters merely increased the size of the tidal prism and thus the velocity, for a fixed mean depth. The variation in the mean tidal depth alters the velocity of the flow; however, it also alters the dispersion coefficient, and the two effects partially cancel. From Figure 2.35 it can be seen that for increasing depth, the resulting equilibrium concentration profile decreases slowly. This result, however, is somewhat misleading because of some of the other physical phenomena not modeled. It is usually concluded for many reasons, such as low flows near the bed if the actually vertical velocity profile is considered, the depth of penetration of light to provide photosynthesis, the effect of re-aeration over a deep water column, and so on, that deep canals are

not desirable as anoxic conditions are known to commonly occur. Thus, this result should not be included in an analysis of proposed canal design except to provide an estimate of the equilibrium profile, but rather the effect of other forcing functions should be studied using the three-dimensional model.

The effects of varying Nikuradse's equivalent sand roughness, k (Figure 2.36), and the dimensionless dispersion coefficient, K (Figure 2.37), have similar effects, as would be expected through their association in the longitudinal dispersion coefficient. Equilibrium concentration profiles increase with decreasing values of these parameters, indicating the fact that rougher canals and bends provide more shear and turbulent eddies that aid the mixing process.

It should be noted that as the magnitudes of the resulting equilibrium profile increase, the time to achieve equilibrium also increases. This could have a potentially serious effect on canal networks which are subject to high loads from time to time. From a statistical point of view, looking at return period relationships, an efficient canal would be one which flushes out a design percentage of the pollutant before the next load was expected. In an inefficient system, a certain amount of the pollutant above the design amount considered acceptable would be retained when the next load arrived. The concentrations would then build up in the system until an equilibrium condition is reached, possibly much above that considered environmentally acceptable by design standards.

The final test used the second model canal network (Figure 2.4) in which a main 1,000 ft canal had a branch at varying locations along its length. The length of the branch was 500 ft. The resulting

concentration profiles at low tide and high tide for location of the branch canal at $x = 200, 400, 500, 600$ and 800 ft are shown in Figures 2.38 and 2.39 respectively. The results indicate that as the branch canal is placed nearer to the dead-end, the resulting concentration profile in the main canal is reduced as the effective excursion of the tidal prism is increased. However, the converse is true for the branch canal and the problem becomes a trade off dependent on acceptable design criteria.

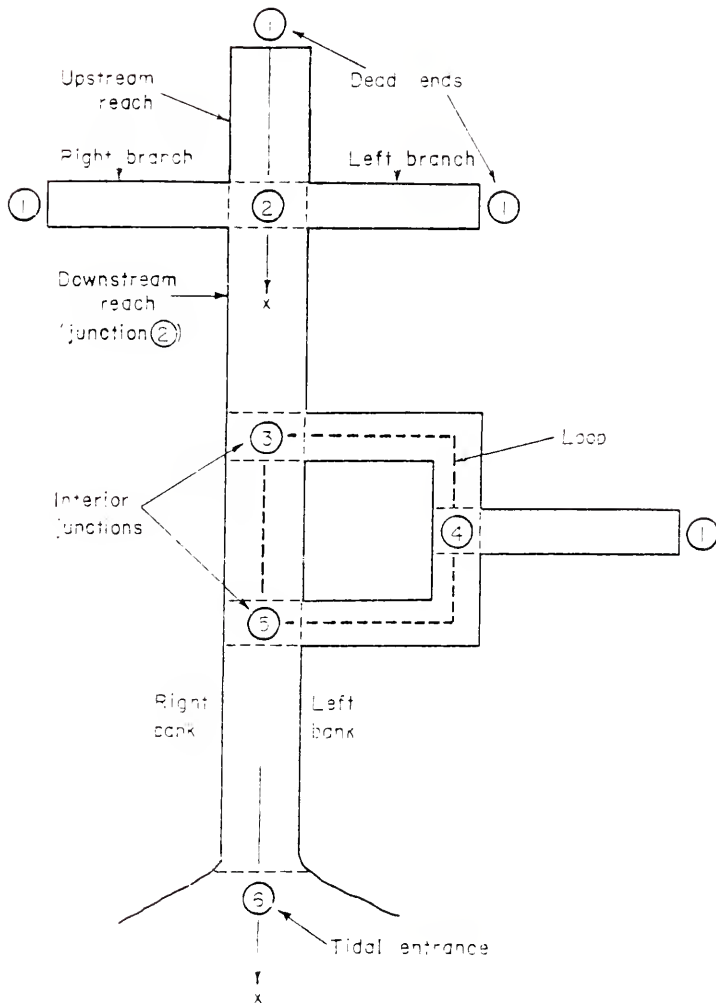


Figure 2.1 - Definition Drawing of Canal Network.

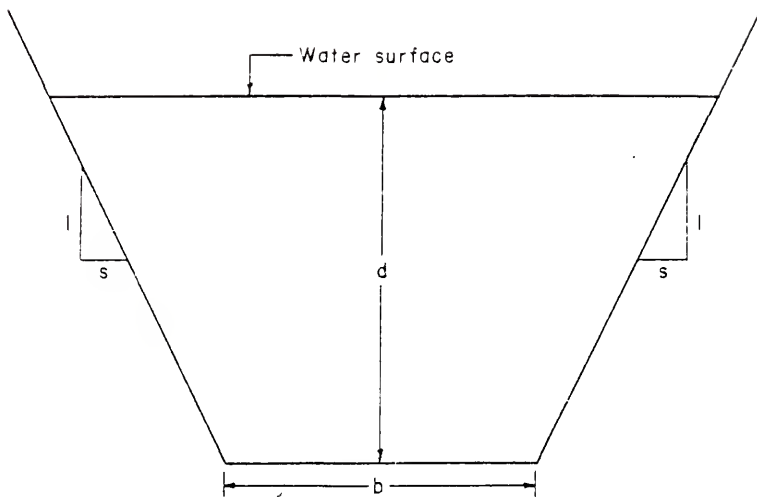


Figure 2.2 - Schematic Drawing of Trapezoidal Cross-Section.

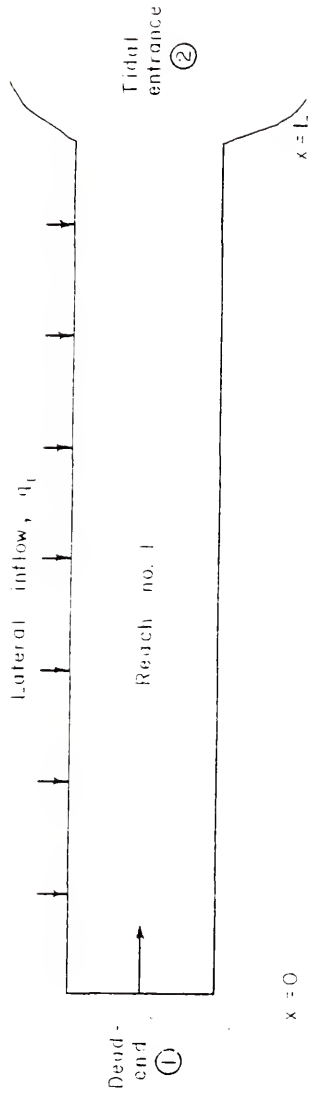


Figure 2.3 - First Test Canal Network.

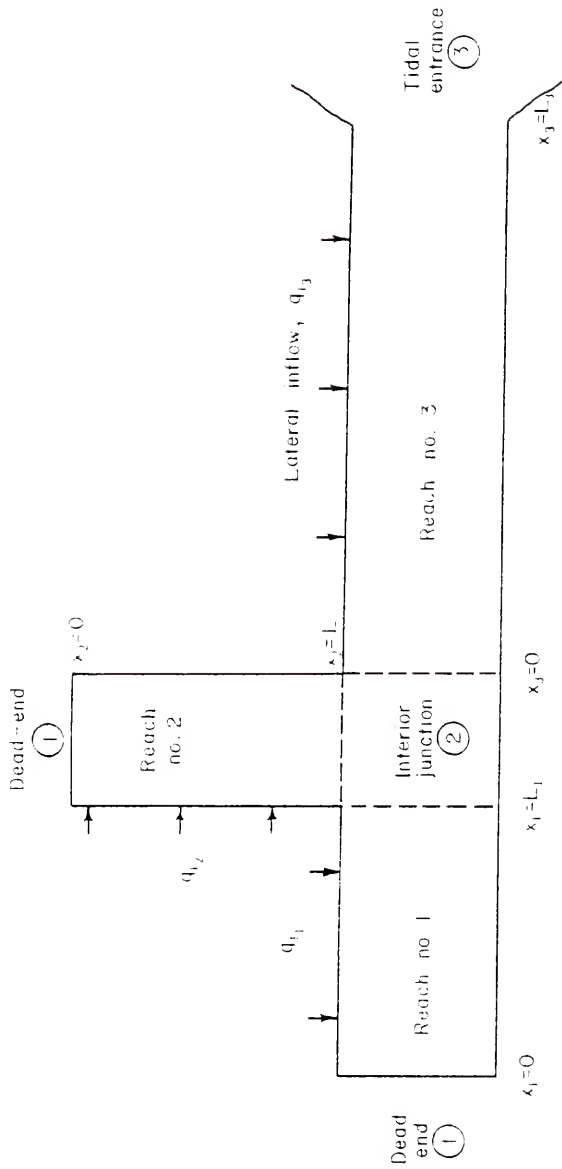


Figure 2.4 - Second Test Canal Network.

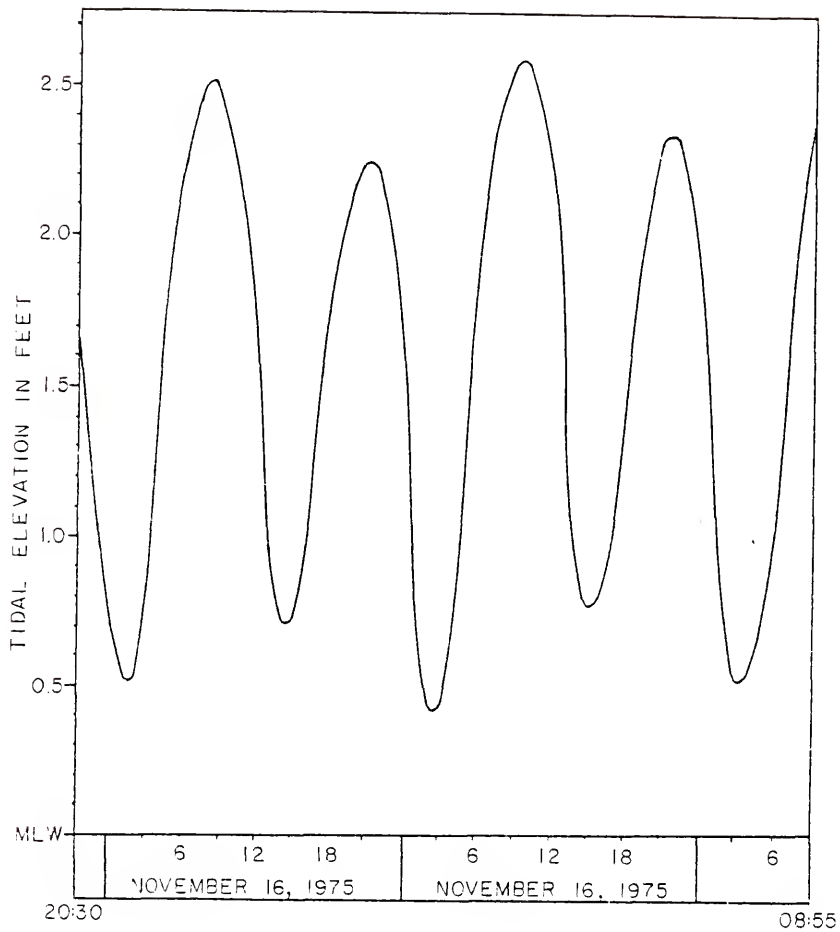


Figure 2.5 - Typical Atlantic Coast Tide Curve.

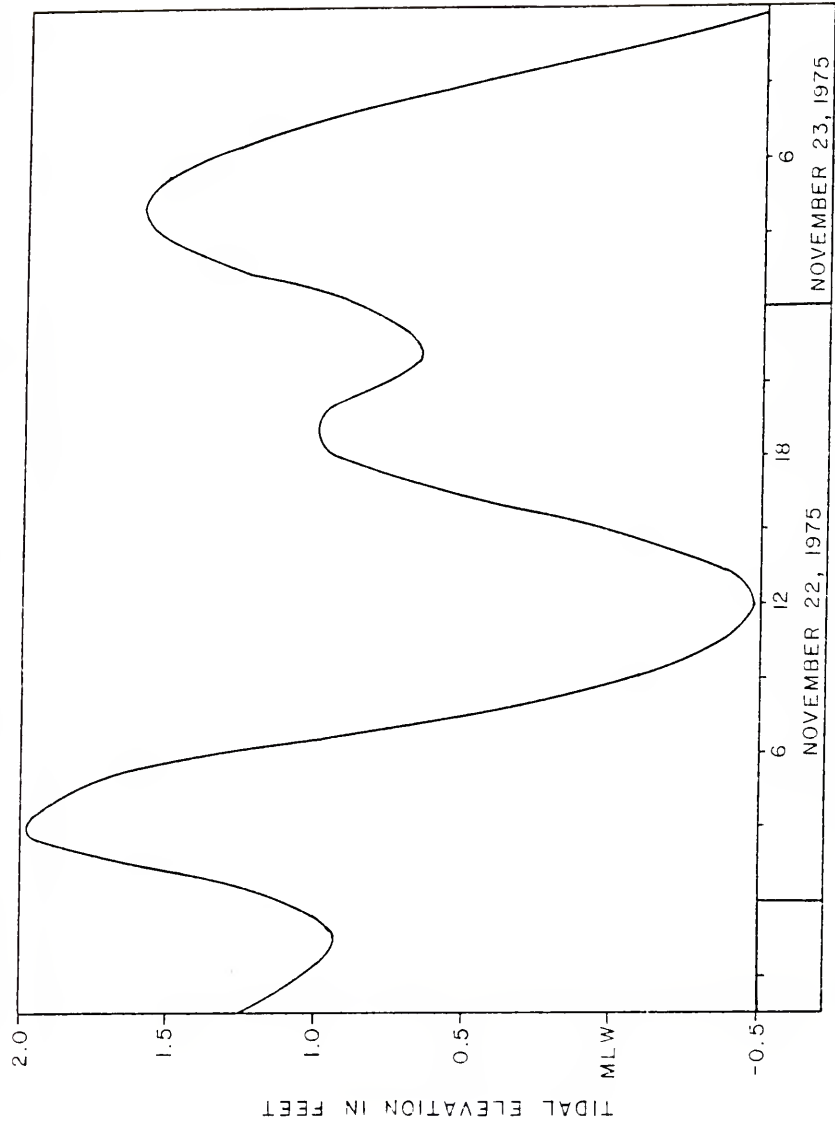


Figure 2.6 - Typical Gulf of Mexico Tide Curve.

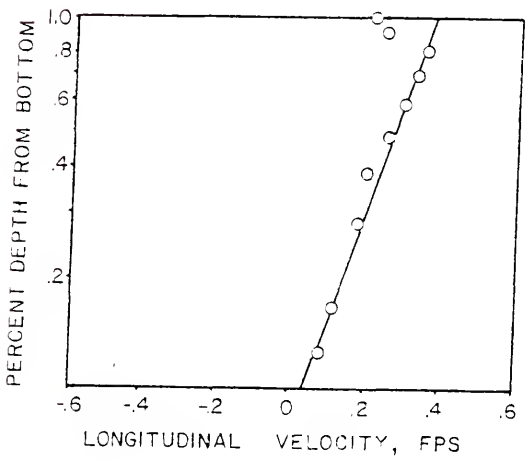
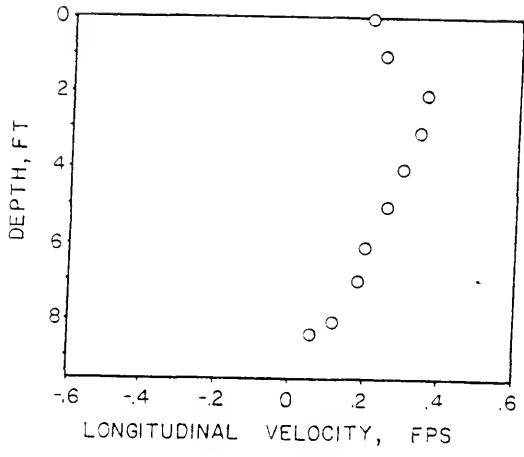


Figure 2.7 - Typical Logarithmic Velocity Profile.

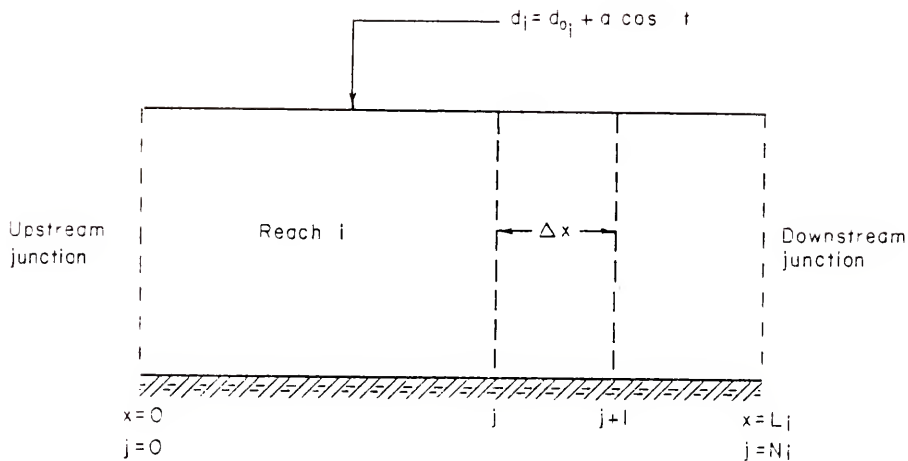


Figure 2.3 - Schematic Drawing of Horizontal Water Surface Assumption.

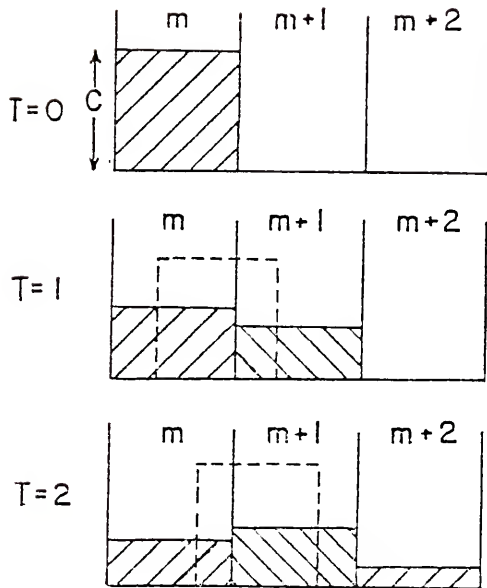


Figure 2.9 - Schematic Representation of Effect of Numerical Dispersion.

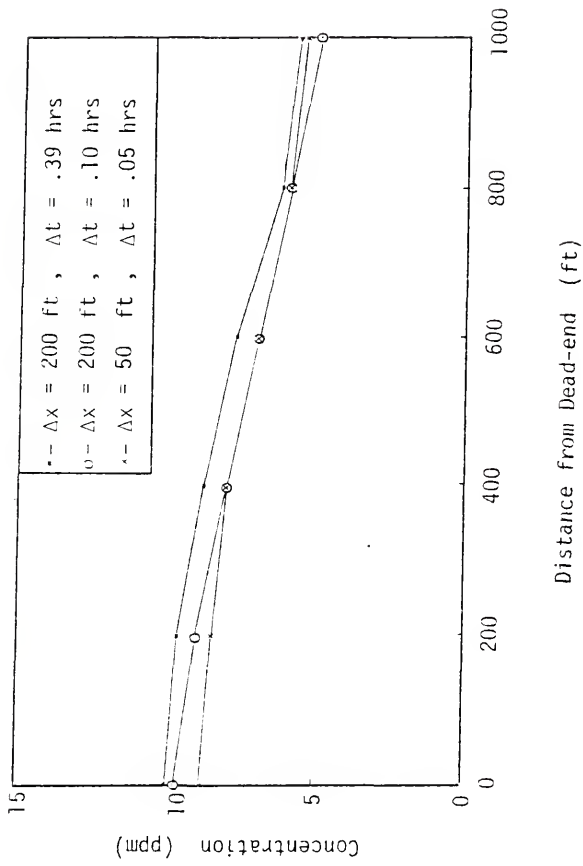


Figure 2.10 - Low Tide Concentration Profiles for Various Δx and Δt - Finite-Difference Method.

CHARACTERISTIC METHODS

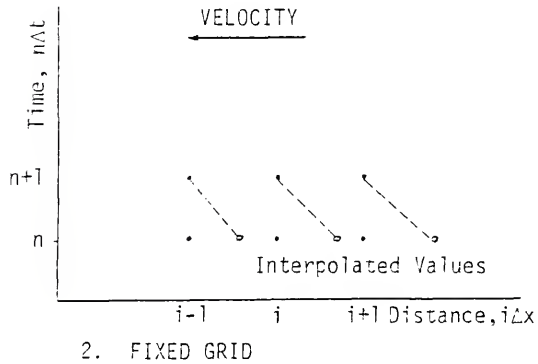
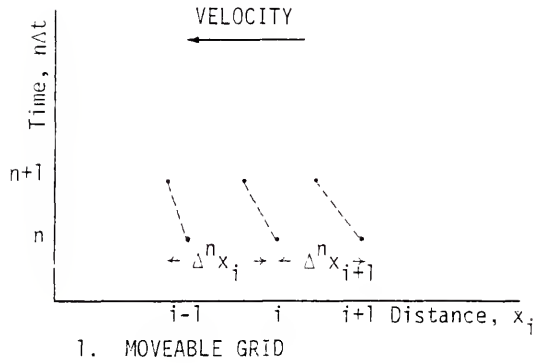


Figure 2.11 - Schematic Representation of Convective Steps of Method-of-Characteristics Methods.

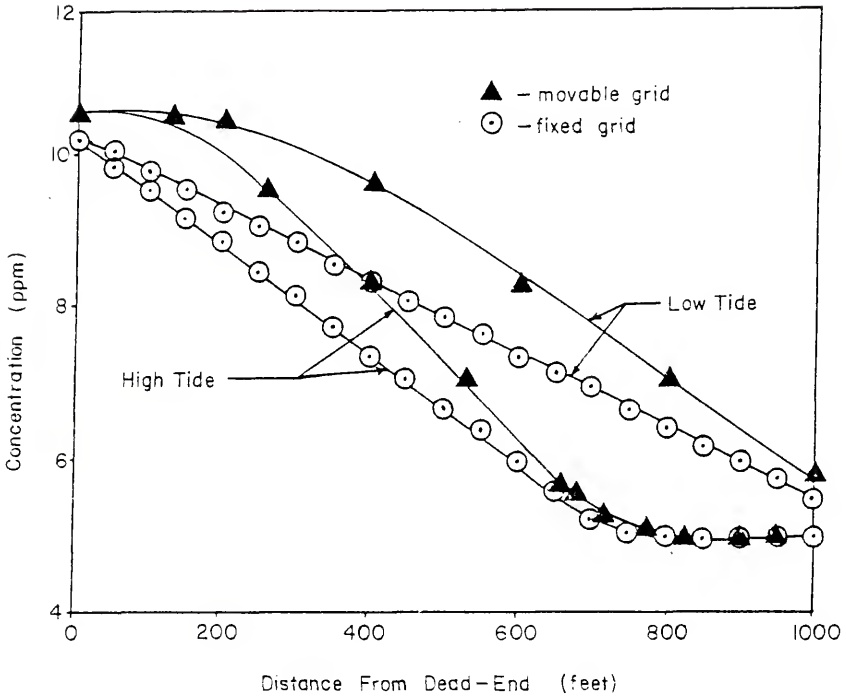


Figure 2.12 - Comparison of Concentration Profiles for Fixed Grids and Movable Grid Method-of-Characteristics.

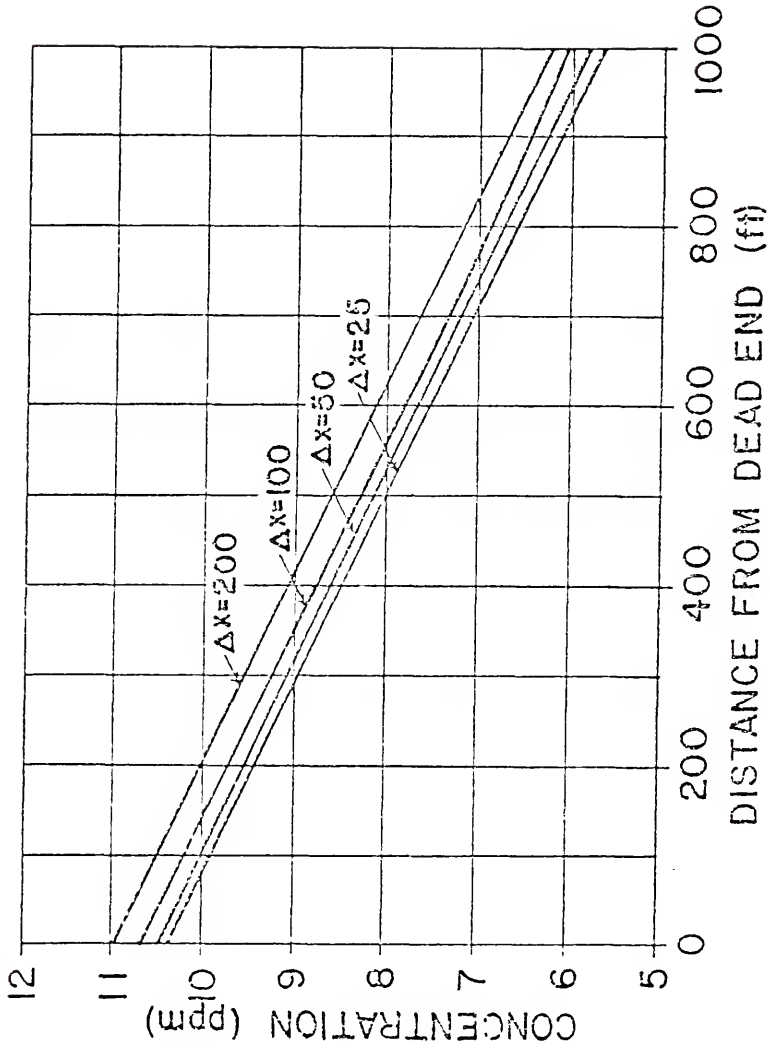


Figure 2.13 - Low Tide Concentration Profiles for Various Δx Fixed Grid Method-of-Characteristics.

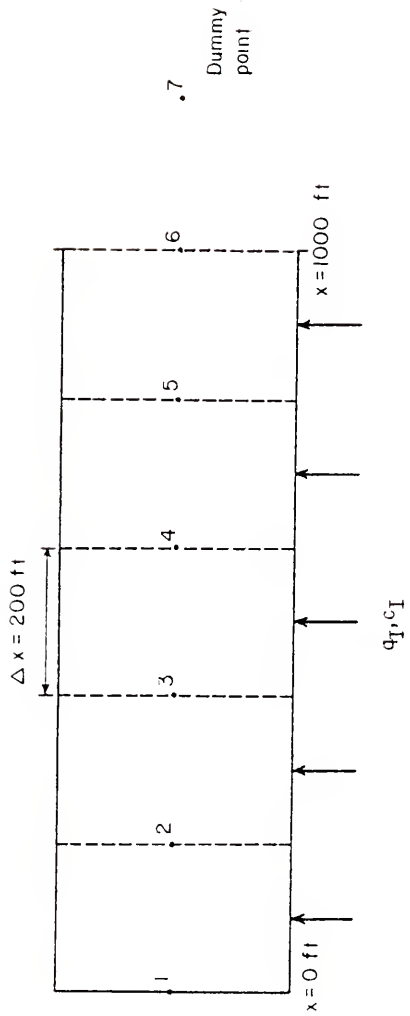


Figure 2.14 - Schematic Drawing of Hybrid Method Test Canal.

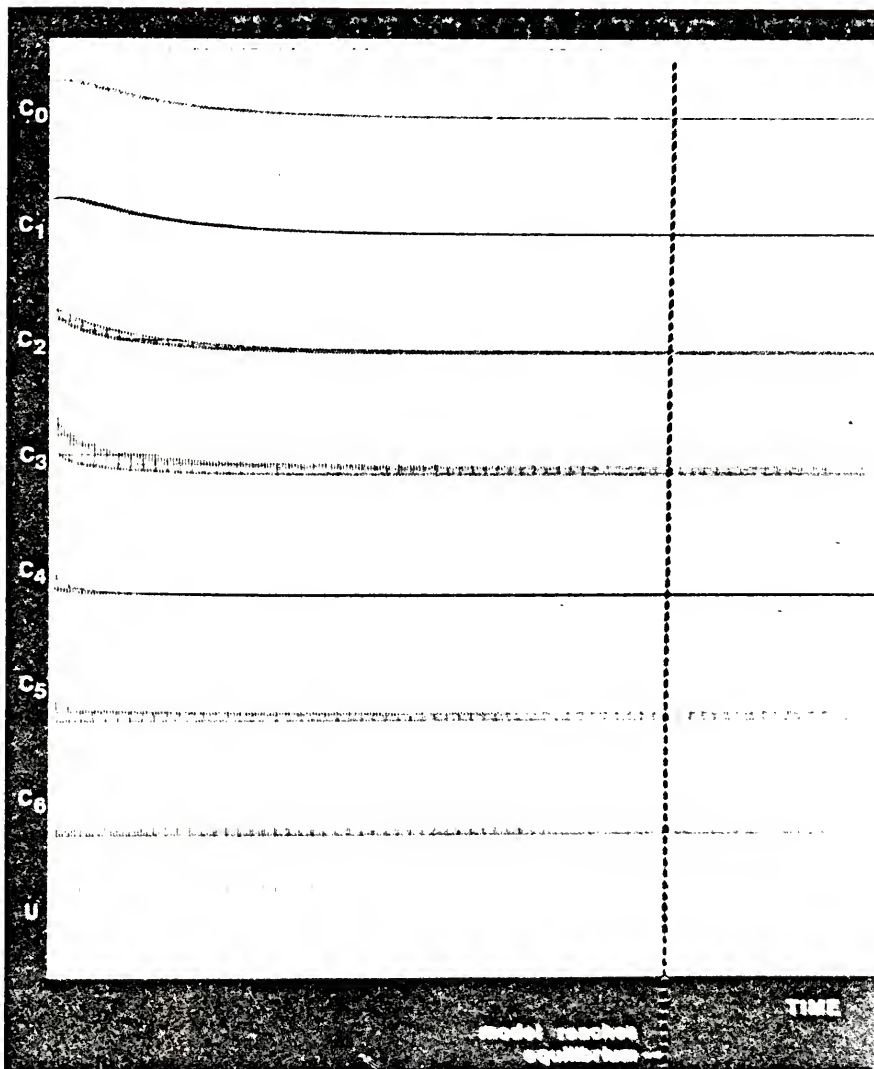


Figure 2.16 - Typical Analog Output.

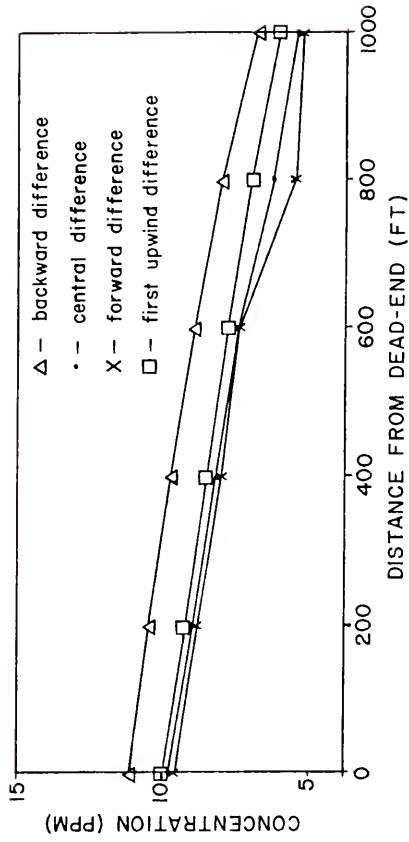


Figure 2.17 - Low Tide Concentration Profiles for Various Analog Methods.

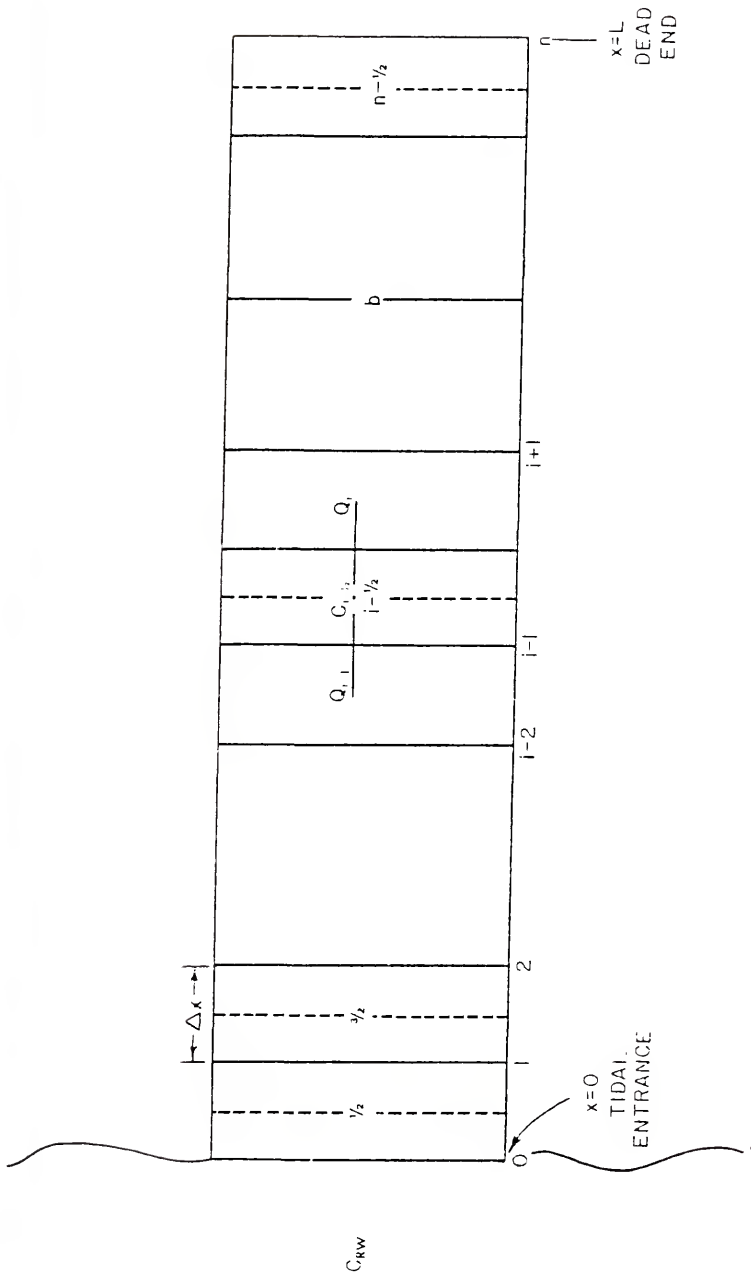


Figure 2.18 - Schematic Representation of Second Upwind Difference Method.

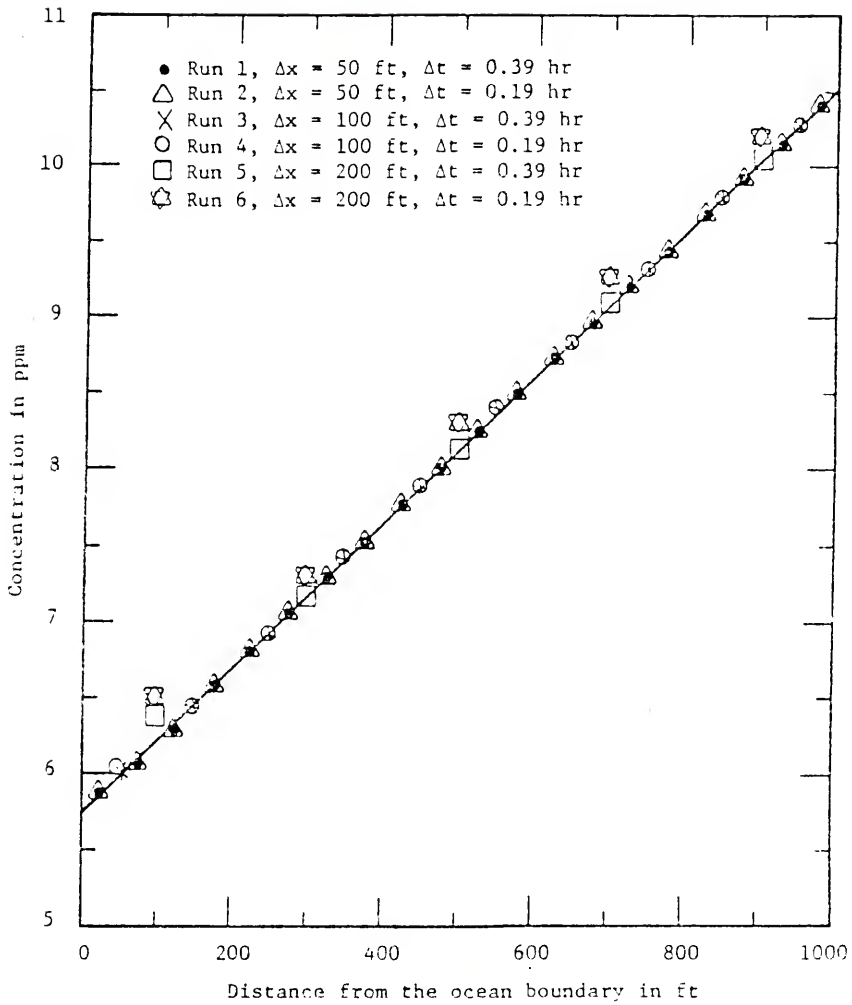


Figure 2.19 - Low Tide Concentration Profiles for Various Δx and Δt - Second Upwind Difference Method.

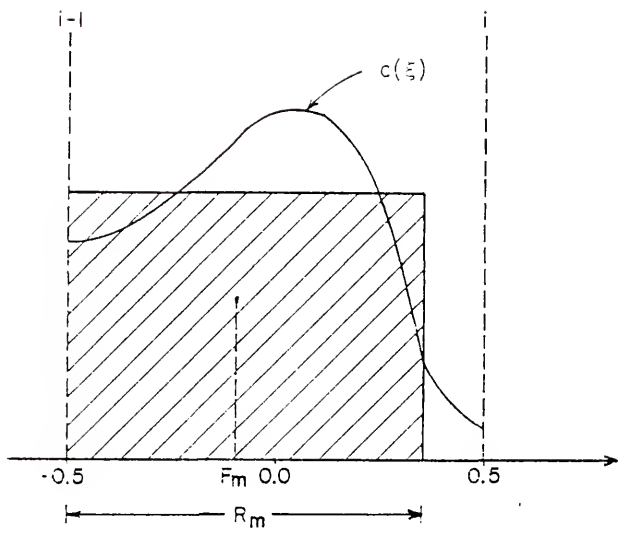


Figure 2.20 - Rectangular Distribution Approximation to Actual Distribution.

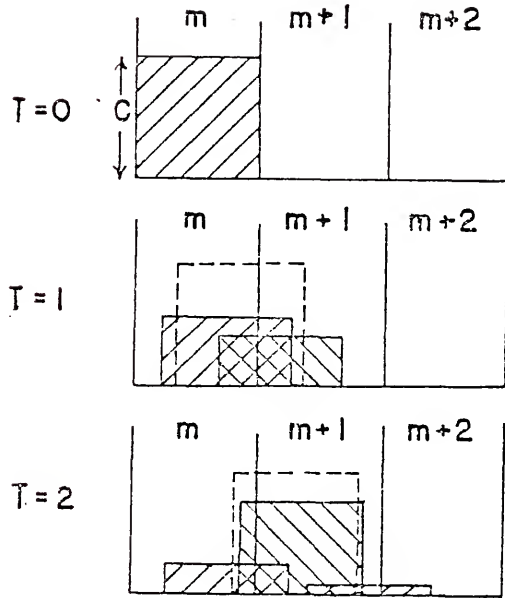


Figure 2.21 - Schematic Representation of Conservation of First Moment.

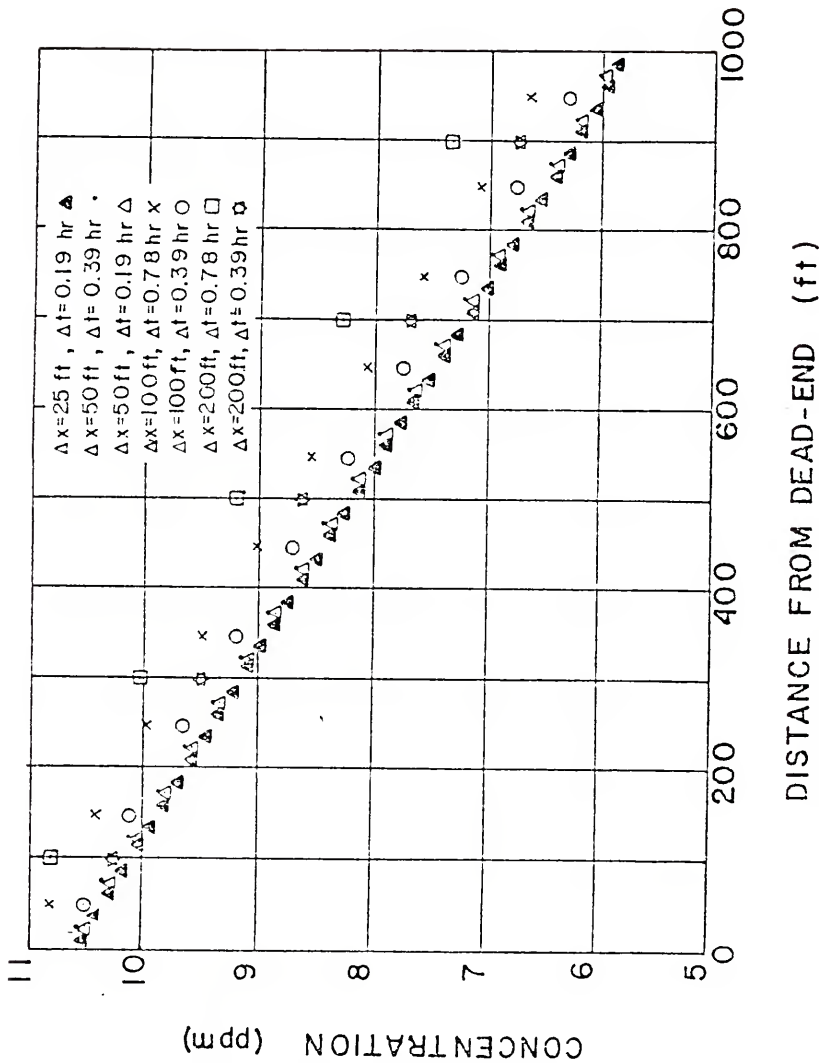


Figure 2.22 - Low Tide Concentration Profiles for Various Δx and Δt - Method of Second Moments.

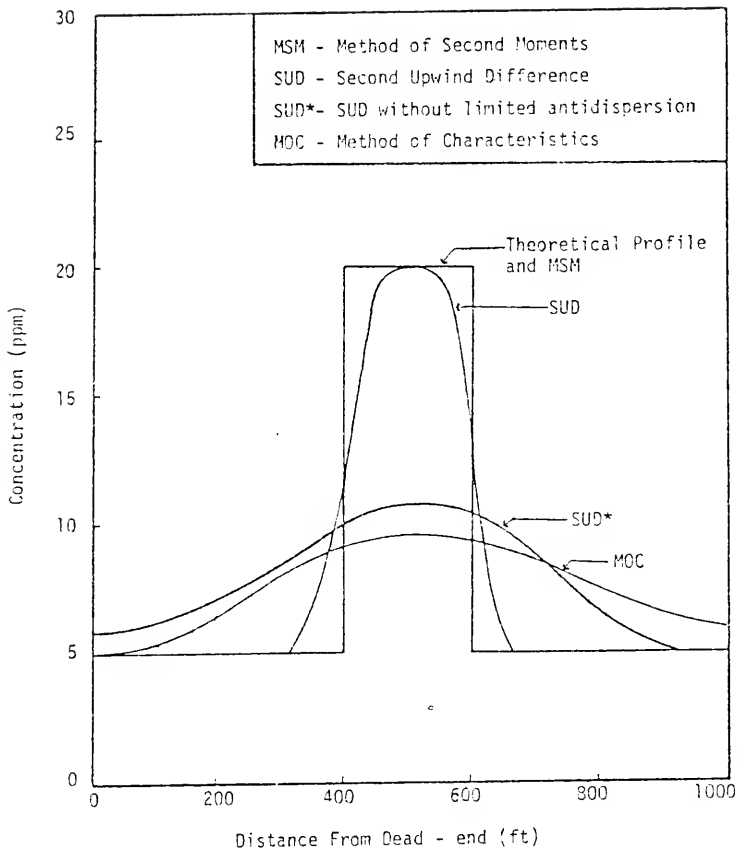


Figure 2.23 - Comparison of Techniques' Accuracy in Modeling Pure Convection.

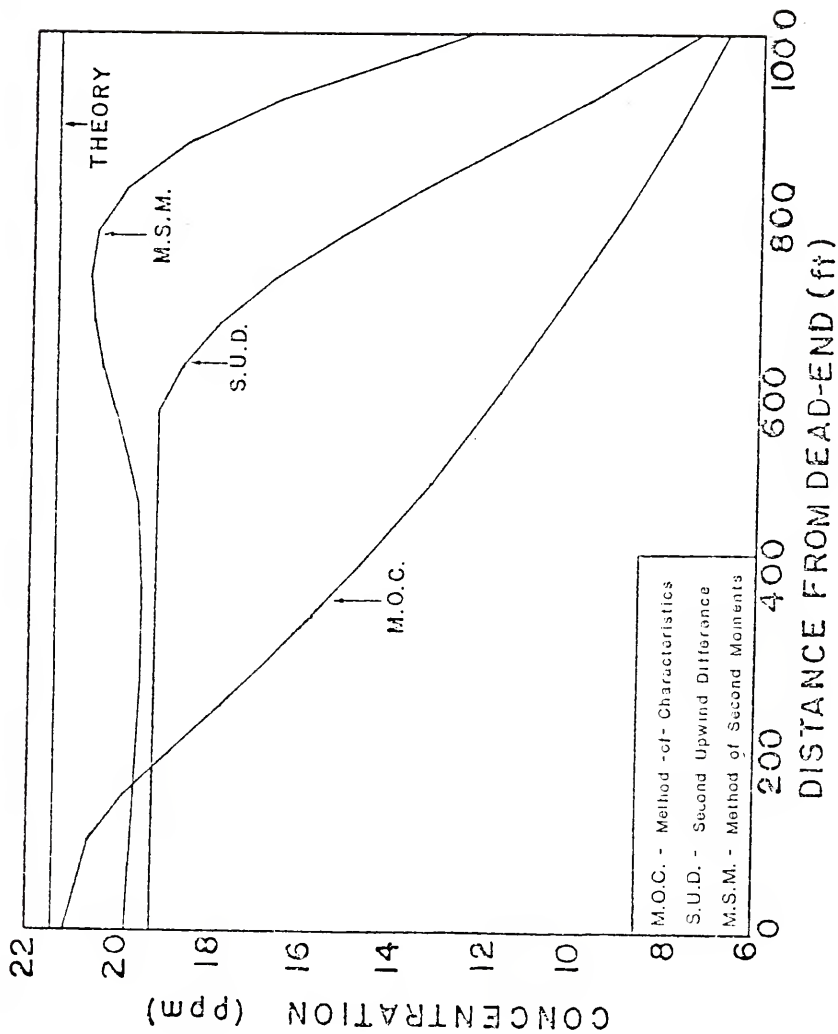


Figure 2-24 - Comparison of Techniques' Accuracy in Conserving Mass.

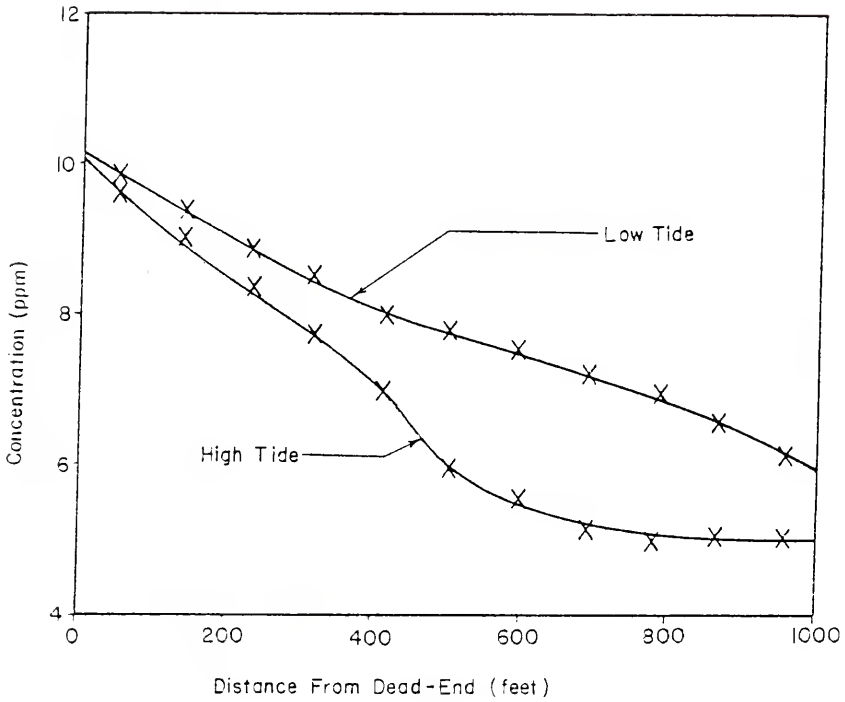


Figure 2.25 - Concentration Profiles for Second Test Canal Network - Second Upwind Difference Method.

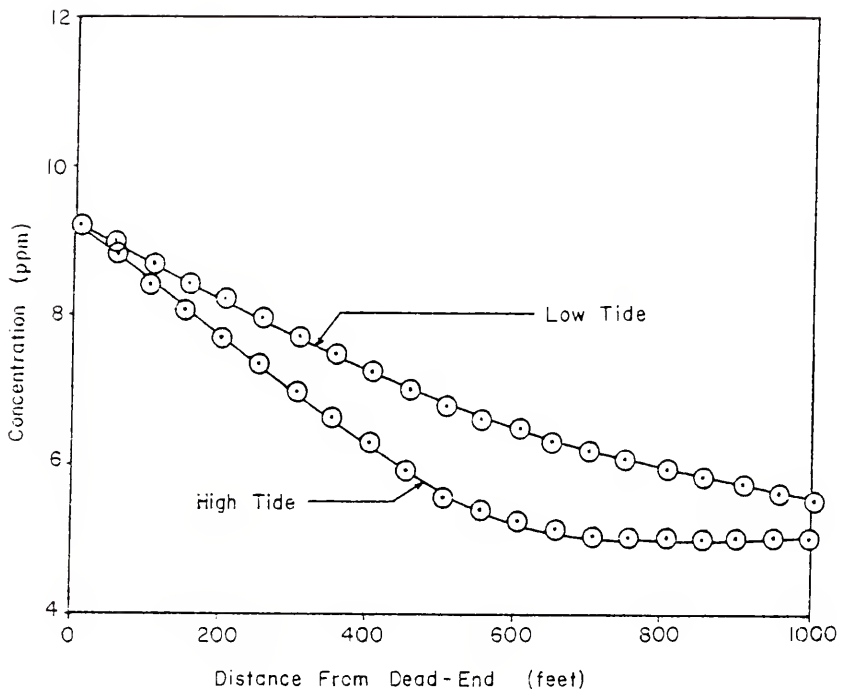


Figure 2.26 - Concentration Profiles for Second Test Canal Network - Method of Second Moments.

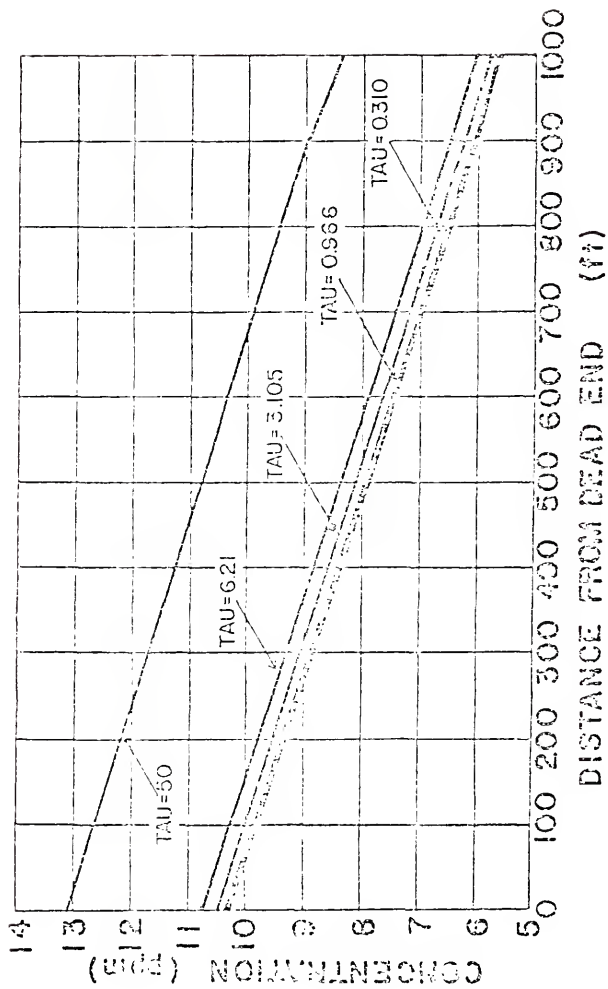


Figure 2.27 - Variability of Tidal Entrance Time Decay Coefficient, τ .

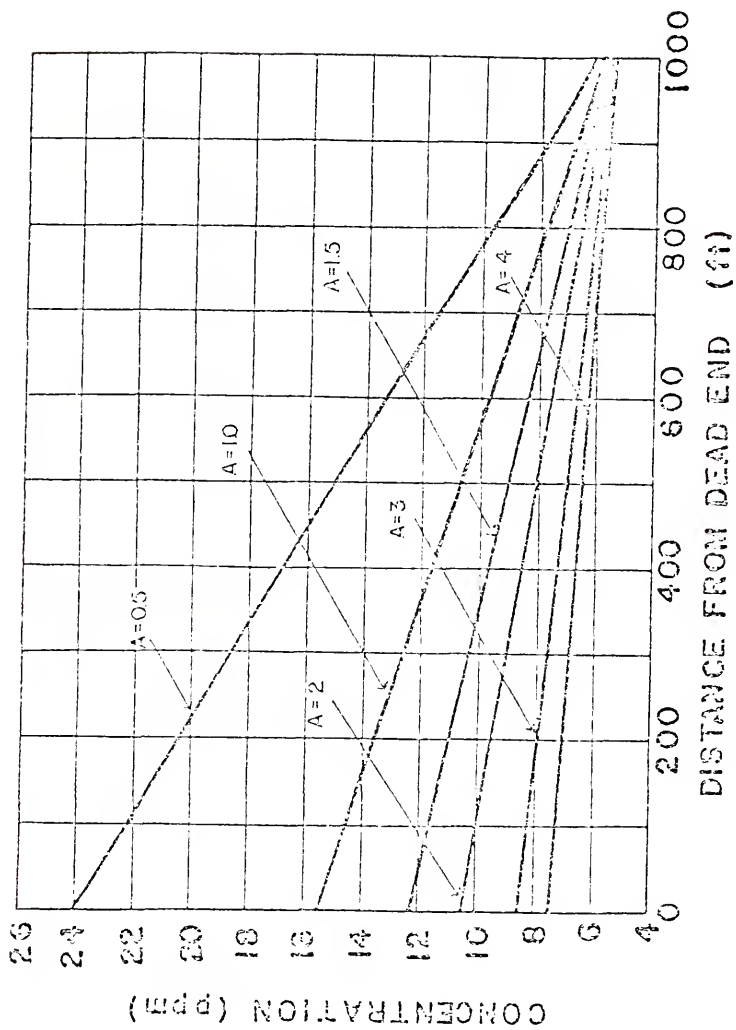


Figure 2.28 - Variability of Tidal Amplitude, a.

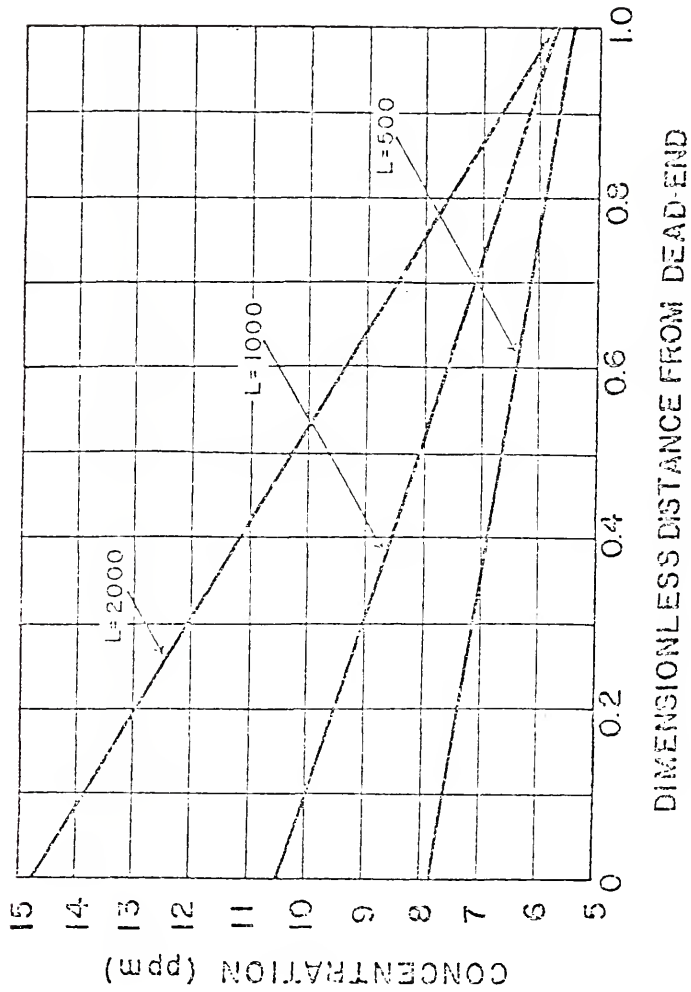


Figure 2.29 - Variability of Canal Length, L

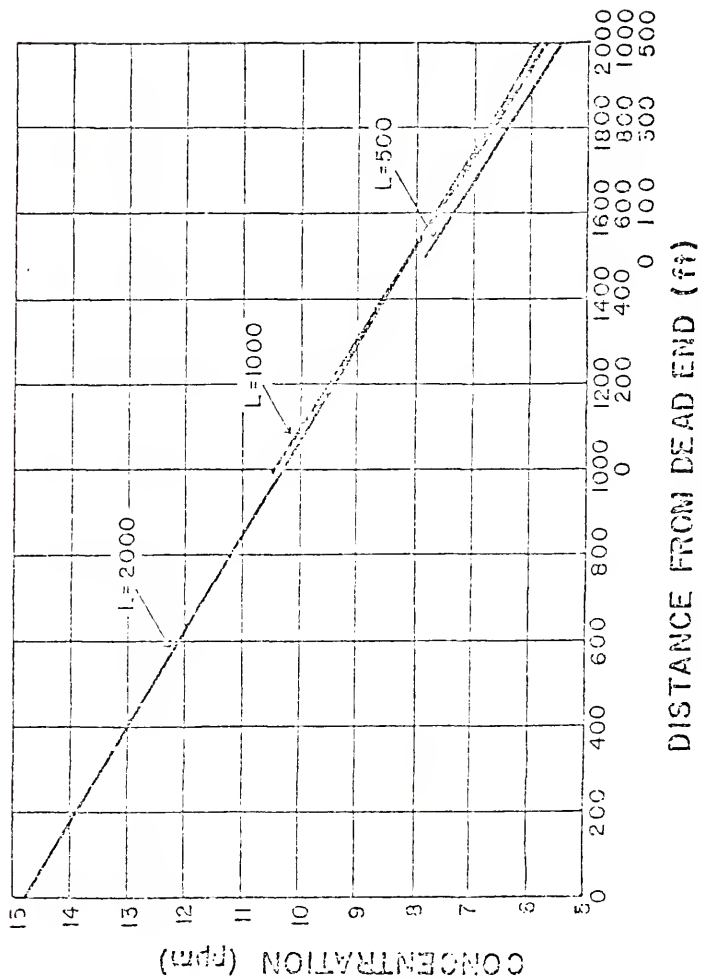


Figure 2.30 - Variability of Dimensionless Canal Length.

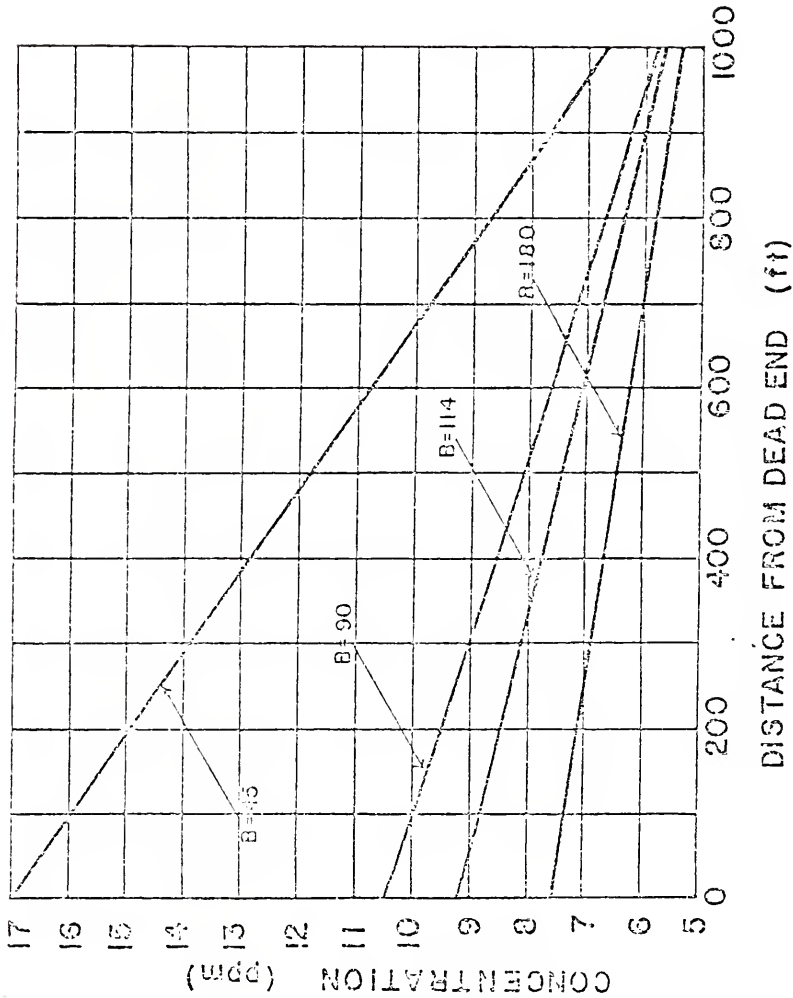


Figure 2.31 - Variability of Bottom Width, b.

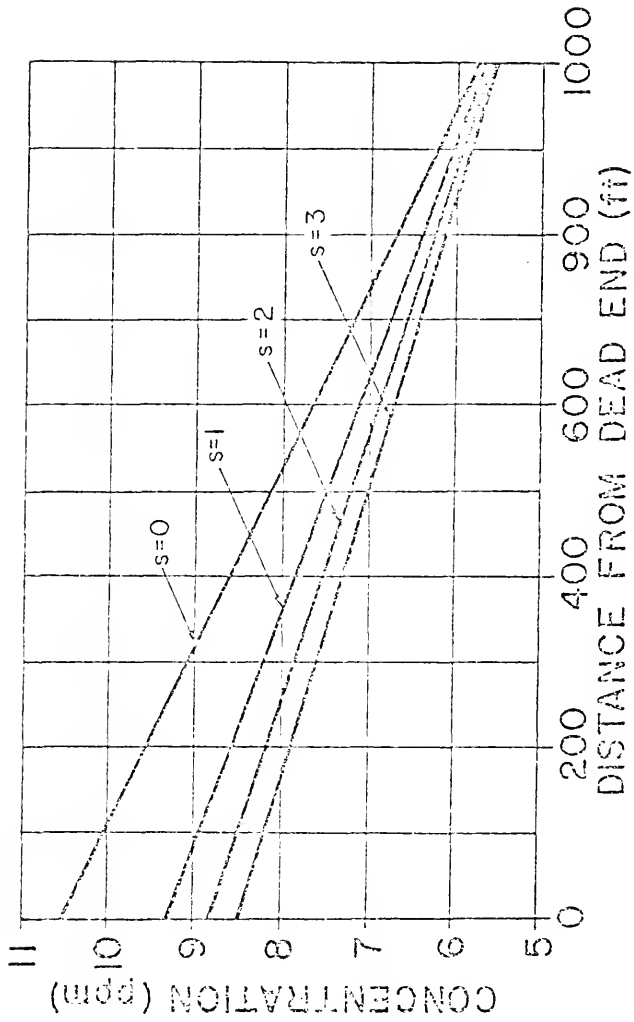


Figure 2.32 - Variability of Inverse Side Slope, s.

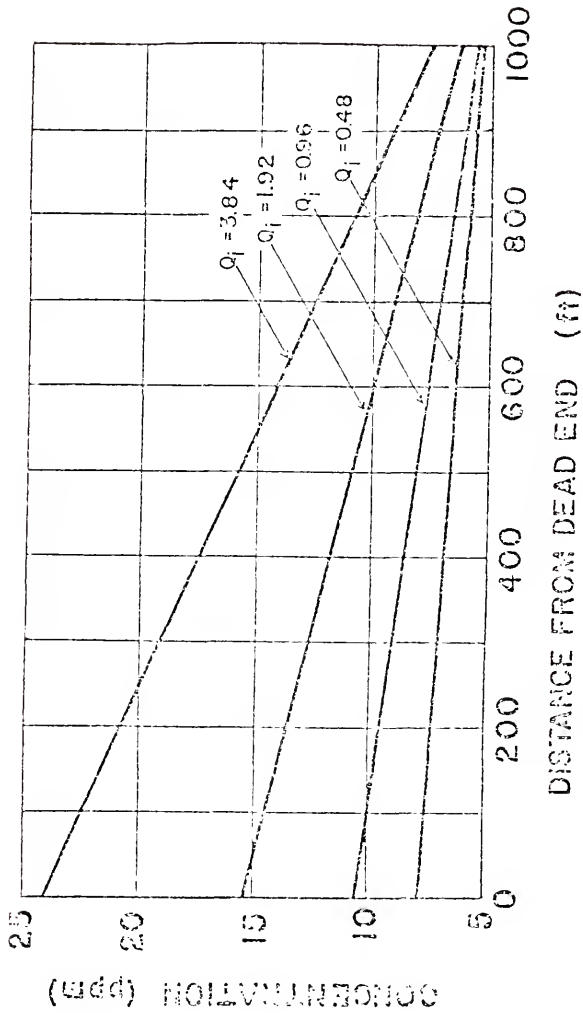


Figure 2.33 - Variability of Lateral Inflow Rate, q_i .

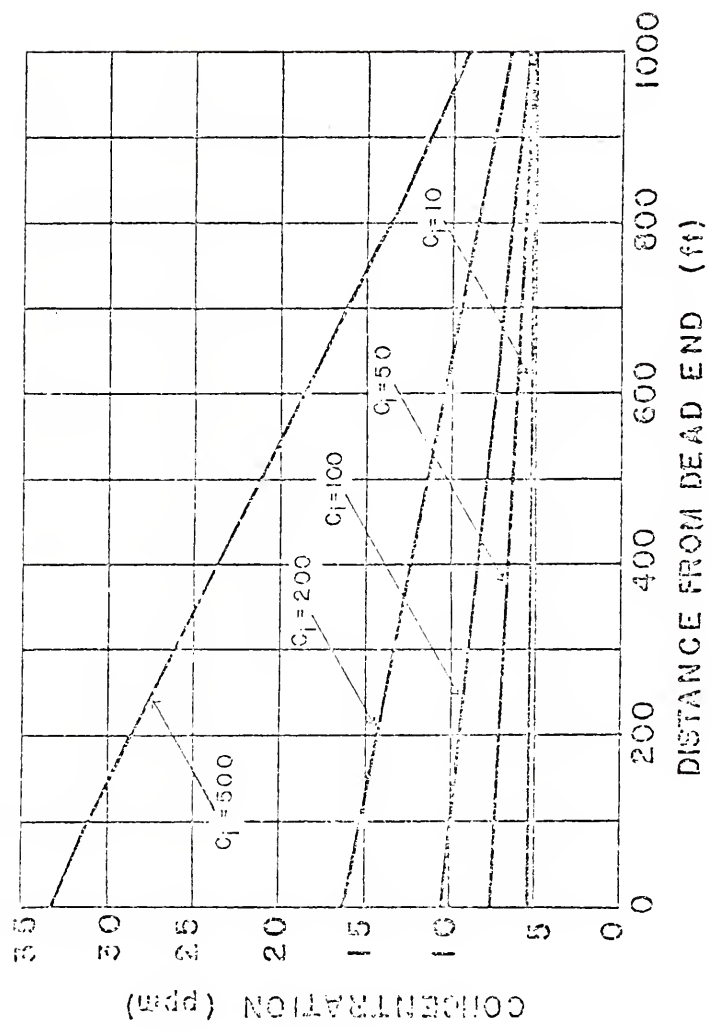


Figure 2.34 - Variability of Lateral Inflow Concentration, c_l .

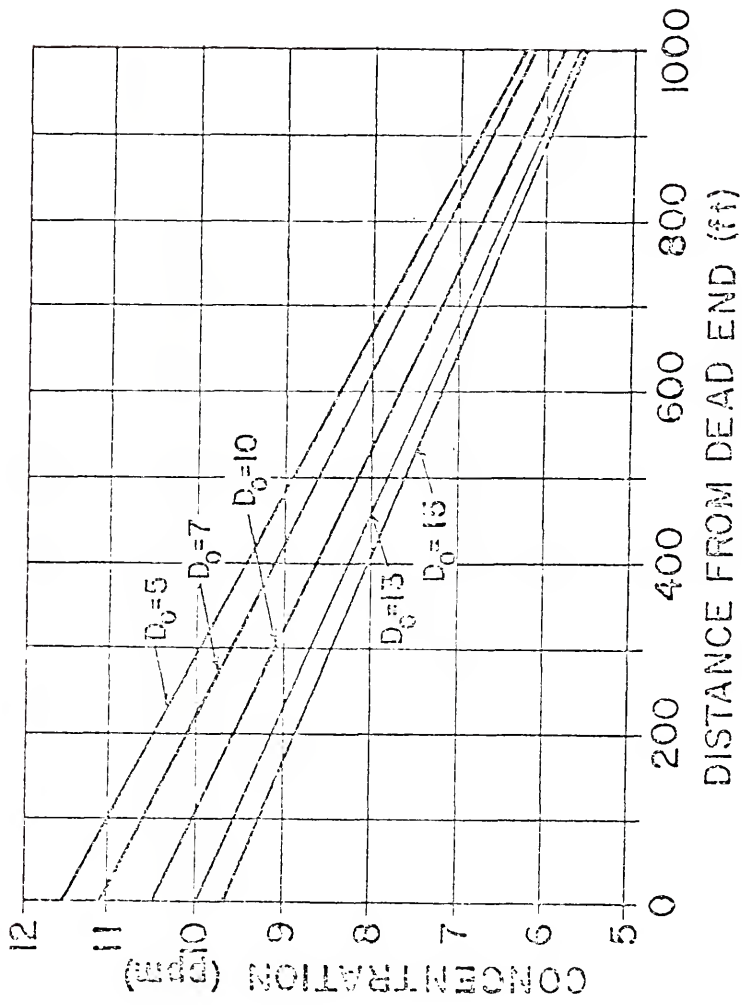


Figure 2.35 - Variability of Mean Tidal Depth, d_0 .

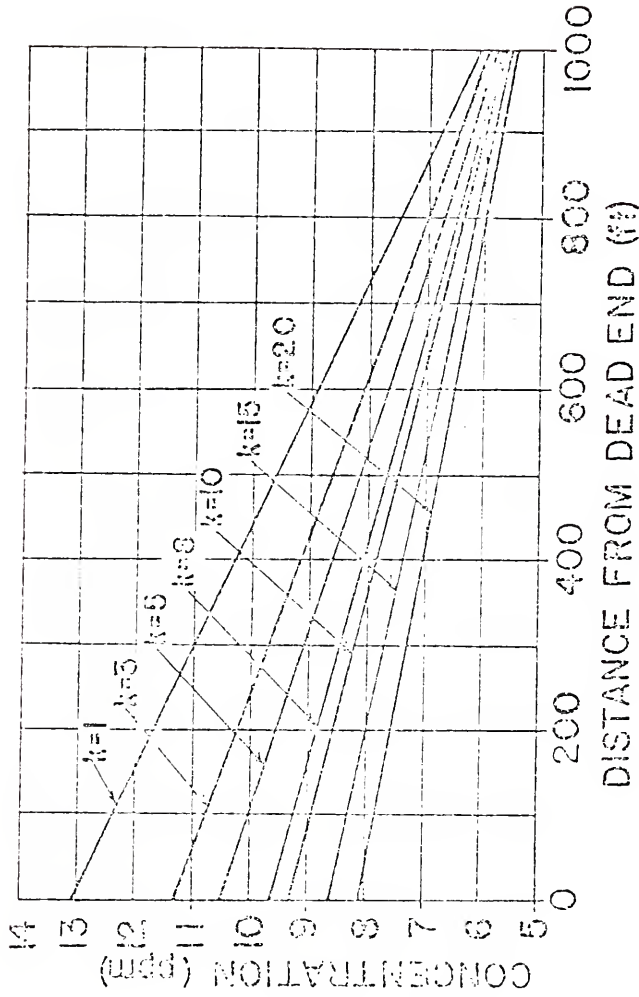


Figure 2.36 - Variability of Nikuradse's Equivalent Sand Roughness, k .

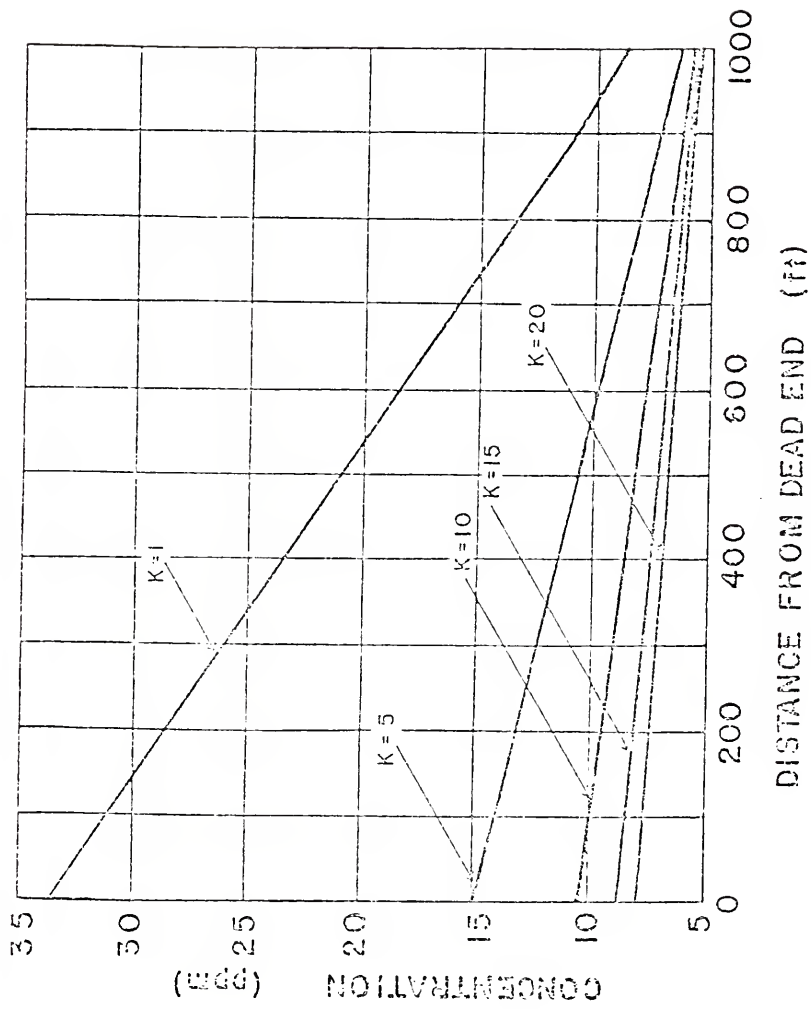


Figure 2.37 - Variability of Dimensionless Dispersion Coefficient, K.

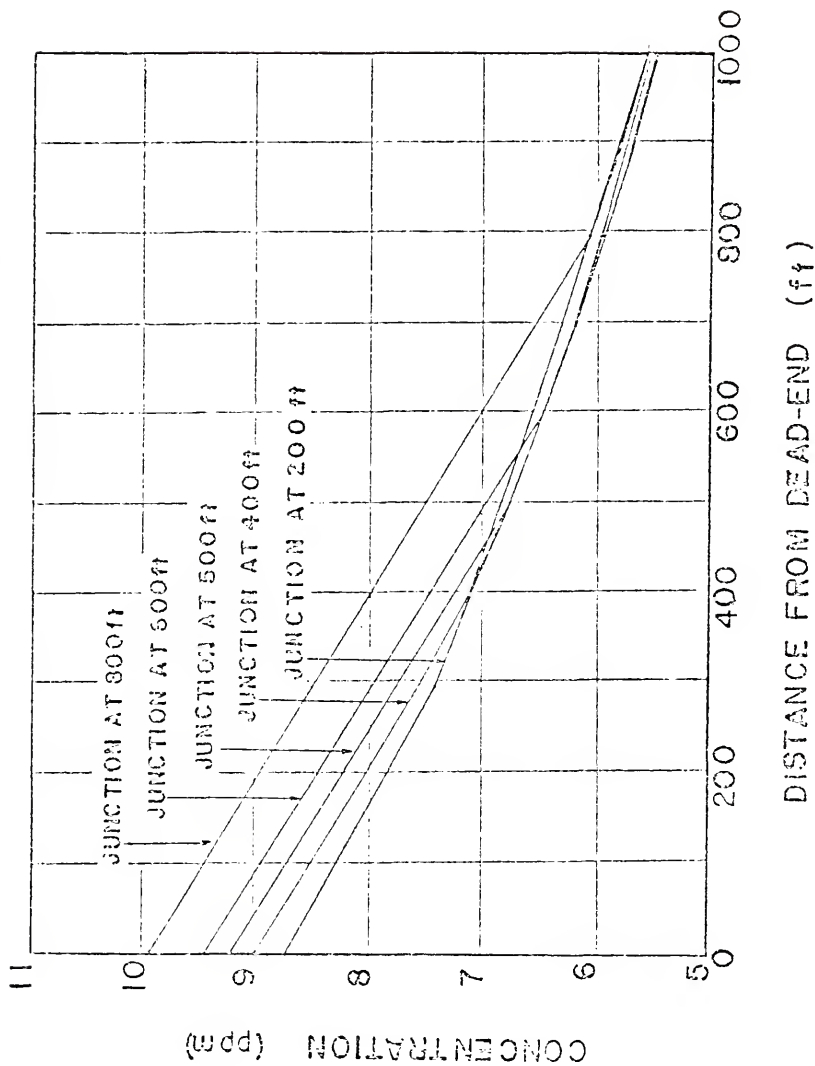


Figure 2.38 - Variability of Low Tide Concentration Profiles for Various Branch Canal Locations.

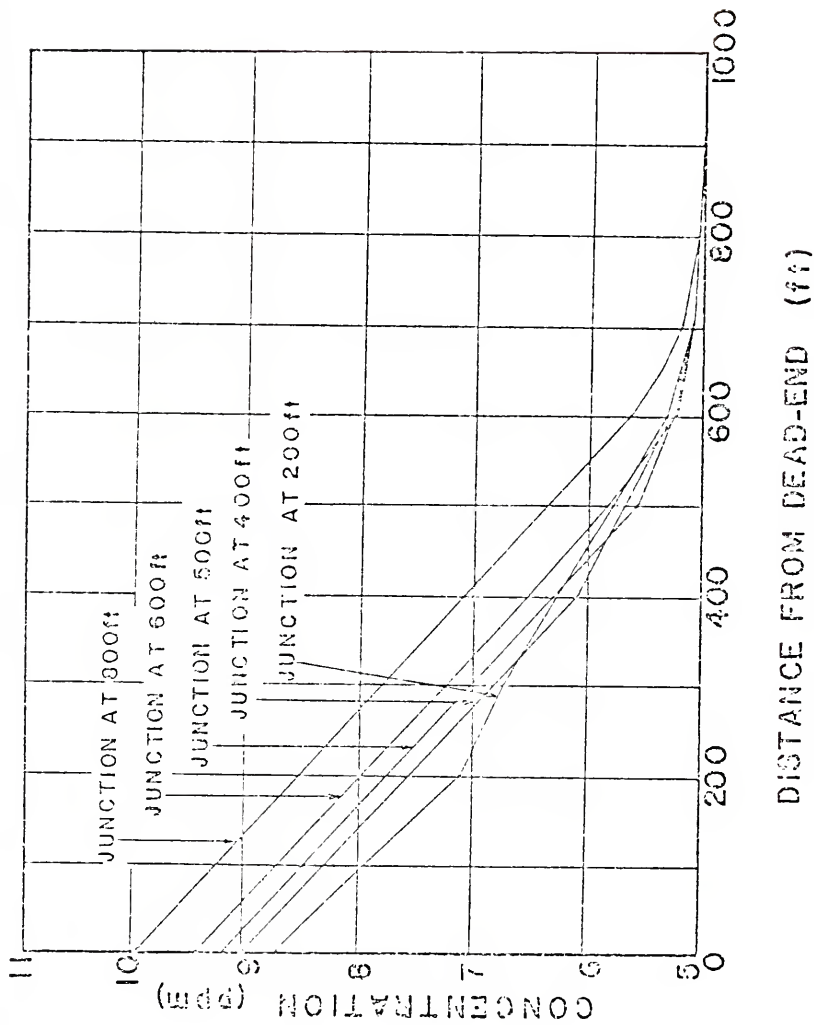


Figure 2.39 - Variability of High Tide Concentration Profiles for Various Branch Canal Locations.

Table 2.1 - Typical Measured Canal Parameters

PARAMETER	RANGE
Length, L	1,500-10,000 ft
Bottom width, b	50-100 ft
Mean tidal depth, d_0	5-12 ft
Inverse side slope, s	0-5
Tidal range, a: Atlantic	2-5 ft
Gulf of Mexico	2-3 ft
Tidal period, T	12.42 hrs
Nikuradse's equivalent sand roughness, k	1-20 ft
Maximum (in canal) longitudinal dispersion coefficient, E_x	0.5-5.0 ft ² /sec
Dimensionless dispersion coefficient, K	2-20 ft
Maximum water surface slope, S	10^{-5} - 10^{-6} ft

Table 2.2 Comparison Between Horizontal Water Surface Assumption and Harleman and Lee's Hydrodynamics Model

Fraction of tidal cycle, t/T	Deviation from time mean depth ft HWSA'	Deviation from time mean depth ft HLM ²	Water surface slope at x , $\partial d/\partial x(x)$ HLM ²
(a) At $x = 500$ ft			
0	-2.00000	-2.00141	-1.41×10^{-6}
0.25	-0.00001	-0.00265	-2.64×10^{-6}
0.50	2.00000	2.00092	9.20×10^{-7}
0.75	0.00548	0.00896	3.48×10^{-6}
(b) At $x = 4,500$ ft			
0	-2.00472	-2.00551	-7.9×10^{-7}
0.25	-0.00729	-0.00800	-7.1×10^{-7}
0.50	2.00309	2.00360	5.1×10^{-7}
0.75	0.01557	0.01675	1.18×10^{-7}
(c) At $x = 9,500$ ft			
0	-2.00693	-2.00709	-1.6×10^{-7}
0.25	-0.00867	-0.00866	1.0×10^{-8}
0.50	2.00453	2.00463	1.0×10^{-7}
0.75	0.01829	0.01837	8.0×10^{-8}

Note: 1. HWSA = horizontal water surface assumption.
 2. HLM = Harleman and Lee's model [1969].

Table 2.3 - Standard Data Set for First Test Canal

PARAMETER	VALUE
Length, L	1000 ft
Bottom width, b	90 ft
Mean tidal depth, d_0	10 ft
Inverse side slope, s	0 ft
Tidal range, a	2 ft
Tidal period, T	12.42 hrs
Nikuradse's equivalent sand roughness, k	5 ft
Dimensionless dispersion coefficient, K	10
Lateral inflow, q_I	0.04 cu ft/hr/ft
Concentration of lateral inflow, c_I	100 ppm
Background concentration, c_{RW}	5 ppm

Table 2.4 - Standard Data Set for Second Test Canal.

PARAMETER	VALUE
Length of Reach No. 1, L_1	450 ft
Length of Reach No. 2, L_2	500 ft
Length of Reach No. 3, L_3	450 ft
Length of Junction, Δx_j	100 ft
Length of Junction, Δy_j	90 ft
All other parameters are as for Table 3.1.	

Table 2.5 - Comparison of Numerical Techniques.

TECHNIQUE	ADVANTAGES	DISADVANTAGES
Finite-element, finite-difference	Ease of formulation, can be conservative.	Suffers from excessive numerical dispersion unless economic choices for Δx and Δt are made.
Method-of-Characteristics	Ease of formulation; very economic.	Suffers from inaccuracies in the interpolation between nodal values; nonconservative.
Hybrid	Ease of formulation; speed of solution; ease of variability studies of nongeometric parameters.	Ties up too much hardware for canal systems with more than 20 nodes; nonconservative.
Second upwind differencing with flux-corrected transport	Accurate; reasonably economic; conservative; transportive.	Complex formulation; artificial physical form.
Method of second moments	Very accurate; reasonably economic; intuitive physical meaning; conservative; transportive.	Suffers some from round-off errors in square root term.

CHAPTER 3
FIELD MEASUREMENTS

3.1 Introduction and Site Descriptions

During the course of this study, a continuous program of hydrodynamic surveys was undertaken on a number of tidal canal networks around the State of Florida. The extent of these data is covered in more detail in a parallel report by Morris [1978]. The aim of this section is to describe some of the data which were used to formulate the numerical model presented in the following chapters.

Two sites will be covered here for the reasons discussed in Section 3.3. They are called the "57 Acres" site and the "Loxahatchee River" site (Figure 3.1). Table 3.1 lists the dates of field investigations and the type of measurements performed.

The study of the 57 Acres site (Figure 3.2) was begun as a private survey [Walton, Morris, Evans, and Christensen, 1975]. Since then, with the late owner's permission, the system has been extensively studied as part of this project, a great deal of data have been collected, and many types of instruments have been tested. The site is located in northern Palm Beach County on the Intracoastal Waterway (Figure 3.1). The project area consists of approximately 1300 acres in sections 18 and 7 of Township 41, Range 43E. The boundaries are the Intracoastal Waterway to the east and the Florida East Coast Railway to the west (Figure 3.2). The canal network has two hydraulic connections to the portion of the

Intracoastal Waterway lying between Jupiter Inlet to the north and Palm Beach Inlet to the south.

The main area of the canal network analysed in this report is the South Loop (Figure 3.2), which is that portion of the system south of the South Straight, including its west branch. Here, extensive data on velocities, wind, salinity, temperature, and dispersion rates calculated from dye dispersion studies have been collected on a number of field trips from early 1975 until late 1977 (Table 3.1). Similar data have been collected, although less extensively, in the remainder of the system, but only the longitudinal dye concentration profiles in the South Loop will be presented to compare model and field results.

The Loxahatchee River site (Figure 3.3) consists of two parallel, straight, prismatic canals joining the Loxahatchee River estuary about five miles upstream from Jupiter Inlet. A study was done at this site in June, 1977, in which tidal elevations, velocities, salinities, wind, and dye concentrations were measured.

The 57 Acres system is an example of a tidal canals network in which the circulation due to wind shear is considered to be the most important factor. The data from this system are used as a basis for developing the wind circulation part of the numerical model presented in Chapter 4. The Loxahatchee River site is an example of a canal network in which a saltwater wedge intrudes into the canals during some part of the flood tide, and retreats during the ebb tide. The data from this site, together with similar data from a report by McKeehan [1975], are used to develop the hydrodynamic portion of the model dealing with the circulation due to saltwater wedges with associated wind shear.

3.2 Geometry and Tides

The South Loop of the 57 Acres system consists of trapezoidal prismatic channels for the most part, with top widths of about 105 feet at mean tide, mean tidal depths of eight feet, and inverse side slopes of approximately three (Figures 3.4 and 3.5; station numbers are given in Figure 3.2). The exception is at the upstream end of the reach where depths of greater than sixteen feet have been measured, and the top width at mean tide is approximately 200 feet.

The center-line depths, measured using a Benmar continuous depth recorder, indicated some variation in the bottom topography not fully indicated by the averaged profile given in Figure 3.4. These fluctuations were on the order of two to three feet from given values, leading to very high values of Nikuradse's equivalent sand roughness, k , typically around twenty feet (Table 3.2).

At the dead-end of the South Loop at station L (Figure 3.2), tidal elevations have been measured using a continuous recorder and a stilling well. A typical tidal curve is that shown in Figure 2.5, having a mean tidal range of 2.5 feet and a mean tidal period of 12.42 hours.

The two Loxahatchee River site canals are straight, prismatic canals of about 2200 in length, six feet deep at mean tide, about seventy feet wide, and have variable inverse side slopes ranging from zero at the tidal entrances to three towards the dead-ends (Figure 3.6). The tide curve shown in Figure 2.5 is also typical for the Loxahatchee River site as the sites are only a few miles apart (Figure 3.1).

3.3 Velocities and Wind

Initially, velocities were measured using a small laboratory type Ott propellor meter (Type C1). However, it was soon found that this instrument was not capable of measuring currents below about 0.16 fps as found in tidal networks around Florida. During the initial 57 Acres study, Robert M. Snyder of Snyder Oceanographic Services in Jupiter, Florida, developed a Savonius current meter using magnetic bearings [Savonius, 1931]. This instrument was calibrated in the Hydraulic Laboratory flume and was found to have a lower threshold velocity than the small Ott meter.

However, the problem with both these meters is that they can only measure a scalar velocity and not a vector, unless one can either see the rotor or propellor turning, or else know the direction of flow beforehand. This problem was not recognized until several dual-axis Cushing electromagnetic current meter probes were purchased and used for the latter part of the 57 Acres project and for the June, 1977, Loxahatchee River field trip. The set-up of the measuring system is shown in Figure 3.7. It was observed that flow reversals are a common part of the hydrodynamic make-up of the canal network. A typical vertical velocity profile for the 57 Acres site is shown in Figure 3.8 and for the Loxahatchee site in Figure 3.9 (other profiles for both sites will be used throughout the remainder of this dissertation when comparisons with analytic and empirical velocity profiles are made).

The main cause of the form of the velocity profiles in the 57 Acres canal network was suspected to be due to wind shear on the water surface. A number of investigators have studied this effect [van Dorn, 1953; Wu, 1969], and relate the shear stress to the square of the wind speed at

some height above the ground. Accordingly, a directional wind meter (Figure 3.10) was erected near the dead-end of the South Loop in October, 1977, and a continuous record obtained during that field survey. The prevailing wind during the period of measurements was from the northeast at about ten to fifteen mph. During the night, however, it was found that the wind tended to die away, and appear again as a light westerly wind in the early morning before changing to the predominant direction by noon (Figure 3.11). The wind data were reduced and plotted in vector form at discrete time intervals in Figure 3.12.

In the Loxahatchee River system, a simple hand-held Davis anemometer was used to measure wind. This instrument has the advantage that it is easy to use, but it must be directed properly to measure either the maximum wind speed, or else its component along the canal.

The reason for considering only the Loxahatchee River site and the 57 Acres site was that only at these two sites were velocities measured using an electromagnetic currentmeter system. These two sites provided the only information on flow reversals due to wind shear and density currents, and hence the only information on which to base a numerical model of these phenomena.

3.4 Salinity and Temperature

A number of salinity measurements versus time made by the Hydraulic Laboratory and Snyder [1976], using a Lamotte conductivity probe meter with a separate temperature meter, and a Lamotte chloride sampling kit, indicated that vertical variations in salinity of 2-3 ppt between surface and bed readings occurred in the 57 Acres system (Figures 3.13 and 3.14). This gradient is probably due mainly to stormwater flow over salinity

structures in the dead-ends of the two west branches (Figure 3.2) as variations in salinity at stations J and H are fairly large. There is also a certain amount of overland flow entering the system over the sides of the canal which may account for the variation in the salinity at stations K and L.

During one field survey to the 57 Acres site in October, 1977, salinities were measured at one point over several tidal cycles. From these results, plotted in Figure 3.15, it appears reasonable to assume that the flow is continuously vertically stratified. However, because of this and the relative uniformity of the salinity it was decided to assume a vertically well mixed system and to use the 57 Acres data to model only the effect of wind induced circulation.

In the Loxahatchee River system, the salinity gradient is much more pronounced (Figure 3.16). From observed velocities (Figure 3.9), it appears that the salt wedge intrusion into the canals is the major factor determining the hydrodynamics of this canal system. Thus, the data for this system were used to develop the model form of the salt wedge induced density current circulation.

3.5 Dye Dispersion Studies

Dye studies were conducted in both systems by "instantaneously" injecting a known amount of 20 percent Rhodamine-WT dye across a reach using a pressurized system to achieve lateral mixing. The water was sampled using a Turner Designs Field Fluorometer Model 10-005 and the concentrations recorded on a Hewlett-Packard dual channel recorder (Figure 3.17).

Two types of tests were performed. Firstly, measurements were recorded at one location so that a concentration versus time curve was

found. This curve was then examined by several techniques, in particular the modified semilog plot method [Holley and Harleman, 1965] to determine the dimensionless dispersion coefficient, K , for that reach. Secondly, at successively high and low tides, longitudinal concentration profiles were measured throughout the system to observe the extent of movement of the dye. Three dye-concentration sequences were performed, in July and October, 1977, in the 57 Acres system, and in June, 1977, in the Loxahatchee River system. An example of one of these dye concentration sequences for the 57 Acres system is given in Figures 3.18-3.24. These data were used to calibrate the numerical model, and to check its accuracy in simulating longitudinal concentration profiles at other times.

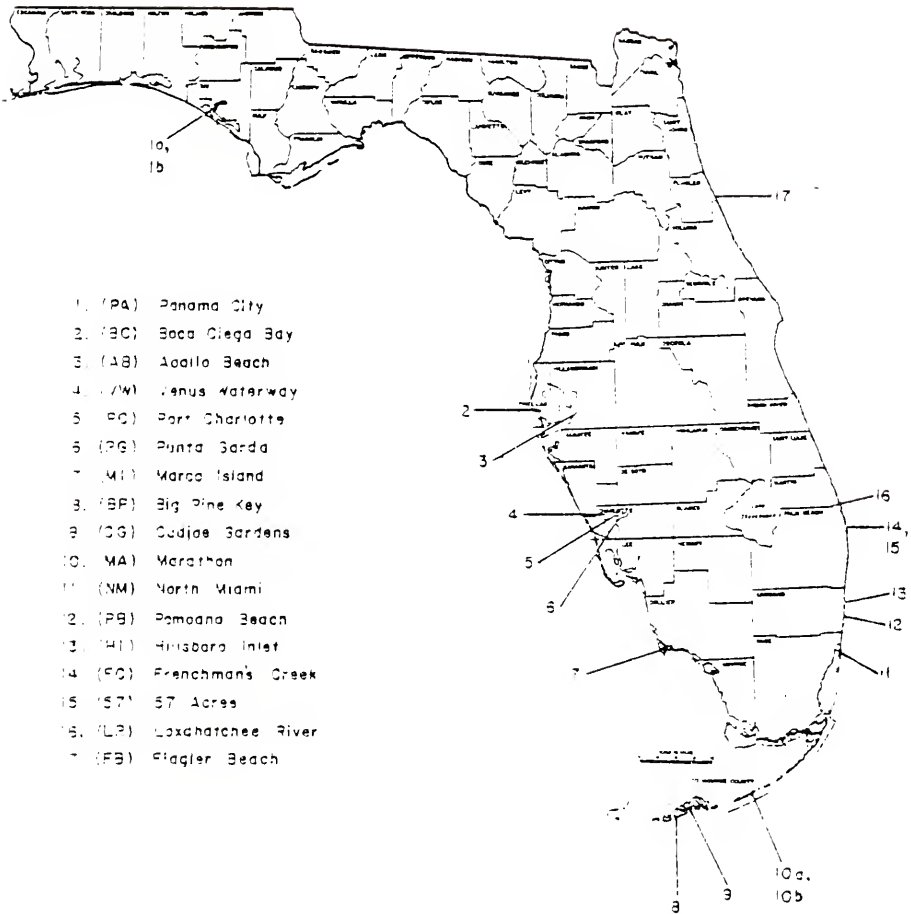


Figure 3.1 - Location Map for Canal Studies.

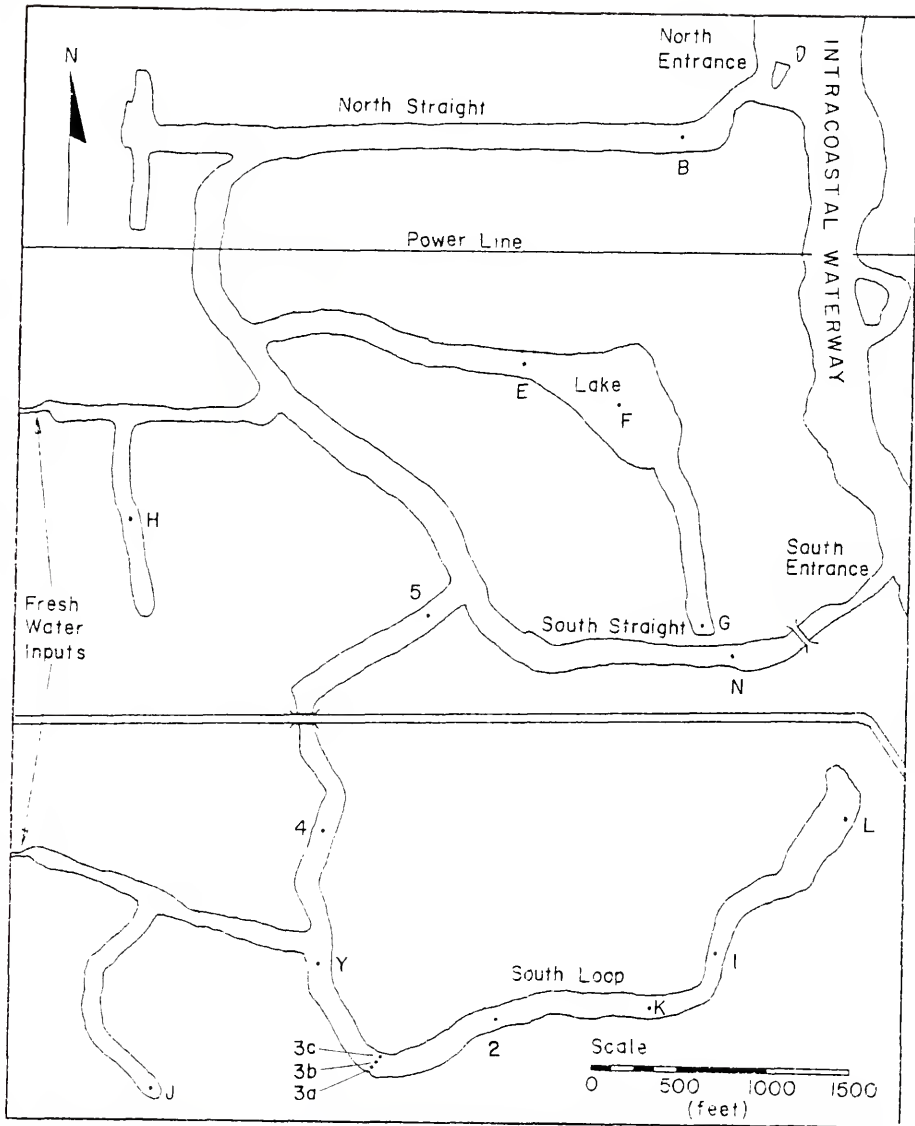


Figure 3.2 - 57 Acres Site Plan Showing Measurement Stations.

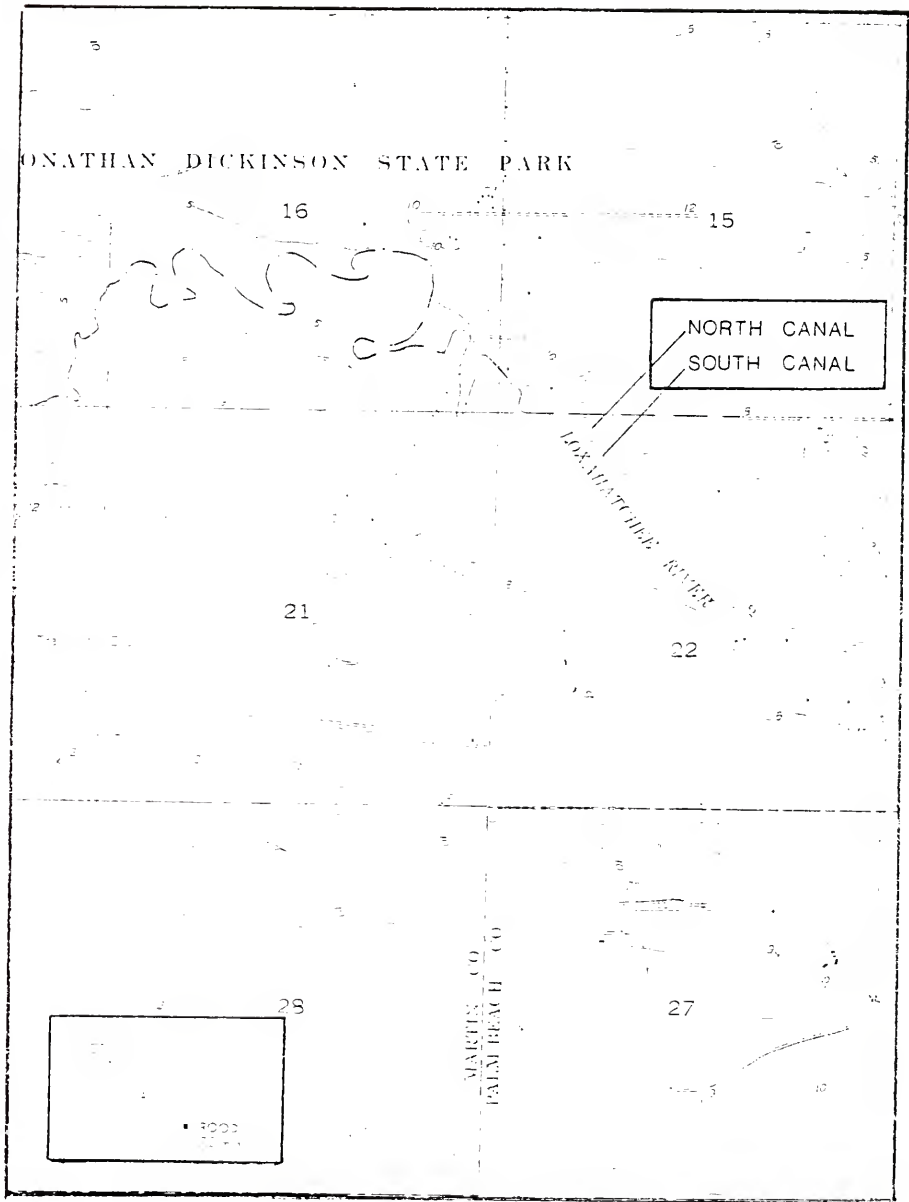


Figure 3.3 - Topographic (7 1/2' quadrangle) Map for Loxahatchee River Canals.

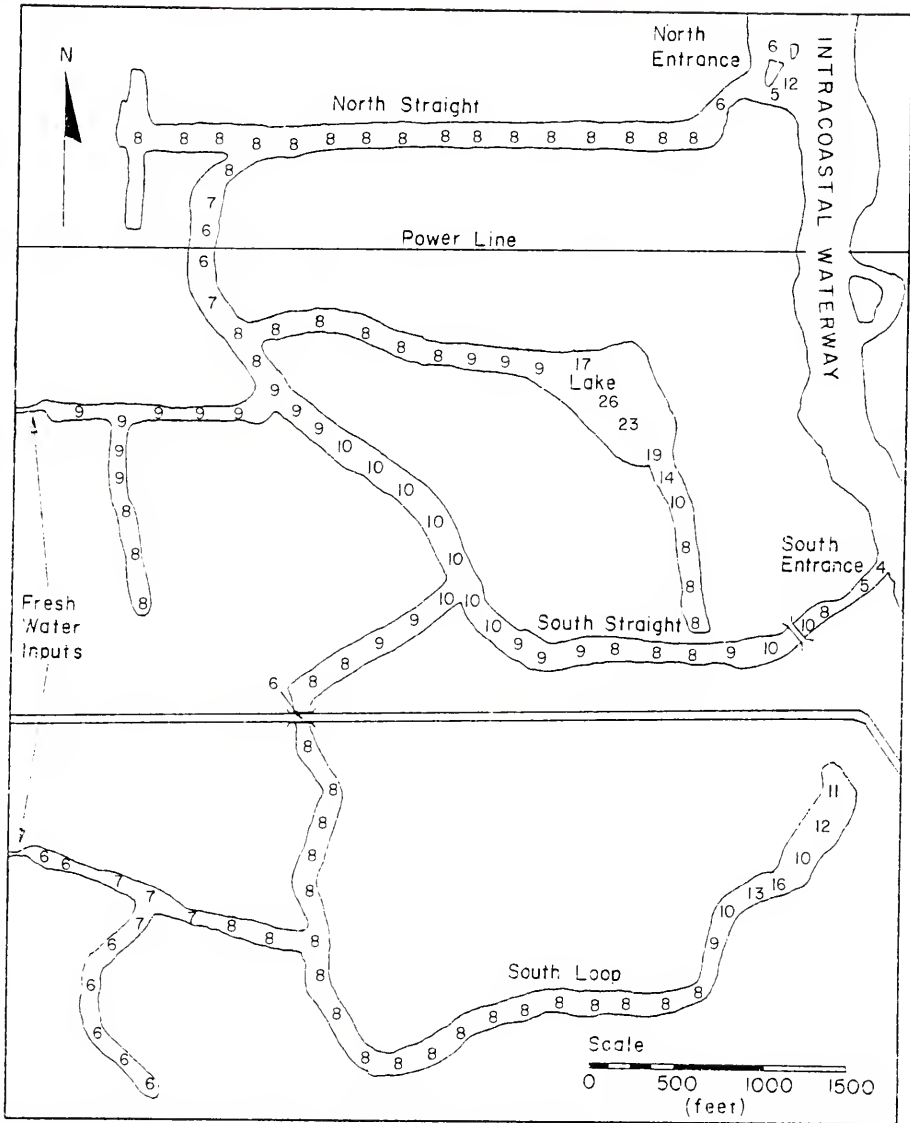


Figure 3.4 - Center Line Depths in 57 Acres System.

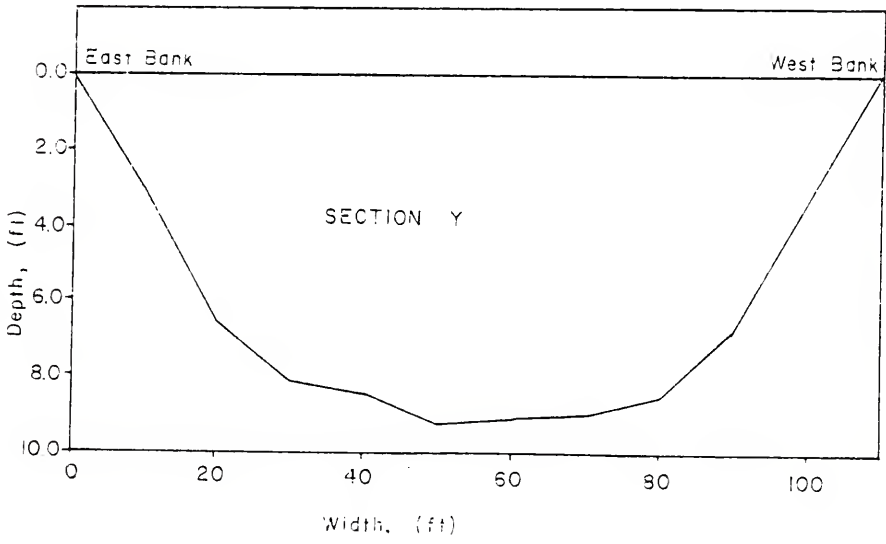
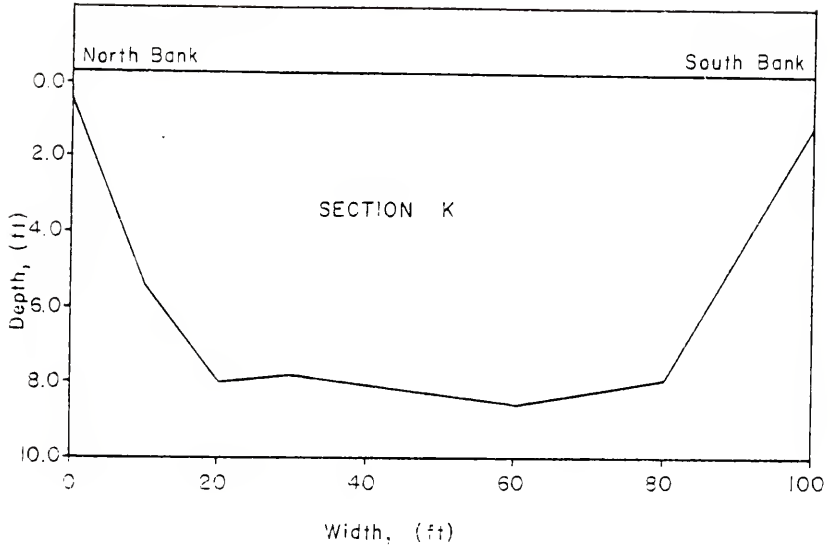
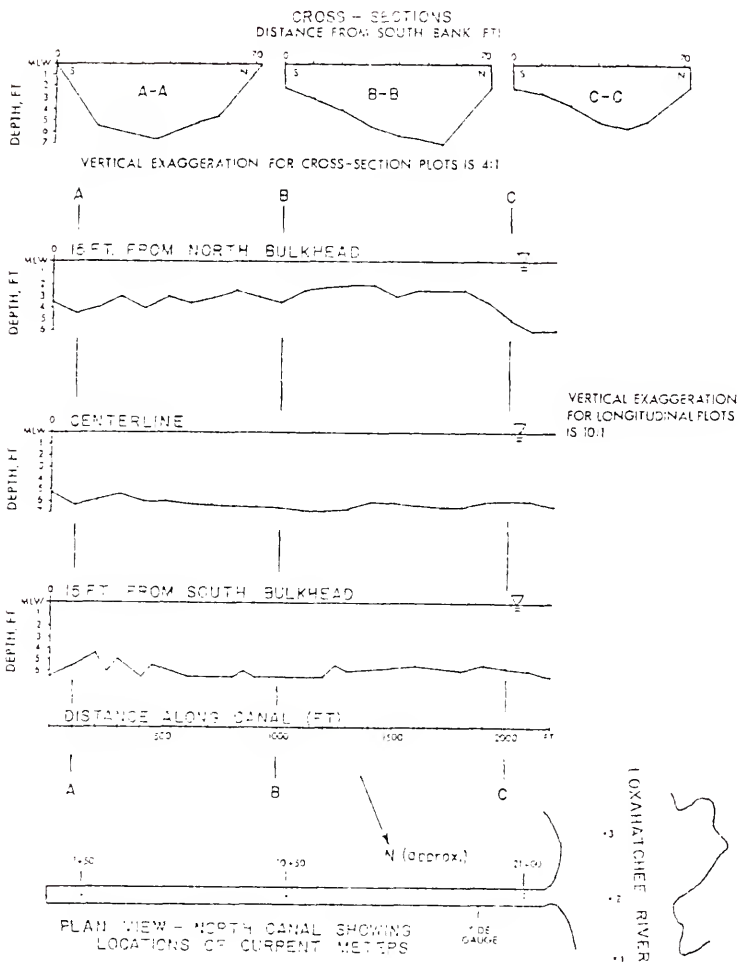


Figure 3.5 - Cross-Sections at K and Y in 57 Acres System.



LOXAHATCHEE NORTH CANAL

Figure 3.6 - Cross-Sections and Plan View of Loxahatchee North Canal, June 1977.

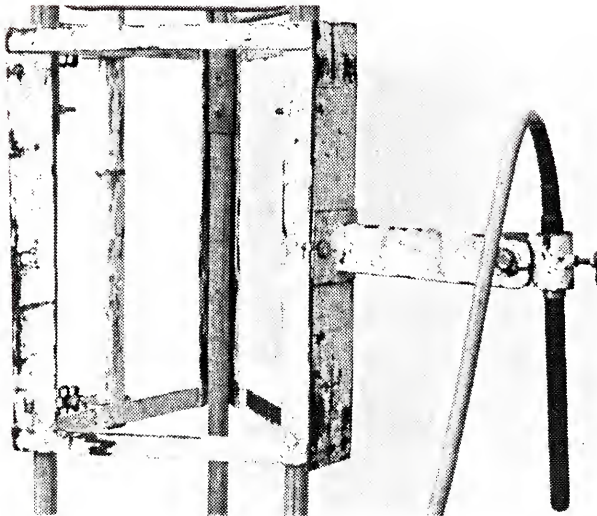


Figure 3.7 - Electromagnetic Velocity Meter Set-Up.

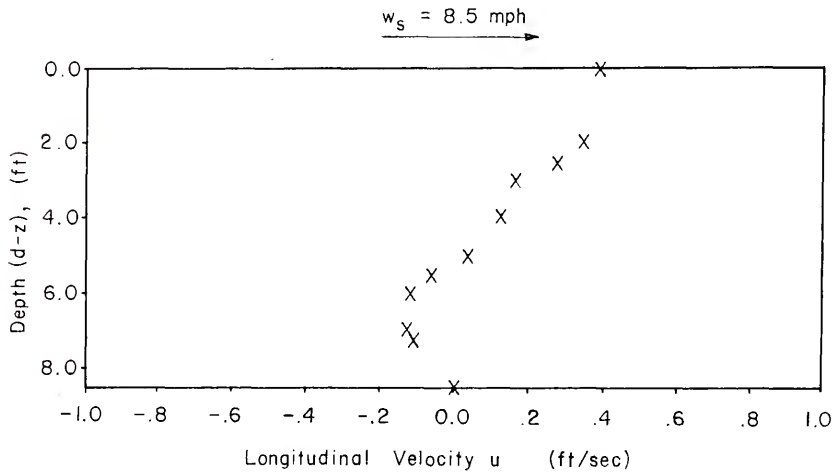
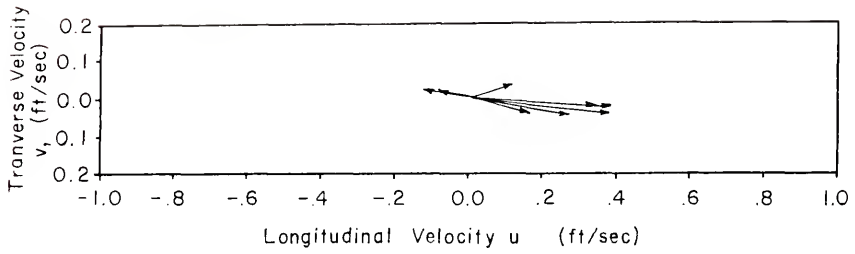


Figure 3.8 - Typical Vertical Velocity Profile in 57 Acres System.

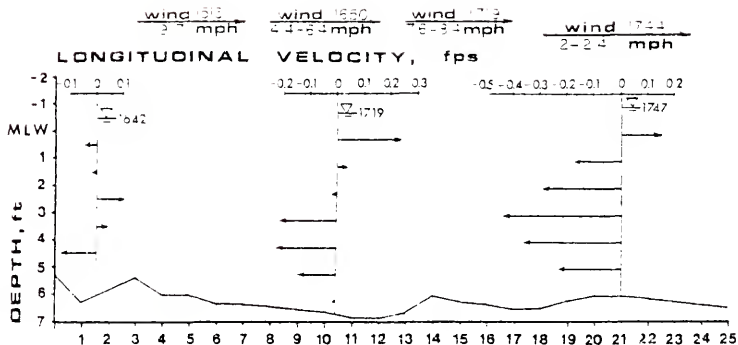


Figure 3.9 - Typical Vertical Velocity Profile in Loxahatchee River System, 13 June, 1977.



Figure 3.10 - Wind Recorder Set-Up.

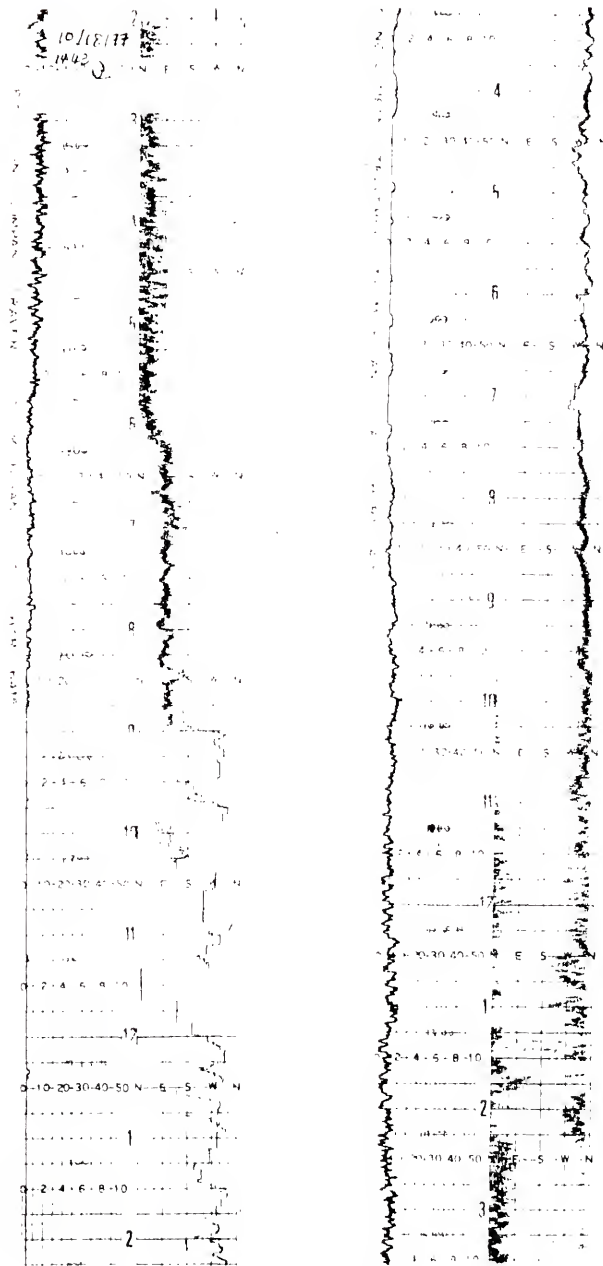


Figure 3.11 - Strip Chart Recording of Wind Data--57 Acres System, October, 1977.

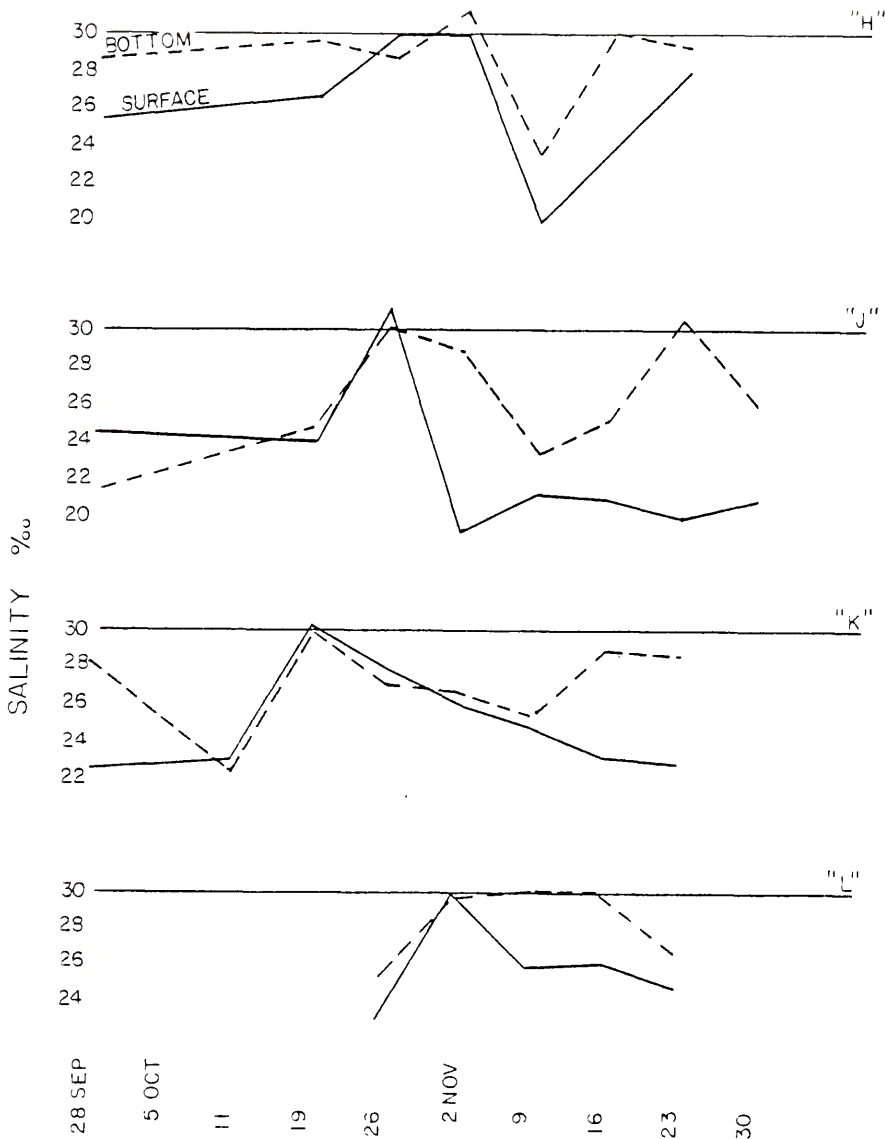


Figure 3.13 - Station Salinities Versus Time in 57 Acres System.

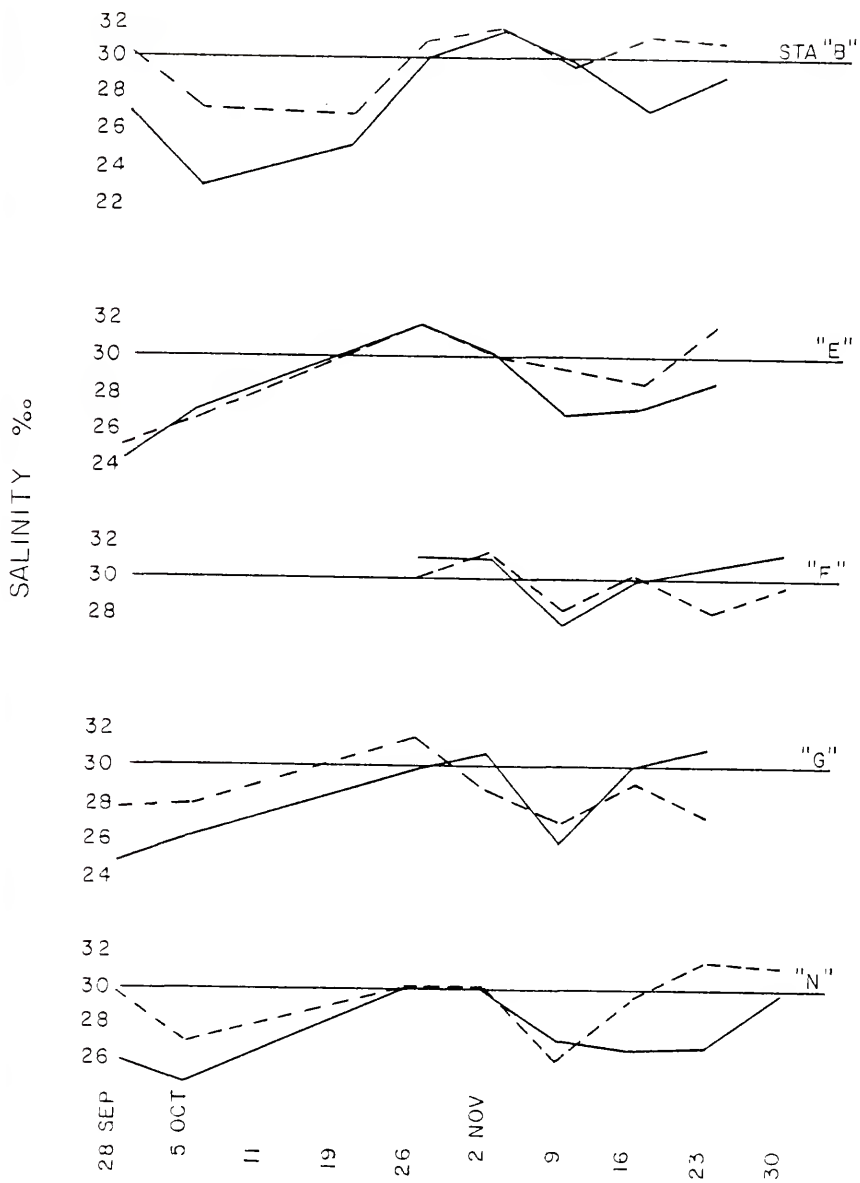


Figure 3.14 - Station Salinities Versus Time in 57 Acres System.

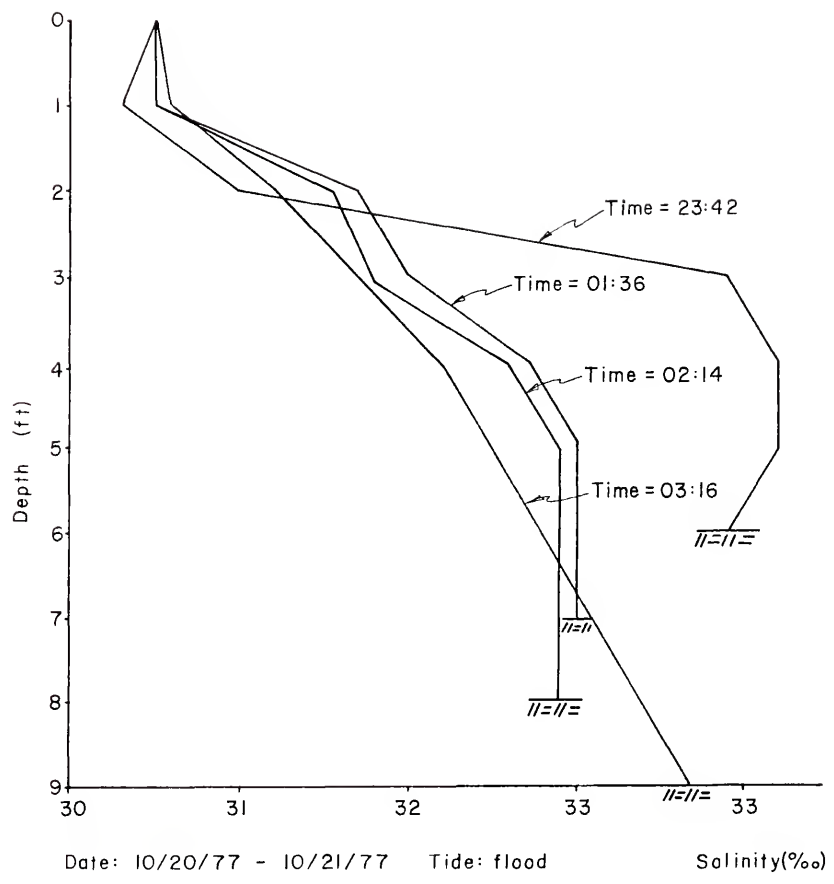


Figure 3.15 - Salinity Versus Time at Station 3 - 57 Acres System, October 1977.

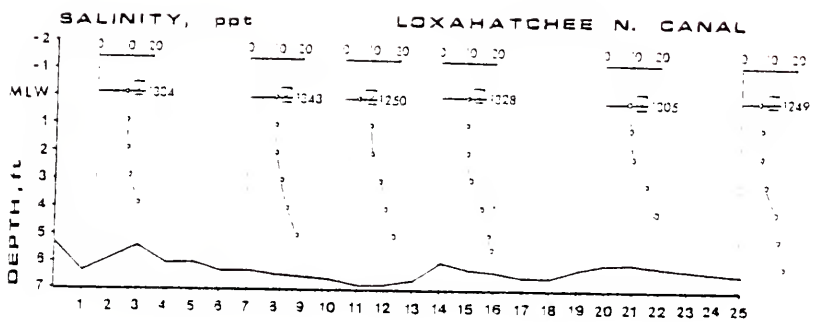


Figure 3.16 - Salinity Profiles--Loxahatchee River System, June 1977.

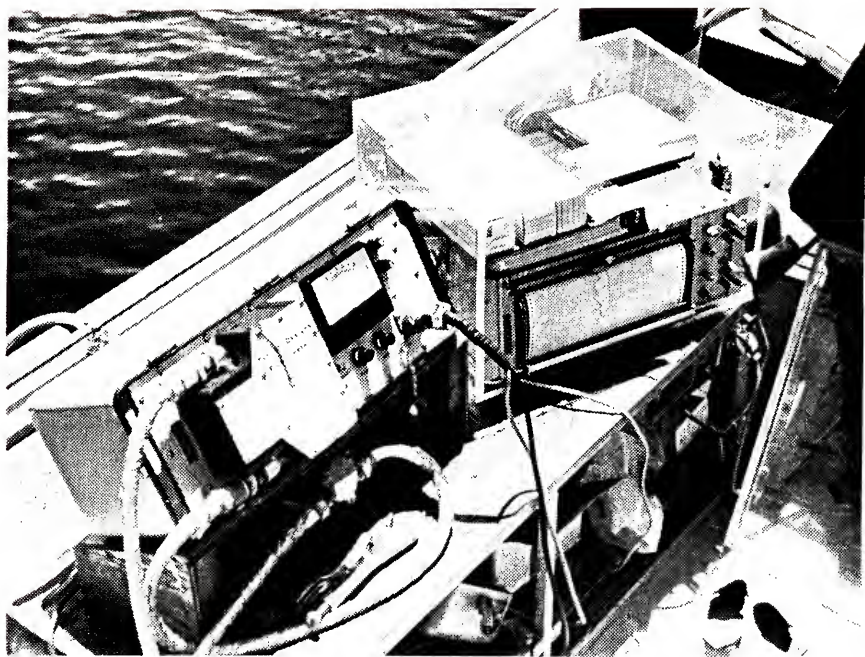
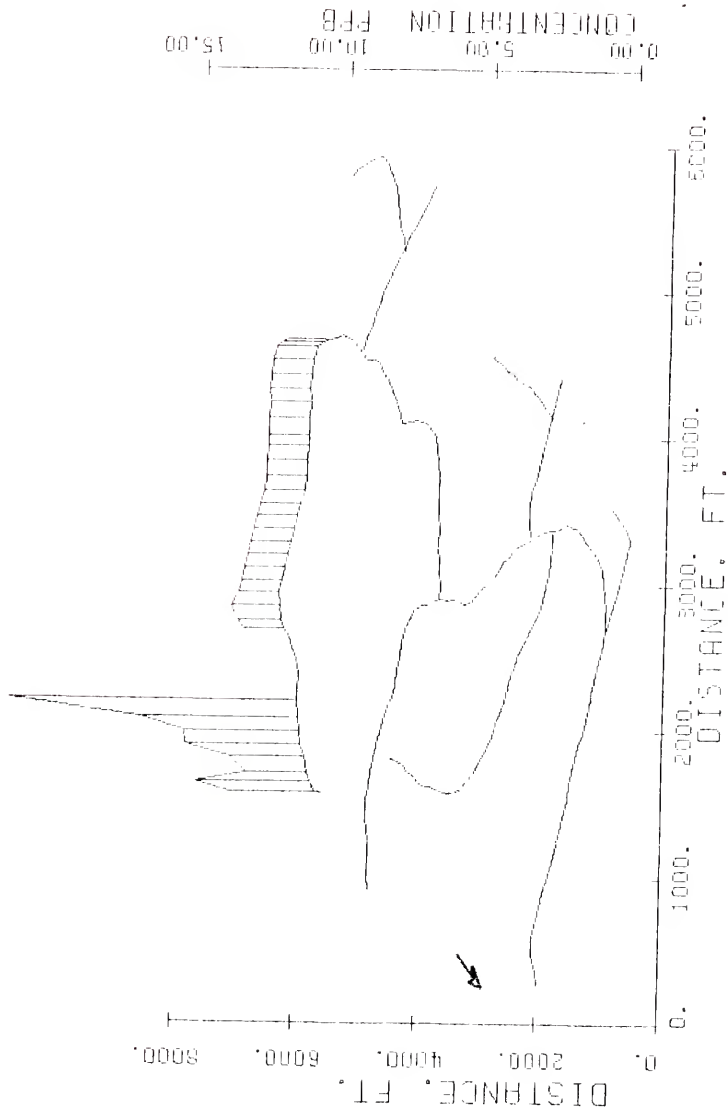


Figure 3.17 - Photograph of Fluorometer and Recorder Set-Up.



MEASURED DYE CONCENTRATION AT 3 FT DEPTH ALONG CENTERLINE
57 ACRES CANAL SYSTEM, PALM BEACH COUNTY, FLORIDA

DATE: 771019. TIDE: LOW. TIME: 2140. PEAK: 10.00 PFB

Figure 3.18 - Longitudinal Dye Concentration Profiles--57 Acres System, October, 1977.

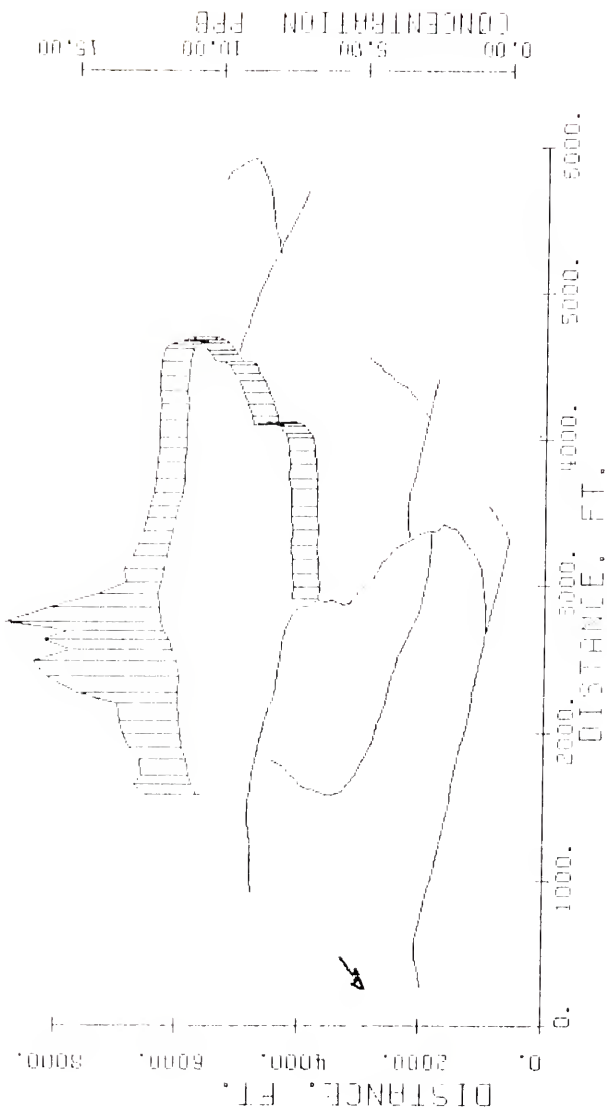
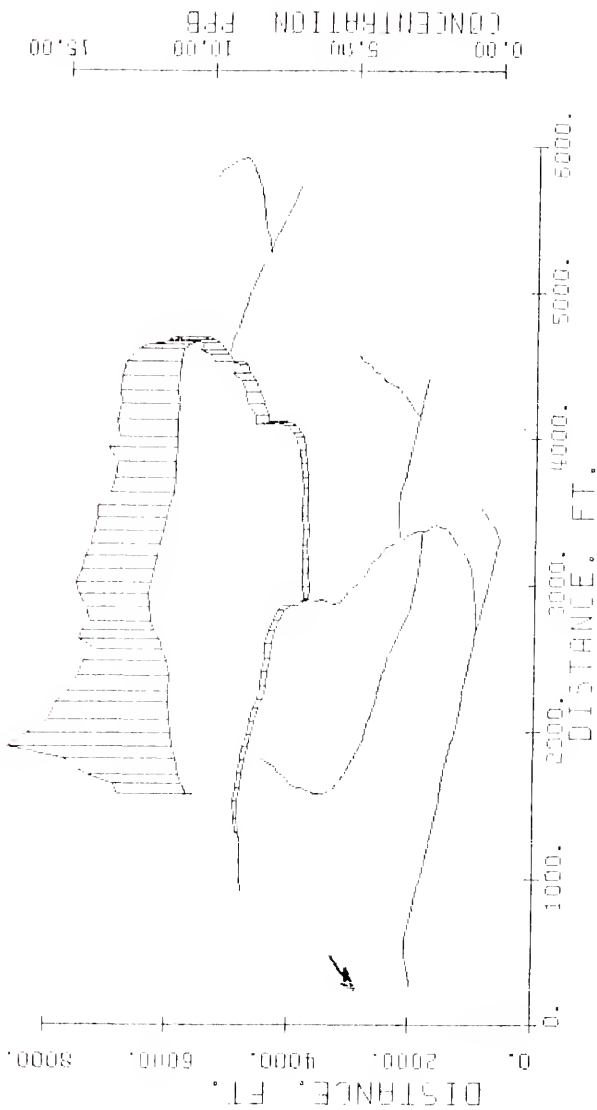


Figure 3.19 - Longitudinal Dye Concentration Profiles--57 Acres System, October, 1977.



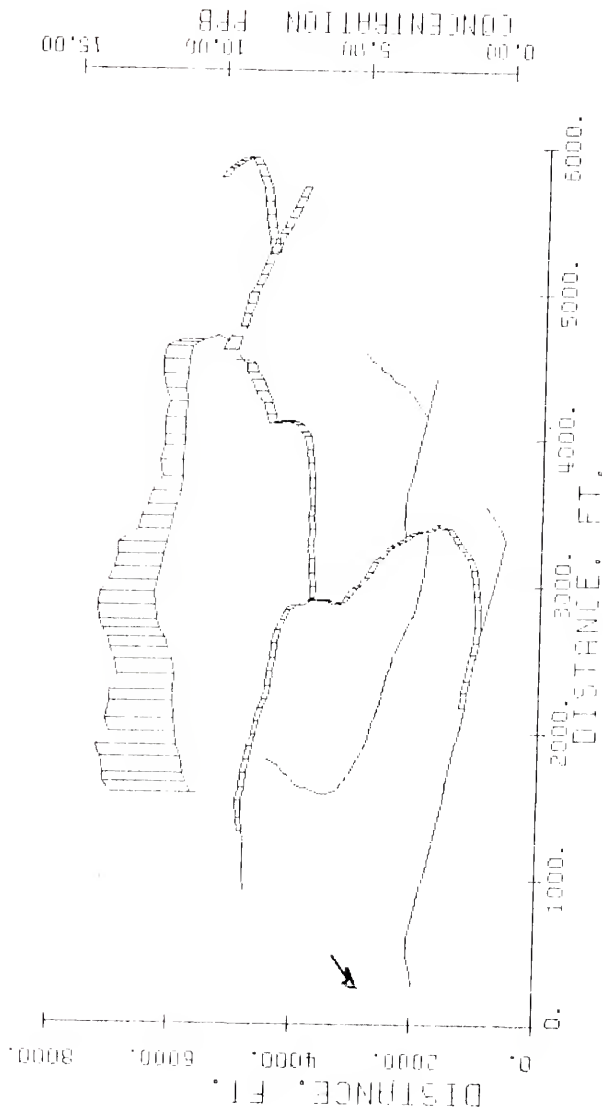
MEASURED DYE CONCENTRATION AT 3 FT DEPTH ALONG CENTERLINE

57 ACRES CANAL SYSTEM, PALM BEACH COUNTY, FLORIDA

DATE: 771020, TIDE: LOW, TIME: 0950, PEAK: 5.70 PPB

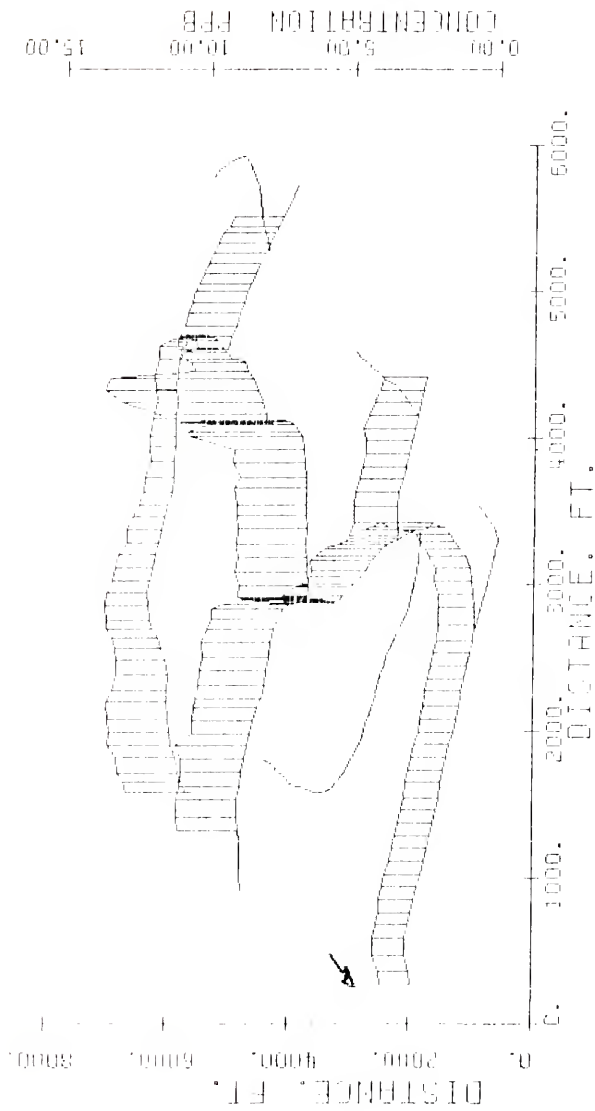
AZIMUTH= 210 DEGREES ELEVATION= 25 DEGREES

Figure 3.20 - Longitudinal Dye Concentration Profiles--57 Acres System, October, 1977.



MEASURED DYE CONCENTRATION AT 3 FT DEPTH ALONG CENTERLINE
 57 ACRES CANAL SYSTEM, PALM BEACH COUNTY, FLORIDA
 DATE: 7/10/70. TIDE: HIGH. TIME: 1610. PEAK: 2.90 PPB
 AZIMUTH= 210 DEGREES ELEVATION= 25 DEGREES

Figure 3.21 - Longitudinal Dye Concentration Profiles--57 Acres System, October, 1977.



MEASURED DYE CONCENTRATION AT 3 FT DEPTH ALONG CENTERLINE
57 ACRES CANAL SYSTEM, PALM BEACH COUNTY, FLORIDA
DATE: 771020. TIDE: LOW. TIME: 2240. PEAK: 5.30 PFB
AZIMUTH= 210 DEGREES ELEVATION= 25 DEGREES

Figure 3.22 - Longitudinal Dye Concentration Profiles--57 Acres System, October, 1977.

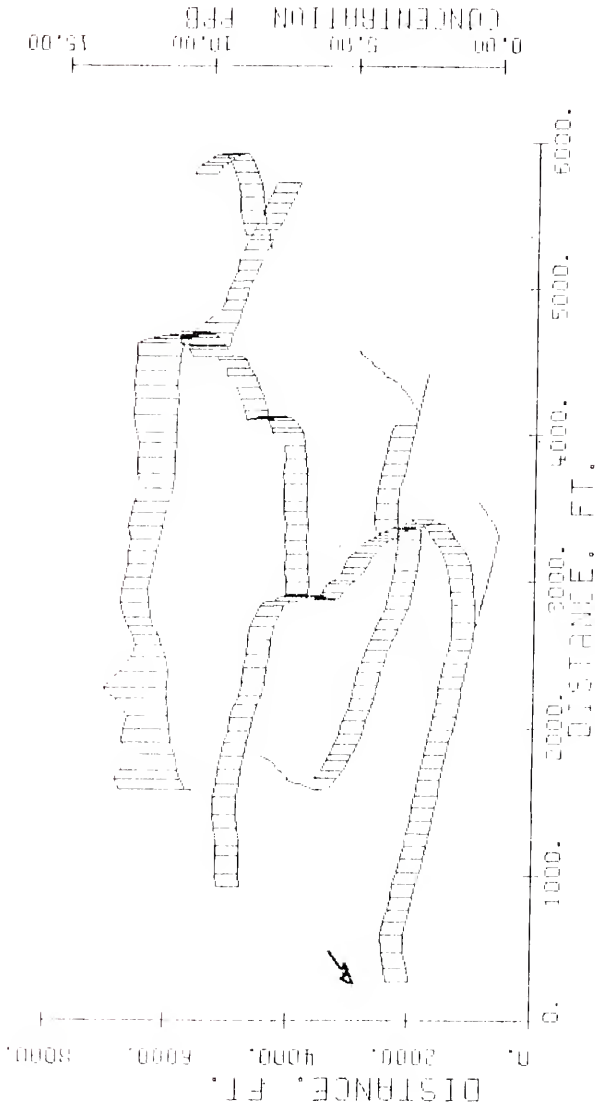
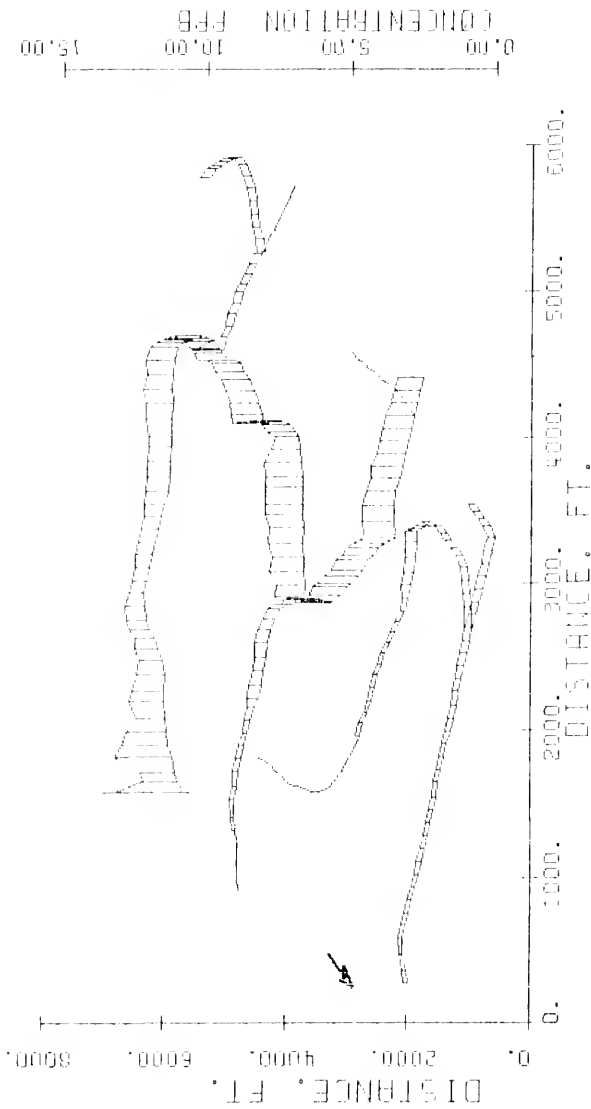


Figure 3.23 - Longitudinal Dye Concentration Profiles--57 Acres System, October, 1977.



MEASURED DYE CONCENTRATION AT 3 FT. DEPTH ALONG CENTERLINE

57 ACRES CANAL SYSTEM, PALM BEACH COUNTY, FLORIDA

DATE: 7/10/21, TIDE: LOW, TIME: 1045, PEAK: 3.00 PPB

AZIMUTH= 210 DEGREES ELEVATION= 25 DEGREES

Figure 3.24 - Longitudinal Dye Concentration Profiles--57 Acres System, October, 1977.

Table 3.1 - continued

Location	Dates	Type	Tide	Depth	Current Speed	Current Velocity	Wind Speed	Wind Velocity	Salinity	Temp.	Dispersion
57 Acres	760401- 760404	FS	X			X	X				
	770719- 771923	FS	X			X	X				X
	771016- 771022	FS	X			X		X			X

Table 3.2 - Summary of Data for South Loop, 57 Acres

Parameter	Station ST	Station Y	Station KU	Station L
Mean depth, ¹ d_m (ft)	5.25	6.76	6.72	
Surface width, ¹ W (ft)	104.0	108.0	100.0	
Cross-sectional area, ¹ A_c (ft ²)	546.0	730.0	672.0	
Hydraulic radius, R (ft)	4.77	6.01	5.92	
Bank slopes	1:3/vert.	1:3/1:3	vertical	
Effective grain size, $d_{35\%}$ (mm)			0.001	0.00024
Soil type (M.I.T.)			Course Clay	Medium Clay
Specific weight of submerged solid, $\gamma_s - \gamma$ (lb/ft ³)			48.3	50.8
Placticity index, P.I.			108.0	98
Angle of repose, ϕ (degrees)			28.0	28.0
Critical horizontal shear stress, $\tau_{cr,h}$ (psf)			0.0600	0.0700
Shear velocity, u^* (fps)	0.046	0.015	0.053	
Bed shear stress, τ_0 (psf)	0.0042	0.0057	0.0056	
Nikuradse's equivalent sand roughness, k (ft)	30.4	13.2	20.2	
Dispersion coefficient, E_d (ft ² /sec): Flood	4.74			
Ebb	3.58		1.84	

Note: ¹To mean low water.

Table 3.3 - Summary of Data for Loxahatchee River North Canal

PARAMETER	VALUE
Length, L	2200 ft
Bottom width, b	50 ft
Mean tidal depth, d_0	7 ft
Inverse side slope, left bank, s_L right bank, s_R	2 2
Tidal amplitude	1 ft
Nikuradse's equivalent sand roughness, k	10 ft
Reach alignment angle	270 degrees
Depth to saltwater interface	3 ft

CHAPTER 4

THREE-DIMENSIONAL HYDRODYNAMICS IN CANAL NETWORKS

4.1 Introduction

The one-dimensional form of the hydrodynamics and transport equation was fine for investigating the numerical dispersion present in solution schemes, their accuracy and stability, and to observe the effects of variations in geometric parameters. However, the flow in a canal network cannot be reduced to this level. Even assuming a logarithmic velocity profile, when wind and salinity effects can be ignored, the excursion of a fluid particle on the surface is greater than that calculated from the mean velocity alone.

When dye, or another source load, is dumped into a canal network, it is rarely mixed as an instantaneous plane source, even with the forced mixing done on a number of field trips [Morris, Walton, and Christensen, 1978; Morris, 1978]. The dye cloud tends to remain in the top half of the cross-sectional area, and not be mixed near the banks. The length scale associated with the so-called "convective period" for the dye is usually on the order of the length of the canal network itself, and thus the material will tend to be convected with the velocities in the upper layers of water, with some mixing to the lower layers. This length is defined as the distance traveled with the mean velocity before the one-dimensional mass-transport equation can be assumed to apply to quasi-steady unidirectional flow. The one-dimensional equation, then, can only be assumed to be applicable when flow reversals are not present.

The equation of this length scale, L, was given by Fischer [1967] as,

$$L > 1.8 \frac{\rho^2}{R} \frac{u}{u^*} \quad (4.1)$$

where

ρ = distance from point of maximum velocity to the farthest bank (L).

Now

$$u^* = \sqrt{gRS_f} \quad (4.2)$$

where

S_f = slope of energy gradient line (dimensionless).

From Manning's equation in the form,

$$u = \frac{8.25 \sqrt{g}}{k^{1/6}} R^{2/3} S_f^{1/2} \quad (4.3)$$

u^* can be written from Equation (4.2) as,

$$u^* = \frac{u}{8.25} \left(\frac{k}{R}\right)^{1/6} \quad (4.4)$$

In Floridian canals, k is of the same order as R, and as the ratio is raised to the 1/6 power, it may be assumed that,

$$\frac{u}{u^*} \approx 8.25 \quad (4.5)$$

Thus, for a typical canal,

$$L > \frac{1.8 \cdot 50^2 \cdot 8.25}{10} = 3,700 \text{ ft} \quad (4.6)$$

which is on the order of the length of the canal, and over which, the one-dimensional mass-transport equation does not apply.

Consider for example, a wind blowing over the canal network in the positive x-direction. Then the excursion of the top layers will

be even greater than for an ebb tide alone with a resulting logarithmic velocity distribution. Added to this, there is a reversal theoretically at the one-third depth, which convects any dye in the lower layer upstream. The combination of this tidal flow and wind circulation produces a dye cloud with a large leading concentration gradient and a long tail, as diffusion occurs not only longitudinally in the top layer of water, but also from the reversal layer to the top layer (Figure 4.1).

This type of dye concentration distribution was frequently measured in a number of canal networks, such as the 57 Acres Site (Figure 3.2), in which the wind circulation was a major factor, and cannot be predicted by any one-dimensional theory. In the site on the Loxahatchee River, and also in two canals investigated by McKeehan [1975], gravity flows due to saline density gradients are an important factor, and according to McKeehan, the dominant factor for his two Gulf Coast canals. In these cases, the canals are hydraulically connected to a tidal estuary with a large river freshwater flow. In this system, a saltwater wedge enters the canal during the flood tide and recedes during the ebb tide in which the freshwater river flow flushes most of the remaining saltwater wedge in the canal leaving a salt dome. It is the exception rather than the rule to measure Gaussian shaped concentration profiles, and a two or three-dimensional theory must be used to explain the physical processes.

Another important phenomenon in these canal networks is secondary currents. This is one of the major mechanisms by which the anoxic water in the benthic layer at the bed may be transferred to the surface where it can be resupplied with oxygen. To include this

effect, the wind circulation, density flows, and tidal flow, requires a three-dimensional model.

The assumption that the water surface can be considered as a horizontal plane, rising and falling through the tidal range, with the tidal frequency, has already been introduced in developing the one-dimensional model. This effect was, of course, measured for a three-dimensional hydrodynamic system, and it therefore seems justifiable to extend this assumption to a three-dimensional model.

The assumption can be supported in theory if the slope of the water surface due to wind set-up alone in a dead-end canal is calculated. Bretschneider [1966], using Saville's work [1953], proposed the following equation for the slope of the water surface under these conditions.

$$\frac{\partial \eta}{\partial x} = \frac{3.3 \cdot 10^{-6} w_s^2}{g(d_0 + \eta)} \quad (4.7)$$

where

η = elevation of water surface from the mean depth, d_0 (L)

w_s = wind speed (L/T)

Typically in Floridian canals,

$$\frac{\partial \eta}{\partial x} = \frac{3.3 \cdot 10^{-6} \cdot 15^2}{32.13 \cdot 10} = 2.3 \cdot 10^{-6} \quad (4.8)$$

which is too small to measure in most networks.

In this chapter, the major hydrodynamic factors such as the tidal flow, wind induced circulation, density currents, and secondary currents are investigated, and closed form expressions derived for their independent effects. It will be assumed that these separate velocity distributions may be superimposed to obtain the network velocity field. This assumption will be supported by field data.

Finally, it remains to define a coordinate system (Figure 4.2). Using the definitions of Section 2.1.2, the x-axis (longitudinal) is in the direction of the ebb tide in each reach, the y-axis (lateral) is from left bank to the right bank when facing in the positive x-direction, the z-axis is vertically upward from the bed of each reach, which is assumed to be a horizontal plane.

4.2 Tidal Velocities

When wind and salinity gradient effects are negligible, the flow is usually found to be logarithmic. The vertical velocity profile based on the volume of the tidal prism, V , upstream of the cross-section of interest, is obtained from Nikuradse's [1933] logarithmic profile as,

$$u(z) = \frac{1}{A} \frac{dV}{dt} \frac{\ln(29.73 z/k)}{\ln(29.73 d/ke)} \quad (4.9)$$

where

e = exponential constant = 2.718.

This form of the equation is satisfactory for a vertically layered model because the mean velocity in the bottom layer, u_b , from $z = 0$ to $z = d_b$, where d_b is the thickness of the bottom layer is given by,

$$u_b = \frac{1}{d_b} \int_0^{d_b} u(z) dz \quad (4.10)$$

Integrating,

$$u_b = \frac{1}{A} \frac{dV}{dt} \frac{\ln(29.73 d_b/ke)}{\ln(29.73 d/ke)} \quad (4.11)$$

as $z \ln z \rightarrow 0$ as $z \rightarrow 0$.

Similarly, the mean velocity in any other layer, u_c , from $z = d_1$ to $z = d_2$ is given by,

$$u_c = \frac{1}{A} \frac{dV}{dt} \frac{(d_2 \ln(29.73 d_2/ke) - d_1 \ln(29.73 d_1/ke))}{(d_2 - d_1) \ln(29.73 d/ke)} \quad (4.12)$$

In a layered model, and particularly one in which the velocities are constant in each layer, it is usual to neglect the no-slip boundary conditions at the bed and the sides of the channel. This is because the thickness of the layer associated with large velocity gradients near the solid boundaries is very small compared to the smallest dimension of a computational cell, a cell being formed by the intersections of planes defining the lateral and vertical layers, and of length Δx .

Instead to allow for vertical and lateral variations in the flow field, the logarithmic velocity defined for any cell was based on the mean depth of the projectors of the horizontal area onto the bed (Figure 4.3). This technique gives a lateral variation to the velocity field for a trapezoidal cross-section.

To give a vertical variation, it was assumed that each cell increases its cross-sectional area by a factor proportional to its mean velocity vector. The constraint placed on this technique is that the cells in a particular layer all expand or contract vertically at the same rate allowing nonuniform expansion only in the lateral direction. The sum of all the expansions or contractions of the cells then equals the change in the total cross-sectional area of the flow in one time interval, Δt .

4.3 Wind Induced Circulation

Many researchers have witnessed and measured flow reversals due to a wind blowing over a waterbody contained in a semienclosed basin [Hellstrom, 1941; Keulegan, 1951; Wu, 1969], and have derived closed form functions or empirical formulae describing the vertical velocity profile. The turbulent momentum equation in the longitudinal x-direction

can be written without density terms,

$$\begin{aligned} \frac{du}{dt} = & g \frac{\partial \eta}{\partial x} + fv + \frac{\partial}{\partial x} \left(\frac{\tau_{xx}}{\rho} \right) + \frac{\partial}{\partial y} \left(\frac{\tau_{xy}}{\rho} \right) + \frac{\partial}{\partial z} \left(\frac{\tau_{xz}}{\rho} \right) \\ & - \frac{1}{\rho} \frac{\partial Pa}{\partial x} \end{aligned} \quad (4.13)$$

where

η = elevation of water surface, (L)

v = lateral velocity, (L/T)

f = Coriolis parameter, (1/T)

$\tau_{xx}, \tau_{xy}, \tau_{xz}$ = shear stress in x, y, z directions with respect to
x-direction, (M/LT²)

ρ = density, (M/L³)

Pa = atmospheric pressure, (M/LT²).

Assuming quasi-steady flow, which is a good assumption as the tidal ranges are very small in Floridian canals, that the atmospheric pressure, Pa , is uniform over the canal network (on the order of a few square miles), that the longitudinal and lateral gradients of the shear stress terms are small, and neglecting the Coriolis effect.

$$g \frac{\partial \eta}{\partial x} = \frac{\partial}{\partial z} \left(\frac{\tau_{xz}}{\rho} \right) \quad (4.14)$$

Considering a rectangular prismatic dead-end canal and assuming that the water surface slope $\partial \eta / \partial x$ is constant, then

$$\frac{\tau_{xz}}{\rho} = gz \frac{\partial \eta}{\partial x} + a_0 \quad (4.15)$$

where

a_0 = constant of integration.

The classical way to write the wind shear stress is,

$$\tau_{xS} = K_W^D w_S^2 \cos\theta \quad (4.16a)$$

$$\tau_{yS} = K_W^D w_S^2 \sin\theta \quad (4.16b)$$

where

K_W = drag coefficient (dimensionless)

θ = angle between wind and positive x-direction of reach
(degrees)

w_S = wind speed (L/T)

τ_{xS}, τ_{yS} = surface wind shear stresses in x and y-directions
respectively (M/LT²).

However, this is assuming a resultant shear stress, τ_x , of the two components, τ_{xS} and τ_{yS} . In a canal reach, the lateral shear stress is very much smaller than the longitudinal, and may be ignored. Hence here,

$$\tau_{xS} = K_W^D w_S^2 \cos\theta |\cos\theta| \quad (4.17a)$$

$$\tau_{yS} \approx 0 \quad (4.17b)$$

The form of the wind drag coefficient, K_W , has been studied by a number of people, notably Van Dorn [1953] and Wu [1969]. Van Dorn's work was considered the standard until Wu did a more thorough investigation incorporating Van Dorn's results. He put forward the following relationship (converting from metric to English units) which will be used in this model,

$$K_W = 0.6 \times 10^{-6} w_S^{1/2} \quad \text{for} \quad w_S < 49.2 \text{ ft/sec} \quad (4.18a)$$

$$K_W = 3.1 \times 10^{-6} \quad \text{for} \quad w_S > 49.2 \text{ ft/sec} \quad (4.18b)$$

With the above boundary condition (Equation (4.17a)), at $z = d$, the depth of water in the reach, the constant a_0 in Equation (4.15) can be evaluated, and,

$$\frac{\tau_{xz}}{\rho} = K_W w_S^2 \cos\theta |\cos\theta| + g(z - d) \frac{\partial \eta}{\partial x} \quad (4.19)$$

The z-component of the turbulent shear stress term can be written

$$\tau_{zx} = (\nu \frac{\partial u}{\partial z} - \overline{u'w'}) \quad (4.20)$$

where

ν = kinematic viscosity (L^2/T)

u' , w' = turbulent fluctuation from turbulent time mean velocities in x and z directions respectively (L/T)

($\overline{\quad}$) = turbulent time mean value.

Using the laminar analogy, which is the first term on the left hand side of Equation (4.20), the turbulent shear stress can be written in terms of a vertical eddy viscosity coefficient, or vertical momentum transfer coefficient, N_z , as,

$$\tau_{xz} = \rho N_z \frac{\partial u}{\partial z} \quad (4.21)$$

Substituting Equation (4.21) into Equation (4.19),

$$N_z \frac{\partial u}{\partial z} = K_W w_S^2 \cos\theta |\cos\theta| + g(z - d) \frac{\partial \eta}{\partial x} \quad (4.22)$$

The next step involves making some assumption about the form of the vertical momentum transfer coefficient, N_z . As $w' = 0$ at the bed, and as $\partial u / \partial z$ is very large (infinite for a no-slip boundary condition), then from Equations (4.8) and (4.9), N_z must be very small or zero there. At the surface most investigators considered $N_z = 0$, or that $w' = 0$

[Cooper and Pearce, 1977; Madsen, 1977]. However, this is only approximately true because there is usually some vertical surface activity in almost all open water bodies. Therefore, N_z may be small but usually not zero.

The classical form of the vertical momentum transfer coefficient is a parabola of the form,

$$N_z = 0.4u^* \frac{z}{d} \left(1 - \frac{z}{d}\right) \quad (4.23)$$

This form has been substantiated by a number of investigators [Jobson and Sayre, 1970; Pritchard, 1956] who measured velocity characteristics both in the laboratory and in the field. The problem arises when such a variation is incorporated into a closed-form solution for the velocity field associated only with the wind.

Many numerical modelers have considered the vertical momentum coefficient to be constant, and have achieved fairly good results [Heaps, 1972, 1974; Wang and Connor, 1975]. Some modelers have tried to go further and incorporate a vertical parabolic distribution. Leendertse and Liu [1975] did this in a layered model by allowing the coefficient to be constant in each layer. Cooper and Pearce [1977] tried to match the distribution of the coefficient using a finite element approach approximating its shape with a series of linear segments. The results were inconclusive, but more importantly, the method introduced two new coefficients instead of the original one, which must be evaluated from field measurements. From Equation (4.22) it can be seen that N_z is a function of z to the first, or higher, power. Integrating Equation (4.23) produces a logarithmic term in z which must be evaluated at $z = 0$, to solve for the constants of integration.

It was felt that, although assuming N_z to be constant is not strictly correct from theoretical considerations or observations, enough people have obtained adequate results from this assumption to justify its use here. Also, introducing two or more new coefficients instead of the original one puts more stress on the accuracy of the field data. Furthermore, when the closed-form solution is derived it will be supported by field data.

Integrating Equation (4.22) again with respect to z gives,

$$u(z) = (K_w w_s^2 \cos \theta |\cos \theta| z + gz(\frac{z}{2} - d) \frac{\partial \eta}{\partial x})/N_z \quad (4.24)$$

The final condition left to use is that there is zero net flow through any cross section,

$$\int_0^d u(z) dz = 0 \quad (4.25)$$

Applying this condition to Equation (4.24) gives,

$$\frac{\partial \eta}{\partial x} = \frac{3}{2} \frac{K_w w_s^2 \cos \theta |\cos \theta|}{gd} \quad (4.26)$$

and substituting back into Equation (4.24)

$$u(z) = \frac{1}{4} K_w w_s^2 \cos \theta |\cos \theta| z(\frac{3z}{d} - 2)/N_z \quad (4.27)$$

This is essentially the same result arrived at by Cooper and Pearce [1977] with a change of axis and has the parabolic form shown in Figure 4.4.

Equation (4.27) can readily be modified for a trapezoidal prismatic dead-end canal to satisfy Equation (4.25), the zero net flow condition, by multiplying the function by a ratio of the top width, B , to the width of the channel at the desired elevation, giving,

$$u(z) = \frac{1}{4} \bar{B}(z) K_w w_s^2 \cos \theta |\cos \theta| z(\frac{3z}{d} - 2)/N_z \quad (4.28)$$

where

$$\bar{B}(z) = (b + d(s_L + s_R)) / (b + z(s_L + s_R)) \quad (4.29)$$

where

b = bottom width (L)

s_L, s_R = inverse side slopes of left and right banks, respectively
(dimensionless).

For a layered model in which the velocity is integrated over a cell from $z = d_1$ to $z = d_2$, this correction factor is then based on the cross-sectional area of each layer. Hence for layer k , the wind induced vertical velocity profile is written,

$$u_k = \frac{1}{4} \bar{A}(k) K_w w_s^2 \cos \theta |\cos \theta| \left[d_2^2 \left(\frac{d_2}{d} - 1 \right) - d_1^2 \left(\frac{d_1}{d} - 1 \right) \right] / N_z (d_2 - d_1) \quad (4.30)$$

where

$$\bar{A}(k) = \frac{(2b + (d + d_{-1})(s_L + s_R)) (d - d_{-1})}{(2b + (d_1 + d_2)(s_L + s_R)) (d_2 - d_1)} \quad (4.31)$$

where

d_{-1} = elevation of base of top layer (L).

From Equation (4.28), an apparent anomaly arises. This is that as the depth increases, the magnitude of the surface velocity also increases as a linear function of the depth. This would therefore result in surface velocities that were greater than the wind speed itself if the canal were made deep enough. Thus, the assumption of a constant vertical momentum transfer coefficient, N_z , is in doubt, and would suggest that if the coefficient is not a function of z , then perhaps it is a function of the total depth, d . It would then be a constant throughout the water column for any given depth.

Looking at Equation (4.28), the vertical velocity profile is described by,

$$u(z) \propto \frac{z}{N_z} \quad (4.32)$$

As it would be reasonable to expect that the surface displacement of fluid would be proportional to the square of the wind speed rather than the flow depth, N_z is assumed to be a linear function of the depth in the form,

$$N_z = \bar{N}_z d \quad (4.33)$$

where

\bar{N}_z = network constant defined by the above equation (L/T).

Substituting in Equation (4.30), the model form of the wind induced vertical velocity profile is obtained,

$$u_k = \frac{1}{4} \bar{A}(k) K_w w_s^2 \cos \theta |\cos \theta| \left[d_2^2 \left(\frac{d_2}{d} - 1 \right) - d_1^2 \left(\frac{d_1}{d} - 1 \right) \right] / \bar{N}_z d (d_2 - d_1) \quad (4.34)$$

For a wind induced circulation model with tidal flow, Equations (4.34) and (4.31), superimposed on the tidal flow Equation (4.12), are used to describe the velocity field.

Figure 4.5 shows a typical measured profile in the 57 Acres canal network (Figure 3.2). Superimposed on the observed data are two plots which represent Equations (4.27) and (4.28), the vertical velocity distribution without and with the width correction factor. It can be seen that the introduction of the correction factor gives a good fit between the theoretical and observed profiles and serves to calibrate \bar{N}_z and N_z used in the three-dimensional model.

One final problem remains, and that is the length of time a change in the wind requires to set-up the induced circulation discussed above. There appears to be little or no discussion on this in the literature, and the data gathered for this report is not long enough to identify the differences between fully developed conditions and the period of set-up. The theory described above is for a fully developed flow and can be calibrated directly only if the measured profile is also fully developed. The ultimate calibration is to run the model between successive periods of dye concentration sampling, and fit \bar{N}_2 to obtain the best fit.

To account for the period of set-up, a time constant can be read into the model over which the wind speeds and directions are averaged, and a resultant vector obtained. The parameter may also be used to calibrate the model. However, it seems fairly clear that the value of this parameter must fall into a certain range. An upper limit to this value would reasonably be expected to be one-quarter of the tidal cycle as changes in the direction of flow for diurnal or semidiurnal tides would tend to break up the set-up.

4.4 Secondary Currents

The secondary current is an important phenomenon in mass transport because it usually offers the quickest means by which parcels of fluid can be transferred to the surface. Even though the velocities associated with this effect are small relative to velocities occurring along the channel, the length scales relative to the length of the channel are even smaller, and thus the time scale is also smaller.

This means that on an average, a parcel of fluid will reach the surface quicker due to secondary currents than due to upwelling in junctions, at dead-ends or at tidal entrances.

The importance of this action is that it transfers fluid from the benthic layer at the bottom of the channel to the surface where it may be reoxygenated, and then transfers it back down to the bottom as the secondary flow persists. This sometimes anoxic water is then "refreshed" and returned to the bottom where it can help cope with the oxygen demand.

The main cause of secondary currents is bends. These occur naturally in open watercourses and usually provide sufficient turnover to prevent stagnant zones of inactive water. However, in many of the man-made canal networks, the reaches are long and straight, particularly the dead-end reaches, and although secondary currents have been found to exist in straight channels, the magnitude of the associated radial component of the velocity is very much smaller than in bends. Thus, it has been observed that anoxic conditions frequently exist in the dead-ends of canal networks, and that when the waters are turned over by a strengthening or shifting wind, pungent odors are sometimes released, much to the chagrin of the residents.

In these straight canals, one method that has been suggested to improve water quality is to stagger roughness elements along each side of the channel to deflect the flow [Swenty, 1977; Parr and Christensen, 1977]. This has the effect of creating a series of bends, and of increasing the effective vertical diffusion coefficient, and the longitudinal dispersion coefficient. Of course, in this layout, the adjacent roughness element creates a helical flow in the opposite direction to

the previous element and returns the fluid parcel to the bed. To overcome this, Christensen and Snyder [1978] suggested an improvement would be to have a continuous bend in one direction causing a helical flow that would persist through the length of the canal and whose direction of rotation would only change with the tide. He theorized that an Archimedian spiral in the direction of the Coriolis effect would accomplish this.

A secondary current is produced when a water column is subjected to a transverse force in a bend. This force is called the centrifugal force, which is a reaction, by Newton's third law, to the centripetal force produced by the bend on the flow. Figure 4.6 shows diagrammatically that when this force, which acts uniformly over the entire water column in a rectangular channel, is retarded at the bed by a friction force, a circulation is set up with the top layer moving towards the outside of the bend and the lower layer moving inward to conserve mass. When this circulatory pattern is superimposed on a longitudinal flow, a helical flow distribution is found (Figure 4.6).

In straight channels, the secondary currents are thought to be caused by the transport of momentum from the center to the sides, as Prandtl intuitively explained it [Ikeda and Kikkawa, 1976], but the mechanism is still not fully understood. The phenomenon has frequently been observed, but it was difficult to quantify because of the small scale of the flow. The usual method was to observe its effect on suspended sediments [Vanoni, 1946] or sand grains [Wolman and Brush, 1961]. With modern instrumentation such as the hot wire anemometer, more accurate measurements are possible, and tend to agree with

Nikuradse's findings [1933] that the largest secondary currents are measured in the corners of the channel.

Recently several theoretical and numerical studies have been undertaken with varying degrees of success [Chiu and Lee, 1971; Ikeda and Kikkawa, 1976]. The latter authors compared their results for secondary flows in a corner with measurements obtained by Brundrett and Baines [1964], and found that they overestimated the magnitude of the velocities by 50-100 percent. For a wide channel, they found that

$$\frac{v}{u^*}, \frac{w}{u^*} > 0.2 \quad (4.35)$$

where

v = lateral velocity components (L/T)

w = vertical velocity component (L/T).

Thus from Equation (4.5),

$$v, w > 0.024u \quad (4.36)$$

For Florida canals where tidal velocities on the order of 0.1 ft/sec are common, the lateral and vertical velocity components are at the threshold level of even the electromagnetic current meters, and smaller than any error term associated with lateral or vertical diffusion. Also, if the banks are sloping, the radial velocities are even smaller. Therefore, secondary currents in straight channels will not be considered, but rather the attention of this study will focus on the circulation due to bends.

The flow of water in bends is the subject of an extensive work by Rozovskii [1957]. He considered a logarithmic vertical velocity profile and derived the radial velocity component and an expression for

the length over which this value decays after the curve ends. The question is whether such an analysis can be applied to a velocity field which includes flow reversals due to wind set-up or saline density flows.

Firstly, there appears to be no literature which attempts to derive a theoretical form for the secondary current in a bend under the influence of a velocity field with a flow reversal. Such a form, which would probably require a separate dissertation at least, is beyond the scope of this report, and as pointed out in the introduction, to model this effect using the full equations of continuity and momentum requires more of the model than the data collection methods can provide. So it is necessary to look to an intuitive argument that attempts to explain the physics of the secondary current process.

Looking at a flow reversal due to a wind set-up or salinity density current, in which there is no tidal action, there is zero net transport through any section. In the bend, secondary currents will then be initiated separately in the top and bottom layers but will act in the same rotational sense when viewed along the longitudinal x -direction. Because of the condition of zero net flow through any section, it is then argued that the two rotational flows will tend to cancel each other out as the momentum associated with each layer (Equation (4.28)) is the same. Therefore, as it was assumed that as the closed form solutions for the velocity field could be superimposed, it follows that the same can be done for the secondary current effect. The only remaining nonzero net effect is then the tidal fluctuation which has a logarithmic vertical velocity profile, consistent with Rozovskii's basis of analysis.

Rozovskii [1957, Ch. 2] considered the linear shear stress distribution that results in a logarithmic vertical velocity profile in turbulent flow in a wide channel, and developed an equation for the radial component of velocity,

$$v = \frac{1}{\kappa^2} u \frac{d}{r} [F_1(\eta) - \frac{\sqrt{g}}{\kappa C} F_4(\eta)] \quad (4.37)$$

where

κ = von Karman's constant = 0.4 (dimensionless)

r = radius of bend (L)

η = z/d , dimensionless depth

C = Chezy's coefficient

and

$$F_1(\eta) = \int 2 \frac{\ln \eta}{\eta-1} d\eta \quad (4.38)$$

$$F_4(\eta) = \int \frac{\ln^2 \eta}{\eta-1} d\eta + 0.8(1 + \ln \eta) \quad (4.39)$$

This is the form of the radial velocity for a rough bed, and differs from the form which Fischer [1969] quoted incorrectly in the second term of Equation (4.39). Without this term, Equation (4.37), with $F_2(\eta)$ now instead of $F_4(\eta)$, is the form for the radial velocity with a smooth bed.

Using Chezy's equation in the form,

$$u = C(RS_f)^{1/2} \quad (4.40)$$

then from Manning's Equation (4.3),

$$C = 8.25 \sqrt{g} \left(\frac{R}{k}\right)^{1/6} \quad (4.41)$$

Again as $R \approx k$ and the ratio is raised to the 1/6 power, Chezy's coefficient can be written,

$$C = 8.25 \sqrt{g} \quad (4.42)$$

Thus, Rozovskii's expression for the radial velocity component is written,

$$v = 6.25 u \frac{d}{r} [F_1(\eta) = F_4(\eta)/3.3] \quad (4.43)$$

Equations (4.38) and (4.39) cannot be solved as indefinite integrals because of the singularities at $\eta = 1$. Rather they may be solved using a numerical integration scheme tending towards the singularity. The results of this integration are given in Rozovskii [1957, p. 42]. Consider the integrand of Equation (4.38),

$$\frac{\ln \eta}{\eta - 1} = \frac{\ln(\eta - 1 + 1)}{\eta - 1} = \frac{\ln(p + 1)}{p} \quad (4.44)$$

defining

$$p = \eta - 1$$

Using an infinite series expansion for the natural logarithm,

$$\frac{\ln(p + 1)}{p} = \sum_{i=0}^{\infty} \frac{(-p)^i}{(i + 1)} \quad (4.45)$$

which is valid for $0 < p \leq 1$. Integrating,

$$\int \frac{2 \ln \eta}{\eta - 1} d\eta = \int \frac{2 \ln(p + 1)}{p} dp = 2 \sum_{i=1}^{\infty} (-1)^{i+1} \frac{p^i}{i^2} + a_0 \quad (4.46)$$

where

$$a_0 = \text{constant of integration.}$$

Matching with the curve in Rozovskii [1957, p. 42], $a_0 = 1.29$, and thus,

$$F_1(\eta) = 2 \sum_{i=1}^{\infty} (-1)^{i+1} \frac{p^i}{i^2} + 1.29 \quad (4.47)$$

As it stands, Equation (4.47) requires about thirty terms to be accurate to two decimal places. However, for a layered model, $F_1(\eta)$ is integrated over each layer to produce an average value, $\bar{F}_1(k)$ given by,

$$\bar{F}_1(k) = \left[2 \sum_{i=2}^{\infty} \frac{(-p)^i}{i^2(i+1)} + 1.29 p \right] \frac{n_2^2}{n_1^2(n_2 - n_1)} \quad (4.48)$$

where

$n_1, n_2 =$ lower and upper dimensionless depths of layer.

This form requires only about five terms to achieve the same degree of accuracy.

As given by Equation (4.39), $F_4(n)$ is much more difficult to reduce to a similar form because integrations are required for terms like $p^i \ln p$, where i is an integer. Thus, it was decided to fit a parabola to its shape given by Rozovskii [1957, p. 42] in the form,

$$\bar{F}_4(n) = -2.88 + 9.36n - 5.19n^2 \quad (4.49)$$

This form was based on the given values of $F_4(n)$ at $n = 0.1, 0.5,$ and 1 so that when layer averaging was performed, errors would tend to cancel out to some degree. Thus, the layer average form of Equation (4.49) is,

$$\bar{F}_4(k) = \left[-2.88n + 4.68n^2 - 1.73n^3 \right] \frac{n_2^2}{n_1^2(n_2 - n_1)} \quad (4.50)$$

The form of the radial velocity given in Equation (4.43) applies in the length of the curved portion of the bend only. Downstream this value decays to almost zero in a distance, L_d , given by Rozovskii [1975, p. 111] as,

$$L_d = \frac{C^2 d}{2g} \ln \frac{\kappa}{P} \quad (4.51)$$

where

$P =$ permissible deviation from the background velocity.

For this model, P was chosen to be 0.02, and writing Chezy's C in terms of Nikuradse's equivalent sand roughness, k , Equation (4.51)

becomes, using Equations (4.4) and (4.5),

$$L_d = \frac{8.25^2 d}{2} \ln(0.4/0.02) = 102d \quad (4.52)$$

Over the decay distance, L_d , the radial velocity decays exponentially to within 100p percent of 0 from its maximum value. $p = 0.02$ was chosen because the decay is then the same type of decay used to describe the flood tide boundary condition for the one-dimension model (Section 3.1.5). With this form, the radial velocity at any point of distance x away from the curved portion of the bend, and less than the decay distance, L_d , is given by,

$$v(x) = v \exp(-3x/L_d) \quad (4.53)$$

This velocity can then be averaged over the length of a cell in which it acts to produce the model from of the lateral velocities due to secondary currents.

Good agreement was found between theoretical and observed radial velocities as seen in Figure 4.7. Here the velocities were measured just downstream of the crown of the bend in the south loop of the 57 Acres system (Figure 3.2), and were compared with those obtained theoretically from Equation (4.43). In each case, velocities on the order of 0.05 ft/sec were found, which is sufficient to cause a considerable amount of overturning of the water.

4.5 Density Induced Currents

In Section 4.4, the equations were developed for the velocity field under the influence of the wind shear stress and tide alone. This development of the hydrodynamics is valid for situations in which there is vertical homogeneity of nonpassive substances, such as saltwater. This situation is likely to be found in a canal network linked directly

to the Intracoastal Waterway of ocean, or above the region of influence of the saltwater in a river estuary. However, in the transition region, the hydrodynamics will be affected by saline wedges intruding and re-treating in the canal networks. McKeehan [1975] considered this to be the most significant effect in understanding the hydrodynamics of this type of canal network.

Most numerical models of stratified flow in fact only model the salt through a mass-transport equation, neglecting the effect of the density gradients on the continuity and momentum equations [King, Norton, and Orlob, 1973; Hess and White, 1974]. This is a fair approximation if the flow is continuously stratified, but cannot be applied to the situation of a salt wedge in a canal because of the discontinuity in the density at the interface between the fresh and saltwaters. There has been a good deal of work done in trying to analyse the movement of a wedge, but mostly this is based on empirical formulae from laboratory and field measurements [Keulegan, 1958], or using grossly simplified equations to model the front of the wedge. Very little work has been done in numerical modeling the governing equations incorporating the density terms, except by people like Leedertse and Liu [1975]. However, this type of model is firstly, very expensive to run, and secondly, its accuracy in tidal canals is doubtful because of the nature of the unknowns, such as bank and bed roughness, being modeled.

The mechanics of a saltwater wedge are depicted in Figure 4.8 and an example from the data collected on the Loxahatchee River (Figure 3.3) shown in Figure 4.9. As the tide floods, a predominantly linear wedge intrudes into the canal. The forcing function for this wedge is the rising saltwater surface in the receiving waterbody. As the tide ebbs, the

saltwater surface in the receiving waterbody falls, and the saltwater wedge in the canal recedes as the wedge loses the potential energy it gained during the flood tide.

The mechanism is very similar to that of a flood wave going overbank onto a flood plain [Walton and Price, 1975]. As the water rises overbank, the flow onto the flood plain is controlled by the dynamic wave that is the flood wave. As the water level in the main channel drops, the velocities associated with flow off the flood plain are then governed by bottom slope and friction. This is called the kinematic wave [Lighthill and Whitham, 1955].

The mechanism becomes even more complicated when a wind shear is applied at the water surface. The difficulties in deriving an accurate theoretical foundation for these complex interactions, dictate that an empirical derivation be investigated to match the conditions observed in the field.

With this in mind, the induced flow in a dead-end canal of a saltwater wedge in a tideless sea was considered. Under these conditions the net mass flux through any cross-section is zero. Studying the form of the saltwater wedge shown in Figure 4.9, the following assumptions were made (and shown in Figure 4.8),

1. the vertical velocity profile, $u_s(z)$, in the wedge is parabolic,

$$u_s(z) = u_1 z^2 \quad \text{for} \quad 0 \leq z \leq d_s \quad (4.54)$$

where

u_1 = constant depending on flow conditions (1/LT)

d_s = depth of wedge (L)

2. the induced counter-flow in the freshwater layer, $u_f(z)$, above the interface is constant,

$$u_f(z) = u_2 \quad \text{for} \quad d_s < z \leq d \quad (4.55)$$

where

$$u_2 = \text{constant } (L/T).$$

The parabolic vertical profile was chosen firstly, because it seems to be in fairly good agreement with measured data. The second reason is that there is only the one calibration coefficient, u_1 , (as u_2 can be found from conservation of mass). If a logarithmic form were chosen, which is certainly more expected, the model would have to be calibrated with not only a coefficient of proportionality, but also with a Nikuradse's equivalent sand roughness, k , which would depend on flow conditions within the wedge. Moreover, the parabolic profile is a reasonable approximation to the logarithmic profile, particularly when it is remembered that integrations are taking place to average conditions over vertical layers.

Keulegan [1958] showed that the velocity of the front of an advancing salt wedge in a tideless sea was a function of several parameters expressed as,

$$\frac{u_F}{u} = f\left(\frac{L_w}{d}, \frac{u_\Delta d}{\nu}, \frac{d}{B}\right) \quad (4.56)$$

where

L_w = length of advancing front (L)

ν = kinematic viscosity (L^2/T)

$f(\)$ = function of ()

and

u_Δ is the densimetric velocity expressed by,

$$u_{\lambda} = \left(\frac{\Delta \rho}{\rho} g d \right)^{1/2} \quad (4.57)$$

In a series of experiments measuring the frontal velocity of the wedge for the case in which two immiscible liquids were initially separated by a vertical barrier which was removed at time $t = 0$, he derived several formulae for the various values of the ratio d/B . For $d/B = 2$, he proposed,

$$\frac{u_F}{u_{\Delta}} = (1.75 + 0.16 \left(\frac{u_{\Delta} d}{v} \right)^{-1/4} \frac{L_w}{d})^{-1} \quad (4.58)$$

An examination of this formula, however, suggests that this may not be a good equation to use to describe the movement of a salt wedge in these prototype conditions. The reason for this is that u_F , expressed in this manner, can vary dramatically with changes in L_w and d . In dead-end canals, the salt wedge may impinge on the dead-end thus altering the character of the flow. Also if a wedge is entering the canal during a flood tide and there is already the remnant of a salt dome left from the previous tidal cycle, then d becomes difficult to define as the velocity field acts throughout the column of salt water.

A better form here might be a dependence on the slope of the interface. If a fluid in a closed frictionless basin is elevated at one end forming a sloping surface, and then released, a simple harmonic motion is set up as the rate of fluctuation of the surface is faster than the time the fluid takes to reach terminal velocity for a given acceleration. In a damped system, such as the movement of a saltwater wedge in a freshwater system over a rough bed, terminal velocities are reached much more quickly than the rate of response of the interface. Thus the velocity of the fluid is controlled by the component of the

gravity term in the horizontal direction, which is proportional to the size of the angle the interface makes with the horizontal. Thus, the mean velocity, u_{sm} , at any vertical section in the wedge is given by,

$$u_{sm} = u_3 u_{\Delta} \sin \phi \quad (4.59)$$

where

$$u_s = \text{constant (L/T)}$$

ϕ = angle between interface and positive x-direction
(degrees).

From Equation (4.54), the mean velocity at any vertical section in the wedge may also be written,

$$u_{sm} = \frac{1}{d_s} \int_0^{d_s} u_1 z^2 dz \quad (4.60)$$

Integrating and substituting Equation (4.59) into the resulting expression gives,

$$u_1 = 3 u_3 u_{\Delta} \sin \phi / d_s^2 \quad (4.61)$$

Thus, the vertical velocity profile can be written,

$$u_s(z) = 3 u_3 \left(\frac{\Delta \rho}{\rho} g d_s \right)^{1/2} \sin \phi \left(\frac{z}{d_s} \right)^2 \text{ for } 0 \leq z \leq d_s \quad (4.62)$$

Finally, the counter-flow velocity in the freshwater layer above the wedge, u_f , can be written from Equation (4.59), to conserve mass, as,

$$u_f = -u_3 \left(\frac{\Delta \rho}{\rho} g d_s \right)^{1/2} \sin \phi / (d/d_s - 1) \quad (4.63)$$

The expressions developed in Equations (4.62) and (4.63) are continuous forms of the vertical velocity profile for a channel of uniform width. To extend these expressions to the three-dimensional

model, an averaging process and a width correction factor are used in exactly the same way as described for the wind induced circulation case in Section 4.3.

Unfortunately, on programming, the method was found to be very unstable. This was due to the variability of the $\sin\phi$ term in Equations (4.62) and (4.63). If a sharp discontinuity appears in the longitudinal profile, the velocity term associated with the flow between adjacent cells can become very large and draw most of the fluid from one of the cells. At the next time step fluid from adjacent cells on either side flows in and the discontinuity becomes even bigger than before. Furthermore, attempts to damp out the instability merely defined the damping term as the condition determining the profile, thus overriding the governing equation.

It was felt that the problem was due to the specification of the angle ϕ locally. In fact, it should more realistically be the slope of the saltwater surface out in the receiving water, particularly during the flood tide, and thus the densimetric velocity, u_{Δ} , would have to be a function of the depth of the receiving water. Clearly, this is not an easy thing to measure, and the ebb tide expression remains unclear. Thus, an alternative expression was sought.

A much simpler condition, and probably a more accurate expression for the flood tide case, would be a mean velocity at the tidal entrance, u_{smTE} , proportional to the rate of rise of the interface at that point in a similar manner to a dynamic flood wave going overbank in a river [Walton and Price, 1975],

$$u_{smTE} = u_4 \frac{dd_s}{dt} \quad (4.64)$$

where $u_4 = \text{constant}$ (dimensionless).

If the salt wedge is assumed to take its simplest form, a triangular distribution, a theory can be developed to predict its passage through the reaches of a canal network. Consider a single rectangular, prismatic canal (the model can easily be extended to a trapezoidal cross-section, but is not done so here to simplify the equations), then during the flood tide, the length of the wedge, L_w , before it impinges on a dead-end is given by,

$$L_w = 2 u_4 d_{sTE} \quad (4.65)$$

where

d_{sTE} = elevation of saltwater interface at tidal entrance
above its low tide value (L)

and the depth at any point, d_s , is

$$d_s = d_{sTE} \left(1 - \frac{x'}{2u_4 d_{sTE}} \right) \quad (4.66)$$

where

x' = distance from tidal entrance (L).

From the linearity of the governing equation then, the mean velocity in the wedge, u_{sm} , at x' is,

$$u_{sm} = u_4 \frac{dd_s}{dt} \quad (4.67)$$

Now from Equation (4.60),

$$u_1 = 3 u_{sm} / d_s^2 \quad (4.68)$$

thus from Equations (4.54), (4.67), and (4.68), the vertical velocity profile in the wedge is given by,

$$u_s(z) = 3 u_4 \frac{dd_s}{dt} \left(\frac{z}{d_s} \right)^2 \quad (4.69)$$

In a similar manner to Equation (4.63), the velocity in the freshwater layer is written,

$$u_f = -u_4 \frac{dd_s}{dt} / \left(\frac{d}{d_s} - 1 \right) \quad (4.70)$$

Once the wedge impinges on the dead-end of the canal, the elevation of the wedge above its low tide value, d_{sDE} , is given by,

$$d_{sDE} = d_{sTE} \left(\frac{2u_4 d_{sTE}}{L} - 1 \right) \quad (4.71)$$

where

L = length of canal (L).

Then, at any point of distance x' from the tidal entrance, the elevation of the salt wedge above its low tide value is written,

$$d_s = d_{sTE} \left(1 + \frac{2x'}{L} \left(\frac{u_4 d_{sTE}}{L} - 1 \right) \right) \quad (4.72)$$

and the mean velocity through this section is,

$$u_{sm} = u_4 \frac{dd_{sTE}}{dt} \left(1 - \frac{x'}{L} \right) \quad (4.73)$$

As before, from Equations (4.54), (4.68), and (4.73), the vertical velocity profile in the saltwater layer at this section is,

$$u_s = 3u_4 \frac{dd_{sTE}}{dt} \left(1 - \frac{x'}{L} \right) \left(\frac{z}{d_s} \right)^2 \quad (4.74)$$

and the constant velocity in the freshwater layer can be written,

$$u_f = -u_4 \frac{dd_{sTE}}{dt} \left(1 - \frac{x'}{L} \right) / \left(\frac{d}{d_s} - 1 \right) \quad (4.75)$$

For the ebb tide, the analogy with the flood wave returning in-bank as the flood wave recedes may be followed. Here, the velocity of the kinematic wave is proportional to the depth and thus the front

of the wedge remains fixed. The velocities are then induced by the decrease in the interface elevation in response to the rate of fall at the tidal entrance. Assuming to first order, that the interface in the canal remains linear, then the depth at any point of a wedge that does not impinge on the dead-end is,

$$d_s = d_{sTE} \left(1 - \frac{x'}{2u_4 d_{sHT}}\right) \quad (4.76)$$

where

d_{sHT} = elevation of interface of salt layer, above its low tide value, at high tide (L)

and the mean velocity,

$$u_{sm} = \frac{1}{2} \frac{dd_{sTE}}{dt} \frac{(L_w - x')^2}{L_w d_s} \quad (4.77)$$

From Equations (4.54), (4.68), and (4.77), the vertical velocity profile in the saltwater layer is,

$$u_s(z) = \frac{3}{2} \frac{dd_{sTE}}{dt} \frac{(L_w - x')^2}{L_w d_s} \left(\frac{z}{d_s}\right)^2 \quad (4.78)$$

and the freshwater velocity is,

$$u_f = -\frac{1}{2} \frac{dd_{sTE}}{dt} \frac{(L_w - x')^2}{L_w d_s} / \left(\frac{d}{d_s} - 1\right) \quad (4.79)$$

Finally, for the case in which the wedge does impinge on the dead-end, the elevation of the interface above its low tide value and any point x' is given by,

$$d_s = d_{sTE} \left(1 - \frac{2x'}{L} \left(1 - \frac{u_4 d_{sTE}}{L}\right)\right) \quad (4.80)$$

and the mean velocity is,

$$u_{sm} = \frac{dd_{sTE}}{dt} \left(\frac{L - x'}{d_s} \right) \left(1 - \left(1 + \frac{x'}{L} \right) \left(1 - \frac{u_4^d d_{sTE}}{L} \right) \right) \quad (4.81)$$

From Equations (4.54), (4.68), and (4.81), the vertical velocity profile in the saltwater layer is,

$$u_s(z) = 3 \frac{dd_{sTE}}{dt} \left(\frac{L - x'}{d_s} \right) \left(1 - \left(1 + \frac{x'}{L} \right) \left(1 - \frac{u_4^d d_{sTE}}{L} \right) \right) \left(\frac{z}{d_s} \right)^2 \quad (4.82)$$

and the constant velocity in the freshwater layer is written,

$$u_f = \frac{dd_{sTE}}{dt} \left(\frac{L - x'}{d_s} \right) \left(1 - \left(1 + \frac{x'}{L} \right) \left(1 - \frac{u_4^d d_{sTE}}{L} \right) \right) \left(\frac{d}{d_s} - 1 \right) \quad (4.83)$$

This method was extended to the case of the canal network with trapezoidal cross-sections and programmed. Data from the Loxahatchee River (Figure 3.3) was used to test the program, and as can be seen in Figure 4.10, fairly good agreement is found. It will also be seen in Chapter 8 that the transient dye concentration profile is fairly well followed, giving some confidence to the theory.

The Loxahatchee River canals are fairly typical canals on both the east and west coasts of Florida in their geometric features, particularly the length. Thus, it was not possible to study the variability of the coefficient u_4 used in Equation (4.64). This value was calibrated to fit the above test case and is assumed to be a reasonable value for similar canals. However, it is possible that the coefficient is dependent on the length of the canal, and thus if possible it should be calibrated on a similar canal to any design canal considered.

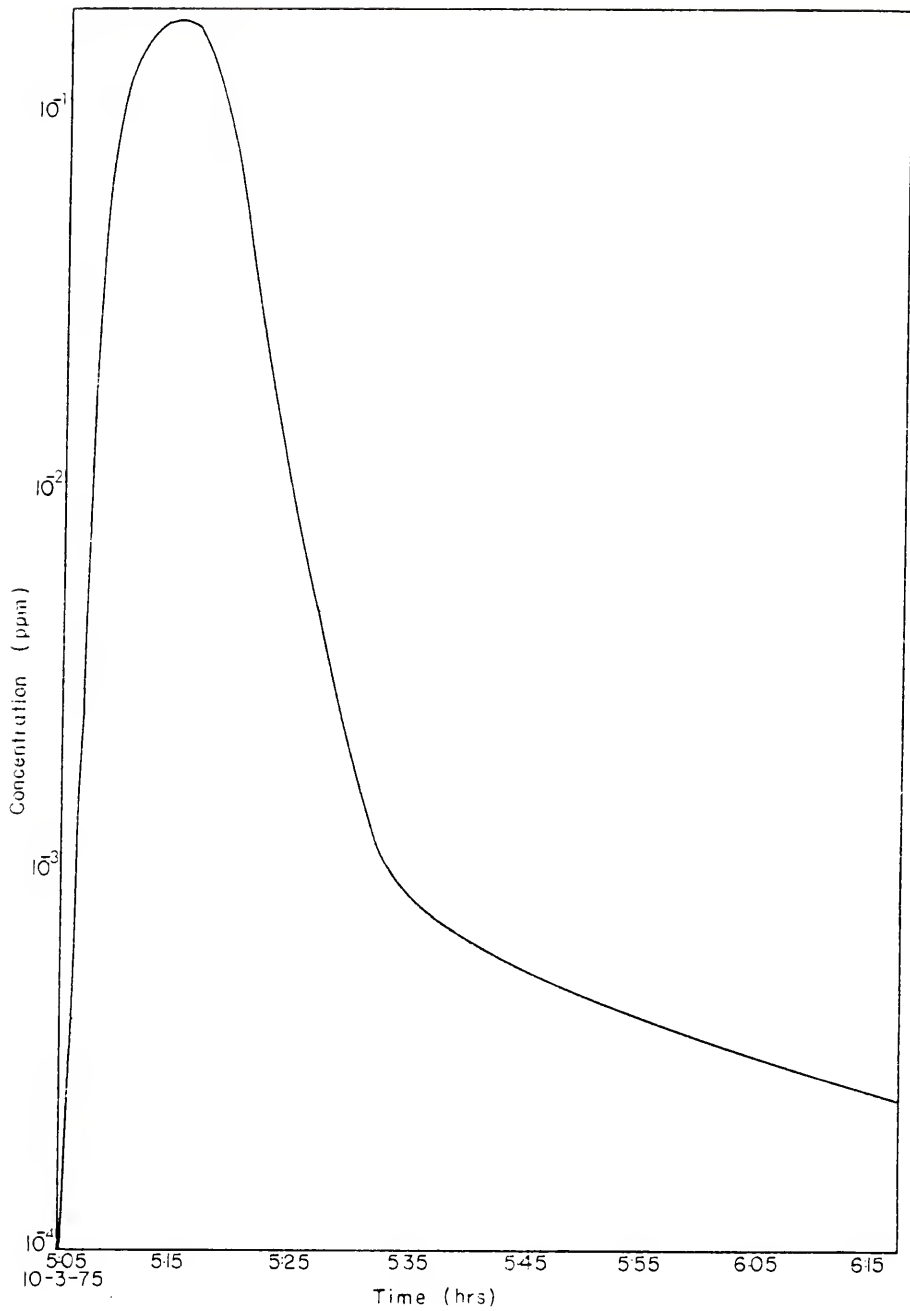


Figure 4.1 - Example of Typical Non-Gaussian Concentration Profile.

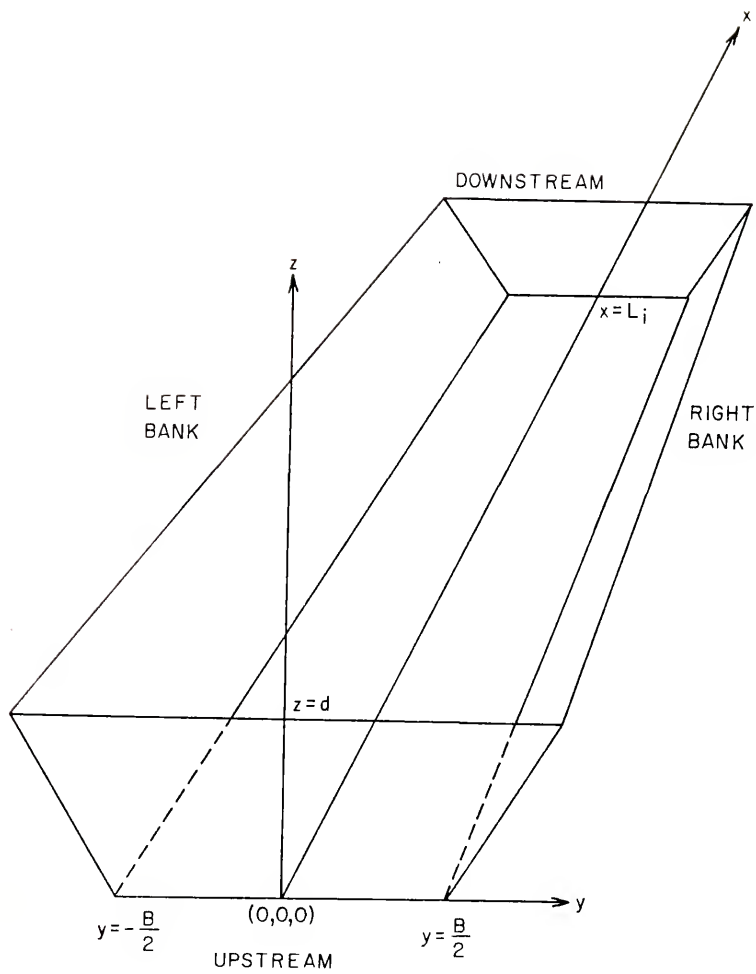


Figure 4.2 - Definition of Coordinate System.

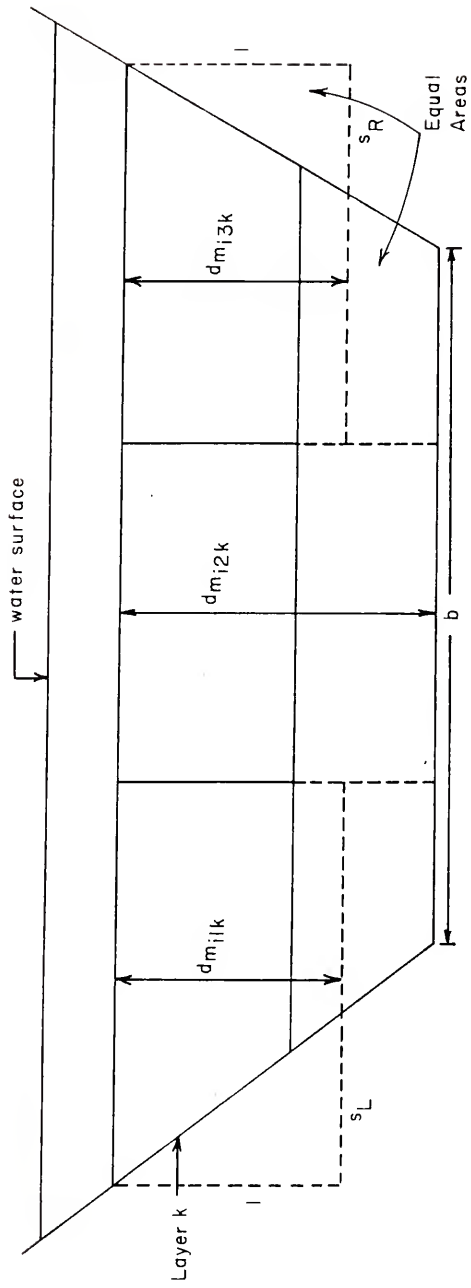


Figure 4.3 - Schematic Drawing of Mean Depths in Lateral Cells of a Vertical Layer.

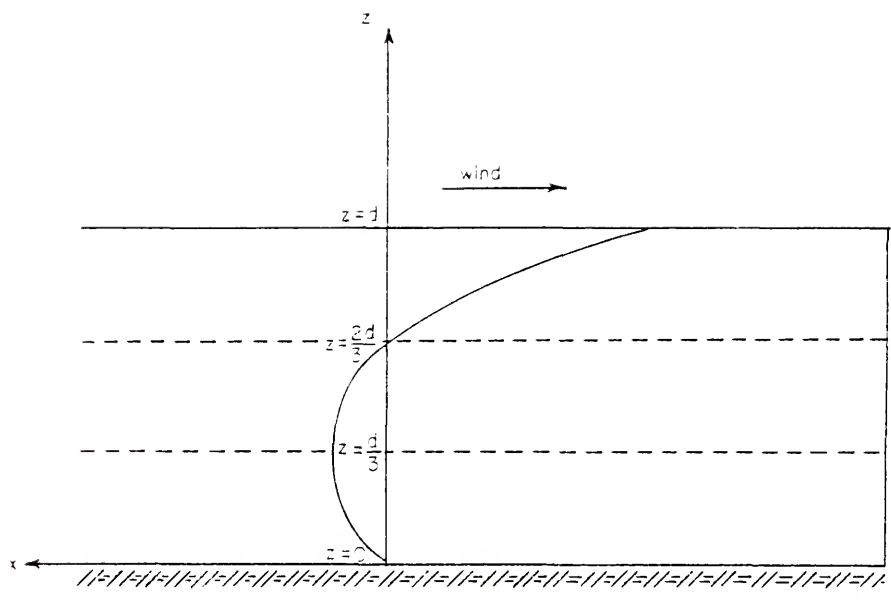


Figure 4.4 - Theoretical Wind-Induced Vertical Velocity Profile.

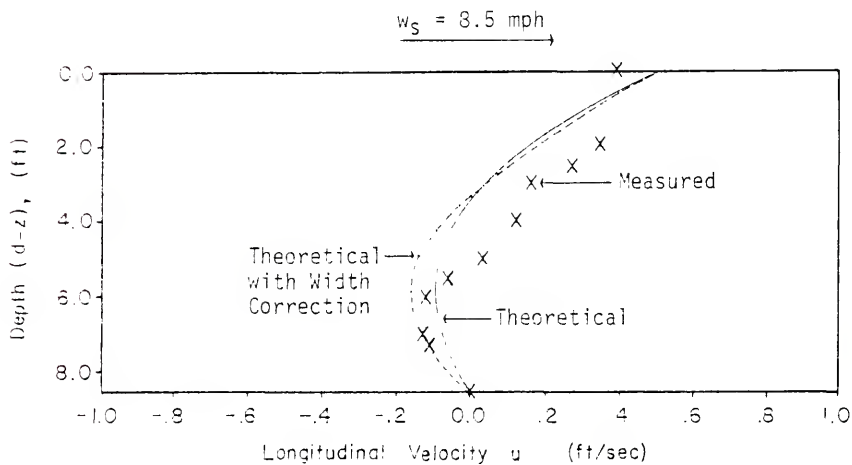
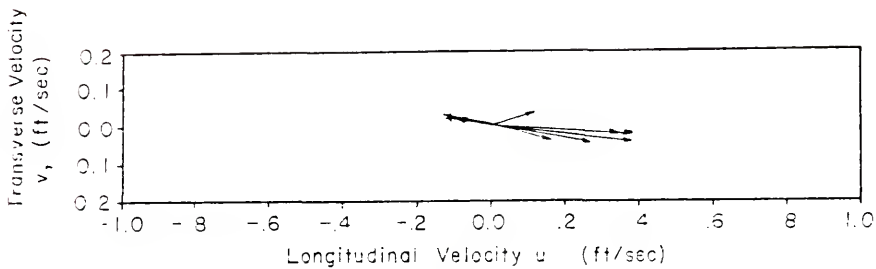


Figure 4.5 - Comparison Between Observed and Theoretical Wind-Induced Vertical Velocity Profiles, With and Without Width Correction ($N_z = 0.002$ ft²/sec) - 57 Acres.

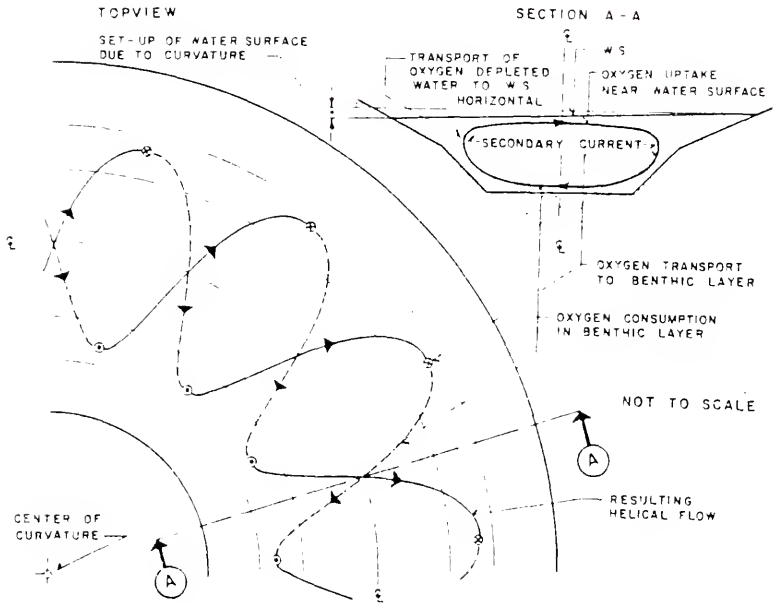


Figure 4.6 - Schematic Drawing of Helical Current Induced by a Bend.

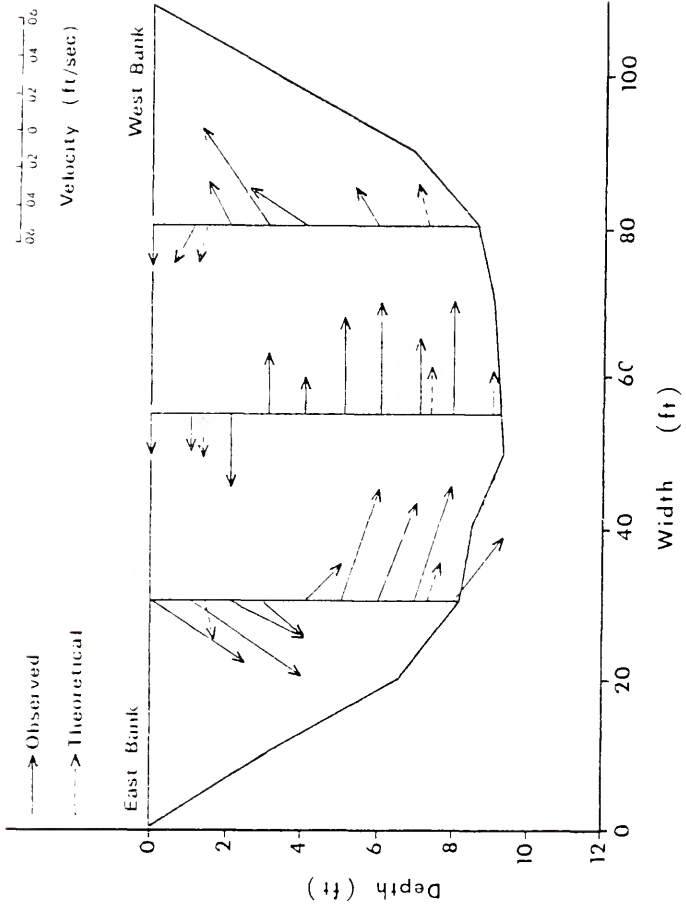


Figure 4.7 - Comparison Between Observed and Computed Lateral Velocities Induced by Bend in South Loop of 57 Acres System.

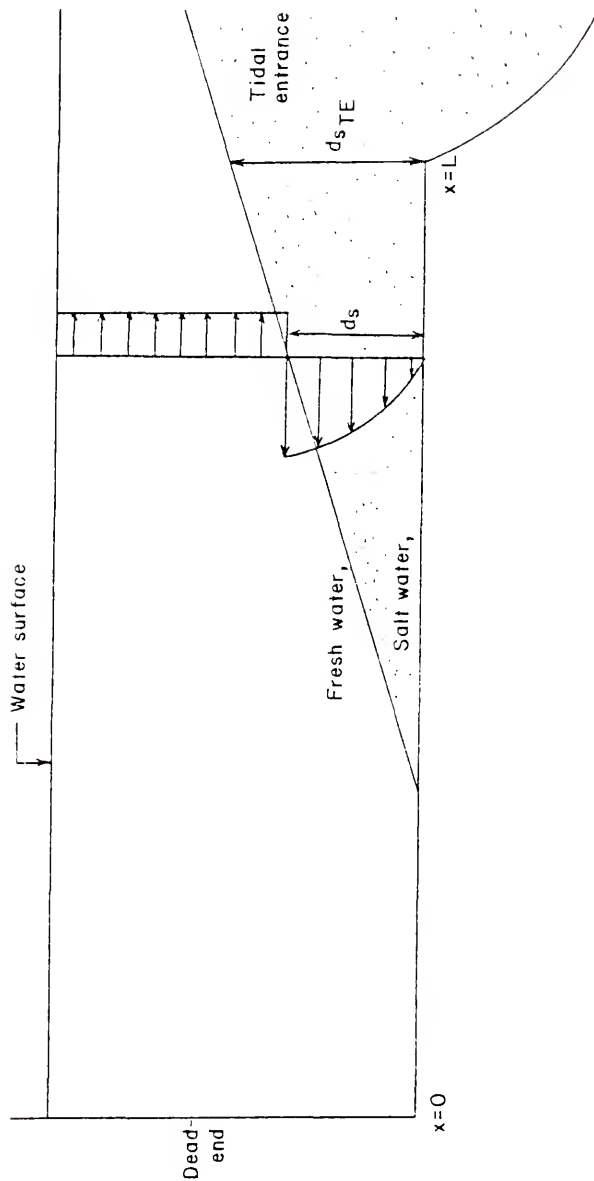


Figure 4.8 - Schematic Drawing of a Salt Wedge Entering a Canal Showing Definitions.

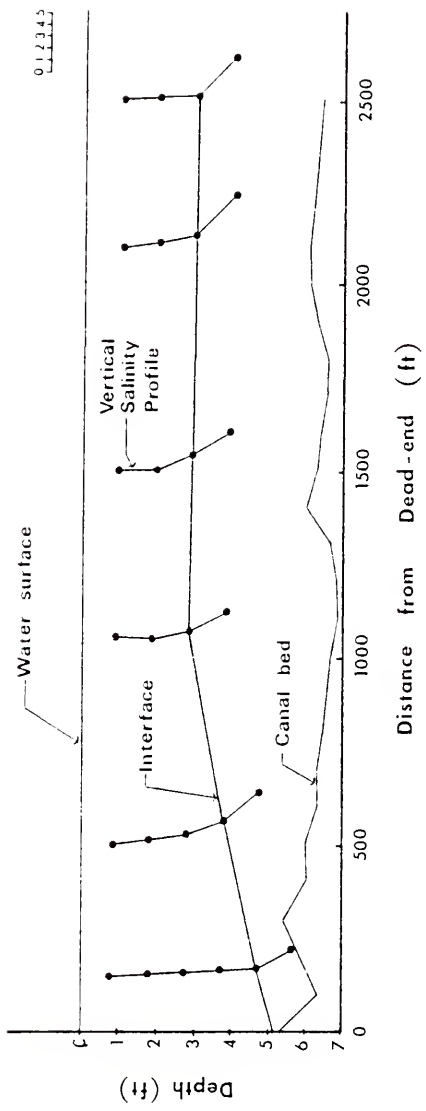


Figure 4.9 - Typical Salinity Profiles in the Loxahatchee River North Canal, Showing Presence of a Saltwater Wedge.

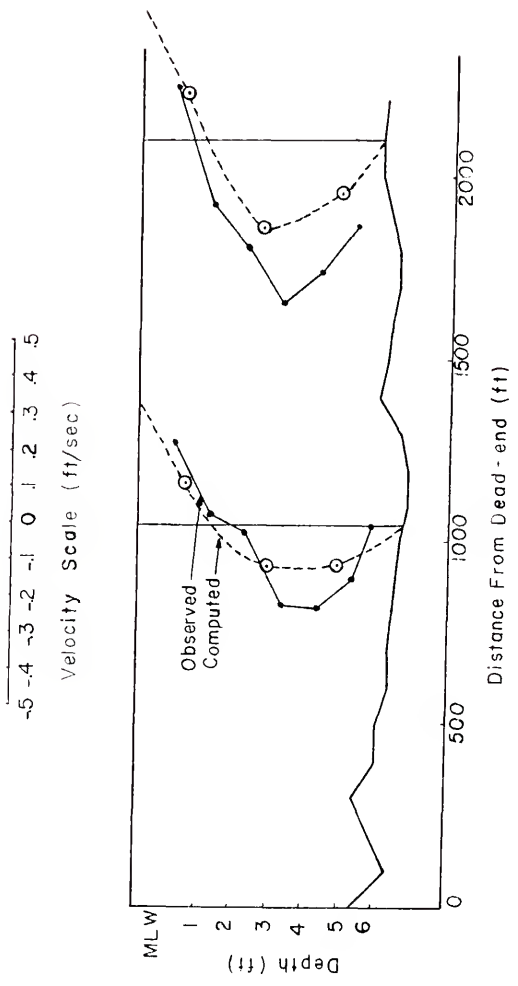


Figure 4.10 - Comparison of Observed and Computed Velocity Profiles for Loxahatchee River Site.

CHAPTER 5

THREE-DIMENSIONAL MASS-TRANSPORT EQUATION

5.1 Transport Mechanisms

The derivation of the three-dimensional mass-transport equation was briefly discussed en route to deriving a one-dimensional model form. The equation was written,

$$\begin{aligned} \frac{\partial c}{\partial t} + \frac{\partial}{\partial x} (cu) + \frac{\partial}{\partial y} (cv) + \frac{\partial}{\partial z} (cw) = \frac{\partial}{\partial x} (E_x \frac{\partial c}{\partial x}) \\ + \frac{\partial}{\partial y} (E_y \frac{\partial c}{\partial y}) + \frac{\partial}{\partial z} (E_z \frac{\partial c}{\partial z}) + r_p \end{aligned} \quad (5.1)$$

The derivation of this equation has been the topic of many works and will be considered without proof as the model transport equation.

The discussion in this chapter rather centers upon the model forms of the three diffusion coefficients, E_x , E_y , and E_z .

It is convenient at this time to introduce the distinction between a diffusion coefficient and a dispersion coefficient used in this report. A *diffusion* coefficient is defined as a coefficient representing a transport analogy which is averaged over a time scale associated with the transport mechanism, such as a molecular time scale or a turbulent time scale. A *dispersion* coefficient is similarly defined as a coefficient representing a transport analogy which is averaged over a length scale associated with the transport mechanism. In the discussion on one-dimensional modeling, a longitudinal dispersion coefficient was obtained by averaging the three-dimensional mass-transport equation over the cross-sectional area. Similarly

dispersion coefficients may be obtained by averaging over just one coordinate direction, or over the length scale of a computational cell. Thus diffusion coefficients are converted to dispersion coefficients by cell averaging, and their associated dimensionless coefficients obtained from field calibration.

The spreading of a substance, such as a dye cloud, involves two component parts which are caused by convection (or advection) and turbulent diffusion. By definition, convection is the transport of a substance with the velocity of the fluid, whereas advection is defined merely as transport in the direction of the flow. The further distinction is made with the meteorological form of convection, which is vertical transport due to thermal gradients. In this report, it is assumed that all substances are transported with the velocity of the fluid and hence convection is being discussed.

The difference between convection and diffusion, or dispersion, is really the scale with which the phenomenon can be measured. If, for example, a substance such as a dye cloud, is instantaneously introduced into a fluid, then its initial transport will be governed by the small time scales associated with turbulent flow, and by spatial variability locally in the velocity field. As the substance begins to spread out under the influence of these small scale eddies, its transport becomes governed by eddies of increasing size up to the size of the largest eddy present in a tidal watercourse, the tide itself.

In the development of Equation (5.1), the diffusive terms on the left hand side of the equation are formed by considering what is called the turbulent fluctuation of the velocity from the turbulent time mean value, \bar{u} , say in the longitudinal direction. Thus

$$u = \bar{u} + u' \quad (5.2)$$

where

u' = instantaneous velocity in x direction (L/T).

Similarly, the fluctuation, c' , from the turbulent time mean value of the concentration, \bar{c} , is written

$$c = \bar{c} + c' \quad (5.3)$$

where

c = instantaneous concentration (dimensionless).

Substitution of terms like these in the initial conservation of mass in an elemental volume [Harleman, 1966], yields terms like $\overline{u'c'}$ which are analogous to Reynolds' stress in turbulent flow.

The use of these terms is to simply say that not enough is known about the true forms of these variables, or that the time interval in the model is greater than the time scale of the turbulent eddies, and so a mechanism must be developed to distribute the substance spatically more than that predicted by following the mean velocity during the time interval.

This is usually done by considering an analogy with Fick's first law of transport due to molecular diffusion. The turbulent analogy is written in the x direction,

$$\overline{u'c'} = - E_x \frac{\partial c}{\partial x} \quad (5.4)$$

and is called the transport due to turbulent diffusion in the

x-direction. Similar expressions are obtained for E_y and E_z , in the y- and z-directions, respectively.

In a similar manner then, as described before, the dispersive transport $E_x \partial c / \partial x$ in a one-dimension model is defined, again using a Fickian analogy. This analogy compensates for the fact that the hydrodynamics are defined in one direction only, and that the spatial variations in the velocity field are providing a three-dimensional transport mechanism.

This idea can be extended to the discretization scheme of any numerical model. Analogous to the mechanism of turbulent diffusion, spatial variations in the velocity field with length scales smaller than the grid size can become lost in the definition of a mean velocity within the grid, unless another dispersion term is established to include this effect. Commonly in three-dimensional models, the turbulent diffusion coefficient in a given direction will be described as a mean of coefficients at the centers of adjacent cells in that direction. This is all right if the variation in the gradient of the velocity field is constant or linear, but for higher order variations the fitting of straight line segments might cause information to be lost, particularly if a coarse grid is being used. To account for this subgrid scale variation, the diffusion coefficients can be adjusted by averaging over the computational cell, thus becoming dispersion coefficients.

Another use of the diffusion term is to account for unknowns in the velocity field. Such an unknown of importance in this study is the circulation at slack tide. Holley and Harleman [1965] were among the first to study the mechanism of dispersion in oscillatory

flow, and developed a form of the longitudinal dispersion coefficient for oscillatory flow based on the work of Taylor [1954] and Elder [1958],

$$E_{\ell} = 20.2Ru^*(t) \quad (5.5)$$

Theoretically, assuming no external forcing functions such as wind or density gradients to exist, E_{ℓ} becomes zero at slack tide. This condition, of course, is unrealistic in tidal canals particularly near the dead-ends of the canals, because it suggests that there is practically no transport taking place at this time. However, it is well known that even during these periods, there is still considerable activity due to eddies whose mechanisms are not entirely understood, but which are probably caused by residual momentum effects or the introduction into the canal systems of oceanic eddies whose time scales are much smaller than the tidal period, but larger than the time scales associated with turbulent fluctuations. In fact, on several field trips, it was felt from some of the velocity readings, that eddies with periods on the order of three seconds were present, which is much larger than turbulent scales, and whose origins were not understood.

With this in mind, a more realistic form of Holley and Harleman's oscillatory dispersion coefficient might be

$$E_{\ell} = 20.2Ru^*(t) + E_0 \quad (5.6)$$

where

$$E_0 = \text{background dispersion coefficient } (L^2/T).$$

In the ensuing sections on the various diffusion and dispersion coefficients, this idea will be incorporated into the model forms of these coefficients.

5.2 Longitudinal and Lateral Diffusion Coefficients

The choice of the model forms of the diffusion coefficients is a difficult one indeed as so many suggested forms have been presented based on "laws" or empirical data merely reflecting our ignorance as to the actual mechanisms operating. Most of these forms are based on assuming that the momentum transfer coefficients, N_x , N_y , and N_z , and the turbulent diffusion coefficients, E_x , E_y , and E_z , are interchangeable. Indeed, there is a foundation of evidence for this assumption based on the work of several investigators [Jobson and Sayre, 1970; Schiller and Sayre, 1973; Dlubac, 1976].

One of the most common of these laws is the so-called "4/3-power law" which is based on the assumption of isotopic turbulence [Richardson, 1926],

$$E_x = k \varrho^{4/3} \quad (5.7)$$

where

k = constant of proportionality ($L^{2/3}/T$)

ϱ = length scale (L).

Isotopic turbulence does not exist in any naturally occurring fluid, but many investigators have gathered data to determine if such a law is approximately valid, or to determine a more realistic form of the power for their data.

One such example is from the work of Okubo [1971], who found that the best fit for his data was

$$E_x = 0.01 \varrho^{1/15} \quad (5.8)$$

From this data, and from the results of other investigators, it appears that the "4/3 power law" gives a good approximation for diffusion in the sea [Christodoulou et al., 1976], however, Zeidler [1976] has

shown that this form of the diffusion coefficient is not acceptable near the shoreline due to bottom and side effects. In canal networks, bottom and side effects are the dominant mechanism affecting the form of the diffusion coefficients, and so the "4/3 power law" method was not used in this study.

Another drawback is the selection of a suitable length scale, l . In canals and rivers this is usually taken to be some characteristic length of the geometry, such as the width, but this could lead to potential errors particularly in tidal canals, due to the presence of a number of eddy sizes ranging from the turbulent scale upward.

The fact that the bottom and side effects are such an important part of the diffusion mechanism, leads us to follow the work of Taylor [1953, 1954], Elder [1959], and Aris [1956] more closely. Their work was more directly affected by the forms of the boundary roughness.

Taylor [1954] showed that for a flow which obeyed the "universal" distribution of velocity in a pipe [Goldstein, 1938, p. 336],

$$\frac{u_m - u}{u^*} = f(z) \quad (5.9)$$

where

$$u_m = \text{mean velocity (L/T)}$$

the longitudinal diffusion coefficient, E_x , could be written,

$$E_x = 0.104 Ru^* \quad (5.10)$$

This form of the longitudinal diffusion coefficient should then hold near any solid boundary, and indeed is assumed to hold for any

velocity field which exhibits logarithmic profiles. The problem arises when the flow is non-logarithmic as evidenced by flow reversals due to wind shear and density gradients. These phenomena occur mainly in the vertical direction and it is argued that, as Equation (5.10) holds near the solid boundaries, it also holds for any horizontal plane in the flow.

For circulation due to wind stress, the vertical velocity profile is only a function of z as shown in Chapter 4. For density flows due to salinity gradients, although lateral uniformity is assumed, the form of the interface is a function of both x and z . However, the interface is a discrete point at which one homogeneous fluid of density ρ_0 is assumed to change to a second homogeneous fluid of density $\rho_0 + \Delta\rho_0$. If it is assumed that an equation like Equation (5.10) holds for each fluid, the solutions can be matched across the interface. Thus the longitudinal diffusion coefficient, E_x , can be written,

$$E_x = K_x Ru^* \quad (5.11)$$

Considering a wide channel in which,

$$R \approx d \quad (5.12)$$

and using Equation (4.5), the longitudinal diffusion coefficient can be written,

$$E_x = K_x du / 8.25 \quad (5.13)$$

Traditionally, the lateral diffusion coefficient, E_y , is related to the longitudinal form by a constant of proportionality. For example, Elder [1959] wrote the lateral diffusion coefficient as,

$$E_y = 0.23Ru^* \quad (5.14)$$

in which he depth-averaged the coefficient and thus produced a

dispersion coefficient. In spite of this fact, a number of people still use Equation (5.14) within a three-dimensional numerical analysis.

The lateral transport mechanism is the same as that discussed in Chapter 4 where the lateral variation in the velocity field was considered. Assuming a logarithmic velocity profile based on the mean depth in the section of flow considered, the mean velocity, v , from one cell to a laterally adjacent cell will be governed by the velocity difference between the cells (Figure 5.1),

$$v \propto u_j - u_{j-1} \quad (5.15)$$

where

$$u_j, u_{j-1} = \text{velocities in laterally adjacent cells (L/T).}$$

Assuming logarithmic velocity profiles,

$$v \propto u^* \ln\left(\frac{d_{m_i}}{d_{m_{i-1}}}\right) \quad (5.16)$$

and hence

$$v \propto u^*$$

Now even though the vertical profiles are not logarithmic, it may be assumed that horizontal profiles are based on lateral logarithmic profiles from the channels' banks. Thus an expression similar to Equation (5.17) can be derived and the interdependence of the longitudinal and lateral velocity profiles shown.

A number of investigators as reported by Fischer [1969] have measured the depth-averaged lateral diffusion coefficient to vary quite considerably. For example, Yotsukura et al. [1970] found the dimensionless diffusion coefficient to be 0.6 for a curved portion of the Missouri River. The fluctuation of the coefficient is undoubtedly due to the fact that secondary current effects were lumped into the diffusion

coefficients and not into the convective terms. In this model, however, an expression for the velocities induced by secondary currents has been included in the model hydrodynamic equations, and so this coefficient should not vary as much as observed by other investigators who do not model this effect.

Accordingly, using a similar argument as before, the form of the lateral diffusion coefficient is

$$E_y = K_y du / 8.25 \quad (5.18)$$

Finally, as suggested in Equation (5.6), a background diffusion coefficient can be used to lump together the effects of unknown eddies occurring during periods of slack tide. However, introducing three different coefficients in the three coordinate directions introduces three new coefficients to be evaluated from the field data collected. This data is considered insufficient in that it is too variable to measure so many diversified effects, and it was decided to assume this coefficient was isotropic. Hence, the model forms for the longitudinal and lateral diffusion coefficients, respectively, are,

$$E_x = K_x du / 8.25 + E_0 \quad (5.19)$$

and

$$E_y = K_y du / 8.25 + E_0 \quad (5.20)$$

where

$$E_0 = \text{background diffusion coefficient } (L^2/T).$$

5.3 Vertical Diffusion Coefficient

The theory that was used to obtain the longitudinal and lateral diffusion coefficients, in Section 5.2, cannot be used here throughout the vertical water column except in rare cases in which the vertical

velocity profile is fully logarithmic. However, this is hardly ever the case due to flow reversals from wind shear and density currents associated with saline wedges. Taylor and Elder's theory will only apply to a small region near the bed of the channel in which the flow can be considered logarithmic. Also the parabolic distribution examined by Jobson and Sayre [1970] cannot be used, as it is also based on a logarithmic vertical velocity profile.

As this theory breaks down, and because there is not enough data to derive an empirical formula for the vertical diffusion coefficient, another form must be selected based on some form of mixing length theory. Having rejected the "4/3 power law" approach because it has been found to be invalid near solid boundaries [Zeidler, 1976], a basic approach such as Prandtl's mixing length theory is considered in which the vertical diffusion coefficient can be written,

$$E_z = K_z \ell^2 \left| \frac{du}{dz} \right| + E_0 \quad (5.21)$$

where

K_z = vertical dimensionless diffusion coefficient.

Considering a layered flow because of the discrete cell structure of the numerical solution technique, Equation (5.21) can be integrated over the thickness, d_ℓ , of the layer k , from $z = d_1$ to $z = d_2$, to produce the vertical dispersion coefficient,

$$E_k = K_z \ell^2 \left| \int_{d_1}^{d_2} \frac{du}{dz} dz \right| / d_\ell + E_0 \quad (5.22)$$

which upon integration gives,

$$E_k = K_z \ell^2 |u(d_2) - u(d_1)| / d_\ell + E_0 \quad (5.23)$$

This theory is now considered for the two cases in which a density gradient due to a saline wedge is firstly absent and secondly present, in a tidal flow with associated wind shear.

From Equations (4.9), (4.28), and (4.31), the vertical dispersion coefficient in layer k is given by,

$$E_k = K_z \ell^2 \left| \frac{1}{A} \frac{dV}{dt} \frac{\ln(d_2/d_1)}{\ln(29.73 d/ke)} + 0.25 K_w W_s^2 \cos\theta \right. \\ \left. |\cos\theta| \left((d_2 - d_1) \left(\frac{3}{d} (d_1 + d_2) - 2 \right) \right) / N_z \right| / d_\ell + E_0 \quad (5.24)$$

The only remaining problem is to define the magnitude of the mixing length, ℓ .

In most studies of diffusion, or dispersion, in rivers and estuaries, this number reflects some uniform geometric length scale such as the mean tidal depth or the width of the reach. Because of the parabolic wind profile, Equation (4.28), derived in Section 4.3, whose characteristic features such as the turning value of the vertical gradient at $z = 2d/3$, and its reversal point at $z = d/3$, are based on the one-third points of the depth (Figure 4.4), a more realistic value of the mixing length for tidal flows with wind shear is one-third of the depth. Thus the model form of the vertical dispersion coefficient is written for layer k ,

$$E_k = \frac{K_z d^2}{9d_z} \left| \frac{1}{A} \frac{dV}{dt} \frac{\ln(d_2/d_1)}{\ln(29.73 d/ke)} + 0.25 K_w W_s^2 \cos\theta \right. \\ \left. |\cos\theta| \left((d_2 - d_1) \left(\frac{3}{d} (d_1 + d_2) - 2 \right) \right) / N_z \right| / d_\ell + E_0 \quad (5.25)$$

For the case of tidal flow with wind shear, and a density current induced by a saline wedge an expression for the layer averaged vertical dispersion coefficient, E_k , similar to Equation (5.25) can be

derived by adding the expressions in Equations (4.69)-(4.83) to the above theory. This form of the equation satisfies Equation (5.23) except at the interface between the two fluids. At the interface, an extra term is required to account for the decrease in interfacial mixing as the density difference between the two fluids increases. The rate of mixing across the interface is usually considered to be governed by the Richardson number, Ri , defined as

$$Ri = \frac{-g/\rho \cdot \partial\rho/\partial z}{(\partial u/\partial z)^2} \quad (5.26)$$

The vertical diffusion coefficient averaged over the layer containing the interface, \tilde{E}_k , is then written,

$$\tilde{E}_k = E_k \phi(Ri) \quad (5.27)$$

where

$\phi(Ri)$ = function of Richardson number to be determined
(dimensionless).

A number of investigators have suggested forms for $\phi(Ri)$. Munk and Anderson [1948] wrote,

$$\phi(Ri) = (1 + \frac{4}{3} Ri)^{-1} \quad (5.28)$$

whereas, Bowden and Hamilton [1975] suggested,

$$\phi(Ri) = (1 + Ri)^{-7/4} \quad (5.29)$$

These forms were compared in a paper by Blumberg [1977] (Figure 5.2) who found that for high Richardson numbers, $\phi(Ri)$ became too small and produced unrealistic salinity distributions. Instead he used a form proposed by Obukhov [1971],

$$\phi(Ri) = (1 - 0.1Ri)^{1/2} \quad \text{for } Ri \leq 10 \quad (5.30a)$$

$$\phi(Ri) = 0 \quad \text{for } Ri > 10 \quad (5.30b)$$

by determining numerically that for Richardson numbers greater than ten there was little or no interfacial mixing. Thus the model form of the layer averaged vertical diffusion coefficient for the layer containing the saline wedge is,

$$\tilde{E}_k = E_k (1 - 0.1Ri)^{1/2} \quad (5.31)$$

This form was found to give satisfactory results for this model.

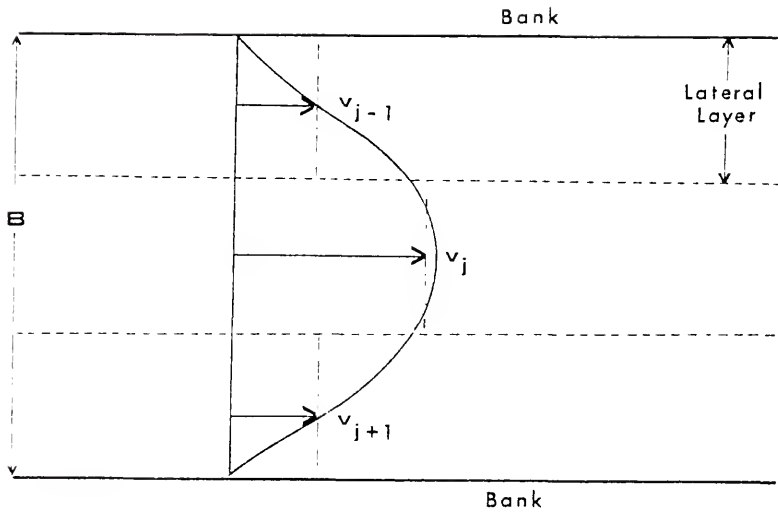


Figure 5.1 - Lateral Variation of Velocity.

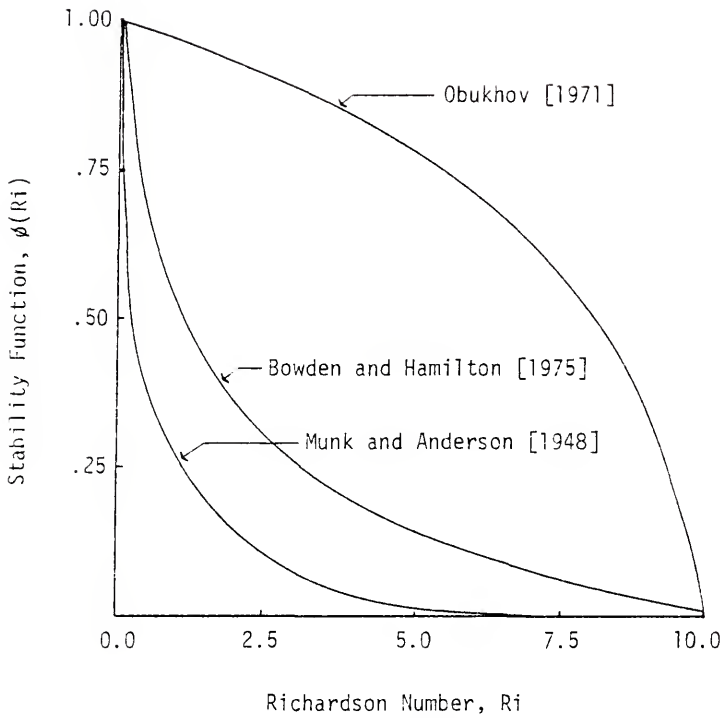


Figure 5.2 - Comparison of Saltwater Interface Stability Function.

CHAPTER 6
DEVELOPMENT OF THREE-DIMENSIONAL NUMERICAL MODEL

In Chapters 4 and 5, the governing equations were developed and arranged in a form for use in this three-dimensional model. In this chapter, these ideas and formulae are placed within a framework that will allow the user maximum flexibility in predicting transient concentration conditions in a variety of the low energy canals found along major portions of the Atlantic and Gulf coasts, while at the same time reducing the amount of "guesswork" involved in calibrating the model, by reducing the number of model coefficients.

The aim of this study was to produce a comprehensive numerical model which is accurate, reasonably economical and relatively simple to use. This requires that the number of input parameters, excluding geometric and forcing function data, be minimized. In fact, as can be seen from the previous two chapters, the only coefficients to be read in, apart from those associated with the tidal entrance boundary condition are the dimensionless dispersion coefficients, the vertical momentum transfer coefficient, and the dimensionless velocity, u_4 . The solution technique is an extension of the method of second methods selected in Chapter 3.

The program, called CANNET3D (standing for CANal NETWORK, 3-Dimensional), was written in FORTRAN IV for an AMDAHL 470 machine. This type of computer is the next sequence up from the IBM 370 Series, as Dr. Andahl was the former chief designer of the 360 and 370 Series

at IBM. The program requires just over 200K bytes of array storage area. The program has a number of subroutines which will be referred to in capital letters as they appear in the remainder of this text. Program variables will also be referred to in the same manner.

A user's manual for the program is given in Appendix A. Appendix B consists of a flow chart for the program, whose coding is listed in Appendix C.

Before proceeding to the discussion of the model development, some of the terms that will be used are defined here. Several of the variables presented have subscripts which are a combination of the letters i , j , and k . These represent spatial reference points in the x , y , and z -directions respectively. Thus, i will denote the number of a segment in the reach, j will denote the lateral location from the left bank, and k will denote the layer number from the bed. If a variable has all three subscripts, then it is a function of the three independent coordinates. However, if a variable has only one or two of the subscripts, its value is uniform with respect to the other coordinate direction(s). Thus, the longitudinal cell length is written Δx_i , in segment i as its length is independent of its location in the cross-section. Similarly, the thickness of a layer is written Δz_k , as it is independent of width and length.

The two superscripts used are n and $n+1$. These denote the time level as a multiple of the time interval, Δt . The time level n , is defined as the last time level at which all the variables were calculated. Thus, time level $n+1$, is the time level currently being evaluated. If these superscripts are omitted, the theory developed can be applied at any time $n\Delta t$.

A wavy bar, $\bar{}$, is written above variables which are calculated during the time level $n+1$ as an intermediate step to the final value of that variable. The subscript av is used where values are averaged between time levels n and $n+1$.

6.1 Layout of Geometry

The first step in numerically evaluating a proposed or existing canal network is to arrange it for input to the model. This consists of dividing and numbering the system into reaches, junctions, dead-ends, tidal entrances, and what will be termed null points.

The *null point* arises out of the need to be able to model transport in canal networks characterized by loops and multiple tidal entrances. Consider a system with two tidal entrances, in which the velocity field is produced entirely by changes in the tidal elevation in the receiving waterbody. Assuming that there is no phase difference between the entrances, it would be expected that the tidal inflows, from each entrance, during the flood tide, would either meet at some point, called a null point (or more correctly an area), within the canal network, or else would recombine to flow into an upstream reach of the system (Figure 6.1). The null point is then a section within the canal network through which the net tidal flux is zero. The general formulation for identifying this type of geometry is extremely complex, requiring a knowledge of systems programming, but an individual case is usually straightforward, and a procedure will be given here to divide the system into program compatible elements.

The procedure, which is carried out at some point of the tidal cycle, usually mean tide, uses the energy equation. If a null point, as defined above (Figure 6.1a), exists, then the head loss along each

series of hydraulically connected reaches and junctions to the point where the flows recombine, or to the receiving waterbody, must be equal,

$$\sum_i \Delta H_i = \sum_j \Delta H_j \quad (6.1)$$

where ΔH = head loss (L)

i, j = reach numbers in each series of canals.

Then from Manning's equation, ignoring losses in junctions,

$$\sum_i \left(\frac{\bar{Q}_i L_i k_i^{1/6}}{A_i R_i^{2/3}} \right)^2 = \sum_j \left(\frac{\bar{Q}_j L_j k_j^{1/6}}{A_j R_j^{2/3}} \right)^2 \quad (6.2)$$

in which the discharge giving the mean head loss in a reach, \bar{Q} , is given by integrating Manning's equation along the length of that reach,

$$\bar{Q}^2 = [Q_u^2 + Q_u \Delta Q + \frac{\Delta Q^2}{3}] \quad (6.3)$$

where

Q_u = discharge at upstream end of reach (L^3/T)

ΔQ = change in discharge along the length of the reach (L^3/T).

For each series of reaches from a null point to the point where the flows recombine, or to the receiving waterbody, the discharge in each reach is based on the volume of the tidal prism downstream of the null point.

The location of the null point is then found by varying its location until the two sides of Equation (6.2) balance. If by following this procedure, it is found that a null point lies upstream of the junction at which the flows recombine, an alternative approach must be used. The problem is in the way a junction is matched with its

upstream, downstream, left and right branch reaches. The requirement of two, or more, downstream reaches cannot easily be met because at least one of the downstream reaches will be laid out with its positive x-axis towards the junction and not away from it in the downstream sense. In other words, one of the downstream reaches must be set up as a left or right branch initially, and its cell structure will be assigned in the wrong direction. The inclusion of such a feature, desirable as it may be in some cases, was too cumbersome to include at this time, and will be left for a future version of the model.

One way in which this shortcoming might be overcome, in certain situations, is if the water surface area above the junction where the flows recombine, can be divided into areas equal to the water surface area required for each downstream reach emanating from that junction, to balance Equation (6.2), and satisfy continuity,

$$\sum_{i=1}^N Q_{u_i} = A_{ws} \frac{dd}{dt} \quad (6.4)$$

Each individual water surface area can then be treated as a lake at an upward limit of the system as described below. Thus, provided the area of specific interest in a canal network with such a feature is far enough away from the junction where the flows recombine that information will not be lost to the "lakes," which are maintained at initial concentration, then the tidal prism volume capacity of the system is retained and an analysis of transport can be carried out in another area of the network.

In an analysis of a proposed design system, all the terms of Equation (6.2) are known from purely geometric considerations, except Nikuradse's equivalent sand roughness, k . As this term is raised to the one-sixth power, its variation may be considered to be small, and the procedure can continue with its cancellation from the equation.

Once the null points are established, they are considered to be the meeting point of two dead-end canals, at which only wind and density induced flows have an influence across the boundary. The adjacent reaches are separately numbered, and the upstream junction number for each reach is assigned the negative value of the adjacent reach. This is to facilitate the model's handling of fluid transfer across the null point. This information is user provided to the model, by detailing the locations of reaches and junctions as described below.

Another geometric feature that sometimes occurs in canal networks is the lake. When they occur, they are usually situated at the upstream limits of the system. To model the flow in the lake would require a separate numerical model as the flow conditions are much different. However, the lake by its very presence, affects the volume of the upstream tidal prism, used in this model to calculate velocities in downstream reaches. Thus, assuming the water surface in the lake remains at the same elevation as the water surface in the remainder of the canal network, the lake is treated as a special case of a dead-end, with finite water surface area, but having no effect on mass transport to downstream reaches.

A junction of the model canal network may be either a null point described above, an area of the system at which one or two branch canals join a main canal, or else it can be a theoretical zone separating two portions of the watercourse with differing geometric features. Once the locations of the junctions have been determined, a reach between two hydraulically adjacent junctions is defined to be a trapezoidal, prismatic channel.

Each reach is assigned a number from 1 to NREACH (the total number of reaches in the system, including reaches formed by the introduction of a null point), in any order desired. This reduces the number of changes in the data with design changes. Once the required information for each reach is read in, the reaches are rearranged, retaining their original identification number, and ordered from the null points and dead-ends of the canal network to the tidal entrances. In this manner, at any junction, the upstream reaches of the junction are placed before the downstream reaches. This is done in the subroutine ORDER, and the new distribution stored in the array NRCH(*).¹ This rearranging is done so that an incremental tidal prism volume can be calculated from the upstream limits of the system to the tidal entrance.

Note: 1. The number of asterisks in parentheses indicates the dimensional order of the array.

In a similar manner, each dead-end, except lakes, is assigned the number 1. Each interior junction (those excluding dead-ends, null points, lakes, and tidal entrances) is assigned a number from 2 to $(NJUNC+1)$, where $NJUNC$ is the number of internal junctions in the system. The lakes are numbered from $(NJUNC+2)$ to $(NJUNC+NLAKE+1)$, where $NLAKE$ is the number of lakes at the dead-ends of the system, and the tidal entrances are numbered from $(NJUNC+NLAKE+2)$ to $(NJUNC+NLAKE+NTES+1)$, where $NTES$ is the number of tidal entrances. An example of a network numbering scheme is shown in Figure 6.2.

Once the reaches and junctions of the system have been thus numbered, the geometric data read in for each reach are its length, bottom width, mean tidal depth, left and right inverse side slopes, the numbers of the junctions upstream and downstream, Nikuradse's equivalent sand roughness, and its alignment angle. The alignment angle is to enable the x-component of the wind vector to be calculated in each reach. Similarly for each junction, its length, width, mean tidal depth, and the identification numbers of the reaches that meet there and fractions of the upstream tidal prism volume, are read in.

Once the canal network geometry is defined, the next step is to divide the system into computational cells. Together with the input data for each reach, the number of longitudinal divisions, $NDIV(*)$, is read in. The number of lateral and vertical divisions, $NLAYX$ and $NLAYZ$ respectively, are defined to be constant for the whole system. This is to ensure proper matching at junctions. At the beginning of the simulation, the depth is divided into $NLAYZ$ layers

of equal thickness. Then each layer is divided into NLAYY cells of equal cross-section area (Figure 6.3).

The junctions between reaches are simply transition zones from one reach to another, and will be used as such for every physical process modeled. To match the lateral and vertical layering of reaches entering the junction perpendicular to one another, the junction is also divided into NLAYZ vertical layers, but each layer has NLAYY² cells (Figure 6.4).

6.2 Treatment of the Velocity Field

The velocity field is obtained as a result of the various forcing functions due to the tide, wind, salinity gradients, bends, and lateral inflows. Each has a slightly different treatment which is discussed in the proceeding subsections, and in Section 6.4.

6.2.1 Tidal Velocities

As discussed in Section 4.2, the tidal velocities are generated by the rate of change of the surface elevation at the tidal entrances to the canal system. The tidal elevation data are input into the model in one of two ways. If the elevations follow a simple harmonic function, here the cosine distribution, so that the transient solution begins at slack tide, the tidal amplitude, AMP, and the period, T, are read in to form the relationship,

$$d = d_{0TE} + a \cos \omega t \quad (6.5)$$

where

d_{0TE} = mean depth at tidal entrance (L).

The tidal amplitude is made positive or negative depending on whether the simulation is to begin at high or low tide respectively. The other method is to digitize the elevations with respect to the mean tidal elevation at each time interval.

When a data set is digitized at fixed time intervals, Δt , it is desirable not to have to alter it because stability criteria dictate that a smaller time step is required. This is true for example, if say hourly tidal elevations are collected and put on magnetic tape. The usual procedure would be to generate a larger data set based on a linear interpolation between existing data points. This may be done within the program in exactly the same way, using the user provided parameter, INTERP.

As the magnitude of the tidal velocities is directly related to the volume of the tidal prism upstream of the section of interest, the calculations begin at the dead-ends of the canal network and proceed towards the tidal entrances. This is the reason for ordering the canals in this manner in the subroutine ORDER, so that an incremental tidal prism volume can be calculated throughout the system.

The vertical velocity profile due to the tidal action alone, was assumed to be logarithmic. This profile for any computational cell, is based on the mean depth of the trapezoidal channel over the width of the cell. The mean depth is calculated in the subroutine MEAND. This logarithmic velocity is then integrated over the vertical extent of the cell, as described in Section 4.2, to form the mean longitudinal velocity in that cell.

Thus, the tidal prism volume, V_i^{n+1} , upstream of segment i in the reach during a time step, Δt , and the mean tidal velocity are known. Defining a flexible cell structure, being flexible in the vertical and lateral directions, such that the mass of fluid transported longitudinally between adjacent cells remains entirely within the receiving cell, the rate at which the cross-section area of the receiving cell varies is proportional to the velocity into it. Thus the system has two degrees of freedom, but only one governing equation. To close the system of equations for solution, the reasonable constraint is applied that the vertical layers respond to the cumulative flow from all the lateral layers as if it were one cell. Thus, the depths of each cell in any layer, except the bottom one, will always be uniform.

Considering j to be the label of a lateral cell, where $j = 1, \dots, \text{NLAYY}$, in the vertical layer, k , where $k = 1, \dots, \text{NLAYZ}$ then,

$$\sum_{j=1}^{\text{NLAYY}} \sum_{k=1}^{\text{NLAYZ}} u_{jk}^{n+1} = V_i^{n+1} / (A^{n+1} \Delta t) \quad (6.6)$$

where

$$u_{jk}^{n+1} = \text{velocity into cell } jk \text{ (L/T)}.$$

If the cross-sectional area of the reach, at the previous time step is A^n , the increase in area is,

$$\Delta A^{n+1} = A^{n+1} - A^n \quad (6.7)$$

Thus, considering the constraint on the vertical layers first, the change in the cross-section area of each layer, ΔA_k^{n+1} , is given by,

$$\Delta A_k^{n+1} = \Delta A^{n+1} A^{n+1} \Delta t \sum_{j=1}^{\text{NLAYY}} u_{jk}^{n+1} / V_i^{n+1} \quad (6.8)$$

Then, the changes in the cross-sectional area of any cell, ΔA_{jk}^{n+1} , in layer k is given by

$$\Delta A_{jk}^{n+1} = \Delta A_k^{n+1} u_{jk}^{n+1} / \sum_{j=1}^{NLAYY} u_{jk}^{n+1} \quad (6.9)$$

This formulation allows the center cells in a cross-section to increase in area during the flood tide as relatively more fluid passes through them, and to contract during the ebb tide. The areas of cells are uniform between adjacent cross-sections of a reach and are stored locally for the reach in ARE(*), and globally for the canal network in AREA(*,*).

Once a flexible cell structure has been defined in this manner, the problem has been reduced to a one-dimensional case of longitudinal flow between adjacent cells, exactly as developed for the one-dimensional model, which is simply one cell encompassing the entire cross-section, in Section 2.6. The method of second moments conserves the mass, C(*); center of mass, FX(*); and the width of its rectangular distribution, RX(*). Each of these three arrays is stored as a continuous string of all the cells in the network to minimize storage and improve access time.

The cells in one reach cross-section change in areas, or as it will be termed from here on, *flex*, at a uniform rate between adjacent cross-sections. However, the flexing of cells from one reach to another may be different. To deal with this problem, the junction, which is treated merely as a transition zone between adjacent reaches, is defined to have cells of equal volume which all flex at the same rate with the tide. The cells at the edge of the junction are then

matched one-to-one with the cells in the immediate vicinity of the adjacent reaches without resorting to complex cell shapes and a three-dimensional form of the method of second moments. Such a form is not desirable because of the unrealistic amount of computer storage and computer time to model an admittedly ill-defined situation. The resulting numerical scheme in the junction is then an upwind difference scheme in which only the mass is conserved. However, as mentioned in Chapter 2, the numerical dispersion of this technique is proportional to the incremental length of the cell. In the junction, the cells are smaller than in the reaches because of the matching of cells from mutually perpendicular reaches meeting at the junction. Also, the surface areas of junctions are usually small compared to the total surface area of the canal network. This partially compensates for the numerical dispersion present in the junction, and the natural dispersion here is not modeled. As pointed out before, the effect of these procedures on the overall system is usually small.

Finally, it should be mentioned, that to ease the computational procedure somewhat, an extra layer of cells is added to both ends of every reach. These are called *buffer cells* (Figure 6.5), and their function is to eliminate the constant testing for junctions that is otherwise necessary for the transfer of mass to occur between adjacent cells in each reach. The buffer cells are then matched with their respective junction edge cells, and the volumes adjusted between the two.

6.2.2 Wind Induced Circulation

As with the tidal elevations, the wind data can be read in one of two ways. If a constant vector wind is blowing then, the constant wind speed, WSC, in mph, and constant wind direction, WANGC, in degrees, are read in, and converted to ft/sec and radians, respectively. Otherwise, the wind speed and direction are digitized. Again, the same INTERP parameter can be specified to be greater than one if the data needs to be provided at a smaller time step.

The velocity induced by the wind in layer k was developed in Equation (4.34) and is constant through the entire length and width of the layer. Also, its net flux through a cross-section of the reach is zero. Therefore, this velocity does not contribute to varying the cross-sectional areas of computational cells in a cross-section, because the increase in the total cross-sectional area due to its action is zero. Once the adjustment has been made to the cross-sectional areas of the cells due to the distribution of tidal velocities, the center of mass of the cell is moved a distance, X , equal to the sum of the component distances of the logarithmic tidal velocity, X_T , and the wind induced velocity, $X_W(*)$, in that layer,

$$X = X_T + X_W(NLZ) \quad (6.10)$$

where

NLZ = number of vertical layer.

As the velocity is uniform in each layer, there is no vertical transfer of mass to conserve mass.

The junction again acts as a transition zone between adjacent reaches. A simple conservation of mass scheme is devised to match the

various conditions in the adjacent cells of the adjacent reaches. This is done by transferring mass vertically in the junction to ensure that the mass entering each layer of the junction equals the mass exiting. The process is distributed throughout the junction depending on the volume flow from each reach boundary cell.

A similar vertical mass transfer is also performed at the dead-ends. If u_{wk} is the wind induced velocity in layer k in the positive x -direction, then the volume of fluid transport out of the dead-end layer in each time step, Δt , is,

$$V_w = u_{wk} A_k \Delta t \quad (6.11)$$

where

A_k = cross-sectional area of layer k (L^2)

V_w = volume of fluid transported out of layer k (L^3).

Beginning with the bottom layer, an equal volume is transferred vertically from the layer above, $k+1$. As the net volume flux is zero, this process is conservative.

Finally, a recommendation is made as to the choice of NLAYZ. As the theoretical expression for the wind induced vertical velocity profile has a reversal at the two-thirds depth and a turning value at the one-third depth, some multiple of three will retain the essential features of the distribution without cancellation in the cell averaging process. In fact, for most practical simulations three layers, and probably no more than six, will provide sufficient information for the design engineer.

6.2.3 Secondary Currents

Secondary currents as defined in Section 4.4 have no effect on the longitudinal velocity distribution. They simply redistribute the fluid mass through the radial velocity pattern developed by Rozovskii [1957, Ch. 2] for a two-dimensional flow in a wide channel over a rough bed. A subroutine, HELIX, was written to describe this process.

For each layer k , at the crown of the bend, a layer averaged velocity, v_{ck} , is given from Equations (4.43), (4.48), and (4.50) by,

$$v_{ck} = 6.25 \frac{d}{r} u_i (\bar{F}_1(k) + \bar{F}_4(k)/3.3) \quad (6.12)$$

where

u_i = mean velocity due to tidal component in segment i (L/T).

This velocity is constant in the layer, throughout the length of the bend, $BENDL(*,*)$, but decays in the direction of flow to within 2 percent of zero according to Equation (4.53). For the y -axis as defined, from the left bank to the right bank, perpendicular to the longitudinal axis, specifying the radius of the bend, r (stored in the array $BENDR(*,*)$), as being positive, defines flow around a bend to the left in the downstream sense. Similarly, if the bend radius is negative, the flow is around a right hand bend.

The input data to the model defines the location of the crown of the bend, the bend radius, and the length of the bend (Figure 6.6). A value for the reach number, NR , of -1 terminates the data. When a bend is located in the model, the pointer backs up against the flow to define the first longitudinal segment of the flow in which the secondary current develops (Figure 6.6). From this point, in the direction of

flow, Equation (6.12) holds throughout the length of the bend, after which the radial velocity decays over the distance PL . For each longitudinal segment, denoted by the subscript i , an averaging procedure based on the length of the bend is performed giving the following cell averaged velocities in layer k , v_{ik} :

1. for segment i totally contained in the bend,

$$v_{ik} = v_{ck} \quad (6.13)$$

2. for segment i of total length x , having length Δx_1 within the length of the bend,

$$v_{ik} = \frac{v_{ck}}{\Delta x} \left(\Delta x_1 + \frac{1}{3} L_d (1 - \exp[-\frac{3}{L_d}(\Delta x - \Delta x_1)]) \right) \quad (6.14)$$

3. for segment i totally outside the length of the bend, but at least partially within the decay distance, L_d , from the bend,

$$v_{ik} = \frac{v_{ck} L_d}{3\Delta x} \left(\exp(-\frac{3x_1}{L_d}) - \exp(-\frac{3x_2}{L_d}) \right) \quad (6.15)$$

where

x_1, x_2 = distance in the direction of flow from the end of the bend to the closest and farthest points of segment i respectively (L).

In each layer of segment i , a volume of fluid, V_{ijk} , given by

$$V_{ijk} = v_{ik} \Delta t \Delta x \Delta z \quad (6.16)$$

where

Δz = thickness of layer (L)

j = number of later cell

is transferred between laterally adjacent cells of the layer, to conserve fluid mass. Once the transfer has been completed in all the cells of a segment of the reach, a vertical mass balance between cells on the outside of the reach is performed as for the wind induced flow case at the dead-ends, to conserve fluid mass between the vertical layers.

6.2.4 Density Currents

The circulation induced by density gradients is treated in a manner similar to the wind induced circulation in the subroutine WEDGE, except that account is taken of the longitudinal variation of the velocity in each layer using vertical transfer to conserve mass. Again, the net mass flux through any cross-section is zero, and thus the flow makes no contribution to the change in cross-sectional areas of the computational cells.

Because of the description of the motion of a saline wedge, that is of a triangular distribution entering the canal network during the flood tide and the lowering of the interface during the ebb tide as described in Chapter 4, the transient simulation to model this phenomenon must start at low tide. Thus, the initial salt wedge configuration in the network is that the elevation of the interface in each reach is the elevation of the low tide interface in the receiving waters. To model multiple tidal entrances and loops, the user must break the canal system up by determining the null points as explained in Section 6.1.

The induced velocity field is provided by the equations in Section 4.5. These velocities are then layer averaged, and the distance

moved by the center of mass in each cell during the time interval, Δt , is stored in the array $XS(*,*)$. Having adjusted the cross-sectional areas of the cells due to the distribution of tidal velocities, the center of mass of each cell is moved a distance X , similar to Equation (6.10), where X is now the sum of the component distances of the tidal velocity, the wind induced velocity, and the density current,

$$X = XT + XW(NLZ) + XS(ND, NLZ) \quad (6.17)$$

where

ND = number of segment of reach.

In longitudinally adjacent segments $i-1$, i say, numbered in the direction of the flow, the longitudinal velocities associated with the density current in layer k are u_{i-1k} and u_{ik} , respectively. Looking at layer k in segment i , a simple fluid mass balance shows that an extra volume of fluid ΔV_{ijk} is added to each lateral cell according to,

$$\Delta V_{ijk} = (u_{i-1k} - u_{ik}) \Delta y \Delta z \quad (6.18)$$

where

Δy = lateral extent of cell.

Then, in each column of cells,

$$\sum_{k=1}^{NLAYZ} \Delta V_{ijk} = 0 \quad (6.19)$$

for conservation of fluid mass. Finally, the fluid mass is adjusted as in the vertical column so that the mass in each cell is conserved.

6.3 Treatment of Dispersive Terms of the Transport Equation

The common method used to treat the dispersive terms of the mass-transport equation is to develop a central finite-difference approximation to the second derivative based on forward and backward expansions of Taylor's series about the point. Such a form was developed for the one-dimensional model in Equation (2.55), and can easily be extended to two and three dimensions [Smith, 1965, pp. 41-45; Roache, 1972]. In most problems this can be done fairly simply by applying the finite-difference approximations to all the internal points of the solution domain and then developing boundary expressions to fit the solution to the edges of the domain. These conditions vary from conservation of mass expressions, to extrapolations, to simply ignoring the dispersive term altogether at this point, and so on. The boundary specification, as artificial as it sometimes may be, is only a small part of the solution domain and if fairly well formed, does not usually impair the results too significantly.

If a numerical solution scheme is developed to model the dispersive process in a tidal canal network, using three layers laterally and three layers vertically, which is a good number for most purposes, then eight out of nine cells are boundary cells. This means that finite-difference approximation to the second derivative term can only be modeled longitudinally, or at the middle cell in each layer, either vertically or laterally. In all likelihood, the application of improvised boundary conditions in so many of the cells would lead to results whose accuracy would be questionable. Thus, a solution scheme must be found through a rearrangement of the governing equation.

Consider a one-dimensional diffusion equation in the form,

$$\frac{\partial c}{\partial t} = \frac{\partial}{\partial x} \left(E_x \frac{\partial c}{\partial x} \right) \quad (6.20)$$

where

$$E_x = \text{diffusion coefficient (L}^2\text{/T)}$$

and introduce a variable, u_{D_x} , defined by,

$$u_{D_x} = - \frac{E_x}{c} \frac{\partial c}{\partial x} \quad (6.21)$$

Introduction of Equation (6.21) into Equation (6.20) gives,

$$\frac{\partial c}{\partial t} + \frac{\partial}{\partial x} (u_{D_x} c) = 0 \quad (6.22)$$

which is the one-dimensional convection equation in which u_{D_x} is a longitudinal velocity term. Here, u_{D_x} is called the diffusion velocity [Spaulding, 1976].

In an exactly similar way, diffusion velocities can be defined in the y- and z-directions, respectively,

$$u_{D_y} = - \frac{E_y}{c} \frac{\partial c}{\partial y} \quad (6.23)$$

$$u_{D_z} = - \frac{E_z}{c} \frac{\partial c}{\partial z} \quad (6.24)$$

such that when applied to the three-dimensional diffusion equation, written in vector form,

$$\frac{\partial c}{\partial t} = \nabla \cdot (\vec{E} \cdot \nabla c) \quad (6.25)$$

the three-dimensional convection equation is obtained,

$$\frac{\partial c}{\partial t} + \vec{u}_D \cdot \nabla c = 0 \quad (6.26)$$

where

$$\bar{u}_D = (u_{D_x}, u_{D_y}, u_{D_z})$$

The diffusion velocities can then be used to transfer mass between adjacent cells, and apply in the boundary cells because the condition of zero flux through the side of the channel is satisfied. As the velocity field has been reduced to a one-dimensional transport between longitudinally adjacent cells using the flexible grid structure defined in Section 6.2, the longitudinal dispersion term is treated slightly differently from the other two dispersion terms.

6.3.1 Longitudinal Dispersion Term

From Equation (6.21) and upwind finite-difference approximation to the longitudinal diffusion velocity, $u_{D_i}^{n+1}$, in segment i , can be derived by considering the transport of mass from cell ijk to cell $i+1jk$,

$$u_{D_i}^{n+1} = - \frac{(\Delta x_i E_{x_{ijk}}^{n+1} + \Delta x_{i+1} E_{x_{i+1jk}}^{n+1}) (\Delta x_{i+1} c_{i+1jk}^n - \Delta x_i c_{ijk}^n)}{(\Delta x_i c_{ijk} + \Delta x_{i+1} c_{i+1jk}) (\Delta x_i + \Delta x_{i+1})} \quad (6.27)$$

where

$$\begin{aligned} \Delta x, \Delta x_{i+1} &= \text{lengths of segments } i \text{ and } i+1, \text{ respectively} \\ E_{x_{ijk}}^{n+1} &= \text{dispersion coefficient in cell } ijk \text{ (} L^2/T \text{)}. \end{aligned}$$

Thus, in an analogous manner to the distances associated with the velocity terms in Section 6.2, a longitudinal diffusion distance XD , or more correctly, a dispersion distance as the coefficient is cell integrated, is defined as

$$XD = u_{D_x} \Delta t \quad (6.28)$$

and added to the other distance terms of Equation (6.17), to give the final model displacement of the center of mass of cell ijk in the time interval Δt as,

$$X = XT + XW(NLZ) + XS(NR, NLZ) + XD \quad (6.29)$$

6.3.2 Lateral and Vertical Dispersion Terms

As there is no specific lateral or vertical velocity term in the model because of the flexible grid structure, except for the case in which secondary flows are present, the lateral and vertical dispersion terms are treated directly as dispersive velocities defined by Equations (6.23) and (6.24), respectively, which transfer fluid between adjacent cells simply conserving mass. Thus, in the lateral and vertical directions a straightforward upwind differencing technique is used.

From Equation (6.23), the mass flux, cu_{D_j} , between lateral cells j and $j+1$, due to lateral dispersion, is written in finite-difference form

$$cu_{D_j}^{n+1} = -\frac{1}{2} (E_{y_{ijk}}^{n+1} + E_{y_{ij+1k}}^{n+1}) (c_{ij+1k}^n - c_{ijk}^n) / \Delta y_{ijk} \quad (6.30)$$

This transfer occurs in the direction of the vector lateral dispersion velocity, u_{D_j} , which is directly related to the lateral concentration gradient.

Similarly, from Equation (6.24), a mass flux, cu_{D_z} , between vertical layers k and $k+1$, due to vertical dispersion, is given as,

$$cu_{D_k}^{n+1} = -\frac{1}{2} (E_{z_{ijk}}^{n+1} + E_{z_{ijk+1}}^{n+1}) (c_{ijk+1}^n - c_{ijk}^n) / \Delta z_k \quad (6.31)$$

Again, transfer occurs in the direction of the negative concentration gradient.

To incorporate vertical dispersion in the presence of a saltwater wedge, the vertical dispersion coefficient, E_z , is multiplied by a function of the Richardson number, as defined in Section 5.3. Even though the saltwater wedge is modeled as a sharp interface, dispersion can be introduced across this interface by defining some distance over which the density varies from ρ_0 to $\rho_0 + \Delta\rho_0$. An obvious choice is the thickness of a vertical layer Δz as an approximation. This is a somewhat crude assumption, but better than assuming no dispersion across the interface at all. Also, field measurements indicate that the thickness of the transition zone varies considerably during the course of a tidal cycle.

Thus, from Equation (5.26), the Richardson number, Ri , is given by,

$$Ri = \frac{-g/\rho_{av}\Delta\rho_0/\Delta z}{(du/dz)^2} \quad (6.32)$$

where

$$\rho_{av} = \text{average density between the two layers (M/L}^3\text{)}.$$

Equation (6.32) is given explicitly as du/dz can be calculated exactly from the various superimposed expressions for the velocity field developed in Chapter 4. The function $\phi(Ri)$ defined by Equation (5.30) is then used to modify Equation (6.31), provided the interface lies within one-half of a cell's depth from the plane separating vertically adjacent cells, giving,

$$cu_{D_k} = \frac{1}{2} (1 - 0.01 Ri)^{1/2} (E_{z_{ijk+1}} + E_{z_{ijk}}) (c_{ijk+1}^n - c_{ijk}^n) / \Delta z_k$$

for $Ri \leq 10$ (6.33a)

$$cu_{D_k} = 0 \quad \text{for } Ri \geq 10 \quad (6.33b)$$

6.4 Lateral Inflows

The rate of production or loss term, r_p , introduced in the three-dimensional mass-transport Equation (2.13), was defined to have the distribution given by Equation (2.16) for the one-dimensional model. This form can be extended to the three-dimensional model by defining $q_{I_{ijk}}$ to be the lateral inflow per unit length of cell ijk . If the concentration of this inflow is $c_{I_{ijk}}$, then the rate of production or loss term, $r_{p_{ijk}}$, is,

$$r_{p_{ijk}} = q_{I_{ijk}} c_{I_{ijk}} / A_{ijk} \quad (6.34)$$

The lateral inflow step is performed as a simple addition of mass to cell ijk , and is done before the convection step. This is so that the lateral inflow rate, q_I , can be added to the tidal prism volume to calculate the velocity through the cell during the current time step. Thus, the concentration of the substance carried in by the lateral inflow is added to the concentration of the substance already in the cell,

$$c_{ijk}^{n+1} = c_{ijk}^n + q_{I_{ijk}}^{n+1} c_{I_{ijk}}^{n+1} \frac{\Delta t}{\Delta y_{ijk}} \Delta z_j \quad (6.35)$$

where

c_{ijk}^{n+1} = resulting concentration in cell ijk after lateral inflow addition (dimensionless)

c_{ijk}^n = concentration in cell ijk at previous time level n
 (dimensionless)

Δx_i = uniform longitudinal length of cell in segment i at reach (L)

Δy_{ijk} = lateral width of cell ijk (L)

Δx_k = vertical thickness at layer k of reach (L) .

Then, the sum of the lateral inflows in segment i is added to the upstream tidal prism volume, V_i^{n+1} , to give

$$\tilde{V}_i^{n+1} = V_i^{n+1} + \sum_{j=1}^{NLAYY} \sum_{k=1}^{NLAYZ} q_{1ijk} \Delta t \Delta x_i \quad (6.36)$$

where

$$\tilde{V}_i^{n+1} = \text{tidal prism volume with lateral inflow added } (L^3).$$

This value of the tidal prism volume is used in the theory presented in Sections 6.2.1 and 4.2, to determine the cell averaged tidal induced velocities, and the change in the cross-sectional areas of cells in each segment.

The advantages of expressing the lateral inflow in this manner are that the resulting model formulation is somewhat simplified. If the effect of the lateral inflow were followed exactly, then it would be necessary to model the lateral circulation produced by the inflow, to both conserve mass, and the horizontal water surface assumption. In the first place, the quality of the data cannot be expected to reflect this mechanism, and secondly the lateral inflow would never be uniformly distributed throughout the length and depth of the cell.

Another advantage is that river flows, or flows over salinity structures, banks, etc., or sinks, can be readily modeled by specifying

the cells into which the inflow or outflow occurs. As the concentration is added before the convective step, the inflow conditions remain in phase with the solution scheme, which means that inflow concentrations are convected with induced velocities at the same time level, and not the next.

In the model, the lateral inflow can be treated in one of two ways. If the inflow rate and concentration remain constant throughout the simulation, then for each such inflow, OPT2(*) is given the value 0, and the reach number, NR, the segment NDX, the number of the cell in the cross-section, NC (based on the coordinate system described in Section 6.1), the lateral inflow rate, QIC(*), and the concentration, CIC(*), are read in initially and are stored for the run. If the lateral inflow and/or its concentration are variable, OPT2(*) is given the value 1 and only the variables NR, NDX, and NC are initially read to determine its location, and are stored in the array LOCV(*) in the subroutine ORDER. Then, OPT2(*) = -1 terminates the data. During the simulation, the variable inflow data are read in at each time interval at which tide or wind data is specified (the INTERP variable will calculate intermediate values as before). However, it should be noted that the inflow data must be in the same order as given initially.

6.5 Decay Coefficients

The three-dimensional mass-transport equation, given in Equations (2.13) and (5.1), describes the transport of a conservative, passive substance in a velocity field (u, v, w) . The term conservative means that the concentration of the substance does not decay due to outside

stimuli such as sunlight, absorption by bank or suspended solids, or reactions with other substances found in the flow field.

If, for example, dissolved oxygen (DO) were being modeled on its own without an interactive process with ultimate oxygen demand (UOD), or nitrites without the conversion process to nitrates, and so on, a decay term could be added at locations where these processes were known to exist to model the phenomena. Similarly, a source term could be added at locations where the substance is produced as described in Section 6.4.

There are many forms of decays which are usually termed first order, second order, or whatever best fits the process. The most common form, however, is the first order exponential decay described by,

$$\tilde{c}_O = c_{RW} + (c_O - c_{RW})\exp(-Kt) \quad (6.37)$$

where

- \tilde{c}_O = concentration after a decay period t (dimensionless)
- c_{RW} = background concentration (dimensionless)
- c_O = initial concentration (dimensionless)
- K = decay coefficient (1/T).

Differentiation with respect to time results in the expression

$$\frac{\partial c_O}{\partial t} = -Kc_O \quad (6.38)$$

As Equations (5.1) and (6.38) are linear, they may be superimposed to produce the three-dimensional mass-transport equation for a nonconservative substance,

$$\frac{\partial c}{\partial t} + \frac{\partial}{\partial x} (uc) + \frac{\partial}{\partial y} (vc) + \frac{\partial}{\partial z} (wc) = \frac{\partial}{\partial x} (E_x \frac{\partial c}{\partial x}) + \frac{\partial}{\partial y} (E_y \frac{\partial c}{\partial y}) + \frac{\partial}{\partial z} (E_z \frac{\partial c}{\partial z}) + r_p - Kc \quad (6.39)$$

In the model, the distinction is made between two different forms of decay, one which exists throughout the volume of a reach, and one that only exists in certain localized portions of the reach. The reach uniform decay coefficient, K , in Equation (6.37), is read in with the other reach data and is stored in the array RDECAY(*). The localized decay coefficients, which are assumed to remain constant throughout the period of the simulation, are input in a similar manner to the lateral inflows. For each coefficient, its reach number, NR, segment, NDX, cell number in cross-section, NC, and decay coefficient, DECAY(*), are read in while the value of OPT for each set of data is nonnegative. A negative value terminates the input.

It is not convenient to model the decay during the convective step in an explicit mass-in-cell technique, such as the method of second moments, because of the increased complexity introduced to follow the various portions of the volume as it is exchanged between adjacent cells. It is easier to model the decay over a time interval Δt , either before or after the convective steps are performed. In this model, the decay step immediately follows the convective step, and a finite-difference scheme, for simplicity, is used to approximate Equation (6.38) in each cell, ijk , in the form

$$c_{ijk}^{n+1} = c_{RW} + (K_R + K_{ijk})(c_{ijk}^{n+1} - c_{RW})\Delta t \quad (6.40)$$

where

K_R = reach constant decay coefficient (1/T)

K_{ijk} = cell constant decay coefficient (1/T)

c_{ijk}^{n+1} = concentration in cell after convective step
(dimensionless).

6.6 Boundary Conditions

As discussed in Section 2.1.5, the three-dimensional mass-transport equation is a second order parabolic equation, being first order in time, t , and second order in the spatial variables (x, y, z). To close the numerical scheme for solution requires one set of initial conditions at all points in the canal network, and specifying conditions on all physical boundaries of the solution domain.

In the same manner as for the one-dimensional model, the initial conditions are either read in (OPT4 = 1), or are generated within each reach to equal the background concentration, c_{RW} (OPT4 = 0).

For each solid boundary, the dead-ends, the banks, the bed, and the air/sea interface at any time, the condition of zero mass flux is applied. One of the advantages of the model formulation presented in the preceding sections of the chapter is the numerical scheme automatically satisfies this condition everywhere, except at the tidal entrances which will be treated separately. Even for the dispersion terms which usually require a boundary condition to replace the spatial second derivative at this point, a dispersion velocity was derived which also satisfies this requirement.

Thus, the only boundary condition which requires some deeper consideration is the tidal entrance condition. The condition adopted

for the model was a revised form of the boundary condition used for the one-dimensional model. Unfortunately, unlike for the one-dimensional model, the flow at the tidal entrance cannot be divided into mass inflow during the flood tide, and mass outflow during the ebb. This is because the circulation patterns produced by wind and salinity gradients may cause flow reversals even at the mouth of the canal networks giving both inflow and outflow from different cells at the same time.

To model this region, it was assumed that once the flow exists the system, it becomes vertically well mixed, and that the resulting concentration decays to the background concentration as described for the one-dimensional model in Equation (2.26). In the model, a cell is generated having a volume equal to that of the last segment in the tidal entrance reach. If the concentration of this cell is \tilde{c}_{TE}^n and the volume is V_{TE}^n , then the resulting concentration at the end of a convective step, c_{TE}^{n+1} , is given by,

$$c_{TE}^{n+1} = \frac{\sum_{j=1}^{NLAYY} \sum_{k=1}^{NLAYZ} V_{jk}^{n+1} c_{jk}^n + (V_{TE}^{n+1} - \sum_{j=1}^{NLAYY} \sum_{k=1}^{NLAYZ} V_{jk}^{n+1}) c_{TE}^n}{V_{TE}^{n+1}} \quad (6.41)$$

where

V_{jk}^{n+1} = volume of fluid transport out of reach from a cell (L^3)

c_{jk}^n = concentration of above volume (dimensionless)

and where the double summation occurs only over cells which have an outflow to the receiving waters. For the remaining cells, an inflow condition is defined so that fluid of concentration c_{TE}^n enters the cell, so that the width of the volume in the cell becomes equal to the

width of the cell, Δx_j ,

$$c_{ijk}^{n+1} = R c_{ijk}^{n+1} + (1 - R) c_{TE}^n \quad (6.42)$$

where

R = width of volume in cell after convective step (L)

c_{ijk}^{n+1} = concentration of fluid in cell after convective step (dimensionless).

Once the convective step is completed, and the uniform concentration c_{TE}^{n+1} is formed in the tidal entrance cell, its value is assumed to decay towards the background concentration, c_{RW} , described by

$$c_{TE}^{n+1} = c_{RW} + (c_{TE}^{n+1} - c_{RW}) \exp(-3\Delta t/\tau) \quad (6.43)$$

where

τ = tidal entrance decay coefficient ($1/T$).

This condition was implemented in the three-dimensional model and was tested under a variety of conditions, including the case in which only the tidal component of the velocity field operated on the flow. In all cases, the condition was found to work satisfactorily, and the comments made in Chapter 2 as to the variability of the coefficient, τ , apply here also, to some degree.

6.7 Results Presentation

The presentation of results is done in three phases, which will be referred to as input data, digital results, and graphical results.

The input data section lists the parameters which are read into the model. After giving the test number, the global parameters such as those associated with the time interval, the tidal amplitude,

AMP, the background concentration, c_{RW} , the dispersion coefficients and parameters detailing the layout and cell structure of the canal network are listed. Following this comes a listing of all the junction parameters, tidal entrance data, lateral inflow data, decay data, bend data, and finally the geometric data for each reach. A typical output showing the listing of input parameters can be seen in Appendix D, for the 57 Acres study canal.

Once these data are listed, the transient solution begins, after specifying the type of problem being investigated, in terms of wind, harmonic or digitized tidal elevations, and so on. Following this, the initial data, in digital form, for concentrations and velocities are listed (the velocities are set to zero initially). First, the time, tidal elevation with respect to mean sea level, the wind speed and direction, are given. Next the reach number is printed, immediately followed by values of concentration and then velocities in that reach. The first line gives the concentration values for the upstream segment list in order from ((j=1, NLAYY), k=1, NLAZY) across the page. Continuation occurs where necessary. The next line lists the velocity values for these cells in the same order. In this manner, each segment's values are printed down to the end of the reach, at which point the values for the next reach are listed. Once the data for all NREACH reaches have been printed, the values for the junctions (concentrations only) are listed in the same manner.

The user controls the number of time intervals between writing by the parameter NPRINT. At every NPRINT time steps, the values for time, tidal elevation, wind speed and direction, concentrations, and velocities are listed as before. When the simulation is completed

the final results are also printed out. A sample output is given in Appendix D.

A second user controlled parameter is NPLOT. If NPLOT is specified to be greater than the total number of time steps, then no graphs are generated. If a lower value is given, then every NPLOT time steps, two graphs are generated for each reach in sequence. The left hand graph gives plot of the concentration values versus distance for each layer, and an average plot over all the layers. The right hand plot shows the same results for the velocities. To keep the plot within bounds, the user must specify the maximum concentration expected, CMAX, and the maximum velocity anticipated, VMAX, so that axial values can be printed. The plots are generated from the upstream section using the parameter DXMIN (the length of the smallest segment in the network), and the results shown for each distance increment, DX(*). A scale is provided between the two plots at DXSC increments. A sample output showing these features is given in Appendix D.

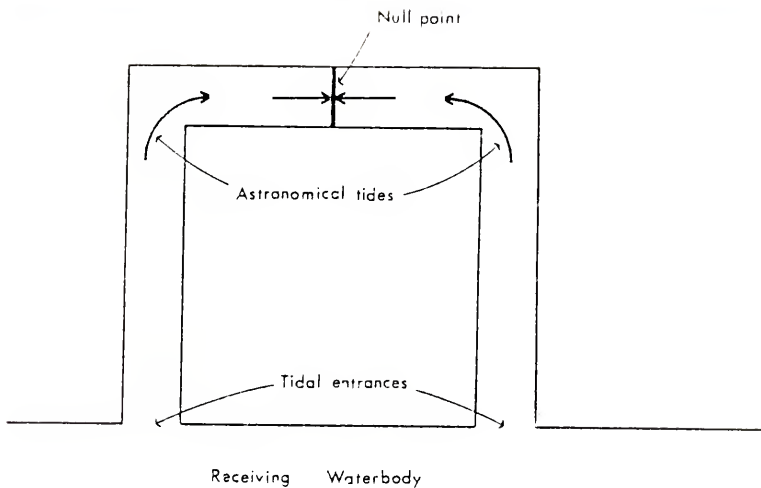


Figure 6.1a - Astronomical Tides Meeting at Null Point.

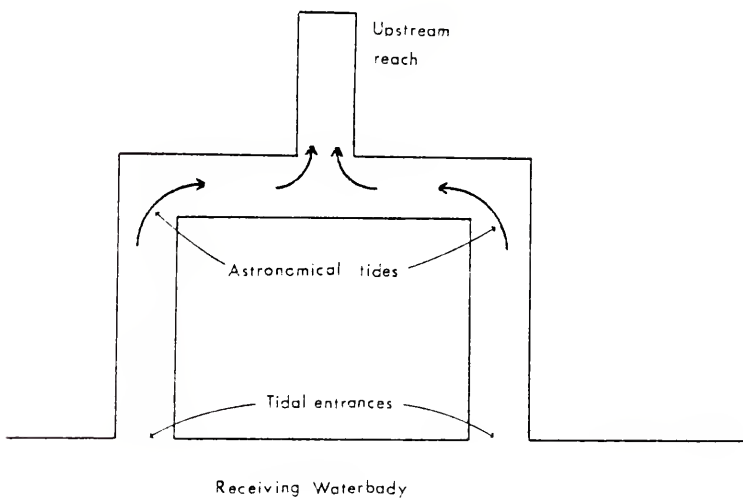


Figure 6.1b - Astronomical Tides Recombining at Upstream Junction.

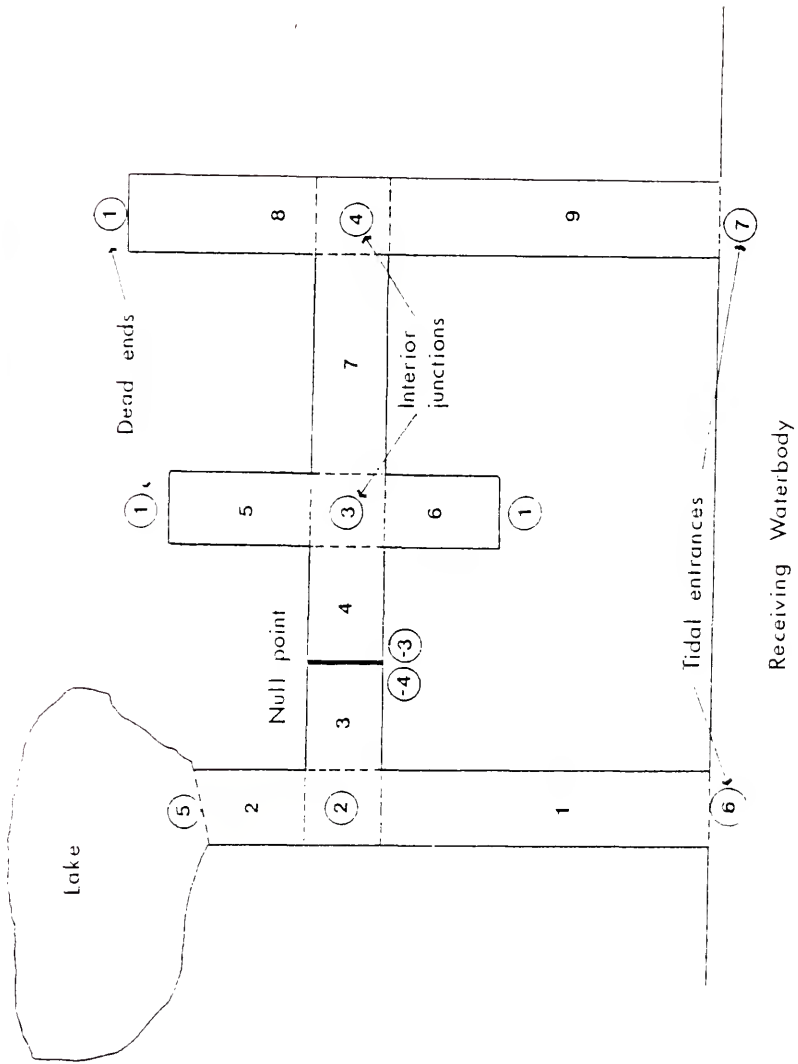


Figure 6.2 - Schematic Layout of Canal Network Showing Features.

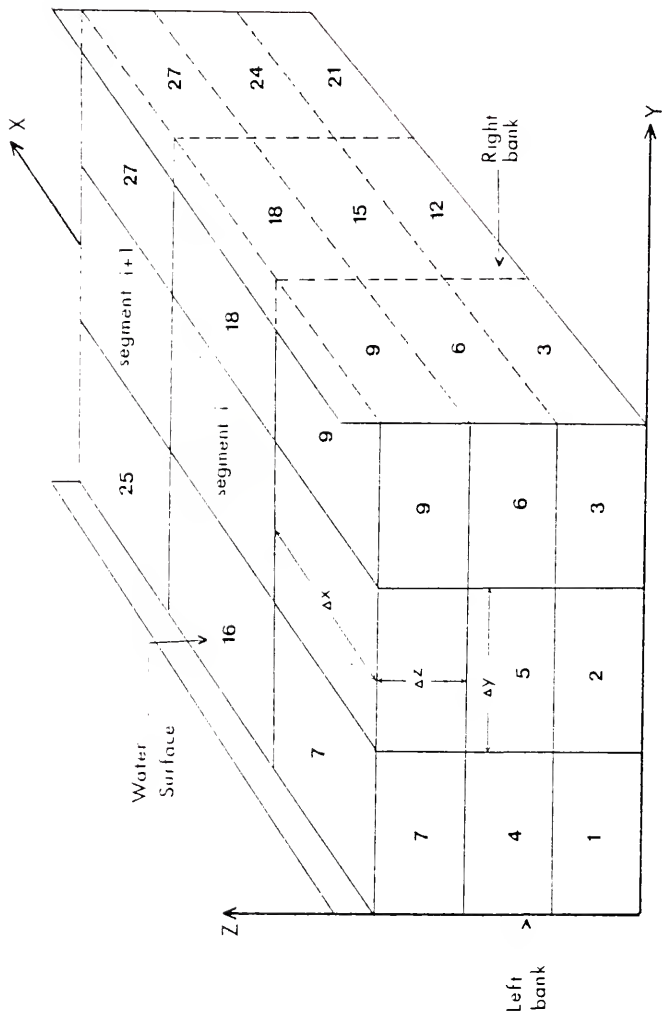


Figure 6.3 - Cell Structure in Reach.

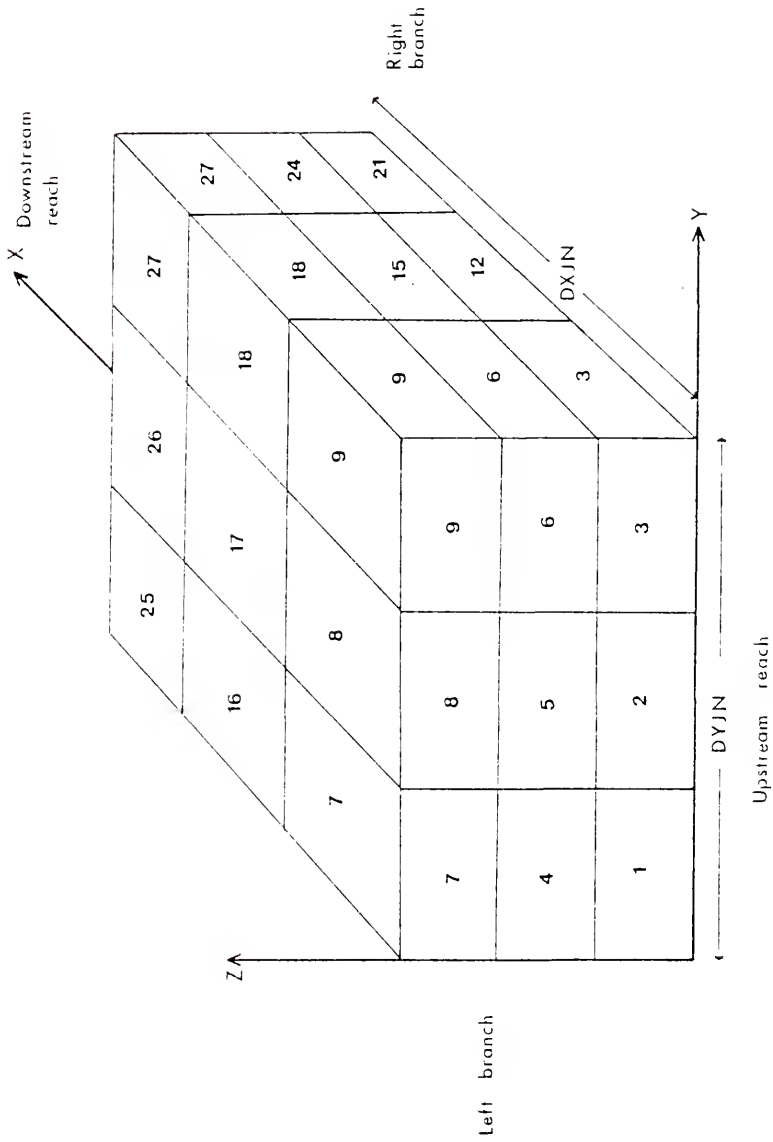


Figure 6.4 - Cell Structure in Junction.

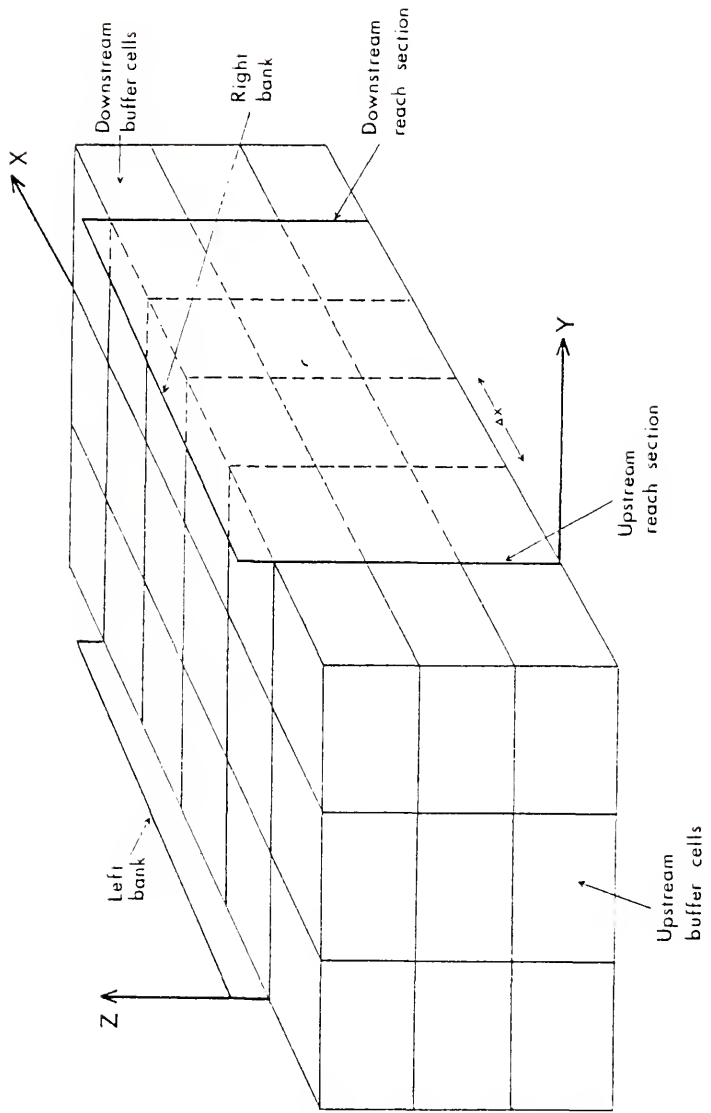


Figure 6.5 - Buffer Cell Structure.

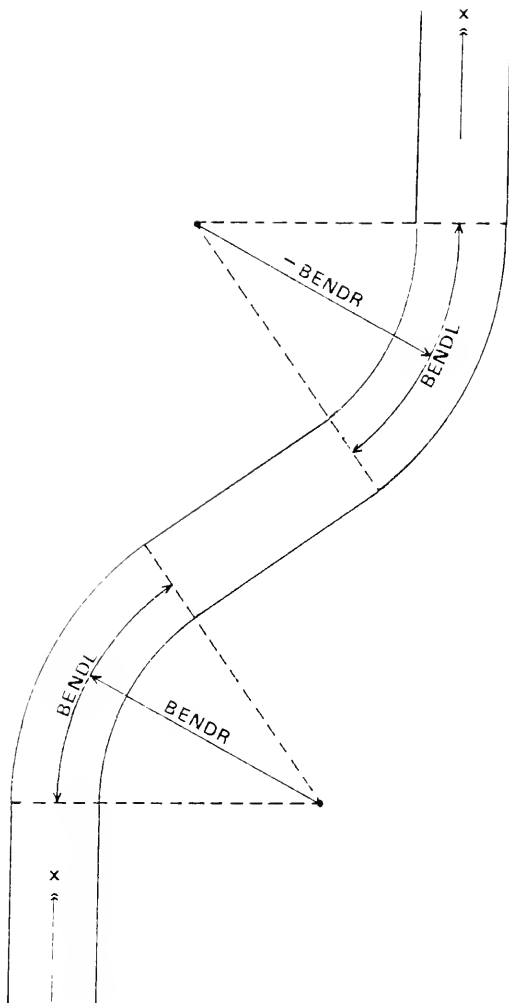


Figure 6.6 - Schematic Layout of Bend.

CHAPTER 7

MODEL STABILITY AND CONVERGENCE CRITERIA

7.1 Conservative Property, Order of Accuracy, and Transportiveness

The method of second moments has been used to develop a model to simulate mass transport in low energy tidal canals. The method is conservative and second order accurate. The conservative property, as discussed by Roache [1972], ensures that the accumulation of mass within the solution domain equals the net flux across the boundaries during both the convection and dispersive processes, as a dispersion velocity term has been used to model the second order terms. Changes then, in the domain, should only occur due to computer round-off error, particularly in the square-root term which is used at each time step and in each cell to calculate the width of the rectangular distribution in the cell.

Most common finite-element and finite-difference methods that have been used to model the mass-transport equation, are first order accurate. This is because, as shown in Chapter 2, there is a second order error, termed numerical dispersion, which results from the approximation to the first-order time derivative, and to the first-order spatial derivative, if the forward or backward-difference methods are used. As the method of second moments, and the second upwind difference scheme with limited antidispersion and flux corrected transport [Lee, 1977], discussed in Chapter 2, eliminate the numerical dispersion, the methods are second order accurate.

The order of accuracy of the numerical scheme is not usually a problem. In many examples, such a formulation is used to model mass transport in rivers and estuaries, in which the natural dispersion being modeled is far greater than the numerical error being produced by the model for reasonable choices of the time and spatial elements, Δx and Δt , respectively. Bella and Dobbins [1968], however, did employ a correction factor based on a theoretical form of the numerical dispersion and subtracted the numerical dispersion coefficient from the natural dispersion coefficient in the model. This technique worked well for them because the resulting coefficient was still positive, and positive dispersion has a smoothing effect on the results.

Unfortunately, in low energy tidal canals such as those investigated in Florida, and indeed which occur throughout the Gulf of Mexico and Eastern United States, dispersion coefficients are very small, maximum coefficients typically being less than $5 \text{ ft}^2/\text{sec}$. This has two effects. Firstly, the numerical dispersion ignored by many investigators in their models, may now be larger than the dispersion being modeled, giving results which are either unstable or severely attenuated. The instabilities arise when the inherent numerical dispersion is negative. Negative dispersion acts in exactly the opposite way from the smoothing effect of positive dispersion. Secondly, correction factors, such as those used by Bella and Dobbins, may also give a resultant negative dispersion coefficient, and hence, instabilities may again arise.

Lee [1977] used this correction technique, but controlled it using flux-corrected transport [Boris and Book, 1973, 1976; Book, Boris, and Hain, 1975]. The method required that no new local maxima or minima be introduced into the solution, and it worked well. Unfortunately, it suffered from

the drawbacks that the formulation, particularly in junctions, was cumbersome and not physically intuitive.

The method of second moments does not suffer from these disadvantages because there is no numerical dispersion to correct for. As a result, the technique is more clearly expressed in a way that is physically meaningful, as it simply conserves the moments of the distribution of each cell about the center of mass in that cell. This leads to a simpler model when dealing with a system as complex as a three-dimensional canal network.

Finally the solution scheme, as arranged in this model, is transportive in every step. Roache [1972] discusses this property by saying that "the effect of a perturbation in a transportive property is advected only in the direction of the velocity" [p. 67]. Upwind difference methods such as the technique developed by Lee [1972] for the convective step, and the method of second moments process this property. No finite-difference formulation of the convective process using space-centered derivatives for the convective term is transportive. In this model, however, because the three-dimensional dispersion terms are treated using a dispersion velocity, the model is also transportive in the second order terms.

7.2 Stability Criteria

Stability is generally defined to be a property associated with the numerical scheme's ability to damp out with time small perturbations in the solution. These perturbations are caused by truncation errors of the infinite series approximation to the governing equations, and by round off errors in the finite word length of computer storage. Usually, this second error is much smaller than the first one, but because of the

large number of square roots calculated, a very inefficient algorithm on some computers, this second error may be important. The second error type is also called random error, because its effect is virtually impossible to analyze.

If "round-off" errors, e_{ijk} , are introduced into the numerical scheme in each cell ijk , such that the exact difference solution, $F(\Delta x, \Delta y, \Delta z, \Delta t)$, is approximated by the numerical solution, $\tilde{F}(\Delta x, \Delta y, \Delta z, \Delta t)$, and if each

$$|e_{ijk}| < \epsilon \quad (7.1)$$

where ϵ = some small number, then if $|F - \tilde{F}| \rightarrow 0$ as $\epsilon \rightarrow 0$, the scheme is said to be stable [Smith, 1965]. Otherwise, the scheme is unstable.

Such a definition is useful because it can give a guideline for analyzing a numerical scheme. However, it is possible that the above condition may not be met, but that the scheme still gives a good approximation to the correct result. This might be the case if the errors accumulated very slowly, or else cancelled each other out. It is often the case in a stability analysis that a scheme is programmed and the results compared with an analytic solution to see whether good agreement is found. If there is good agreement, the model is said to be stable.

In some numerical schemes, it is possible to use a conventional stability analysis, such as the discrete perturbation stability analysis or the von Neumann stability analysis [Roache, 1972, pp. 36-53], to examine the expected accuracy. Usually such an analysis can only be based on a simplified form of the governing equations, as an extension to include extra terms makes the analysis too difficult. Thus, in most cases, stability criteria are developed that make sense physically for the problem being investigated, and these are adjusted in view of the model results obtained.

Such an investigation was performed for the one-dimensional model developed in Chapter 2, and will be extended here to include all three coordinate directions. The criteria are divided into velocity criteria and dispersion criteria, and are examined in the following two subsections.

7.2.1 Velocity Criteria

The simplest and most obvious velocity criterion is that pollutant mass should only be transferred between adjacent cells during one time step. The model is set up this way, so that if too large a velocity is present, such a transfer of mass will probably cause an error in the square root term associated with the width of the distribution in a cell, because this width is now negative. In its simplest form, this condition can be written,

$$|u_{\max ijk}| < \frac{\Delta x}{\Delta t} \quad (7.2)$$

where

$$u_{\max ijk} = \text{largest velocity expected in cell } ijk \text{ (L/T)}.$$

Before setting up the model, then, the condition expressed by Equation (7.2) should be examined in each proposed cell of the model, particularly in junctions. However, this would be both cumbersome and unnecessary if the condition in only the most critical cells of each reach and junction can be examined. To select these cells, the type of velocity field expected must be considered, and points of maximum anticipated velocities identified.

For the case of an astronomical tide alone, the maximum velocity in each reach and junction is expected at the downstream end since the

tidal velocity is a linear function of distance from the dead-end. Also, as the vertical velocity distribution is assumed to be logarithmic, based on the mean depth of flow in each cell, the maximum velocity in the vertical will occur in the middle cell of the top layer. Thus, the critical cell is the middle cell in the top layer at the downstream end of the reach or junction, assuming the length of each segment, Δx , is either constant, or does not vary significantly.

For wind induced circulation alone, the maximum velocity is at the water surface. Thus, the critical cells will be those in the top layer of each reach.

For density currents alone, induced by movement of a saline wedge, the maximum velocities occur at the downstream end of each reach. However, because of the parabolic vertical velocity distribution within the wedge, the location of the critical cells at the downstream end of the reach may vary between one or more cells. Thus, one cell in each vertical layer at the downstream end of each reach should be examined for this case.

The remaining two components of the velocity field are the induced circulation in bends, and the flow due to the volume rate of lateral inflow. However, unless a river is modeled, using the lateral inflow capability, these two effects produce velocities whose magnitudes are small compared with other velocities present, and hence they will not be included in the following analysis.

When this model is run, it will usually be for one of two combinations of conditions, and these will be examined separately. For the case of wind induced circulation superimposed on an astronomical tide, the critical cell is the middle cell in the top layer at the

downstream end of each reach. From Equation (4.30), the maximum wind induced velocity expected, u_{wmax} , can be expressed as a function of the maximum component of the wind $|w_s \cos \theta|_{max}$ along the longitudinal axis of the reach,

$$u_{wmax} = K_w |w_s \cos \theta|_{max}^2 (d - \Delta z)^2 / 4dN_z \quad (7.3)$$

where Δz = thickness of top layer (L).

A similar expression can be developed for the maximum astronomical tide component of the velocity field, u_{tmax} , from Equation (4.12),

$$u_{tmax} = \left(\frac{1}{A} \frac{dy}{dt} \right)_{max} \left(\frac{d}{\Delta z} \ln \frac{d}{d-\Delta z} + \ln \frac{29.73(d-\Delta z)}{ke} / \ln(29.73 d/ke) \right) \quad (7.4)$$

Thus for this case, the velocity stability criterion is given from Equations (7.2), (7.3), and (7.4), as,

$$|u_{wmax}| + |u_{tmax}| < \frac{\Delta x}{\Delta t} \quad (7.5)$$

This form assumes that either Δx is constant throughout a reach, or else its variation is small (particularly if the variation is to increase its value from that at the downstream end of the reach). If Δx does vary throughout the reach, it may be necessary to examine the criterion of Equation (7.5) at other top-center cells in the reach. Merely checking the stability condition at the tidal entrance can be dangerous if a wind induced circulation is present, because the criterion may be violated in an upstream reach whose channel is aligned closer to the direction of the prevailing wind. When a wind is blowing, its induced flow is usually greater than the flow produced by the astronomical tide, and care must be taken to check conditions carefully in all reaches.

For the case in which a density current exists due to the motion of a saline wedge, the vertical velocity profile within the saltwater wedge during the flood tide is given in Equation (4.69), before the wedge impinges on a dead-end of the canal network. In the top layer of the saltwater wedge, the maximum velocity, u_{smax} , is given by,

$$u_{smax} = \frac{u_4}{\Delta z} d_s \left(\frac{dd}{dt} \right)_{max} \left(1 - \left(1 - \frac{\Delta z}{d_s} \right)^3 \right) \quad (7.6)$$

where Equation (7.6) is applied at the downstream section of each reach. This expression is added to Equation (7.5), to establish a criterion for the longitudinal velocity field in the presence of a density current,

$$u_{max} = |u_{wmax}| + |u_{tmax}| + |u_{smax}| < \frac{\Delta x}{\Delta t} \quad (7.7)$$

The condition of Equation (7.7) leads to a conservative criterion as the worst case conditions for the wind induced circulation and the density current occur in different cells. However, this form of analysis is simpler than a rigorous application of the equation to each cell in the cross-section at the downstream section of each reach.

The conditions for wind induced circulation and density currents in junctions cannot be analysed as above, because the junctions are simply defined as transition zones between adjacent reaches. To determine the effect of junction spatial increments, Equation (7.2) can be used directly using the estimated velocities in cells adjoining the junction. However, this may not always produce stable results because of the coupling of two different numerical schemes, the upwind difference scheme in the junction and the method of second moments in the adjacent reaches, at this point. On a number of occasions, with stability criteria seemingly met, the results become unstable at, and

propagated from the cells adjoining a junction of the network. In all cases it was found that halving the time step rectified the problem.

7.2.2 Dispersion Criteria

Written in terms of mass transfer between adjacent cells, the vector form of the dispersion terms of the three-dimensional mass-transport equation can be written using the dispersion velocities developed in Chapter 5,

$$c \bar{u}_D = -\bar{E} \nabla c \quad (7.8)$$

A stability criterion can then be established in the reaches of the system, as dispersion is not modeled in junctions, to state that not more than half the difference in the mass of the substance modeled can be transferred between adjacent cells in the direction of the negative concentration gradient, in one time step Δt . This means that the dispersion coefficient in each coordinate direction has to satisfy the condition,

$$(E_x, E_y, E_z) \leq \frac{1}{2\Delta t} (\Delta x^2, \Delta y^2, \Delta z^2) \quad (7.9)$$

Looking at the longitudinal dispersion coefficient, a criterion can be developed from Equations (5.19) and (7.9), for the associated dimensionless dispersion coefficient, K_x ,

$$K_x \leq \left(\frac{\Delta x^2}{2\Delta t} - E_0 \right) \frac{8.25}{u_{\max}} \quad (7.10)$$

where u_{\max} is given from Equation (7.7). For all practical applications, $E_0 \ll \Delta x^2/2\Delta t$, and the condition becomes,

$$K_x \leq 4.125 \Delta x^2 / \Delta t u_{\max} \quad (7.11)$$

A closer look at the magnitude of the right hand side of Equation (7.11) indicates that this value will usually be much larger than the value of

K_x (Taylor's analysis [1954] shows that K_x is on the order of 0.1).

Thus, for most simulations, this condition will be well satisfied, and can be ignored for all practical purposes.

Similarly from Equations (5.20) and (7.9), the stability criterion for the lateral dimensionless dispersion coefficient, K_y , can be written,

$$K_y \leq 4.125 \Delta y^2 / \Delta t d u_{\max} \quad (7.12)$$

where E_0 is again small compared to $\Delta y^2 / 2\Delta t$. This condition although more readily violated than the condition for the longitudinal dimensionless dispersion coefficient, K_x , is well satisfied in most practical cases as K_y is an order of magnitude less than K_x . The danger arises when many lateral divisions are chosen, and the time step Δt , is large. However, most systems can be reasonably simulated using only one lateral cell in each vertical layer, thus eliminating the need for this condition.

The criterion for the vertical dimensionless dispersion coefficient, K_z , is by far the most critical, and usually the one which will be violated first in a simulation. From Equations (5.21), (5.25), and (7.9), the condition can be written,

$$K_z \frac{d^2}{9} \left| \frac{du}{dz} \right|_{\max} + E_0 \leq \frac{\Delta z^2}{2\Delta t} \quad (7.13)$$

In this case, E_0 can be of the same order of magnitude as $\Delta z^2 / 2\Delta t$, for reasonable choices of these model parameters. The condition for K_z is then,

$$K_z \leq \left(\frac{\Delta z^2}{2\Delta t} - E_0 \right) 9/d^2 \left| \frac{du}{dz} \right|_{\max} \quad (7.14)$$

where a first condition is that the right hand side of Equation (7.14) must be positive.

Equation (7.14) could be further expanded by introducing the closed form functions of the various components of the velocity field, and differentiating twice to find $\left. \frac{du}{dz} \right|_{\max}$. However, this would result in a theoretically valid, but extremely cumbersome, expression to be evaluated at many locations in a canal network. Two simpler expressions can be obtained by considering the conditions, as before, of a wind induced circulation with and without a density current. In both cases the tidal velocity term will be ignored to first order, as its effect is usually small and would automatically be satisfied alone for most practical choices of a network cell structure.

For the first case of the wind induced circulation, Equation (4.30) can be differentiated to give the stability criterion,

$$K_z \leq \left(\frac{\Delta z^2}{2\Delta t} - E_0 \right) \frac{18N_z}{d^2 K_w |w_s \cos \theta|_{\max}^2} \quad (7.15)$$

This condition uses the value of du/dz at the water surface and hence is conservative.

For the second case in which a saltwater wedge is also present, the condition is much more complicated as it depends on the relative thicknesses of the fresh and saltwater layers. Again, a conservative condition can be established by assuming that the velocity in the freshwater layer is the maximum velocity in the wedge multiplied by an inverse ratio of the thicknesses of the layers. Incorporating this, along with the condition for the wind induced circulation, gives,

$$K_z \leq 9 \left(\frac{\Delta z^2}{2\Delta t} - E_0 \right) / d^2 \left(\frac{K_w |w_s \cos \theta|_{\max}^2}{2N_z} + 3u_4 \left(\frac{dd_s}{dt} \right)_{\max} \left(1 + \frac{d_s}{d-d_s} \right) \right) \quad (7.16)$$

The criteria expressed in the equations throughout Section 7.2 give guidelines for choosing values of the spatial increments Δx , Δy , and Δz , and the time increment, Δt . In most cases, the spatial increments will be chosen first, reflecting the amount of detail the user wishes to see in the results. Once these values are established, the time increment can be chosen to meet all the stability criteria. The conditions given in this section act only as a guide to the user. Once the model is operational, an examination of the calculated velocity field will show whether the criteria were met, and simpler forms of the conditions, such as Equation (7.9) directly, can be used for this analysis.

7.3 Convergence Criteria

Let $F(x, y, z, t)$ denote the exact solution of the three-dimensional mass-transport equation in terms of its independent variables x, y, z , and t , and let the exact solution of the difference equation used to approximate it be $\tilde{F}(i\Delta x, j\Delta y, k\Delta z, n\Delta t)$, in terms of its incremental variables $\Delta x, \Delta y, \Delta z$, and Δt . Then, the numerical scheme is said to be convergent if $\tilde{F} \rightarrow F$ as $\Delta x, \Delta y, \Delta z$, and $\Delta t \rightarrow 0$ [Smith, 1975].

In a numerical scheme, there must be a point at which the results are considered to be close enough to the exact solution. Above this point the solution either diverges rapidly from the exact solution, or else the results are not considered to be accurate enough for further use. Below this point, decreasing the incremental variables increases the accuracy of the solution but at the expense of computing time and cost. In other words this point is a point of diminishing return in an economic sense.

For numerical solutions to the three-dimensional mass-transport equation, once the stability conditions are met, the scheme will usually converge to the exact solution. For this equation, with variable coefficients, necessary and sufficient convergence criteria are difficult to establish, particularly with respect to the expected accuracy of the model. In order to establish such a criterion, the model must be run for a variety of values of the incremental variables, and their results compared.

In Table 7.1, a standard data set is given for a 1600 ft long canal with a wind of 5 mph blowing along its longitudinal axis from the tidal entrance to the dead-end (Figure 7.1). Several test cases were run assuming that the initial concentration in the canal was 100 ppm, and that the concentration of the receiving waters was 5 ppm. In all cases the results were depth averaged.

The first test, and the most important, varied the longitudinal spatial increment, Δx , and the time increment, Δt , while using three vertical layers and one lateral layer. For a variety of values of Δx from 50-200 ft and of Δt from 0.097-0.388 hrs, the results are shown in Figure 7.2. It can be seen from this figure that the resulting concentration profiles are very similar and predict values that vary by less than 5-6 percent of the initial concentration at any point. This set of results is very encouraging because it includes some combinations of Δx and Δt that are extremely coarse, and which might violate stability conditions for other cases. From Figure 7.2, it can be concluded that the convergence characteristics of the model are such that once the stability criteria are met, the model will yield accurate results.

The second test looked at the number of vertical layers that might be used to simulate a case with wind induced circulation. One lateral layer was defined for simplicity, and the number of vertical layers varied from one to six. It can be seen from Figure 7.3, that the use of only one vertical layer, as expected, averages out the wind effect altogether leaving only a one-dimensional representation of the astronomical tide. The use of two to six vertical layers gave surprisingly similar results for the downstream 2/3 of the canal. However, at the dead-end, the profiles fan out, and for simulations using layers which are not multiples of three, higher concentration values are predicted. It can further be seen that as the number of layers increases from two to five, the concentration profiles at the dead-end tend towards the profiles for the cases of three and six layers. This is not really surprising, because the more layers that are used, the better is the representation of the wind induced vertical velocity profile. Also, even though the depth averaged concentrations are similar, the actual concentrations in each layer differ somewhat from the simulations using three and six layers. The use of many layers to accurately represent the wind induced velocity profile is clearly seen to be an unnecessary waste of time and money, when a simulation using a multiple of three layers will be at least as accurate, and definitely more efficient. For most practical case, three layers are sufficient to model transport conditions, but more can be used if more detailed vertical concentration profiles are required.

The third test was to model the case for three vertical layers, but to vary the number of lateral layers from one to three. As can be seen from Figure 7.4, the results are virtually identical as expected in this

case. From this result it may be concluded that one lateral layer is usually sufficient for a simulation. However, two or three layers should be specified in the flow in a bend is considered to be important, or the lateral distribution of concentration is specifically desired. The problem with specifying more than one layer in each cross-section is that the longitudinal distance increment through the junction may be made unreasonably small, as it is the width of the branch canal divided by the number of lateral layers. One method of overcoming this is to specify a large value for the length of the junction $DXJN(*)$, to give a suitable distance step.

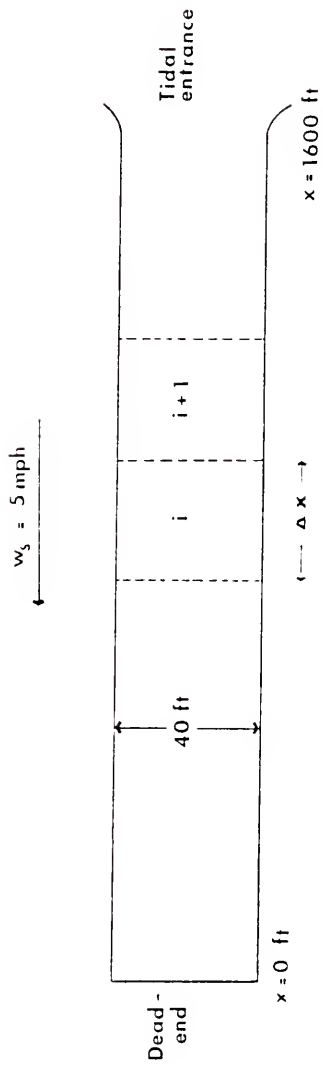


Figure 7.1 - Schematical Canal for Three-Dimensional Model Tests.

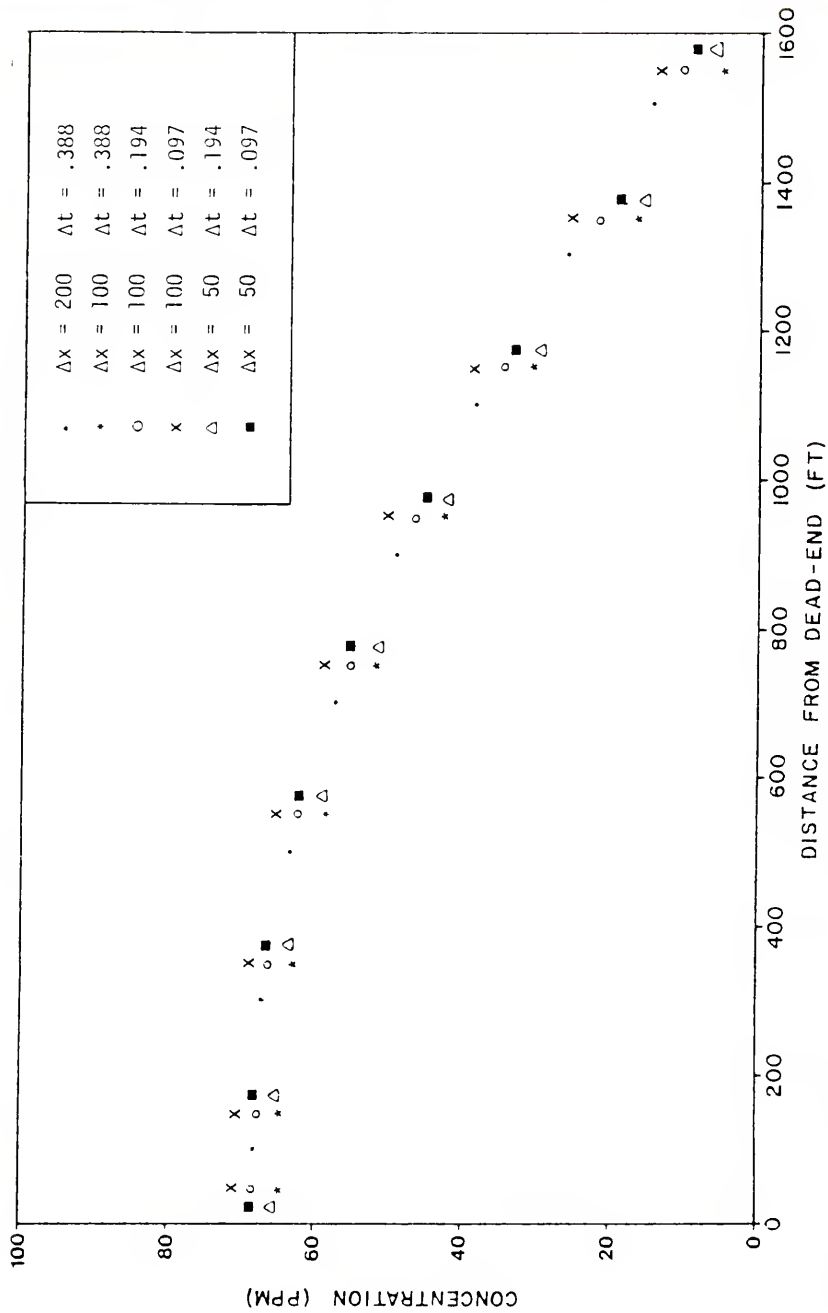


Figure. 7.2 - Variation of Δx and Δt after 50 Tidal Cycles.

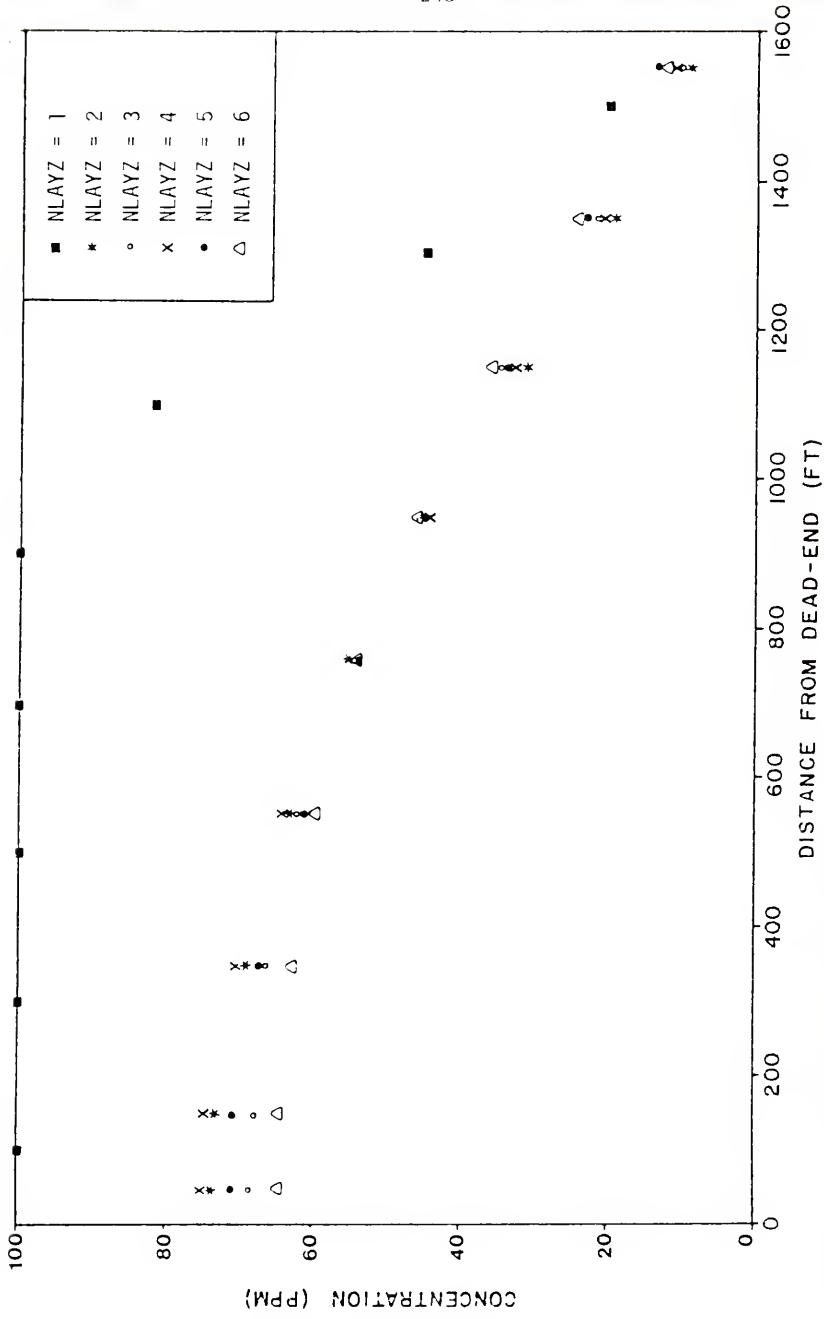


Figure 7.3 - Variations of NLAYZ (NLAYZ = 1).

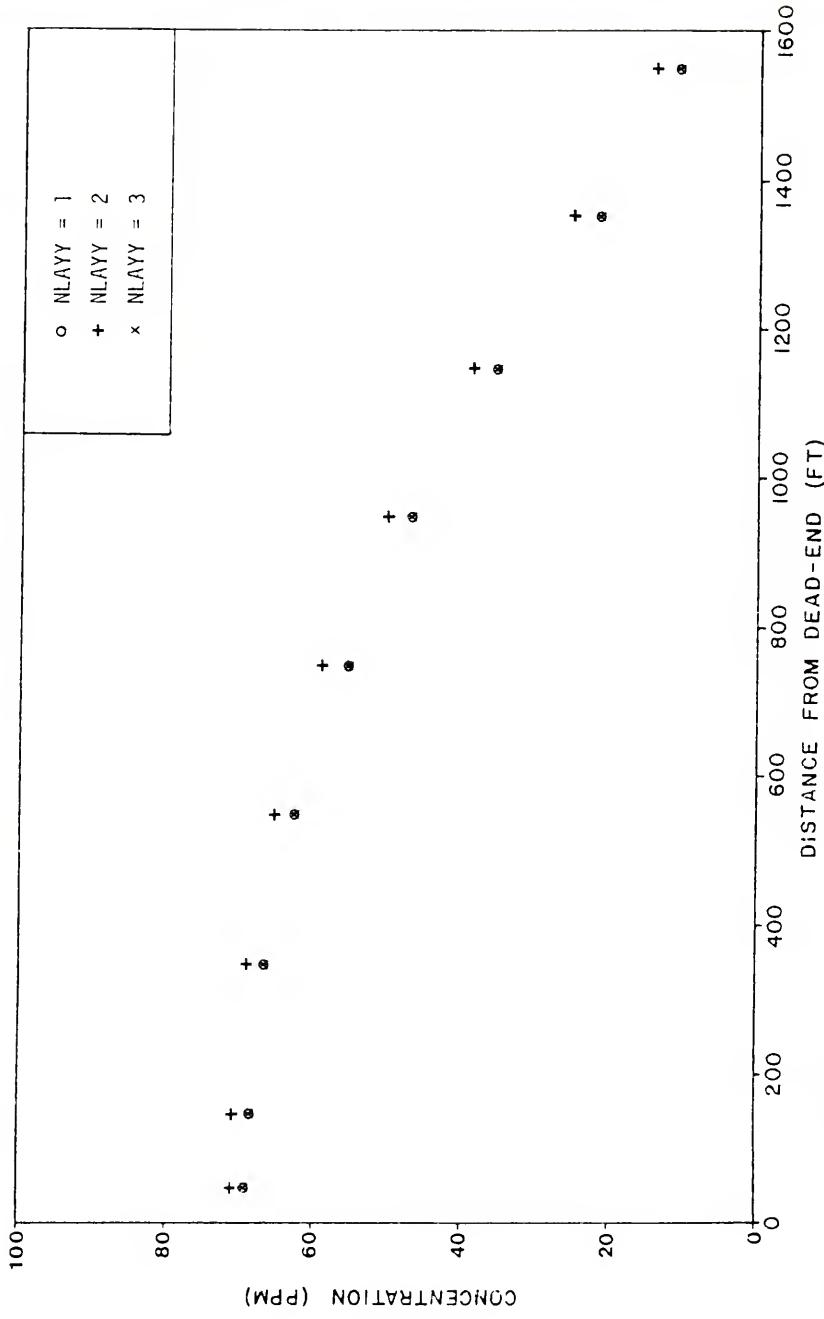


Figure 7.4 - Variation of NLAYY (NLAZY = 3).

CHAPTER 8
MODEL TESTS AND RESULTS

8.1 Introduction

In the previous four chapters, a numerical model has been developed to simulate three-dimensional mass-transport in a canal network. The model equations were presented, the organization discussed, and a set of user oriented stability and convergence criteria established.

In this chapter several case histories are examined to both calibrate the model and to check its accuracy against field data. The first case examines a study on Big Pine Key, Florida, done by the Environmental Protection Agency [EPA, May, 1975]. Looking in particular at what was called Big Pine Key Canal III, Lee [1977] tested his one-dimensional model against EPA's field data, and arrived at some interesting results. These will be discussed in Section 8.2 and the case will also be analysed from a two-dimensional point of view in an attempt to explain the actual physical processes occurring.

The second case study looks at the measured data collected from the 57 Acres Canal Network, in July and October, 1977 [Morris, Walton, and Christensen, 1978; Morris, 1978]. This canal network (Figure 3.2) was considered to be influenced only by the astronomical tides and wind induced circulation. During each field investigation, an amount of Rhodamine WT dye was injected near the dead-end of the South Loop (Figure 8.1) at slack tide, and the resulting longitudinal concentration profiles at several successive slack tides measured using a Turner

Designs Field Fluorometer. These data were used to calibrate the unknown parameters of the model between adjacent high and low tide longitudinal concentration profiles at the beginning of each study, and were then used to determine whether longer term conditions could be accurately simulated. A discussion is presented in Section 8.3.

The third case, presented in Section 8.4, is the Loxahatchee River study (Figure 3.3), which was considered to be an example of a canal influenced by the progress of a saline wedge into the canal during the flood tide. A field investigation was carried out in June, 1977, and the data used to calibrate the saline wedge parameters associated with the model, and to examine the accuracy of the model in simulating measured conditions through time.

Finally, in Section 8.5, a test canal is set up, and some of the features of the three-dimensional model, which could not be analysed using the one-dimensional model presented in Chapter 2, are examined. The effect of winds of varying magnitude and directions were modeled for several different cases of lateral inflow loadings. Also, the effect of a saltwater wedge on such a system was studied.

8.2 Case History #1: Results of Big Pine Key Canal III Runs

Big Pine Key Canal III is one of several canals in the Florida Keys studied by the EPA [May, 1975]. The canal (Figure 8.2) is almost 1600 ft long, 40 ft wide, and 10 ft deep at mid tide. It has a rectangular, prismatic cross-section, and is aligned with its longitudinal x-axis (defined as positive from the dead-end) predominantly NNW.

On November 3, 1973, at high water slack, 500 ml of Rhodamine WT dye was injected at mid-depth, 50 ft from the dead-end of the canal. At regular intervals after the injection, dye concentrations were measured

using a fluorometer sampling at mid-depth along the longitudinal center-line of the canal [EPA, May, 1975, Figure 22, p. 45].

Once the data were collected, EPA tried to simulate the profiles using firstly the June, 1973, version of the Storm Water Management Model (SWMM) [Langer et al., 1971; Metcalf and Eddy et al., 1971], and then the Columbia River Model (CRM) [Callaway et al., 1969; Callaway and Byram, 1970]. The reason given for turning away from the SWMM model was that [p. 207]:

SWMM did not satisfactorily reproduce observed profiles. The field study showed the dye mixing rapidly throughout the length of the canal and then slowly "bleeding" out. The model, however, shows the dye cloud centroid remaining in one place and slowly flattening out, similar to classical diffusion without advection. As the SWMM neglects diffusion in its transport equation, this apparent diffusion is probably due to "numerical dispersion," or "pseudo-dispersion," associated with the numerical methods employed in this model.

Turning to the CRM, which incorporates a dispersion term, several of the canals examined were studied and the results presented. Although a computer simulation was not shown for Big Pine Key Canal III, one was done for Big Pine Key Canal V, which is an identical, adjacent canal to the west. Using a measured longitudinal dispersion coefficient of 24×10^{-4} sq mile/day ($0.77 \text{ ft}^2/\text{sec}$) at the mid-point of the canal as a uniform coefficient, they managed to reproduce the measured profiles by making an adjustment to the dispersion term, effectively by dividing it by five.

Interestingly, Lee [1977] also tried to model Big Pine Key Canal III using a one-dimensional model which corrects for numerical dispersion (described in Chapter 3), with a linearly varying longitudinal dispersion coefficient that matched the measured value of 26×10^{-4} sq mile/day ($0.84 \text{ ft}^2/\text{sec}$) at mid-canal. However, in obtaining a fit between computed and observed profiles he had to increase the dispersion term by two orders of magnitude (Figure 8.3).

From these results, two conclusions may be drawn. Firstly, the CRM suffers from severe numerical dispersion when used to model low energy canals such as those along the Gulf and East Atlantic coasts. This is not really too surprising, as the CRM and SWMM are interrelated models, both having been developed from the Dynamic Estuary Model (DEM) [Feigner and Harris, 1970]. The inclusion of a dispersive term in the CRM cannot be expected to produce any better results, as the main source of error has not been addressed.

Secondly, as stated in the EPA report [May, 1975, p. 207], "the dye cloud centroid remaining in one place" must be expected in a model which, due to its one-dimensional form, can only model the velocity field induced by the astronomical tide. In the Pig Pine Key area of Florida, the tidal range is on the order of 1 ft. A simple volumetric tidal prism analysis indicates that maximum velocities of no greater than 0.01 ft/sec can be expected, and then only at the tidal entrance. At the dead-end of the canal, the tide induced velocities will be much lower, and certainly not enough to move the dye cloud any appreciable distance.

In such a system which is directly open to the ocean, and which does not appear to be influenced by density currents, the main forcing function producing circulation in the canal must be the wind. This effect cannot be modeled in one-dimension, although many people apparently have tried. The altering of dispersion coefficients to match prototype conditions, using an ill-defined model, can only give results good for that particular case--and no other! Any predictive analysis based on such a model calibrated in this manner, must be at best questionable.

To illustrate this point, the three-dimensional model, CANNET3D, was run for this case. One lateral layer and three vertical layers

were used and the wind speed and direction estimated from monthly averages for the Key West area (Table 8.1). From these data, a resultant wind in the canal appeared to be about 5 mph blowing from the tidal entrance to the dead-end. The remaining coefficients left to vary were the vertical momentum transfer coefficient, N_z , the background dispersion coefficient, E_0 , and the three dimensionless dispersion coefficients, K_x , K_y , and K_z . As the wind speed was constant, E_0 was set to zero, and thus its effect is combined with that of K_z . As there was only one lateral layer, K_y had no effect. Also, the effect of K_x is very small, and the two important parameters are N_z and K_z .

To calibrate these parameters, N_z was altered until the center of mass predicted by the model corresponded with its observed location after 12 hrs. Then, K_z was altered until the concentration values at the same time matched. It can be seen from Figure 8.3 that good agreement was found by setting $N_z = 0.005 \text{ ft}^2/\text{sec}$, and $K_z = 0.008 \text{ ft}^2/\text{sec}$ (Table 8.1). As will be seen in the next section, these are very reasonable values for N_z and K_z particularly considering that the variability of the wind could not be introduced into the model, as wind data were not collected at the site, and also that an estimate was made, however realistic, of the magnitude of the wind. As the wind induced velocity depends on the wind speed raised to the power 2.5 (Equations (4.18) and (4.27)), N_z could easily have the same value as found for the 57 Acres Canal Network, discussed next. Furthermore, decay was not introduced because the time sequence and atmospheric conditions at the time of the test were unknown.

In conclusion, it has been demonstrated quite clearly, that a one-dimensional model is quite useless in predicting water quality conditions

in low energy canal systems. In many cases, the tidally induced flow is one of the least significant forcing functions, and thus field conditions cannot be hoped to be simulated using only one component of the physical phenomena at work. In a simple testing of the three-dimensional model, using only a two-dimensional capability, a much more realistic set of results were obtained, using values of the variable parameters that will also be seen to be applicable to other canal networks in different locations and operating under different conditions.

8.3 Case History #2: Results of 57 Acres Model Runs

The 57 Acres Canal site has been extensively investigated by the Hydraulic Laboratory since early 1975 (Table 3.1). However, two particular field studies have been isolated for this analysis because each contains a detailed study of the movement of a dye cloud introduced into the system.

During both the July and October field trips in 1977, 1500 ml of Rhodamine WT were released into the end section of the South Loop of the system (Figure 8.1) at slack tide. For the July study the dye was released as a point source, while in October it was mixed throughout the width, over the top 1/3 of the depth, using the pressurized release technique discussed in Chapter 3 [also, Morris, Walton, and Christensen, 1978; Morris, 1978]. At each successive high and low tide, a longitudinal concentration profile was measured at a depth of 2 ft below the water surface, using a Turner Designs Field Fluorometer. The sampling was done by driving the boat at low speed down the center-line of each reach of the system.

A wind gauge was installed for the October field survey so that a continuous record of wind speed and direction could be maintained throughout the course of the investigation. To investigate the results of the July study, a wind record for the closest permanent wind gauge at West Palm Beach Airport, Florida, was obtained. These two records showed quite different wind conditions. From Figure 3.12, it can be seen that the wind during the October investigation was fairly light, becoming very calm at night, whereas for the July study, the wind was much stronger and more uniform with 10-13 mph winds out of the East for much of the time. During both investigations, a continuous recording tide gauge was set up in the dead-end of the South Loop to obtain a time history of tidal elevations which, like the wind speed and direction, was digitized for input to the model.

For both these test cases, it was decided to simulate mass transport in the South Loop only, for computational economy, and because not much of the dye escaped from this area during the 40-50 hrs of simulation in each case. Thus the entrance to the South Loop was set up as a tidal entrance, and a high time decay rate, $\tau = 6.21$ hrs (half the tidal period) was specified because of the small receiving waterbody present.

For the July study, the 1500 ml of dye was released about 250 ft from the dead-end of the South Loop. Reach number 1 (Figure 8.1) was divided into 100 ft segments, and one lateral layer and three vertical layers were chosen for the model. Therefore, it was assumed that initially, the dye was well mixed throughout the upper layer of the third segment from the dead-end (200-300 ft). This gives an initial concentration in that cell of,

$$c_i = \frac{(1500 \text{ ml})(3.531 \times 10^{-5} \text{ cu ft/ml})}{(3 \text{ ft})(100 \text{ ft})(100 \text{ ft})} \times 10^9 \text{ ppb}$$
$$= 1750 \text{ ppb} \quad (8.1)$$

The background concentration, c_{RW} , was estimated to be 20 ppb from field observations. The observed and computed longitudinal concentration profiles for reach numbers 1 and 5, and junction number 2 are shown in Figure 8.4.

During the October study, a similar amount of dye was injected into the canal a little further away from the dead-end. For this study case, it was decided to digitize the longitudinal concentration profile in reach number 1 at the first high water slack tide after the injection. Again from field observations, the background concentration was found to be 0.2 ppb. The observed and computed longitudinal concentration profiles for reach numbers 1 and 5, and junction number 2, for the October study, are shown in Figure 8.5.

As for the Big Pine Key Canal III study case, the important parameters to investigate were the momentum transfer coefficient, N_z , and the dimensionless vertical dispersion coefficient, K_z . However, in this case, as the wind conditions during each investigation were different, the effect of the background dispersion coefficient, E_0 , could also be studied.

For both the July and October simulations, the first runs in each case were designed to vary N_z until the model predicted the observed location of the center of mass after half a tidal cycle (or to the following slack tide). Both runs met with some success and some difficulty. For the July run, the fact that wind data was from an off-site source,

was reflected in the fact that it was difficult to accurately simulate actual conditions. However, it can be seen from Figure 8.4 that the general movement of the dye cloud is fairly well followed.

The results for the October simulation (Figure 8.5) indicate that the center of mass is followed fairly well after the first slack tide from the beginning of the simulation. However, it is not fully understood why the initial fit to the profile after one-half tidal cycle is not better. During this period from 10 p.m. on October 18, 1977, until 4 a.m. on October 19, it can be seen from Figure 2.35 that there was no wind blowing, and yet the dye cloud moved downstream against a flood tide. The probable explanation of this apparent inconsistency is data error.

For both cases it was found that a value of $N_z = 0.002 \text{ ft}^2/\text{sec}$ gave fairly good agreement between the simulated and observed locations of the center of mass of the dye cloud throughout the period of investigation. This result agrees with the value obtained from the Big Pine Key Canal III study case (Section 8.2), when it is recalled that an estimated wind velocity was used. In fact, as the wind induced velocity in the canal is related to the wind speed to the power $5/2$ for moderate winds (Equations (4.18) and (4.27)), the wind speed in the latter case would only have to be multiplied by a factor of 0.7 to give exact agreement between the two simulations.

Once the transient locations of the center of mass of the dye clouds had been simulated, the next step was to reproduce the peak values of dye concentration profile. First runs indicated that using K_z alone would not match both sets of field data. During the initial period of the October investigation, the winds were either very light

or dead calm. Thus, it was decided to use the background dispersion coefficient, E_0 , to match the peak concentration values for the first measured profile after the start of the simulation. When this was done, E_0 was held constant and K_z adjusted to match the peak concentration values for the first measured profile after the start of the July simulation. This formed the basis of an iterative procedure on the values of E_0 and K_z until good agreement over the initial period of the two simulations was found. The values obtained were $E_0 = 0.0005$ ft^2/sec and $K_z = 0.0001$.

With these values, and others given in Table 8.2, the simulations were then run to the end of the periods of record. The results are plotted in Figure 8.4 for the July investigation and in Figure 8.5 for the October investigation. From these figures, it can be seen that reasonably good agreement was found considering the difficulties inherent in obtaining accurate data over a long time period. Most of the disagreement is believed to have been caused by the continual recalibration of the fluorometer during each study. The results show that the mass of dye present in the canal varies during the measurement period in a manner not consistent with decay, mixing to lower layers, and loss through the tidal entrance. Considering this to be the case, the degree of fit between model and prototype values is good.

In the South Loop at Station 3 (Figure 3.2), there is a sharp bend. For the simulations described above this feature was not included because of the variability of measured concentration, and because the concentrations were only measured at a depth of 3 ft. During the October field investigation, three velocity towers were set up just downstream of the bend, and a period of record obtained. To investigate the

accuracy of the model, this bend was included and the model run for the October study case with three lateral layers and three vertical layers. A predicted and measured lateral velocity field were shown in Figure 4.7, where the theory of secondary currents was discussed. From this figure it can be seen that in spite of the assumptions made, field conditions are well modeled.

During this same run, the vertical dispersion coefficients, E_z , were also printed out, and are shown in comparison with the component of wind down reach number 1 (Figure 8.1) in Figure 8.6. From this figure, the importance of modeling this parameter based on the velocity gradient can be seen. Many modelers simply specify E_z to be constant in their models. However, this can be unrealistic in low energy tidal canals in which flow reversals are common. In the reversal layer, a good deal of mixing, not predicted by a constant vertical dispersion coefficient, is expected and can only be modeled using a form of E_z based on the value of the vertical velocity gradient at this point.

In conclusion of this section, good agreement was found between the various studies for the value of the vertical momentum transfer coefficient, $N_z = 0.002 \text{ ft}^2/\text{sec}$. The results of simulating the July and October dye studies yielded $E_0 = 0.0005 \text{ ft}^2/\text{sec}$ and $K_z = 0.0001$. These values gave good results considering the difficulties involved in obtaining accurate field measurements.

A sample test run for the October simulation is shown in Appendix D. The input parameters are listed, the results printed out after every 5 hrs of simulation, and longitudinal concentration profiles plotted at two time intervals during the simulation.

8.4 Case History #3: Results of Loxahatchee River Runs

The Loxahatchee River site (Figure 3.3) consists of two parallel canals, the North and South Canals, which are 2200 ft long, 70 ft wide, and 7 ft deep at mid-tide (Figure 3.6). The alignment angle of the canals is approximately 270 degrees (west). During a field investigation by the Hydraulic Laboratory in June, 1977 (discussed in Chapter 3), 75 ml of Rhodamine WT dye was injected and mixed in the upper half depth, across the width, 200 ft from the dead-end of the North Canal at high water slack. Sampling was performed at regular intervals at discrete points in the vertical and along the longitudinal centerline of the canal, as indicated by the readings in Figure 8.25.

During the field investigation, several wind speed readings were taken using a hand-held meter. However, because of the infrequency of the readings, and because of the difficulty in obtaining an accurate direction, wind data collected at the closest permanent station, West Palm Beach Airport, were used for simulation purposes. This record was digitized, together with the tidal elevations obtained from a continuous tide recorder located near the mouth of the canal, as input to the model. The tidal entrance decay coefficient, τ , was assigned the value 1, as the receiving waterbody was large and good mixing could be anticipated.

Measured salinity profiles (Figure 3.16) indicate that this is a system which is influenced by the movement of a saline wedge entering the canal during the flood tide, and receding during the ebb tide. Thus, it was decided to analyse this system by including the saline wedge capability of the model, as coded in the subroutine WEDGE. As

discussed in Chapters 4 and 6, modeling a saline wedge requires that the simulation begins at low tide. Unfortunately, the dye was injected into the system 3 hrs before low tide. However, the first set of measurements were taken during the following low water slack tide, and these readings were digitized as the initial concentration profile in the computational cells of the model. The background concentration, c_{RW} , was measured to be 0.03 ppb.

The canal was divided into one lateral layer and three vertical layers, and the simulation proceeded for 50 hrs. This test run was used to study the salt wedge parameter, u_4 , introduced in Equation (4.64). The remaining parameters, N_z , K_x , K_y , K_z , and E_0 , assumed the values chosen for the 57 Acres simulation runs. The values of the various parameters are listed in Table 8.3.

From Figure 8.7, it can be seen that good agreement was found between observed and computed concentration values for $u_4 = 3000$. Also, giving confidence to this value, the computed vertical velocity profile, as shown in Figure 4.10, matches well the observed profile measured at the corresponding time.

As stated before, only one canal exhibiting these conditions was studied, and although it is fairly typical in geometry to other canals influenced by density currents, the value of u_4 may have a variation which is dependent on the length of the canal. Thus, it is recommended that before a simulation of a proposed canal network is begun, it would be advisable to first check the value of this parameter on a canal of similar length, to determine both u_4 and its dependence on the length of a system.

8.5 Effect of Varying Model Parameters on Three-Dimensional Mass-Transport

In Section 2.8, the effects of the different parameters of the one-dimensional model were studied and some conclusions drawn. The main parameters varied were geometric, and thus their qualitative effect as presented in the variability analysis will also be the same for the three-dimensional model. However, the one-dimensional model does not have the capability of modeling phenomena which produce zero net flux through any cross-section of a reach. These phenomena, such as wind induced circulation and density currents, can only be studied by a two- or three-dimensional model, and will be the subject of the following two subsections.

The following analysis was based on a single prismatic canal whose dimensions are those of the Big Pine Key Canal III discussed in Section 8.2 (Figure 8.1), but whose longitudinal axis is directed south (180 degrees). The other parameters were chosen fairly arbitrarily, being selected to provide a constant data set rather than reflect actual conditions in that particular canal. This data set is listed in Table 8.4.

The analysis of the following two subsections serves to provide the reader with a qualitative idea of the effect of wind induced circulation and density currents on a simple system. A much more in-depth look at these effects is presented in a separate report [Morris, Walton, and Christensen, 1978], and in a separate dissertation [Morris, 1978]. In those discussions, the entire canal network design process is studied, and a procedure outlined for investigating proposed systems with a view to optimizing their flushing characteristics.

8.5.1 Effect of Wind Induced Circulation

In this section, the effect of wind induced circulation will be studied in the absence of a density current. For each case considered, five different wind conditions were used which are zero wind (0,0), 5 mph blowing out of the canal (5,0) (positive x-direction), 5 mph blowing into the canal (5,180) (negative x-direction), 10 mph blowing out of the canal (10,0), and 10 mph blowing into the canal (10,180). In the following figures, these conditions will be labeled on the plots as "(wind speed, wind direction)."

The first case, case 1W (see Table 8.5, where W refers to wind induced circulation only), examined the rates of flushing of the system due to wind. The initial concentrations in the canal, c_i , were set to 100 ppm and the background concentrations, c_{RW} , was 5 ppm. Such might be the case of a catastrophic pollutant loading on the canal. The resulting vertically integrated longitudinal concentration profiles after ten and fifty tidal cycles are shown in Figure 8.8 and 8.9, respectively.

As expected, the resulting profile with no wind shows that very little of the substance has been removed from the canal. In fact, it would take many hundreds of tidal cycles to cause any significant effect on the system. This result is in complete accord with results obtained for a similar system using the one-dimensional model, and clearly demonstrates a one-dimensional model's inability to accurately model the flushing characteristics of low energy tidal canals.

From these figures it can be seen that the 10 mph wind has flushed half the substance from the canal in ten tidal cycles, and virtually all of it after fifty tidal cycles. The results for the 5 mph wind are much more interesting. Examining Figure 8.9, it can be seen

that with the wind blowing out of the canal, over 50 percent of the substance was removed after fifty tidal cycles, whereas with the wind directed into the canal, about 10 percent more has been retained in the same time. This is due to the fact that transport out of the canal in the lower layers for this wind condition is slower, because of friction at the bed, than for transport out in the upper layer with an out-blowing wind.

This can also be seen in the second test case, case 2W (Table 8.5), in which the two concentrations are reversed. The initial concentrations in the canal were 5 ppm and the background concentration of the receiving waters set at 100 ppm. This might be an example of a "clean" canal connected to a polluted waterbody.

The results after ten and fifty tidal cycles are shown in Figures 8.10 and 8.11 respectively. From these figures it can be seen that the exact opposite of the previous case is found. For zero wind, hardly any intrusion is found, which would be an underestimation in any practical situation. For wind speeds of 10 mph, the concentrations in the canal virtually increase to the background after fifty tidal cycles, and as can be seen for the case of the 5 mph winds, the higher concentrations result when the wind is blowing into the canal from the tidal entrance towards the dead-end.

The next series of runs examines the effect of wind induced circulation for the case in which there is a uniform lateral inflow of a substance with concentration $c_I = 100$ ppm, distributed in various ways along the length of the canal. In each case, the total volume rate of the substance entering the canal per unit time is constant.

In the first simulation, case 3W (Table 8.5), a uniform lateral inflow rate of $q_1 = 0.04$ cu ft/hr/ft, with a concentration $c_1 = 100$ ppm was specified along the length of the canal. The resulting longitudinal concentration profiles after ten and fifty tidal cycles are shown in Figures 8.12 and 8.13 respectively. Here it can be seen that for the case of no wind, the concentration at the dead-end is steadily increasing. Also, the wind blowing out of the canal is much more effective in removing the substance than for a wind blowing into the canal. The result is not too surprising, as a wind blowing into the canal transports the substance towards the dead-end in the upper layers, and then towards the tidal entrance in the lower 2/3 of the depth. Thus the substance has further to go to reach the tidal entrance and takes much longer to do so than for either case of the wind blowing out of the canal. In fact, for a 10 mph wind blowing out of the canal in this case, no measurable amount of the substance above the background value remains in the canal, and for a 5 mph wind, the increase in concentrations throughout the length of the canal is small.

The second distribution, case 4W (Table 8.5), results from an inflow rate $q_1 = 0.08$ cu ft/hr/ft in the upper half of the canal. The resulting concentration profiles after ten and fifty tidal cycles are shown in Figures 8.14 and 8.15 respectively. The build-up at the dead-end for no wind or for a wind blowing into the canal, is now more pronounced. As before, a 10 mph wind blowing out of the canal succeeds in keeping pace with the inflow rate in this case, and the increase in concentrations is small.

The 5 mph wind blowing out of the canal is not as efficient as before because more of the substance is now diffused into the lower

layers as the concentration difference is larger than before, and carried back towards the dead-end. For a 5 mph wind blowing into the canal, the concentration is building up at the dead-end, as the induced velocities in the lower layers are not sufficient to carry out all the inflow. An equilibrium position will be reached with time. However, the 10 mph wind in this case induces a sufficiently large return velocity to cause the concentrations at the dead-end to increase very slowly through time.

The final simulation, case 5W (Table 8.5), considers a large loading at the dead-end of the canal. In this case, the lateral inflow rate is 0.32 cu ft/hr/ft along 200 ft adjacent to the dead-end. The resulting profiles after ten and fifty tidal cycles are shown in Figure 8.16 and 8.17 respectively. In all cases, the wind induced circulation was unable to deal with the continuous loading. However as before, concentration values were lower with the wind blowing out of the canal than blowing into the canal for each wind speed.

In case 5W, however, the 5 mph wind blowing out of the canal was not as effective in reducing concentration values as the 10 mph wind blowing into the canal. This shows that there is some point in the variability analysis at which the transfer of substance vertically becomes important when compared to purely convective transport of the velocity field. In this case, the 5 mph wind blowing out of the canal, is not able to transport the substance out of the canal quickly enough to prevent a considerable amount of vertical transfer to the lower layers which is transported towards the dead-end.

In conclusion, most cases of lateral inflows of pollutants into canals occur into the top layers of the canal; such as run-off from

lawns, leaking septic tanks, etc. In these situations, the above analysis shows that the resulting pollutant mass is better flushed when the wind is blowing down the length of the canal from the dead-end towards the tidal entrance, and that peak concentrations in the canal are smaller than for winds of equal magnitude blowing into the canal.

Also, in cases in which the receiving waterbody has higher concentrations than those desired in the canal, a wind blowing out of the canal is more effective in flushing whatever pollutant does enter the system. Again maximum concentration values in the canal are smaller in this case than for a wind blowing into the canal.

However, if the main pollutant source is in the lower layers, and is located away from the dead-end where it might quickly be transferred to the top layer and transported out of the canal, then a wind blowing into the canal might be more desirable to obtain optimum flushing.

8.5.2 Effect of Density Current

The previous section described the flushing characteristics of the test canal under the influence of wind induced circulation alone. In this section, a density induced circulation is superimposed on the same system and the results analysed for the test cases 1S-5S listed in Table 8.5. For this discussion, only two wind conditions were used, a 5 mph wind blowing into the canal, and a 5 mph wind blowing out of the canal.

The salt wedge interface used in these test runs was located 5 ft below the mean tidal elevation at the tidal entrance to the canal, and the coefficient, u_4 , of Equation (4.64) was assigned the value 4000.

The simulations were carried out to fifty tidal cycles and the results from this analysis presented only at the completion of each run.

For the first test case, case 1S, in which the initial concentrations in the canal were 100 ppm, and the background concentration was 5 ppm, the results are shown in Figure 8.18. Because of the greater circulation induced by the movement of the salt wedge, sufficient to overcome the smaller wind circulation in this case, the resulting longitudinal concentration profiles are significantly lower. As before, the resulting profiles with the wind blowing out of the canal are lower than for the wind blowing into the canal, because the wind induced reversal in the lower layer aids the passage of the salt wedge into the canal and much more mixing occurs across the interface. Conversely, in the case in which the wind blows into the canal, the induced flow reversal tends to impede the density current reducing velocities and thus decreasing vertical dispersion.

In case 2S, in which the initial concentrations in the canal are 5 ppm, and the background concentration of the receiving waterbody is 100 ppm, the opposite is true (Figure 8.19). As the passage of the salt wedge dominates the wind induced circulation for these wind speeds, much more of the higher concentration receiving waterbody is circulated in the canal giving higher concentrations than before. In this case, the 5 mph wind blowing out of the canal does not serve to retard this effect, but instead increases it by aiding the passage of the wedge with a flow reversal towards the dead-end in the lower layers. Also, larger vertical velocity gradients are present which increase vertical dispersion.

In cases 3S to 5S, which examine various lateral inflow distributions, q_I , of constant concentration, $c_I = 1.0$ ppm (Table 8.5), the results show that in each case (except case 3S with the wind blowing out of the canal) the resulting longitudinal concentration profiles are similar to the cases of no density current, but that the effect of the density induced circulation is to improve mixing and lower the range of values of the profiles (Figures 8.20-8.22). The discrepancy in the case 3S result is probably due to some small instability present in the salt wedge computations in which two different schemes are matched. The wedge induced circulation increases the flow out of the canal in the upper layer of the flow, and also increases the vertical dispersion to the lower layers. As the wedge retreats during the ebb tide, the mass of substance in the lower layers is carried out to the receiving waters.

From these results, it would appear that the effect of the movement of a saltwater wedge in a freshwater canal is to improve the circulation in that canal and flush out substances carried by both the fresh and saltwaters. However, the results also show that if a substance is being introduced from the receiving waterbody, such as saline water itself, the transition to a similar type condition in the canal will be quicker than for the case of wind induced circulation alone.

The results in this and the previous subsection are included to provide some qualitative idea of the effect of different external phenomena on water circulation and the flushing characteristics of tidal canals. They can serve as a guide only because there are so many combinations of conditions that can occur, that an all-inclusive analysis

is not possible. Each case must be examined on its own merits. For example, in Floridian canals, the above analysis might indicate that the West Coast (or Gulf Coast) canals have better flushing characteristics than East Coast (or Atlantic Coast) canals when they are built off tidal estuaries with large freshwater river inflows. However, the effect of the salt wedge movement in such a comparison must be weighed against the usually small tidal ranges in this region.

Thus, a proposed canal network should be analysed comparing different conditions which might be expected at a site in that location. Accurate wind and tidal elevation records should be obtained in the area, and a comparative analysis performed for that site with variations in canal network layout. The techniques used in such an analysis are the subjects of separate reports [Morris, Walton, and Christensen, 1978; Morris, 1978].

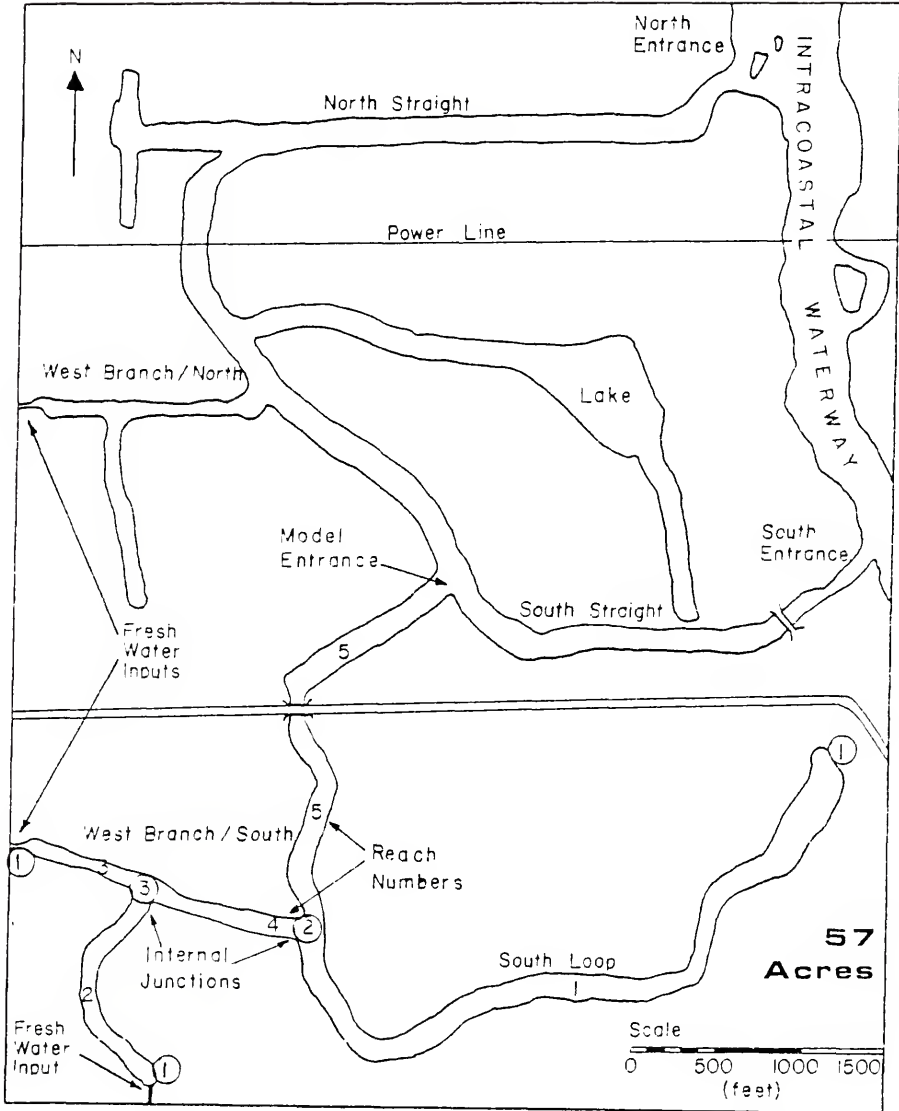


Figure 8.1 - Model Layout of Reaches and Junctions in 57 Acres System.

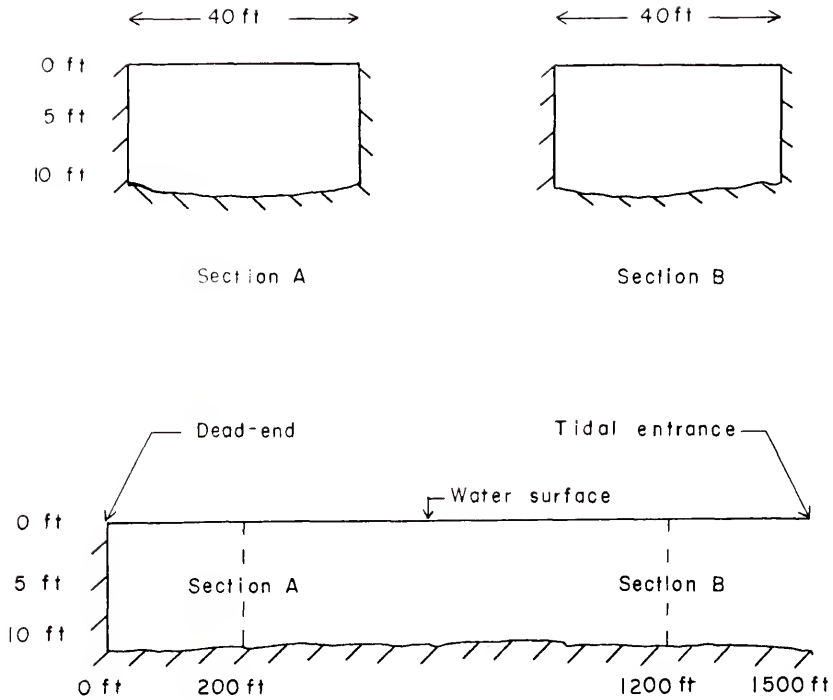


Figure 8.2 - Typical Longitudinal Sections and Cross-Sections, Big Pine Key Canal III, Florida [EPA, May, 1975].

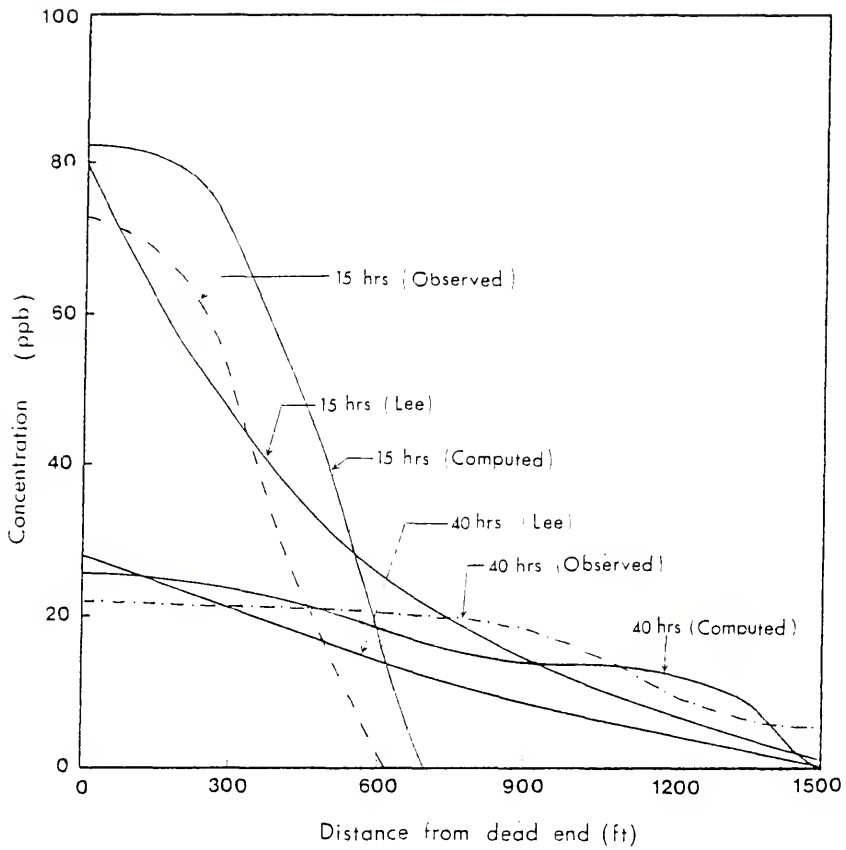


Figure 8.3 - Observed and Predicted Concentration Profiles for Big Pine Key Canal III Case History.

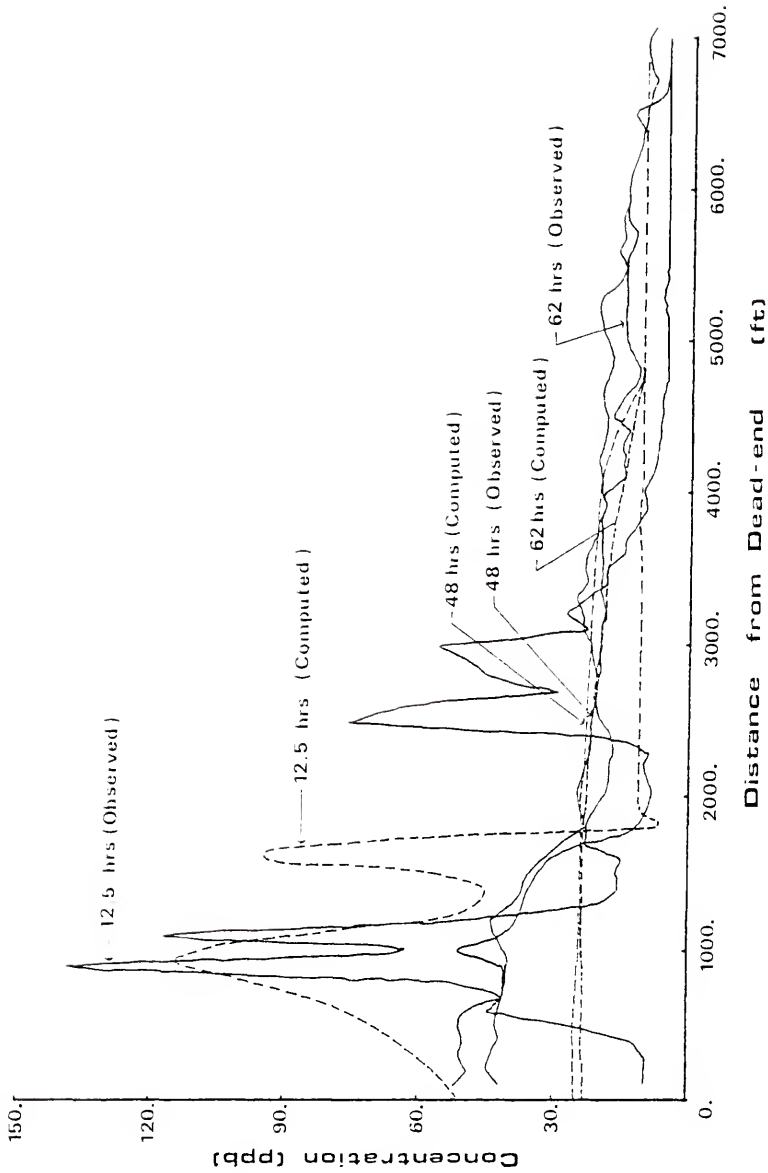


Figure 8.4 - Observed and Predicted Concentration Profiles for 57 Acres July, 1977 Case History.

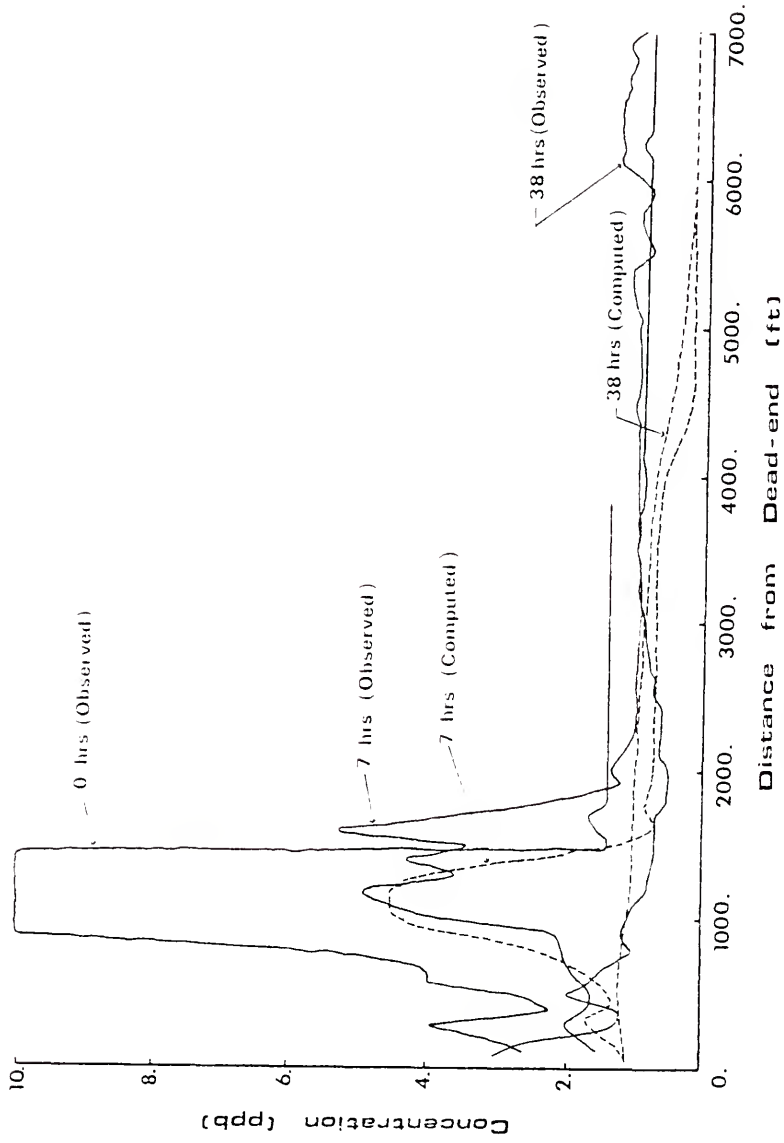


Figure 8.5 - Observed and Predicted Concentration Profiles for 57 Acres October, 1977 Case History.

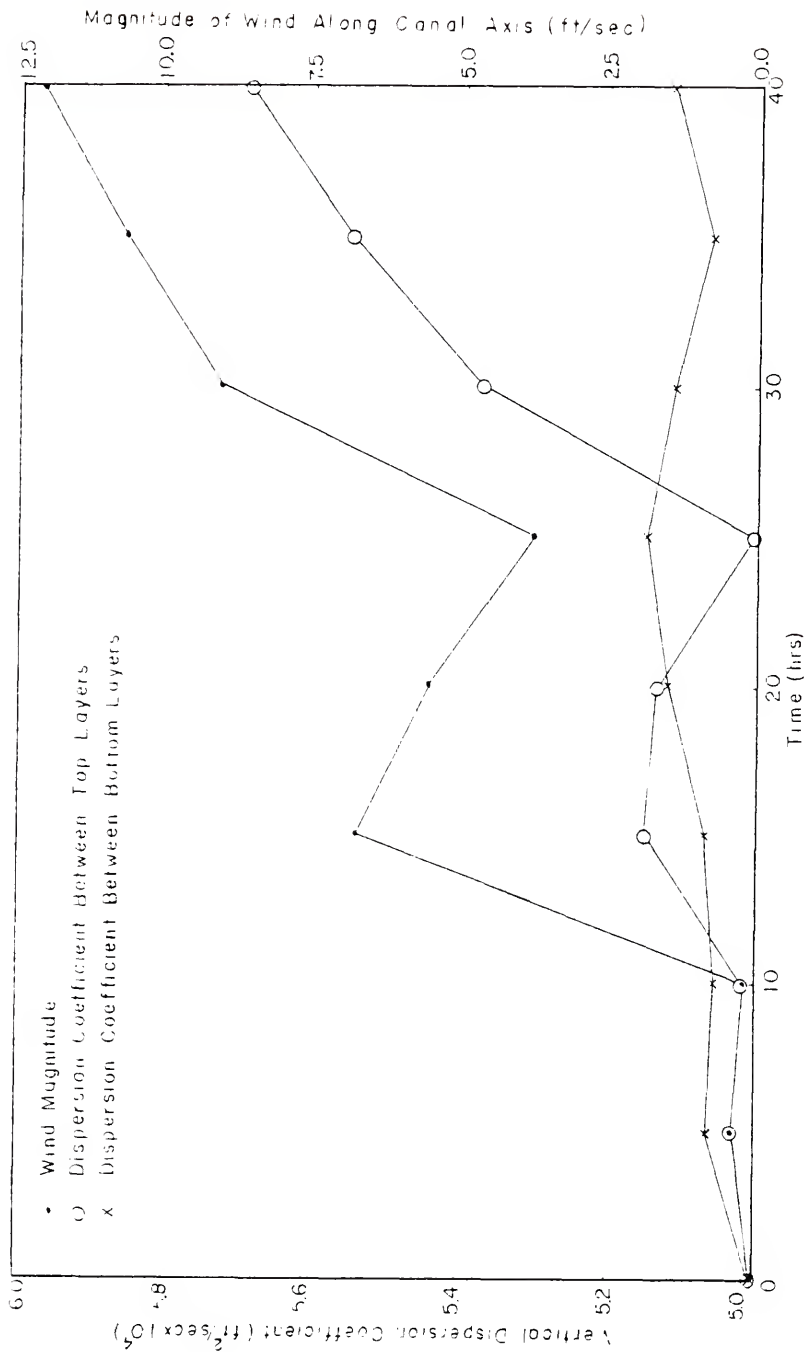


Figure 8.6 - Variation of Vertical Dispersion Coefficient With Time and Wind Speed at Mid-Point of Reach 1 (Figure 8.1), 57 Acres October, 1977 Case History.

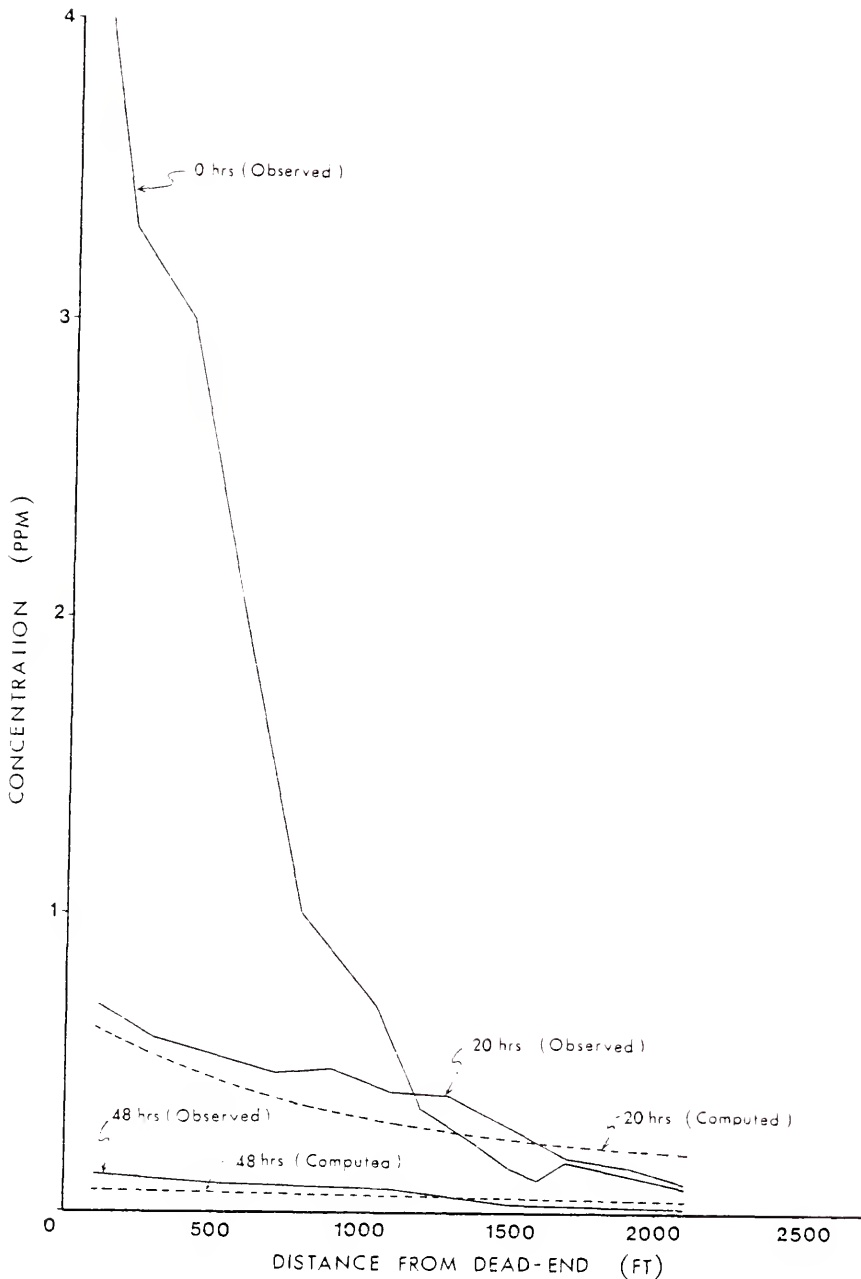


Figure 8.7 - Comparison Between Observed and Computed Concentration for Loxahatchee River North Canal, June, 1977.

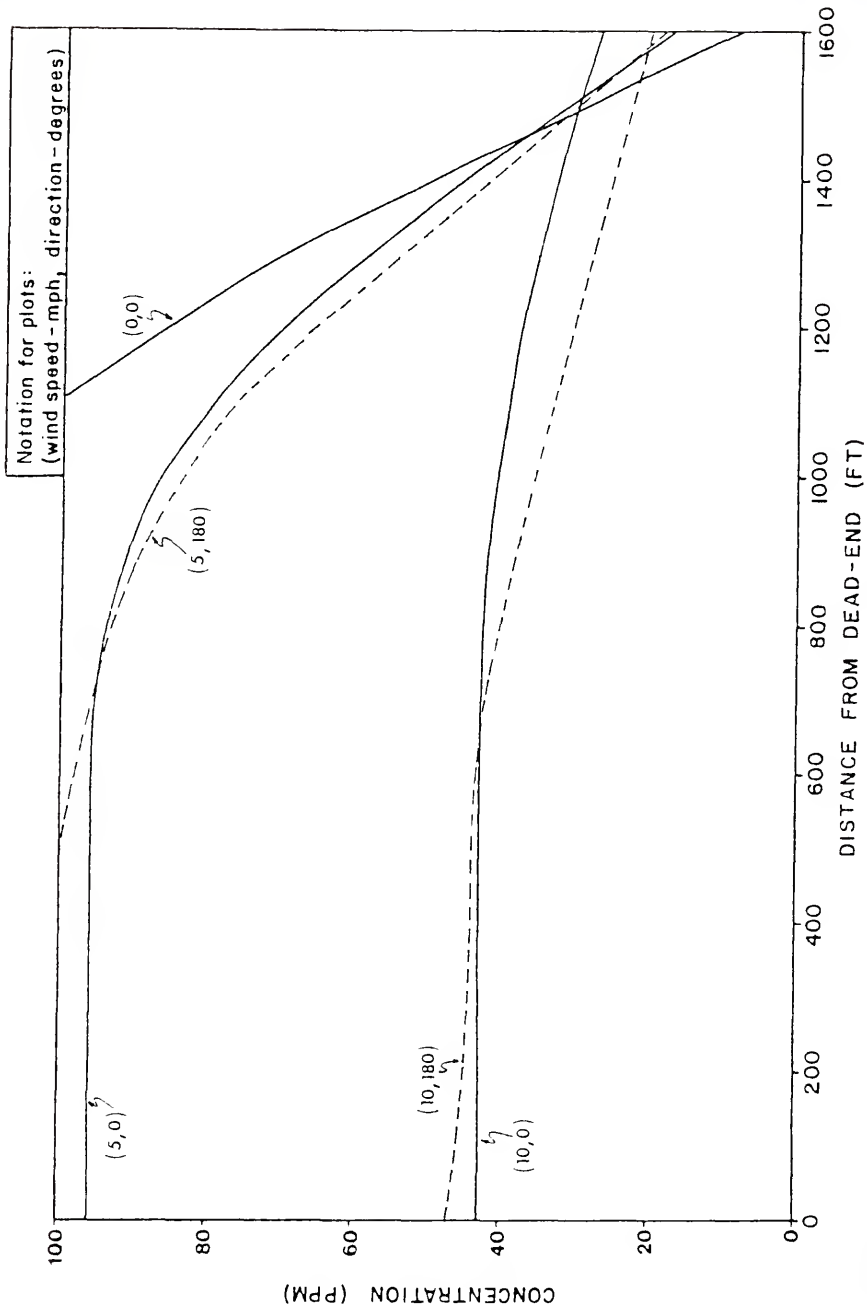


Figure 8.8 - Case 1W; Initial Concentrations, $c_i = 100$ ppm, Background Concentration, $c_{RW} = 5$ ppm - Ten Tidal Cycles.

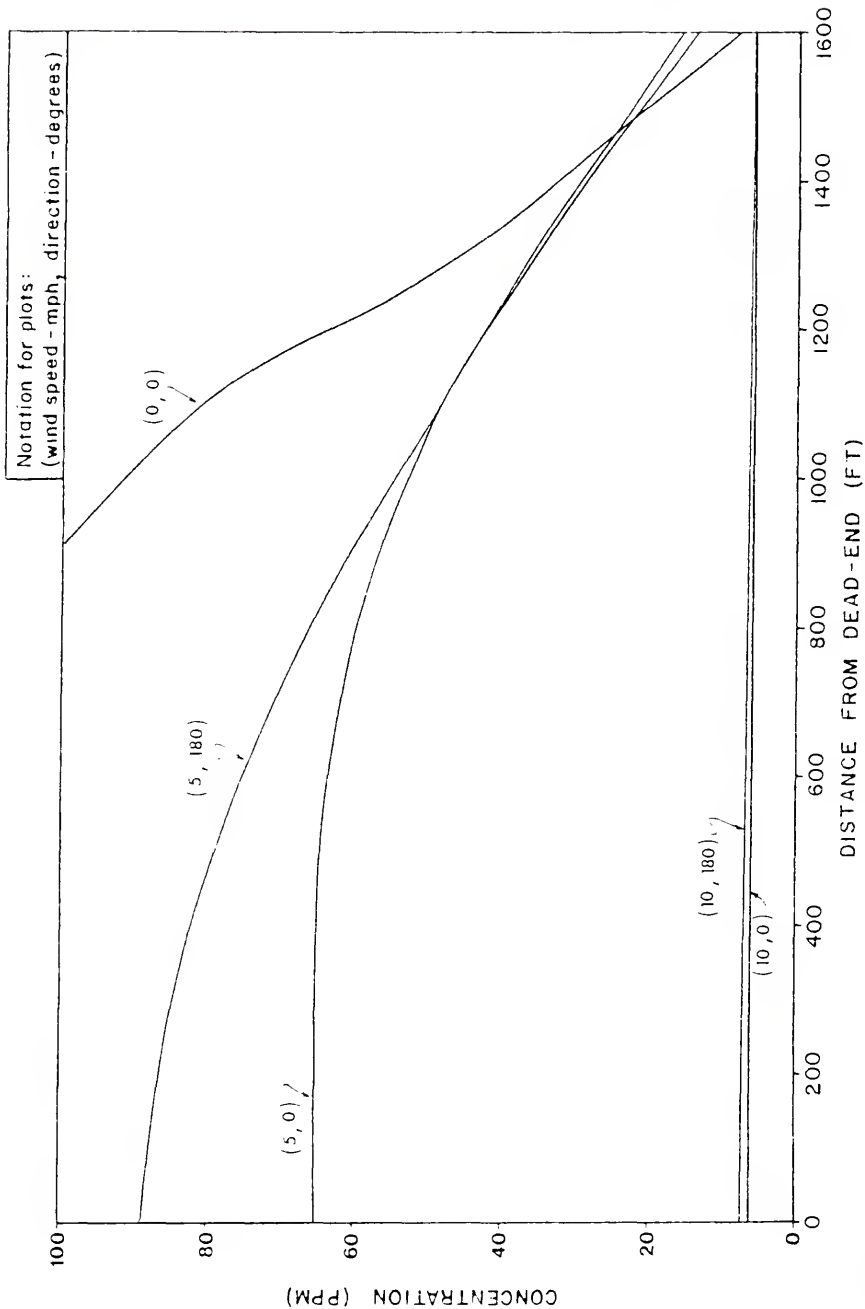


Figure 8.9 - Case IV: Initial Concentrations, $c_i = 100$ ppm, Background Concentration, $c_{RW} = 5$ ppm - Fifty Tidal Cycles.

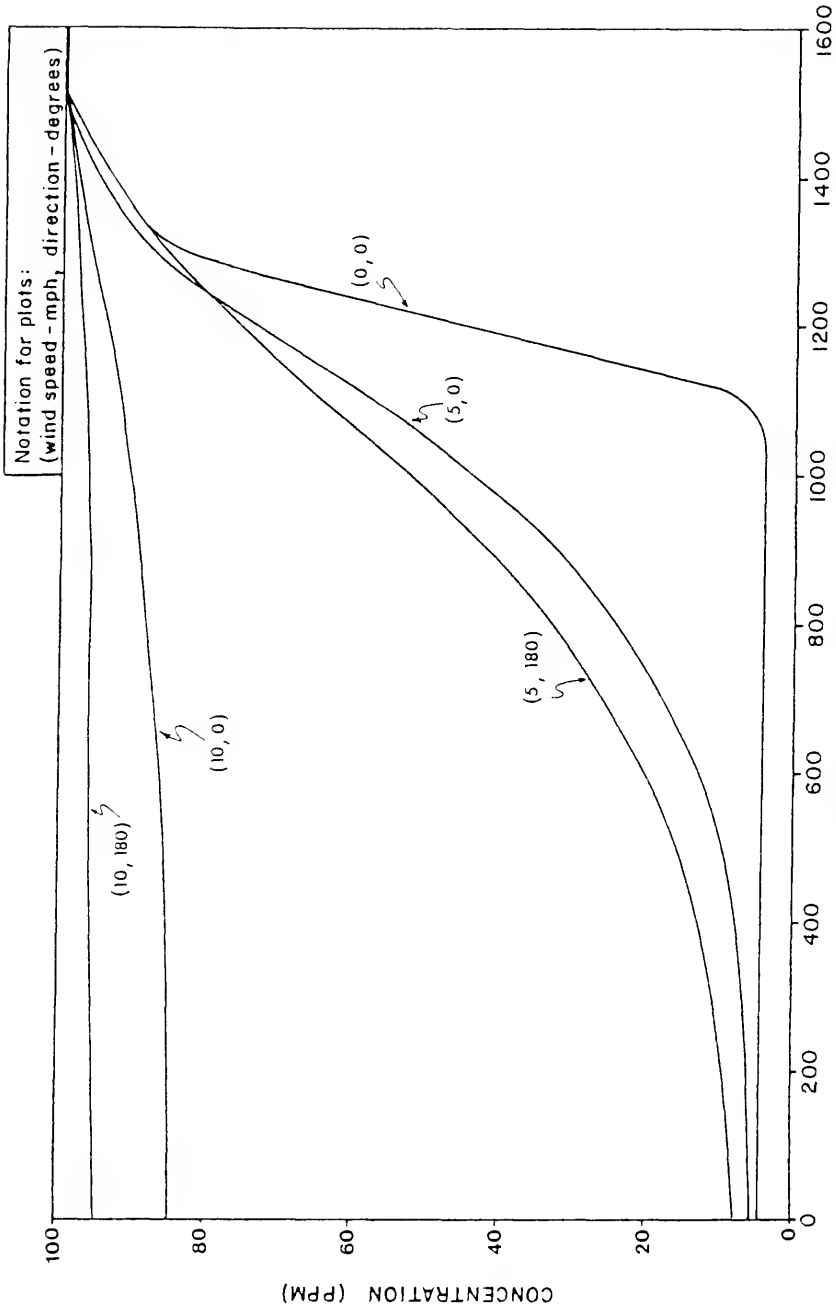


Figure 8.10 - Case 2M: Initial Concentrations, $c_i = 5$ ppm, Background Concentrations, $c_{RW} = 100$ ppm
- Ten Tidal Cycles.

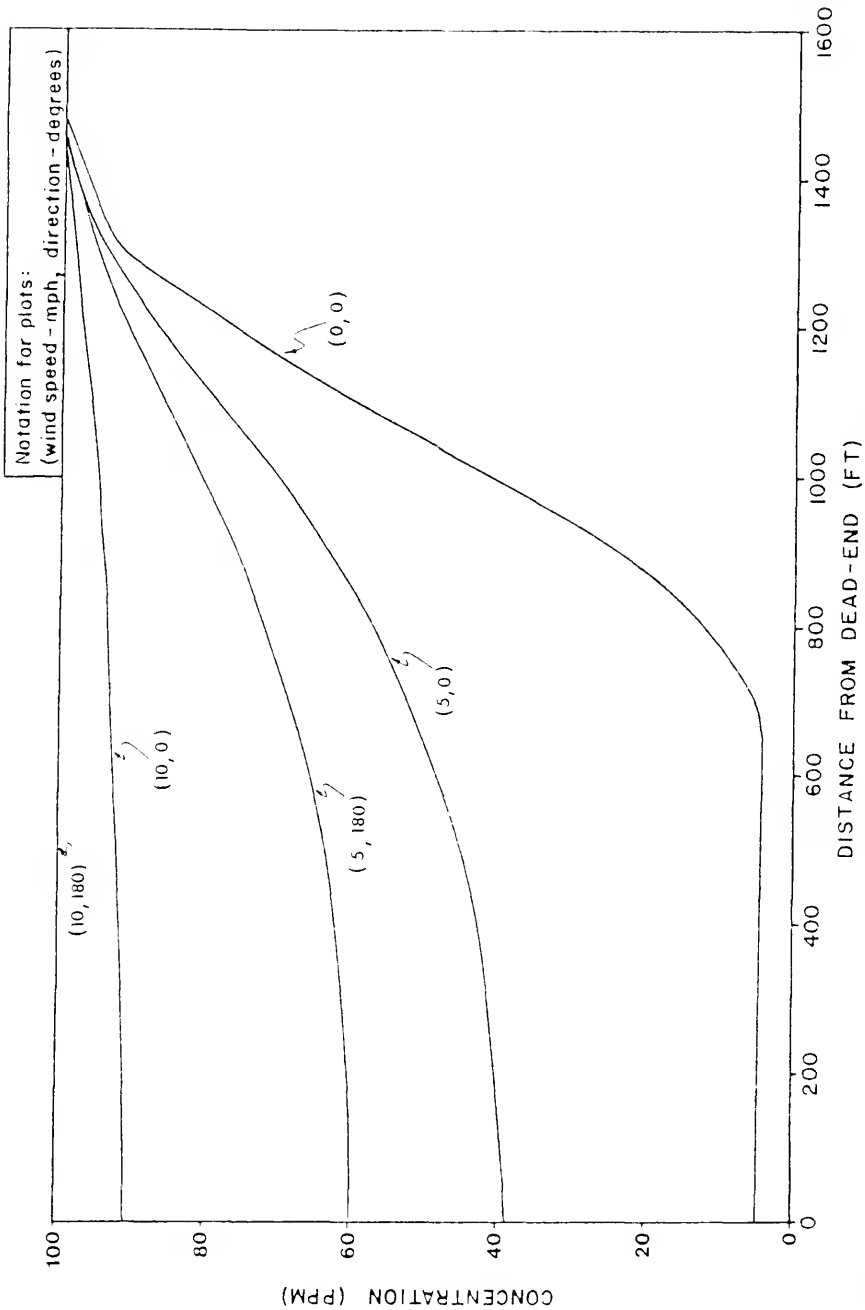


Figure 8.11 - Case 2W: Initial Concentrations, $c_i = 5$ ppm, Background Concentration, $c_{RW} = 100$ ppm
- Fifty Tidal Cycles.

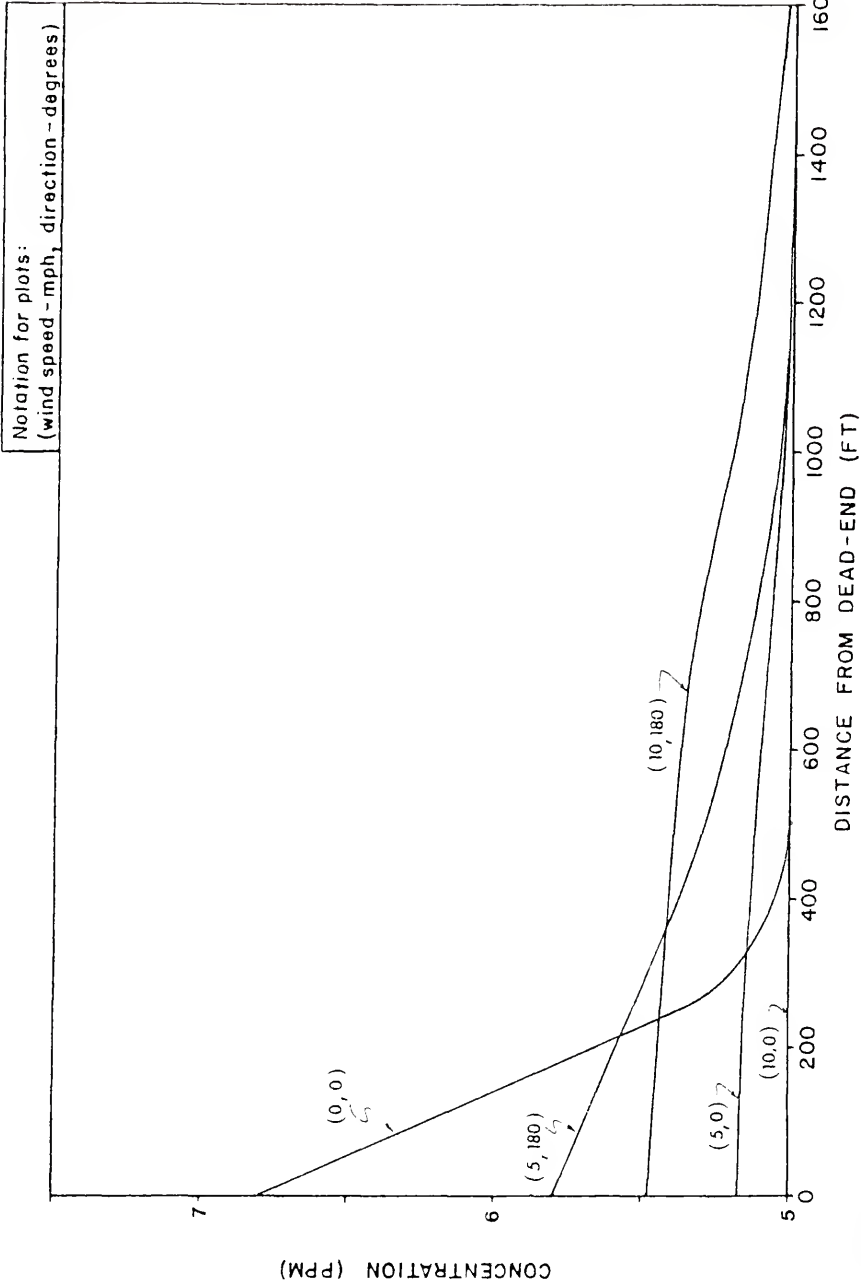


Figure 8.12 - Case 3W: Lateral Inflow Distribution Along Length of Canal - Ten Tidal Cycles.

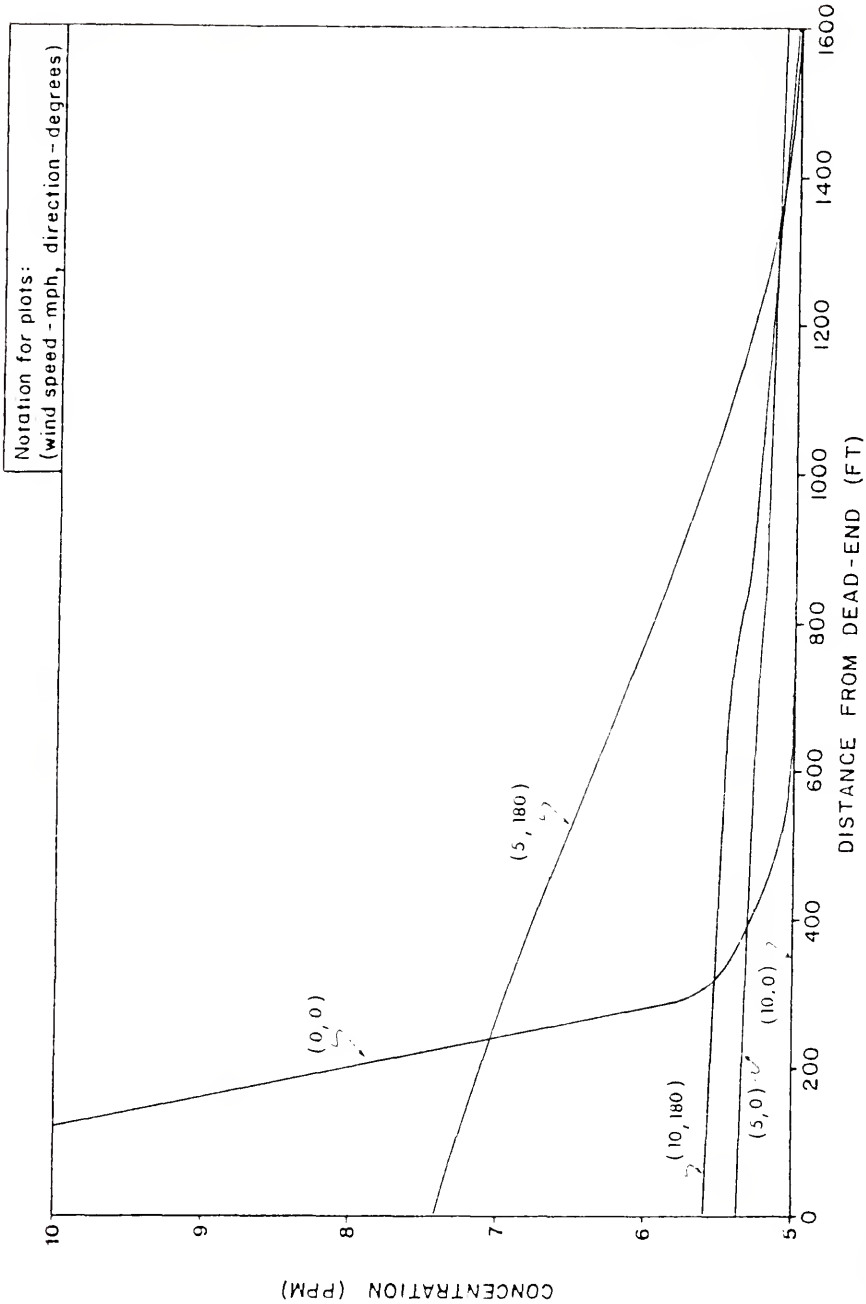


Figure 8.13 - Case 3W: Lateral Inflow Distribution Along Length of Canal - Fifty Tidal Cycles.

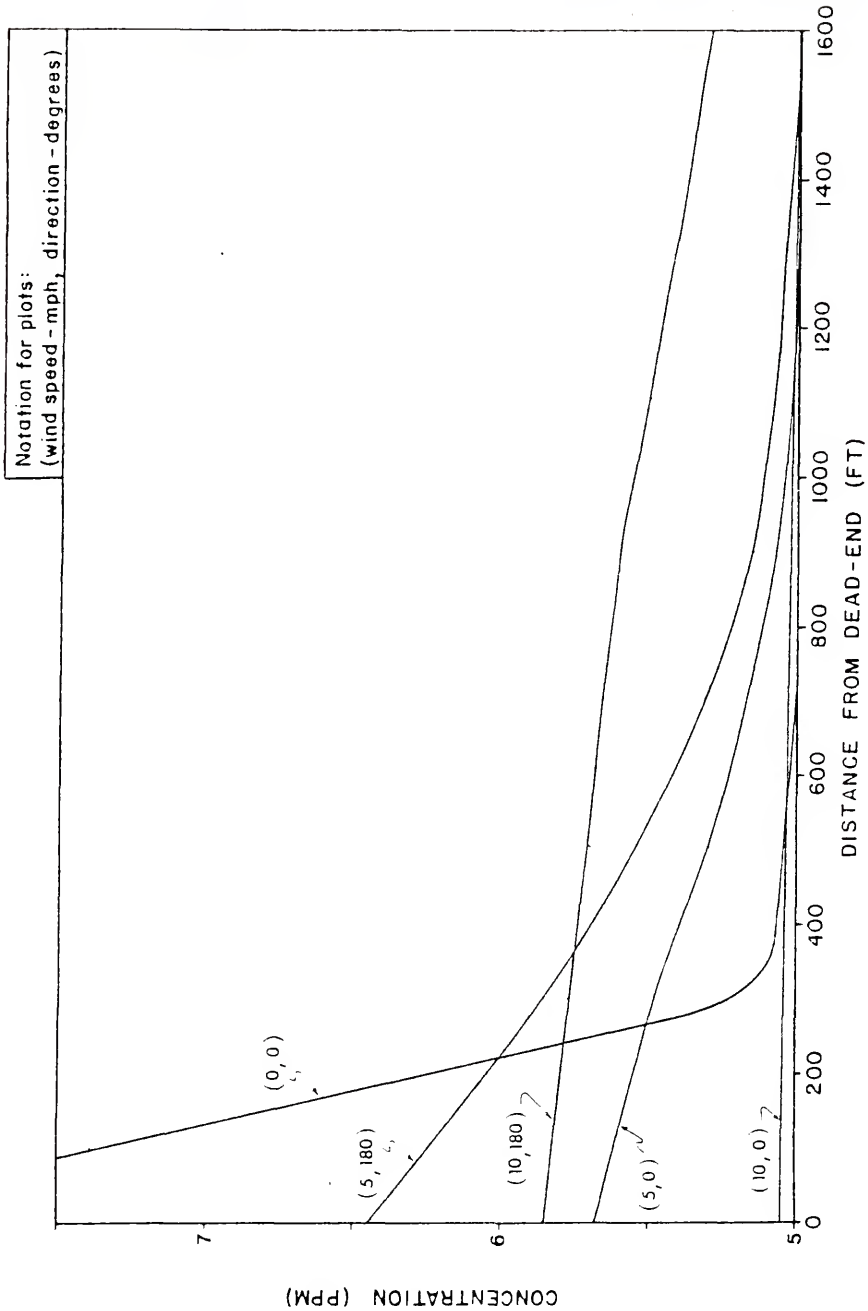


Figure 8.14 - Case 4W: Lateral Inflow Distribution Along Upper 1/2 of Canal - Ten Tidal Cycles.

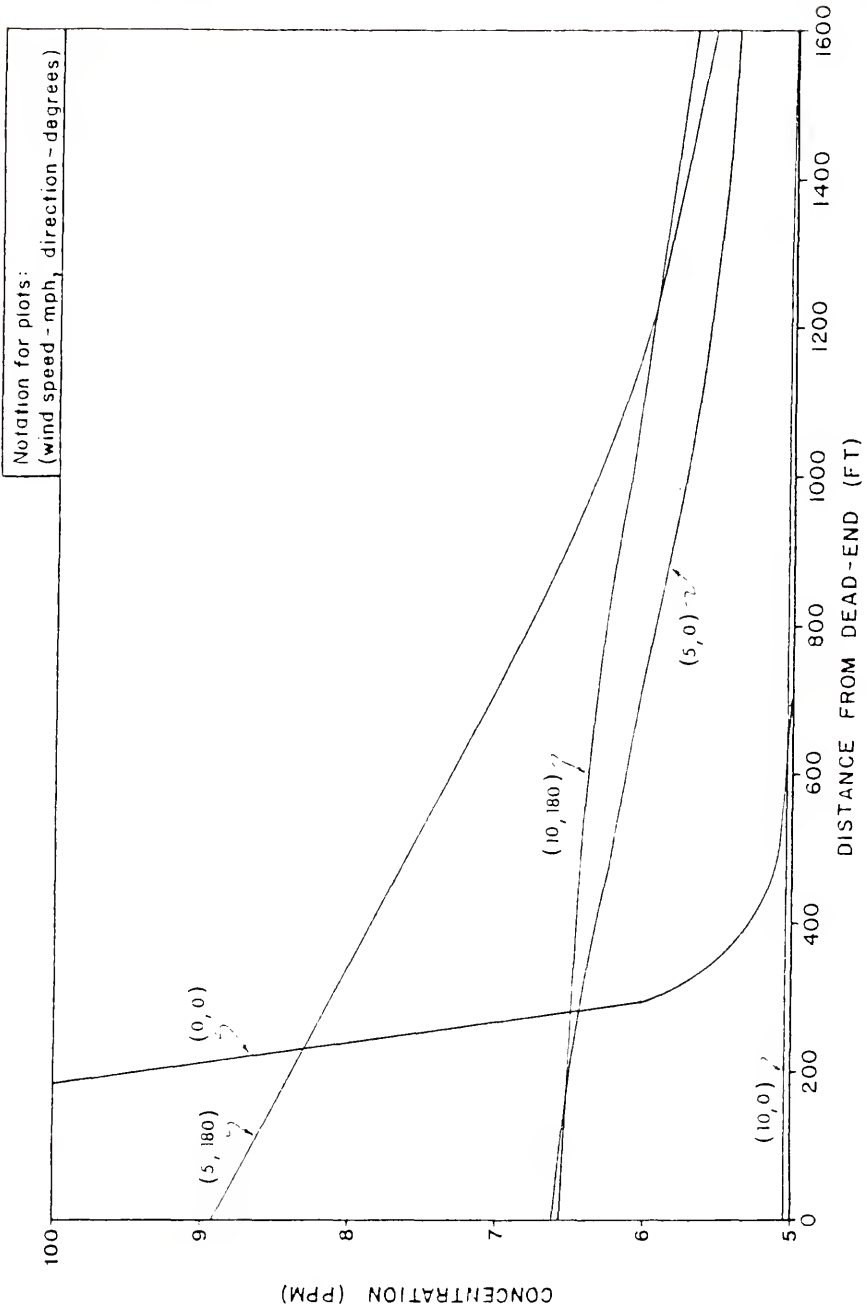


Figure 8.15 - Case 4W: Lateral Inflow Distribution Along Upper 1/2 of Canal - Fifty Tidal Cycles.

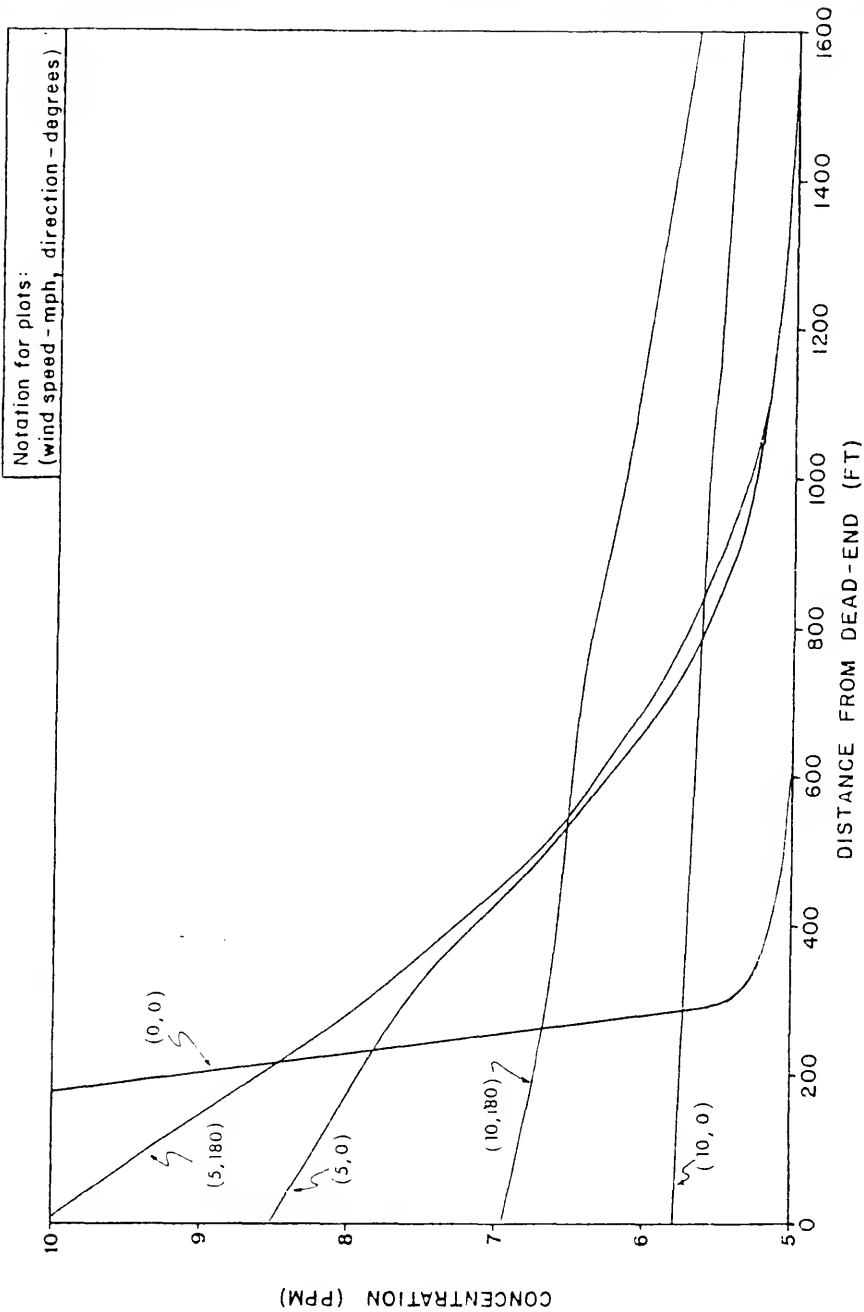


Figure 8.16 - Case 5W: Lateral Inflow at Dead-End - Ten Tidal Cycles.

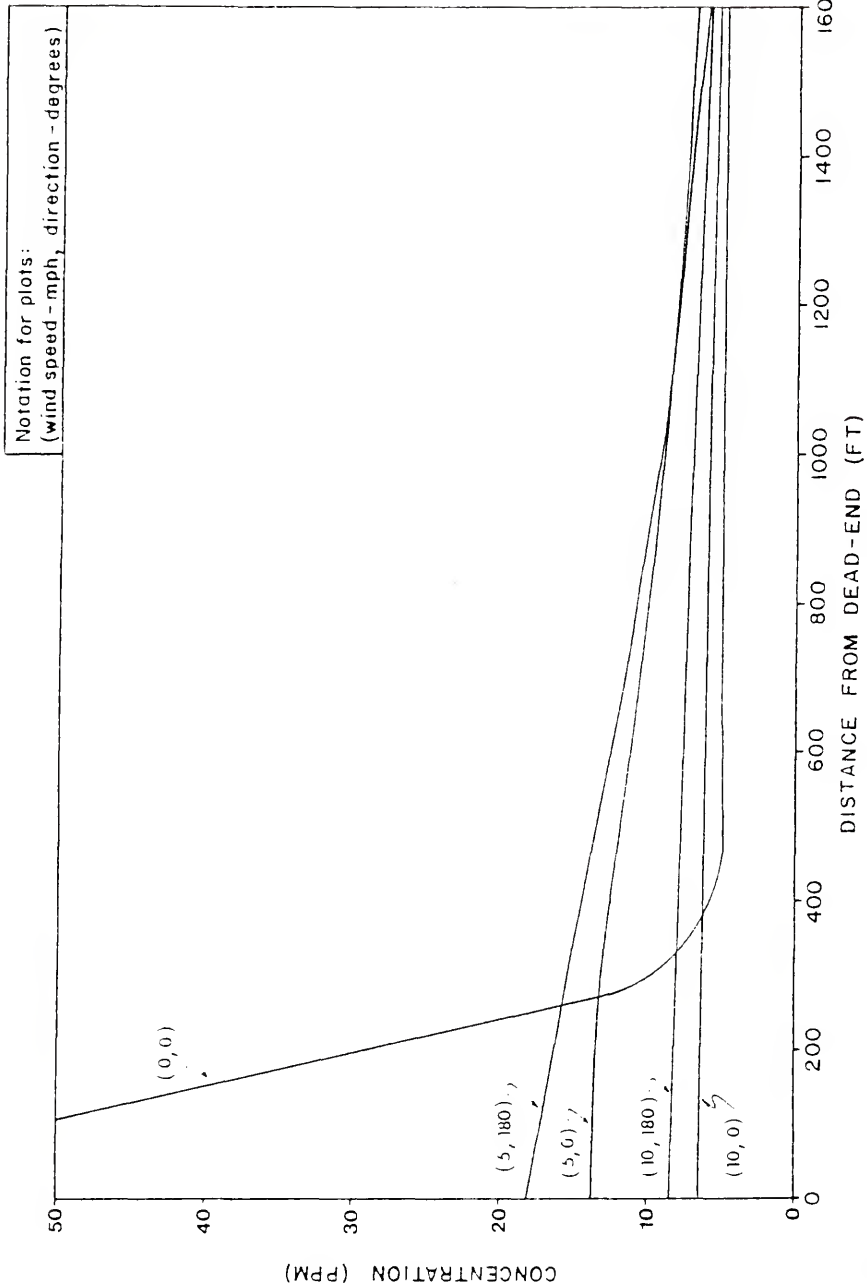


Figure 8.17 - Case 5W: Lateral Inflow at Dead-end - Fifty Tidal Cycles.

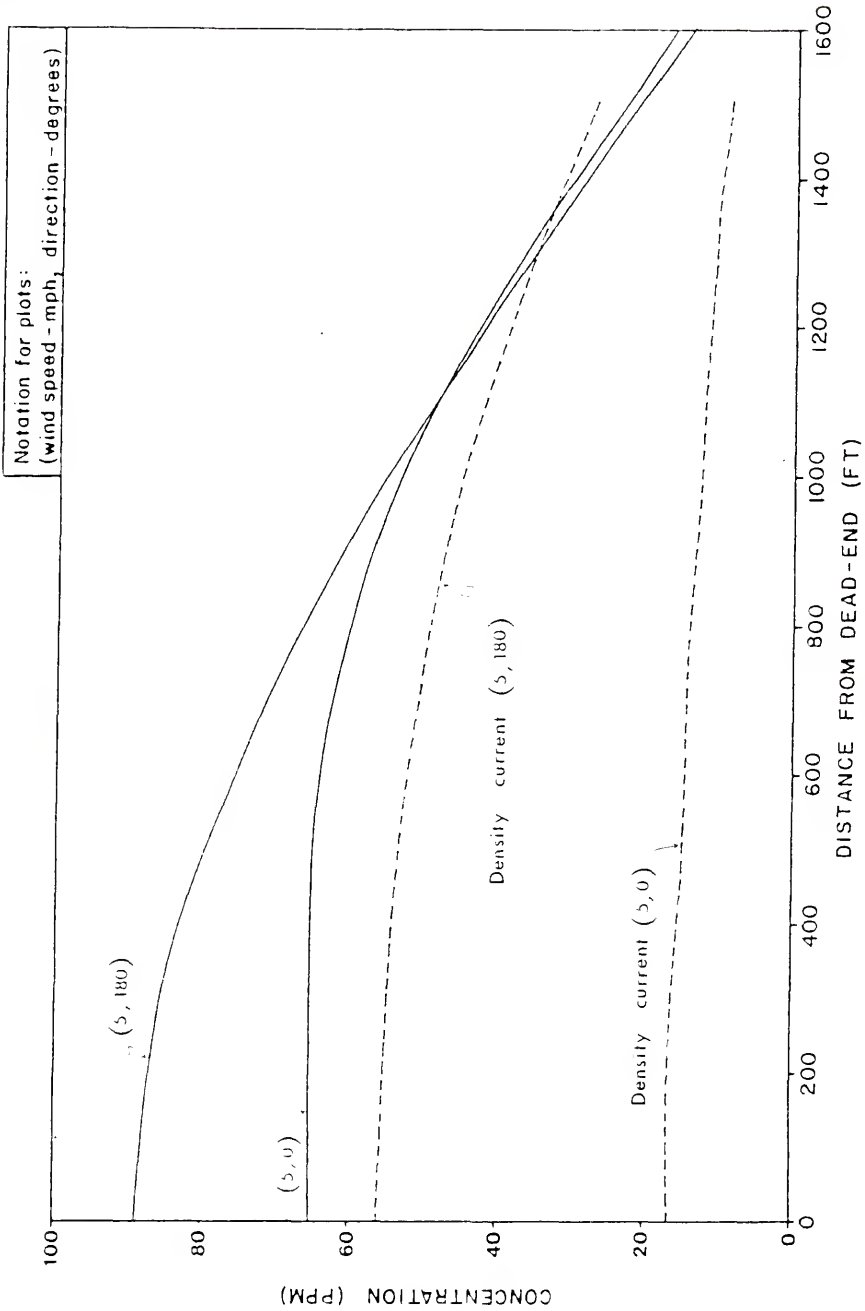


Figure 8.18 - Case 1S: Effect of Salt Wedge With Initial Concentration, $c_i = 100$ ppm, Background Concentration, $c_{RW} = 5$ ppm - Fifty Tidal Cycles.

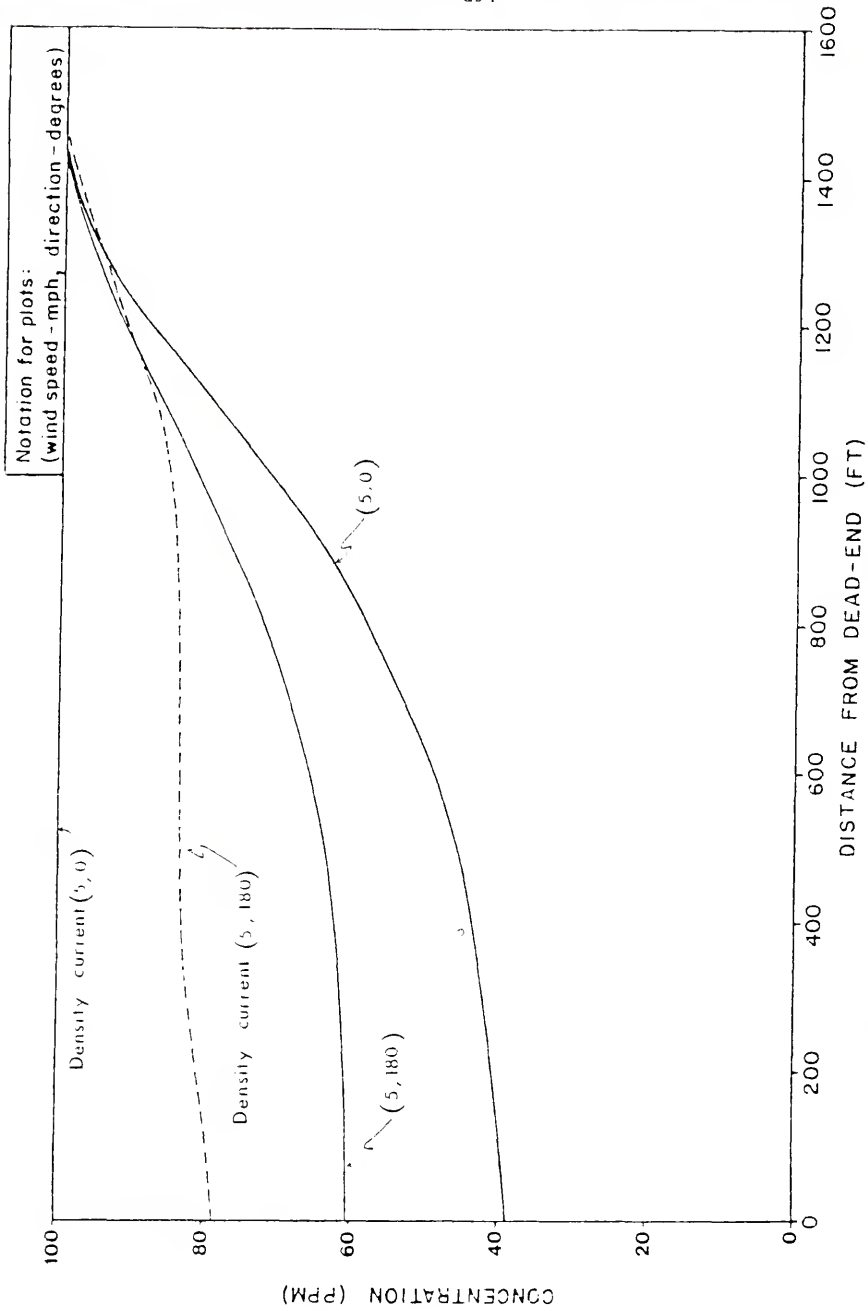


Figure 8.19 - Case 2S: Effects of Salt Wedge With Initial Concentrations, $c_i = 5$ ppm, Background Concentration, $c_{RW} = 100$ ppm - Fifty Tidal Cycles.

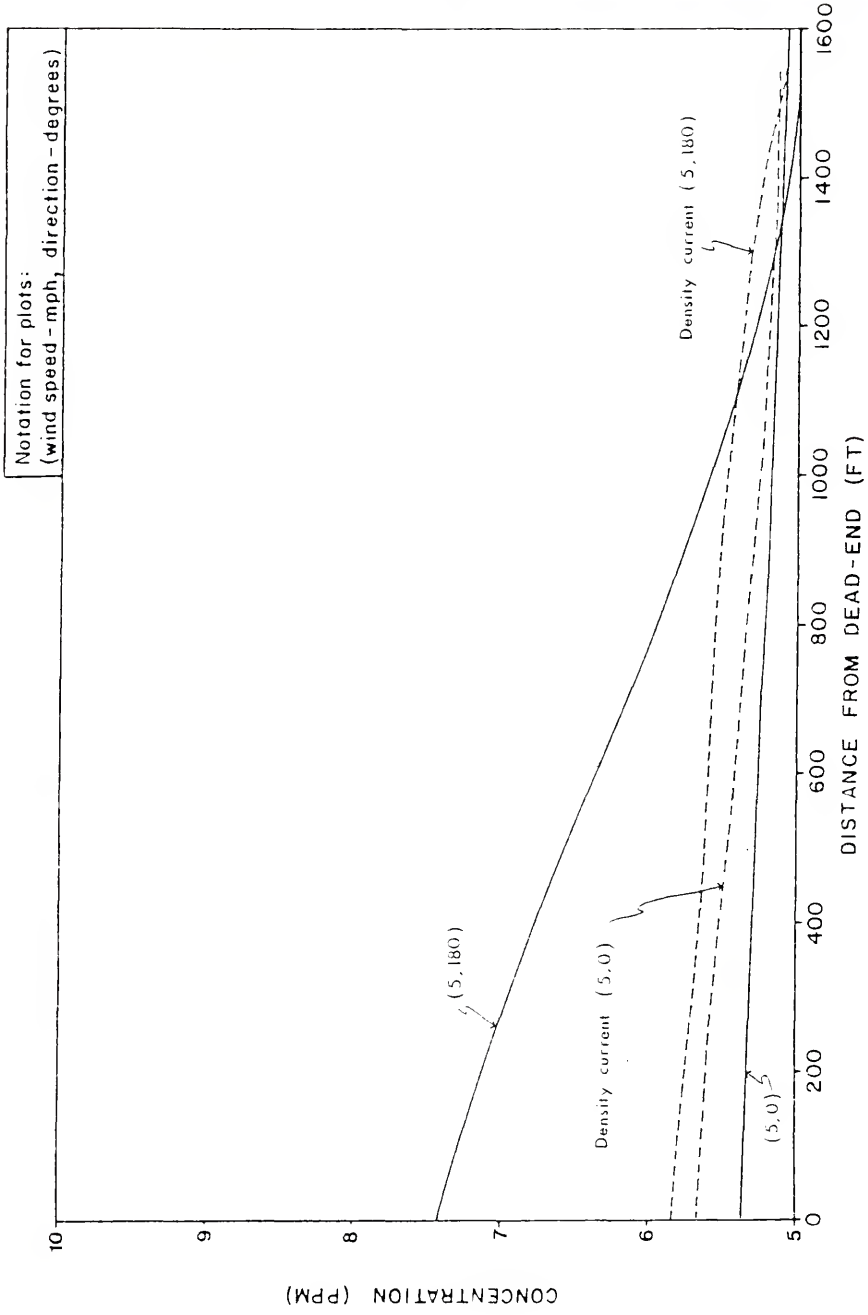


Figure 8.20 - Case 35: Effect of Salt Wedge With Lateral Inflow Distribution Along Length of Canal - Fifty Tidal Cycles.

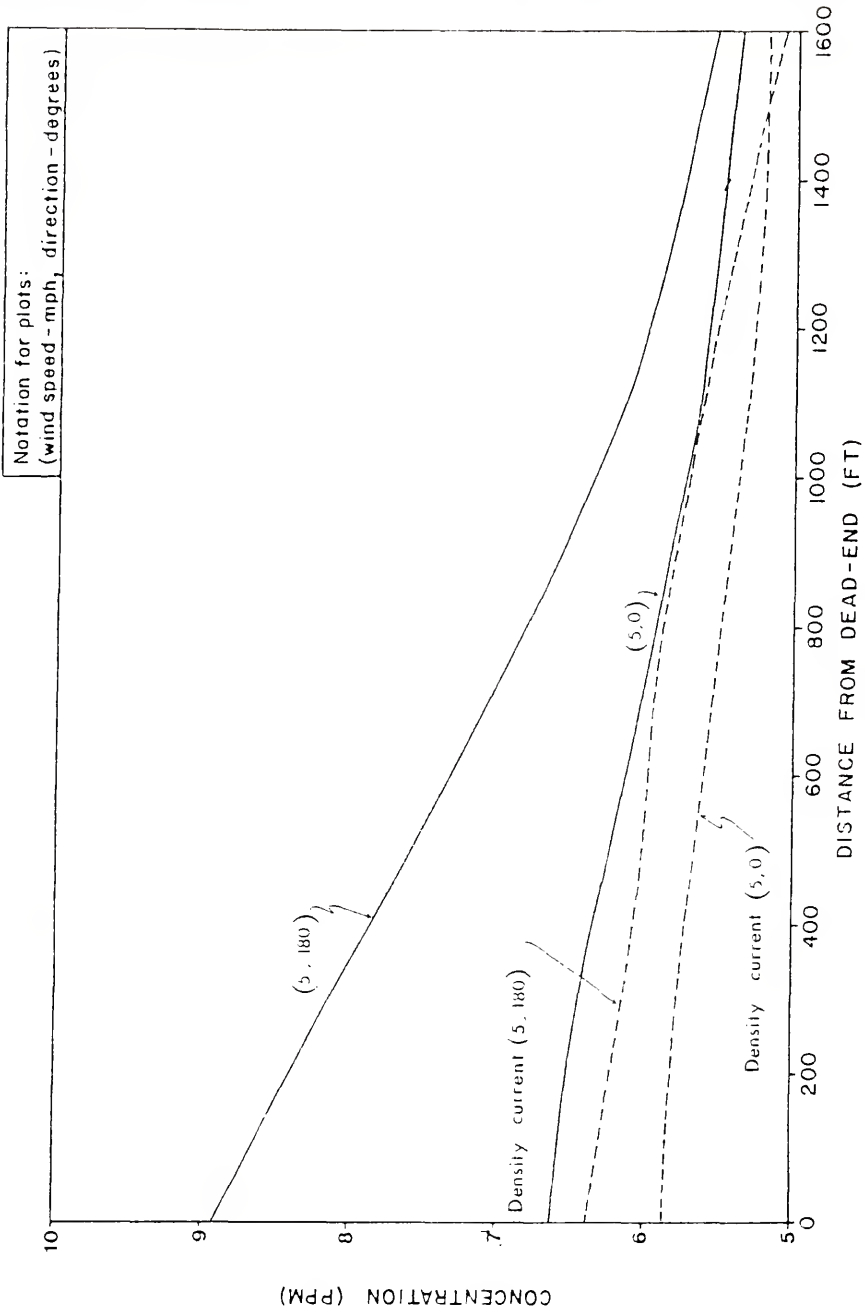


Figure 8.21 - Case 4S: Effect of Salt Wedge With Lateral Inflow Distribution Along Upper 1/2 of Canal - Fifty Tidal Cycles.

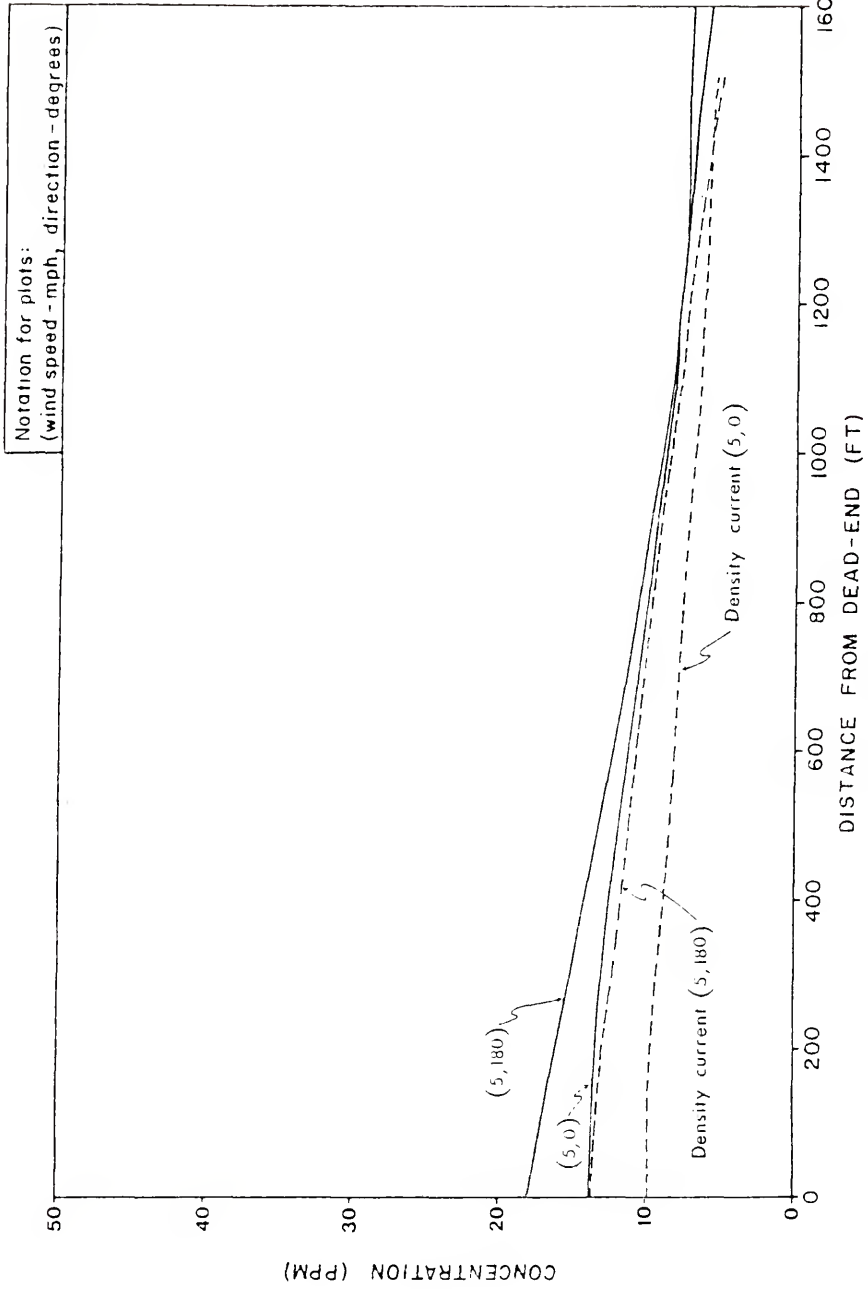


Figure 8.22 - Case 5S: Effect of Salt Wedge With Lateral Inflow Distribution at Dead-End
- Fifty Tidal Cycles.

Table 8.1 - Parameters for Big Pine Key Canal III Case History

PARAMETER	VALUE
Length, L	1600 ft
Bottom width, b	40 ft
Mean tidal depth, d_0	10 ft
Inverse side slope, left bank, s_L right bank, s_R	0 0
Tidal amplitude a	0.5 ft
Nikuradse's equivalent sand roughness, k	5 ft
Reach alignment angle, RANG	0 degrees
Reach decay coefficient, RDECAY	0/hr
Dimensionless dispersion coefficient longitudinal, K_x lateral, K_y vertical, K_z	0.1 0.001 0.008
Background dispersion coefficient, E_0	0 ft ² /sec
Vertical momentum transfer coefficient, N_z	0.005 ft ² /sec
Background concentration, c_{RW}	0 ppm
Constant wind speed, w_s	5 mph
Constant wind direction	0 degrees

Table 8.2 - Parameters for 57 Acres Case History

PARAMETER	REACH 1	REACH 2	REACH 3	REACH 4	REACH 5
Length, L (ft)	4200	1300	700	900	2500
Bottom width, b (ft)	65	50	50	60	70
Mean tidal depth, d_0 (ft)	8.0	6.2	6.3	7.7	8.0
Inverse side slope: left bank, s_L right bank, s_R	3 3	3 3	3 3	3 3	2 4
Reach alignment angle, RANG	240	340	110	110	30
Equivalent sand roughness, k (ft)	15	15	15	15	15
Reach decay coefficient, RDECAY (1/hr)	0.0	0.0	0.0	0.0	0.0
Number of upstream junction	1	1	1	3	2
Number of downstream junction	2	3	3	2	4

Table 8.2 - continued.

PARAMETER	VALUE
Tidal amplitude, a (ft)	1.15
Dimensionless dispersion coefficient, longitudinal, lateral, K_x vertical, K_y K_z	0.1 0.01 0.0001
Background dispersion coefficient, E_0 (ft ² /sec)	0.0005
Vertical momentum transfer coefficient, N_z (ft ² /sec)	0.002
Background concentration, C_{RW} (ppm): July, 1977 October, 1977	6 0.2
Number of layers: lateral, NLAYY vertical, NLAYZ	1 3

Table 8.3 - Parameters for Loxahatchee North Canal Case History

PARAMETER	VALUE
Length, L	2200 ft
Bottom width, b	50 ft
Mean tidal depth, d_0	7 ft
Inverse side slope, left bank, s_L right bank, s_R	2 2
Tidal amplitude, a	1 ft
Nikuradse's equivalent sand roughness, k	10 ft
Reach alignment angle, RANGE	270 degrees
Reach decay coefficient, RDECAY	0/hr
Dimensionless dispersion coefficient longitudinal, K_x lateral, K_y vertical, K_z	0.1 0.01 0.001
Background dispersion coefficient, E_0	0.0005 ft ² /sec
Vertical momentum transfer coefficient, N_z	0.002 ft ² /sec
Background concentration, c_{RW}	0.03 ppb
Depth to saltwater interface, DSM	3 ft
Coefficient of Equation (6.64), u_4	3000
Density of freshwater, RHOF	1.94 slugs/cu ft
Density of saltwater, RHOS	1.99 slugs/cu ft

Table 8.4 - Parameters for Three-Dimensional Model Test Canal

PARAMETER	VALUE
Length, L	1600 ft
Bottom width, b	40 ft
Mean tidal depth, d_0	10 ft
Inverse side slope, left bank, s_L right bank, s_R	0 0
Tidal amplitude	0.5 ft
Nikuradse's equivalent sand roughness, k	5 ft
Reach alignment angle, RANG	180 degrees
Reach decay coefficient RDECAY	0/hr
Dimensionless dispersion coefficient, longitudinal, K_x lateral, K_y vertical, K_z	0.1 0.01 0.05
Background dispersion coefficient, E_0	0 ft ² /sec
Background concentration,* c_{RW}	5 ppm
Tidal entrance decay coefficient, τ	6.21 hrs
Number of lateral layers, NLAYY	1
Number of vertical layers, NLAYZ	3
Depth of saltwater interface,** DSM	5 ft
Coefficient of Equation (6.64),** u_4	4000
Density of freshwater,** RHOF	1.94 slugs/cu ft
Density of saltwater,** RHOS	1.99 slugs/cu ft

*Unless otherwise stated.

**Values for wedge analysis (Section 8.5.2).

Table 8.5 - Variability Studies Using Three-Dimensional Model

CASE NUMBER	VARIATION
1W,* 1S	Initial concentration, $c_i = 100$ ppm Background concentration, $c_{RW} = 5$ ppm
2W, 2S	Initial concentration, $c_i = 5$ ppm Background concentration, $c_{RW} = 100$ ppm
3W, 3S	Lateral inflow rate, $q_I = 0.04$ cu ft/hr/ft along whole length of canal Inflow concentration, $c_I = 100$ ppm
4W, 4S	Lateral inflow rate, $q_I = 0.08$ cu ft/hr/ft along upper 1/2 length of canal Inflow concentration, $c_I = 100$ ppm
5W, 5S	Lateral inflow rate, $q_I = 0.32$ cu ft/hr/ft in 200 ft adjacent to dead-end Inflow concentration, $c_I = 100$ ppm

*W refers to wind induced circulation only (Section 8.5.1),
S refers to density induced circulation (Section 8.5.2).

CHAPTER 9
SUMMARY OF NUMERICAL MODELING

9.1 Summary of One-Dimensional Modeling

As an initial step in the development of a numerical model to accurately, and inexpensively, simulate mass-transport in low energy tidal finger canal networks, a simple one-dimensional numerical model was developed based on the horizontal water surface assumption and the one-dimensional, mass-transport equation. The horizontal water surface assumption was significant in that it greatly reduced the complexity of the governing equations, thus making solution techniques simpler and cheaper. As shown in Section 2.1.3, this assumption is reasonable when compared with field measurements and another numerical model based on the full equations of continuity and momentum (or the dynamic equation). Being able to model the velocity field using the continuity equation alone, it was found that velocities in the canal network could be obtained as closed form functions of the longitudinal displacement, x , from the dead-end of each reach.

Furthermore, as shown in Section 2.1.4, using a classical form of the longitudinal dispersion coefficient, E_L , this coefficient could also be found as a closed form function of x . This greatly simplified the problem, and by including a lateral inflow term $q_1 c_1/A$ for the rate of production or loss term of Equation (2.15), the number of unknowns was reduced to one, the concentration, c .

However, upon programming this model using the more common finite-element and finite-difference techniques, such as the central-difference explicit method, it was found that a severe damping term was present in the schemes. This term is called numerical dispersion, and like natural dispersion is a second order effect produced when infinite Taylor series expansions to the first order time derivative and the first order spatial derivative are truncated after the second term.

Analysis of this problem, and an extensive literature review, showed that for economic choices of the time increment, Δt , and the spatial increment, Δx , the numerical dispersion term can have a significant effect in systems in which the natural dispersion coefficient is small. In Floridian canals, and other low energy canal networks around the Gulf Coast and along the Eastern Atlantic Seaboard, measured maximum dispersion coefficients are on the order of $5 \text{ ft}^2/\text{sec}$. This is very small when compared with dispersion coefficients in rivers and estuaries, which are often two orders of magnitude larger. In these canals, the numerical dispersion inherent in most common finite-element and finite-difference techniques can swamp the natural dispersion being modeled giving the damped concentration profiles found in early models.

The main problem, then, in a one-dimensional analysis of mass-transport in tidal networks, and indeed one of the major research efforts of the entire project, became the developing of a numerical technique which would eliminate, or at best greatly reduce the amount of numerical dispersion in the method, so that error terms would be

small compared with the longitudinal dispersion term. A variety of methods were investigated as discussed at length in Chapter 2.

Two method-of-characteristics techniques were developed, one using a fixed grid structure and the second using a movable grid system. The latter method was dropped because it was found that when lateral inflow was being modeled, the grid system tended to drift out of the canal with the net positive velocity induced by the inflow. The fixed grid method-of-characteristic technique appeared to be much more promising at first, until tests showed that the interpolation routine between grid points could not handle curvature in the concentration profile without damping the results.

Another technique extensively investigated was an analog model approach using the hybrid facilities of Martin-Marietta Aerospace in Orlando, Florida. Investigation of the theoretical form of the numerical dispersion term for uniform flow conditions showed that the numerical dispersion might be reduced to zero as the time step, Δt , was made smaller. An analog machine models time as a continuous variable, and encouraging results were obtained from a model using finite-difference forms of the spatial variables. Unfortunately, the conclusion of the research showed that the method could not be realistically extended to a two- or three-dimensional model because of severe hardware limitations, and that the nodal structure of the model was fairly inflexible.

The continuing research effort finally produced two numerical models which satisfied the objectives being sought. The first model used a second upwind differencing technique with limited anti-dispersion and flux corrected transport [Lee, 1977]. As was seen in

Section 2.5, the method was very successful in minimizing numerical dispersion and gave accurate results fairly inexpensively. The second model used a variation in the method of second moments, to incorporate the change in the depth of flow with the tide. The results obtained were equally as accurate as produced by the first model, and the runs required slightly less CPU time.

Comparing the two techniques, it was decided to use the method of second moments to develop a three-dimensional numerical model. The reasons for choosing this technique were that it seemed more physically meaningful to model conservation of moments than to continually make corrections for errors, and that its formulation was simpler, particularly in junctions.

Once a one-dimensional model had been developed, it was used to analyse the effects of changing geometric parameters of the canal layout (see Section 2.8). Most of the results presented in that section are intuitively obvious, and usually showed that equilibrium concentration profiles were lower when a bigger volume of canal water was present to dilute incoming lateral inflow. This analysis also clearly showed that a one-dimensional model was not sufficient to adequately simulate prototype conditions. For small tidal amplitudes, the exchange volume with the receiving waterbody is small and very little flushing is obtained in the canal. The other interesting result was that the tidal entrance decay coefficient, τ , could be varied through a fairly wide range of values without significantly affecting the equilibrium concentration profile within the canal. This result was gratifying because the tidal entrance boundary condition is not well understood and many modelers assume a decay type condition during flood tide. The insensitivity of the parameter means that its value

can be assigned from field measurements without the need for an exhaustive analysis in that region of the canal network.

The one-dimensional model was adequate for showing the qualitative effect of varying geometric and inflow parameters, results which would be expected to be duplicated using a two- or three-dimensional model. However, as the variability study of the tidal amplitude showed, a one-dimensional mass-transport model is not adequate in simulating prototype conditions influenced by wind and density currents.

This point was illustrated in Section 8.2, in which an EPA study of the Big Pine Key Canal III was analyzed [EPA, May, 1977]. In simulating the observed transport of a dye cloud introduced into the canal using the CRM, the dispersion coefficient in the model was reduced by a factor of 5. In fact, the SWMM model was first used, but was found to suffer from numerical dispersion, and could not predict the passage of the center of mass of the dye cloud.

In testing his model, Lee [1977] also tried to model this canal and found that he had to increase his dispersion coefficient by two orders of magnitude. This result clearly indicated that SWMM and CRM are not suited to investigations of transport characteristics in low energy tidal canals, and also that a one-dimensional investigation of these systems is meaningless. Lee's model could not predict the movement of the center of mass of the dye cloud either, as theoretical tidal induced velocities were on the order of 0.001 ft/sec.

The conclusions arrived at from this initial study were that at least a two- and possibly three-dimensional model would be required to model the transport characteristics of these canal systems.

The tidal flux in the canal system was seen to be often one of the least important phenomenon in short canals, and that the important factors such as wind and density induced circulation needed to be incorporated into such a model. The second conclusion was that the method of second moments was well suited for an extension to such a model and was chosen over the other methods investigated.

9.2 Summary of Three-Dimensional Modeling

In Chapters 4, 5, and 6, a three-dimensional mass-transport model was developed to simulate the transport characteristics of low energy tidal canal networks. The model incorporated not only the tide, but also wind induced circulation, density currents, lateral inflows, and decay. The numerical technique used was an extension of the method of second methods outlined in Section 2.6.

The extension to the three-dimensional model was made by giving the cell structure of the model the capability of expanding and contracting with the tidal flux. By allowing the cross-sectional areas of each layer to "flex" in proportion to the volume flux through the layer, and then allowing the lateral cells in each vertical layer to change in cross-sectional areas depending on the volume flux through them, a model was developed in which the cell structure could change its shape in response to the change in tidal elevations and velocities, and in which mass-transfer could be modeled by only considering the exchange between longitudinally adjacent cells in the same vertical layer. The model uses a longitudinal dispersion velocity, added to a convective transport term, and lateral and vertical dispersive transfer using a similar approach. Decay was introduced on an individual cell basis, or as a uniform coefficient for the whole reach.

The various component parts of the velocity field were identified as unique closed form functions, and their forms superimposed to synthesize the model velocity field. The tidal component, as for the one-dimensional model, was derived using the horizontal water surface assumption, but was assumed to have a vertical logarithmic distribution. The magnitude of the tidal flow was obtained using an upstream volumetric tidal prism incorporating the lateral inflow rate. Secondary currents in bends were derived from Rozovskii's theory [1957] of logarithmic flow over a rough bed. A wind induced vertical velocity profile was theorized by simplifying the momentum equation, using a parabolic distribution with a flow reversal at the one-third depth from the water surface. Finally, a density current, induced by the movement of a saline wedge in a freshwater canal, was introduced by making an analogy with the passage of a flood wave going over bank in a river. The movement of a triangular wedge is governed by the dynamic response to the rate of rise of the saltwater interface in the receiving waterbody during the flood tide, and by the kinematic wave produced as the salt wedge in the canal loses potential energy during the ebb tide.

In the model, junctions were treated as transition zones between flow conditions in adjoining reaches. Only conservation of mass is modeled in junctions, and dispersion is ignored because of the inherent numerical dispersion present in this region.

Chapter 7 outlines stability and convergence criteria for the model. On the whole, the model is stable and has good convergence characteristics. The problem areas are the interfacing of schemes at the junctions, and in the modeling of density currents. Although

instabilities were generally not a problem, particularly for nondensity flow simulations, the case of uniform lateral inflow along the length of a test canal influenced by the movement of a saline wedge resulted in instabilities which were of a sufficient magnitude to affect the very small concentration differences being modeled. However, in all other cases, the model performed well.

The model was used to first simulate the movement of a dye cloud in the Big Pine Key Canal III [EPA, May, 1977], and the results clearly showed the power of a two-dimensional formulation of the velocity field. Using values for the model parameters which were consistent with other case studies, the observed longitudinal concentration profiles through time were accurately simulated using an estimated value for wind speed. With the wind induced circulation being incorporated into the model, not only the peak concentration values could be accurately reproduced but also the center of mass of the distribution.

Other case histories simulated observed conditions in the 57 Acres canal network and the Loxahatchee River site, both located on the East Coast of Florida. The first site was considered to be influenced primarily by wind induced circulation, whereas salinity measurements at the second site showed the existence of a saltwater interface. In modeling these systems, good agreement was found as discussed in Chapter 8. More importantly the agreement was achieved without altering the values of the vertical momentum transfer coefficient, N_z , the dimensionless vertical dispersion coefficient, K_z , and the background dispersion coefficient, E_0 , between the sites. In all of these case histories, values of $N_z = 0.002 \text{ ft}^2/\text{sec}$,

$K_2 = 0.0001$, and $E_0 = 0.0005 \text{ ft}^2/\text{sec}$ were used. For the Loxahatchee River site, in which density circulation was included, a value of 3000 was determined for the coefficient, u_4 , of Equation (4.64).

The fact that the various systems could be modeled with uniform values of the major parameters was the important finding of the study. It shows that a more physically correct approximation to prototype transport phenomena is being modeled, a process which cannot be incorporated into a one-dimensional model. However, the need to use a background dispersion coefficient, E_0 , shows that there is still much to be learned about the diffusion process.

The final part of Chapter 8 was a variability analysis of the effects of wind induced circulation and density currents. The results showed that a wind blowing down a canal (in the positive x-direction) was more efficient in flushing a canal and resisting the entry of polluted receiving waters than a wind blowing up the canal from the tidal entrance towards the dead-end. Furthermore, the addition of a density current to the system increased the rate at which the canal flushed, but also increased the rate at which canal water was exchanged with the receiving waterbody.

The variability analysis showed only a qualitative effect. It would be dangerous to base a proposed scheme on the basis of the results obtained from a variability analysis without first undergoing an extensive analysis based on the actual conditions present at the existing or proposed site. Once wind, salinity, and tidal elevation data have been obtained, the canal layout can be varied in a systematic manner to best utilize the available energy sources.

9.3 Future Research

The three-dimensional, mass-transport model presented in this dissertation was developed to simulate the transport properties of low energy tidal canal networks. The aim of the study was to show that a model of this nature was required to accurately model field conditions. This has been clearly demonstrated, and thus future research should be centered around expanding this model to improve its versatility and scope of application. Also, improvements in the numerical techniques used in the model could be studied.

The aspects of the model which might bear further examination are the matching of numerical schemes, the method of second moments, and the upwind difference method, at junctions and in modeling density currents. The junction is a very complex area of the canal system in which transitions are occurring between the various adjoining reaches. It may prove to be very difficult to accurately model this area without resorting to a fully three-dimensional model. However, the density current theory might be improved by considering the change in centers of mass and widths of distributions in cells in which an upwardly induced flow is present to conserve mass. Also, the condition through junctions and at canal dead-ends might be further investigated, as instabilities appear to originate in these areas.

The present model was only able to model flow in loops, or with multiple tidal entrances, in situations where the flows came together again at a null point. The model cannot handle the case in which the flows recombine and enter an upstream reach. This is because at a junction, one downstream reach must be specified. In the case described above, two reaches can be considered to be downstream

reaches for that junction, but one of them has to be specified as a left or right branch. With the present layout of the model, in which the cells are numbered from upstream to downstream in each reach, the lower numbered cells of a reach adjoin an upstream junction, but the high numbered cells of a branch canal adjoin the same junction. Thus, in effect, the "second" downstream reach is defined the wrong way around, and some additional work to rectify this problem is required.

Further desirable extensions of the model include the more obvious ones of being able to model not just one isolated substance, but combinations of substances including chemical and biochemical interactions. The incorporation of a water quality package would give the model the ability to simulate the major transport and quality phenomena present in canal networks. However, the danger of such a compound model, as mentioned in the introductory chapter, is that the number of unknown parameters is dramatically increased, and unless a careful field calibration study is undertaken by experienced scientists, there is the possibility of producing numbers which appear to be correct but which in reality have no relationship to actual conditions. The lesson to be learned from the comparative analysis with one-dimensional, mass-transport models, is to model only those phenomena whose effects are well understood and which play an important part in the overall process, and to avoid confusing the results with a multitude of factors whose sum effect could give entirely erroneous results.

9.4 The Numerical Model as a Design Tool

CANNET3D has been designed to be user oriented and incorporates few parameters which need to be calibrated. In fact, for most practical applications, the longitudinal and lateral dispersive terms play an insignificant part in changing concentration values. The major parameters are the vertical momentum transfer coefficient, N_z , the dimensionless vertical dispersion coefficient, K_z , the background dispersion coefficient, E_0 , the dimensionless density current coefficient, u_4 (defined in Equation (4.64)), and the tidal entrance decay coefficient, τ .

Although in the case histories examined in this report, values for these parameters varied little between the different sites, it is recommended that a field study be conducted to determine the actual values that would apply to a unique location. The values of these parameters together with measured wind and tidal elevation data, form the base from which a design study can be carried out.

The model has been designed in such a way that the geometric features of a proposed layout can easily be read in, as described in Chapter 6. Furthermore, the program has been arranged so that design changes in the layout, or changes in the time interval, can be easily made without extensive revisions to the data.

Once set up, the model simulates the transport of a substance through the canal network, and writes and plots the results at user-specified time intervals. This means that the designer can follow the course of a flushing simulation to determine whether the rate of transport of the substance is sufficient to meet design criteria.

In summary, the numerical model, CANNET3D, developed to simulate mass-transport in low energy tidal finger canal networks, is a very useful design tool to enable the design engineer to evaluate and develop a canal network to conform to design and water quality criteria. In two separate reports [Morris, Walton, and Christensen, 1978; Morris, 1978], the model is used as the major component in a design procedure outlined to give the design engineer an approach to laying out a canal network that will make best use of the available energies of the wind and the tide for flushing. Once an initial design is formulated, the ability of the model to handle different pollutant load conditions is evaluated. Design changes are then made in a systematic manner based on the variability analysis to determine what features might be incorporated into the proposed system to improve its flushing action. In this iterative manner, an initial design layout can be taken, and with some alterations converted into an efficient system which will benefit the surrounding ecosystem, and the prospective residents.

APPENDIX A
USER'S MANUAL

A program designed to simulate mass transport in low energy tidal canal networks, CANNET3D, has been programmed in FORTRAN IV (Level G) for solution on an AMDAHL 470, a machine which is entirely compatible with IBM 360 and 370 series machines, at the Northeast Regional Data Center, Gainesville, Florida. An explanation of FORTRAN language and formats can be found in the manual IBM System/360 and System/370, FORTRAN IV Language [1974].

Once a canal system has been schematized as described in Chapter 6, and time and spatial increments have been chosen to meet stability and convergence criteria, as outlined in Chapter 7, an input card deck is prepared for the program as described below. The cards, as they appear in order in the program, are listed giving the variables to be read in, in terms of program names and their format. This is followed by a listing in alphabetical order of these variables, giving a description and an order magnitude if applicable. This comprises Section A.1.

Section A.2 discusses the limits of the model in terms of array storage area specified and how this can be extended. Section A.3 discusses the output from the model.

A.1 Input Data Cards

Type of Data	Content of Card	Condition/Comment	Format	No. of Cards
Title	Title #1		20A4	1
Title	Title #2		20A4	1
Initial	NTESTS	NTESTS sets of data below and required	I5	1
Initial	T, NDT, DTH, NPRINT, NPLOTT		F10.0, I5, F10.0, 2I5	1
Initial	CMAX, VMAX, DXMIN, DXSC		4F10.0	1
Initial	AMP, CRM, KX, KY, KZ, EO, NZ		7F10.0	1
Initial	NREACH, NJUNC, NLAKE, NTES, NLAYY, NLAYZ		6I5	1
Initial	OPT3, OPT6, OPT7, OPT8		4I5	1
Reach Geometry	{ NDV, NJU, NJD, OPT1, OPT4	First 5 columns for reach number	5X, 5I5	1
	{ RL, RB, RDO, RSL, RSR, RANG, RNK, RDECAY		8F10.0	1
	{ DX(I), I = 1, NDV	IF OPTI = 1	8F10.0	NDV/8

A.1 - continued

Type of Data	Content of Card	Condition/Comment	Format	No. of Cards
Junction	DXJN, DYJN, DOJN, NRU, NRD, NRL, NRR	First 5 columns for junction number IF NJUNC + NLAKE 0	5X, 3F10.0, 4I5	NJUNC + NLAKE
Tidal Entrance	TAU (I), I = 1, NTES		8F10.0	NTES/8
Lateral Inflow	OPT2, NR, NDX, NC, CQI, CCI	CQI, CCI = 0, if OPT2 = 1	4I5, 2F10.0	No. of Inflows
Decay	-1	Terminates inflow cards	I5	1
Decay	NR, NDX, NC, DEC	Terminates decay cards	3I5, F10.0	No. of decays
Bend	-1	Terminates bend data	I5	1
Bend	NR, NDX, BR, BL		2I2, 2F10.0	No. of bends
Salt wedge	DSM, RHOF, RHOS, U4TE	IF OPT8 = 1	4F10.0	1
Initial data in reach	C(NC), NC = 1 NLAYZ, NLAYZ-NDV	IF OPT4 = 1	9F8.0	NREACH sets of (NLAYZ-NLAYZ-NDV)/9
Initial data in junction	CJ(NJC), NJC = 1 NLAYZ, NLAYZ	IF OPT5 = 1	9F8.0	NJUNC + NLAKE sets of (NLAYZ-NLAYZ)/9
Interpolation	WTIME, INTERP	IF OPT6 and/or OPT7 = 1 (if OPT7 = 0, WTIME = 0)	F10.0, I5	1

A.1 - continued

	Content of Card	Condition/Comment	Format	No. of Cards
Time	COSINE, WS, WANGLE	IF OPT6 and/or OPT7 = 1 (if OPT6 = 0, COSINE = 0) (if OPT7 = 0, WS, WANG = 0)	3F10.0	1
Transient Solution	$\left\{ \begin{array}{l} \text{COSINE, WS, WANGLE} \\ \text{QIV(IQ), CIV(IQ), IQ = 1,} \\ \text{NIQ} \end{array} \right\}$	IF OPT6 and/or OPT7 = 1 (if OPT6 = 0, COSINE = 0) (if OPT7 = 0, WS, WANG = 0) NIQ = no. of varying lateral inflows	3F10.0 8F10.0	$\left. \begin{array}{l} 1 \\ \text{NIQ/8} \end{array} \right\} \frac{(\text{NDI}-1)}{\text{INTERP}}$

AMP tidal amplitude in feet.

BL length of bend in feet.

BR radius of bend in feet.

C(*) initial concentrations in reach cells in ppm.

CCI constant concentration of lateral inflow in ppm (OPT = 1).

CIV(*) concentration of lateral inflow in ppm (OPT = 1).

CJ(*) initial concentration in junction and lake cells in ppm.

CMAX maximum concentration anticipated in network. This is a parameter for graph plotting. If CMAX is exceeded, an error will be generated and no plot appears. Also for neatness for the display, CMAX/5 should give a reasonable number for a display heading.

COSINE elevation of tide from mean sea level in feet.

CQI constant lateral inflow rate in cu ft/hr/ft (OPT = 0).

CRW background concentration in ppm.

DEC decay coefficient in cell in 1/hr.

DSM depth to saltwater interface from sea level at mid tide in feet.

DTH time interval in hours.

DX(*) longitudinal cell length in segment of a reach in feet.

DXJN(*) longitudinal length of junction in feet.

DXMIN minimum value of DX(*) in canal network in feet.

DXSC suitable length scale for graph plots in feet.

DXJN(*) lateral width of junction in feet.

EO background dispersion coefficient in ft^2/sec (0.0005).

INTERP if OPT6 and/or OPT7 = 0, this parameter interpolates between data points of the original data set. This is to eliminate having to redefine a data set if the time interval was originally too large. If INTERP is changed, NDT must be also.

KX dimensionless longitudinal dispersion coefficient in ft^2/sec (≈ 0.1).

KY dimensionless lateral dispersion coefficient in ft^2/sec (≈ 0.01).

KZ dimensionless vertical dispersion coefficient in ft^2/sec (≈ 0.0001).

NC number of cell in cross-section (bottom left-top right).

NDT number of time steps in simulation.

NDV stored in NDIV(*), the number of longitudinal segments in a reach.

NDX number of segment in reach from dead-end of that reach.

NJD(*) assigned number of junction at downstream end of reach.

NJU(*) assigned number of junction at upstream end of reach (= 1 for dead-end, = reach number of adjacent reach meeting a null point).

NJUNC number of internal junctions in network (excludes dead-ends, null points, lakes, and tidal entrances).

NLAKE number of lakes in system (at upward limits).

NLAYY number of lateral layers in system.

NLAYZ number of vertical layers in system.

NPLOT number of time steps between plots (if NPLOT > NDT no plots are generated).

NPRINT number of time steps between written data outputs.

NR assigned number of reach.

NREACH number of reaches in system.

NDR(*) assigned number of downstream reach at junction.

NRL(*) assigned number of left branch at junction.

NRR(*) assigned number of right branch at junction.

NRU(*) assigned number of upstream reach at junction.

NTES number of tidal entrances in system.

NTESTS number of simulations to be run consecutively. All the data must be read in again for each run.

NZ vertical momentum transfer coefficient in ft^2/sec (≈ 0.002).

OPT1 spatial increment option. If OPT1 = 0 the reach is subdivided into NDV equal segments, DX(*). If OPT1 = 0 the DX(*) are read in.

- OPT2 lateral inflow option. If OPT2 = 0, the lateral inflow rate, COI, and its concentration, CCI, are constant for the simulation. If OPT2 = 1, the lateral inflow and/or its concentration are variable and are read in throughout the simulation.
- OPT3 initial tidal condition option. If OPT3 = 1, the simulation begins at high tide. If OPT3 = -1, the simulation begins at low tide. So, OPT3 only has an effect when OPT6 = 0. If OPT6 = 1, OPT3 can take any value.
- OPT4 initial conditions in reach option. If OPT4 = 0, the initial concentrations in each cell of the reach are set to the background concentration, CRW. If OPT4 = 1, they are read in.
- OPT5 initial conditions in junction option. If OPT5 = 0, the initial concentrations in each cell of the junction are set to the background concentration, CRW. If OPT5 = 1, they are read in.
- OPT6 tidal elevations option. If OPT6 = 0, the tidal elevations from mean sea level are generated as a cosine distribution with amplitude AMP and frequently, $2\pi/T$, where T is the tidal period. If OPT6 = 1, they are read in every INTERP time intervals.
- OPT7 wind option. If OPT7 = 0, the wind speed, WS, and direction, WANG, are constant. If OPT7 = 1, they are read in every INTERP time intervals.
- OPT8 salt wedge option. If OPT8 = 0, no salt wedge is present. If OPT8 = 1, a salt wedge is present and the simulation must begin at low tide, no matter whether the tidal elevations are generated or read in.
- QIV(*) variable lateral inflow rate in cu ft/hr/ft.
- RANG(*) reach alignment angle in degrees.
- RB(*) reach bottom width in feet.
- RDECAY(*) reach constant decay coefficient in 1/hr.
- RDO(*) mean tidal depth in reach in feet.
- RHOF density of freshwater in slugs/cu ft (= 1.94).
- RHOS density of saltwater in slugs/cu ft (= 1.99).
- RL(*) reach length in feet.
- RNK(*) value of Nikuradse's equivalent sand roughness in reach in feet.
- RSL(*) inverse side slope of left bank of reach.

RSR(*)	inverse side slope of right bank of reach.
T	tidal period in hours (≈ 12.42 hrs).
TAU(*)	tidal entrance concentration decay coefficient in 1/hr.
VMAX	maximum velocity anticipated in network at time of plot. For a display heading, VMAX/2 should give a reasonable number.
WANG	wind direction in degrees.
WS	wind speed in mph.
WTIME	time over which wind speeds are averaged in hours.

A.2 Program Area

The arrays used in CANNET3D are such that the program, listed in Appendix C, can handle 50 reaches, 50 junctions, 2000 reach cells, 1000 junction cells, 6 lateral layers, 6 vertical layers, 5 tidal entrances, 50 constant and 50 variable lateral inflows, 100 cell constant decay coefficients. The user may wish to change array size by simply modifying the DIMENSION and COMMON statement cards at the beginnings of the main program and subroutines.

A.3 Output Description

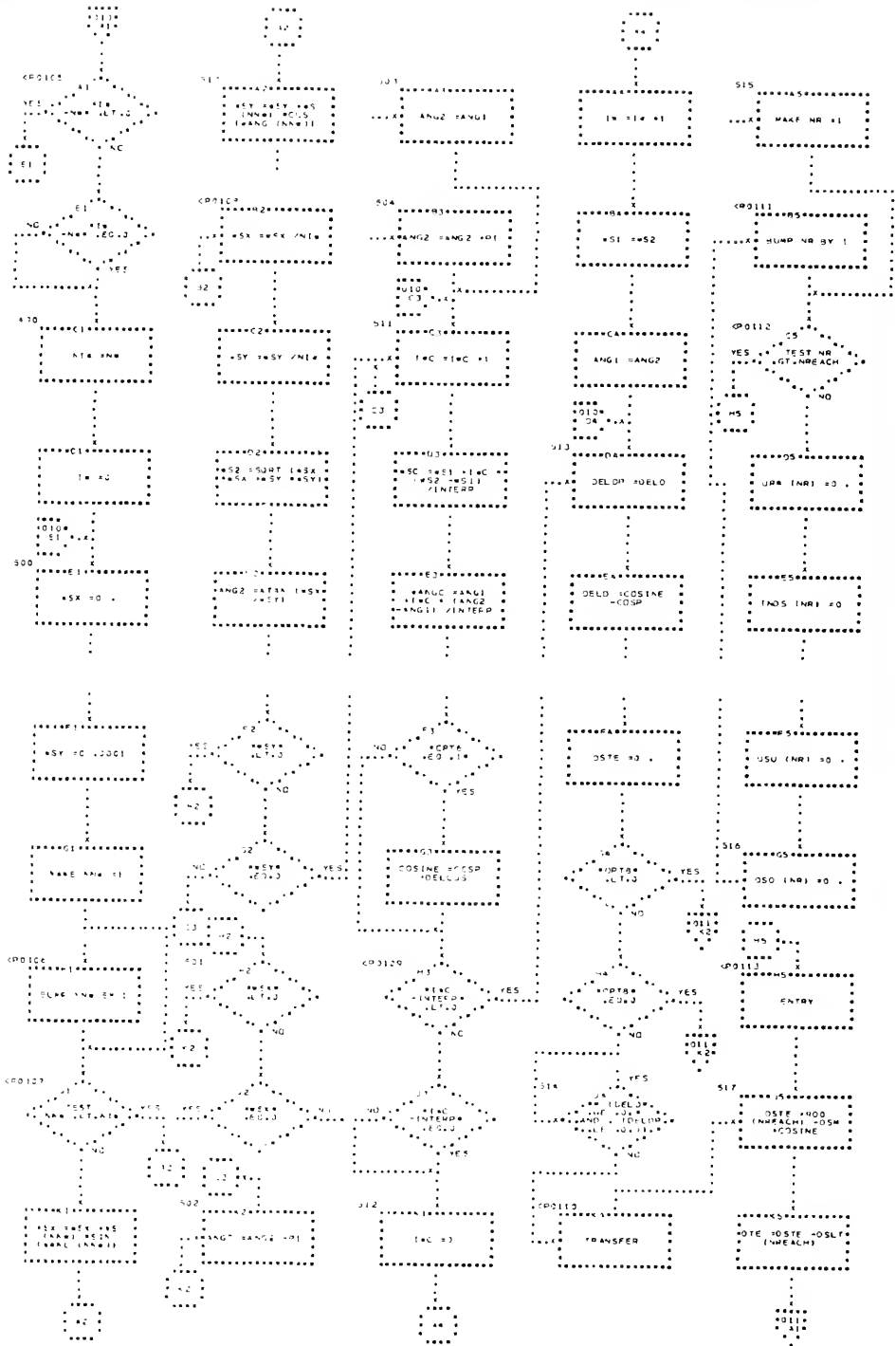
The output from the program is well documented. Input data is printed first, followed by descriptions of the junctions, tidal entrances, lateral inflows, cell constant decay coefficients, and bends.

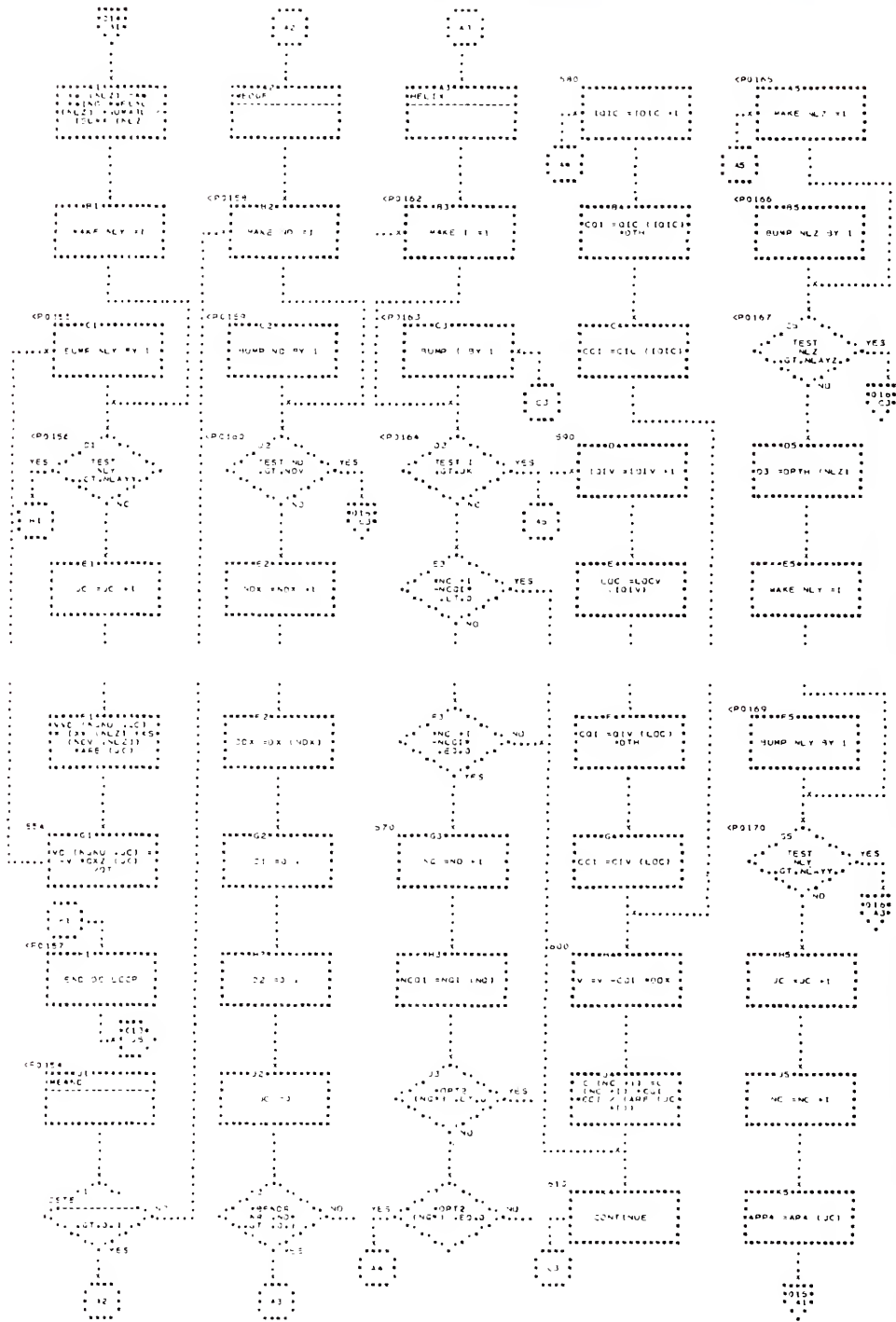
Then, written output is generated every NPRINT time steps and comprises the time, tidal elevation, wind speed and direction, followed by concentrations and velocities for each reach, and the concentrations in the junctions. The subroutine WRITIT also produces this information at the completion of the simulation.

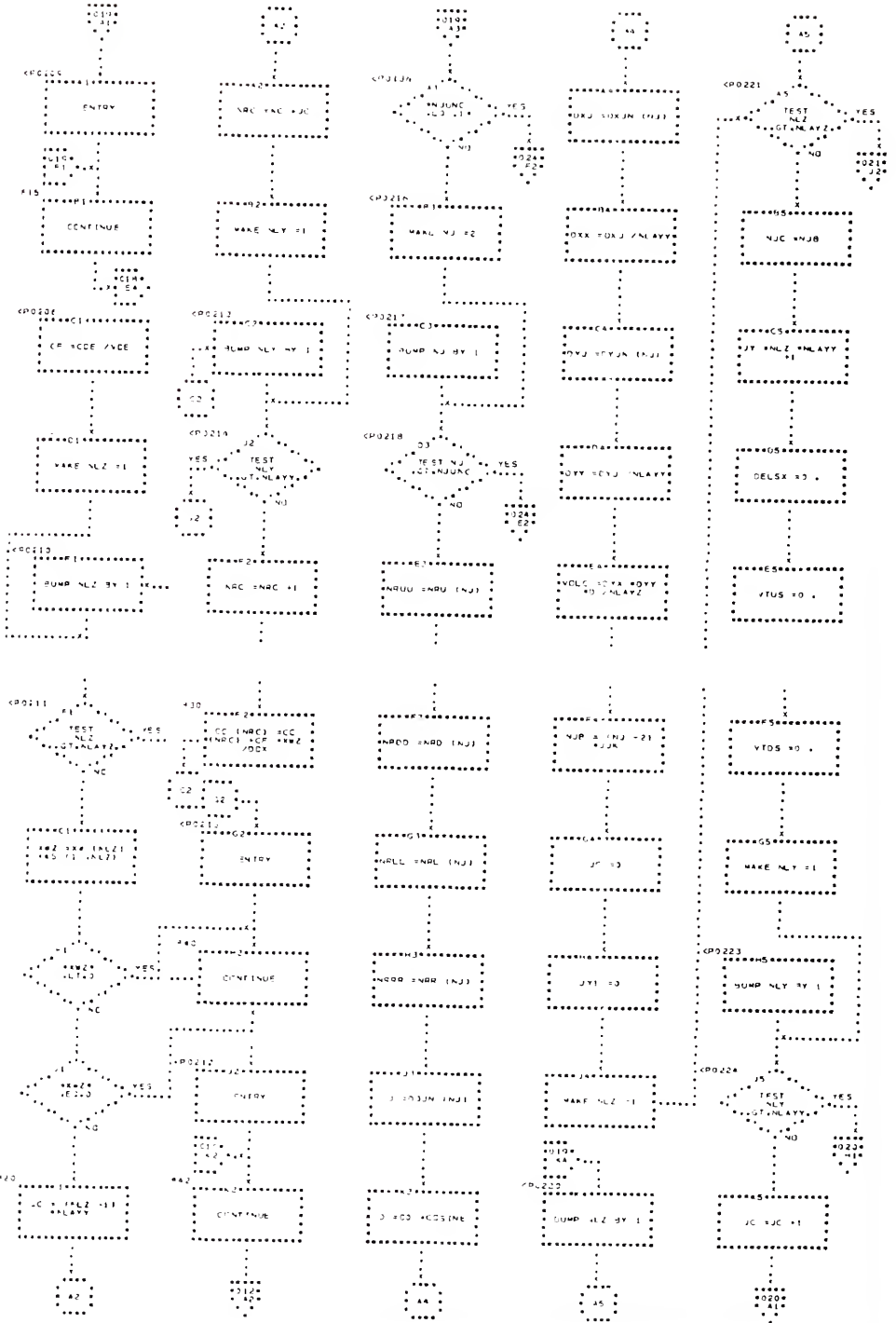
Graph plots are produced every NPLOT time intervals by the sub-routine SHOWIT, unless NPLOT > NDT, in which case no plots drawn. For each reach, the longitudinal concentration profiles and velocity profiles in each layer, and layer averaged values, are produced.

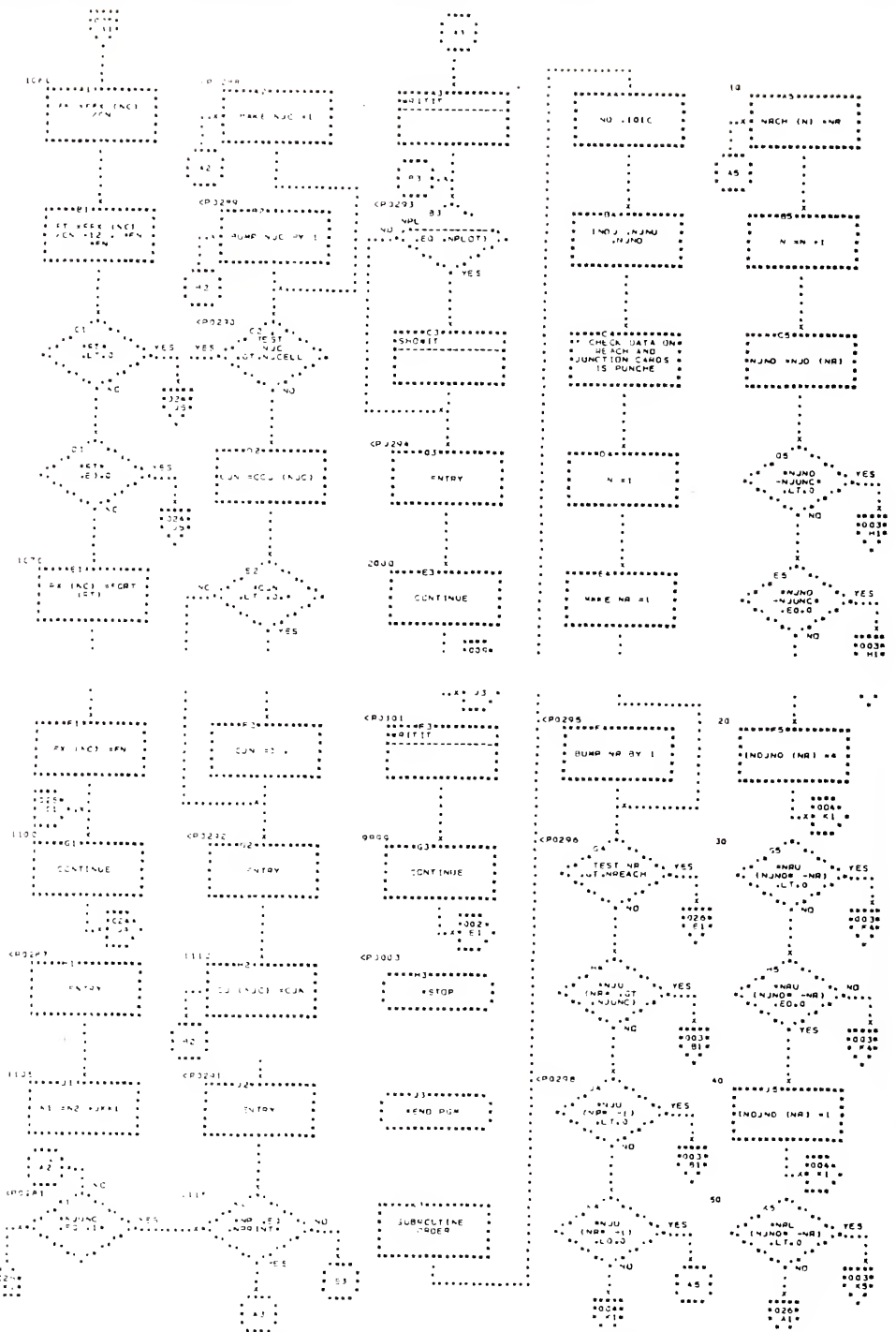
APPENDIX B
FLOW CHART FOR THE COMPUTER PROGRAM

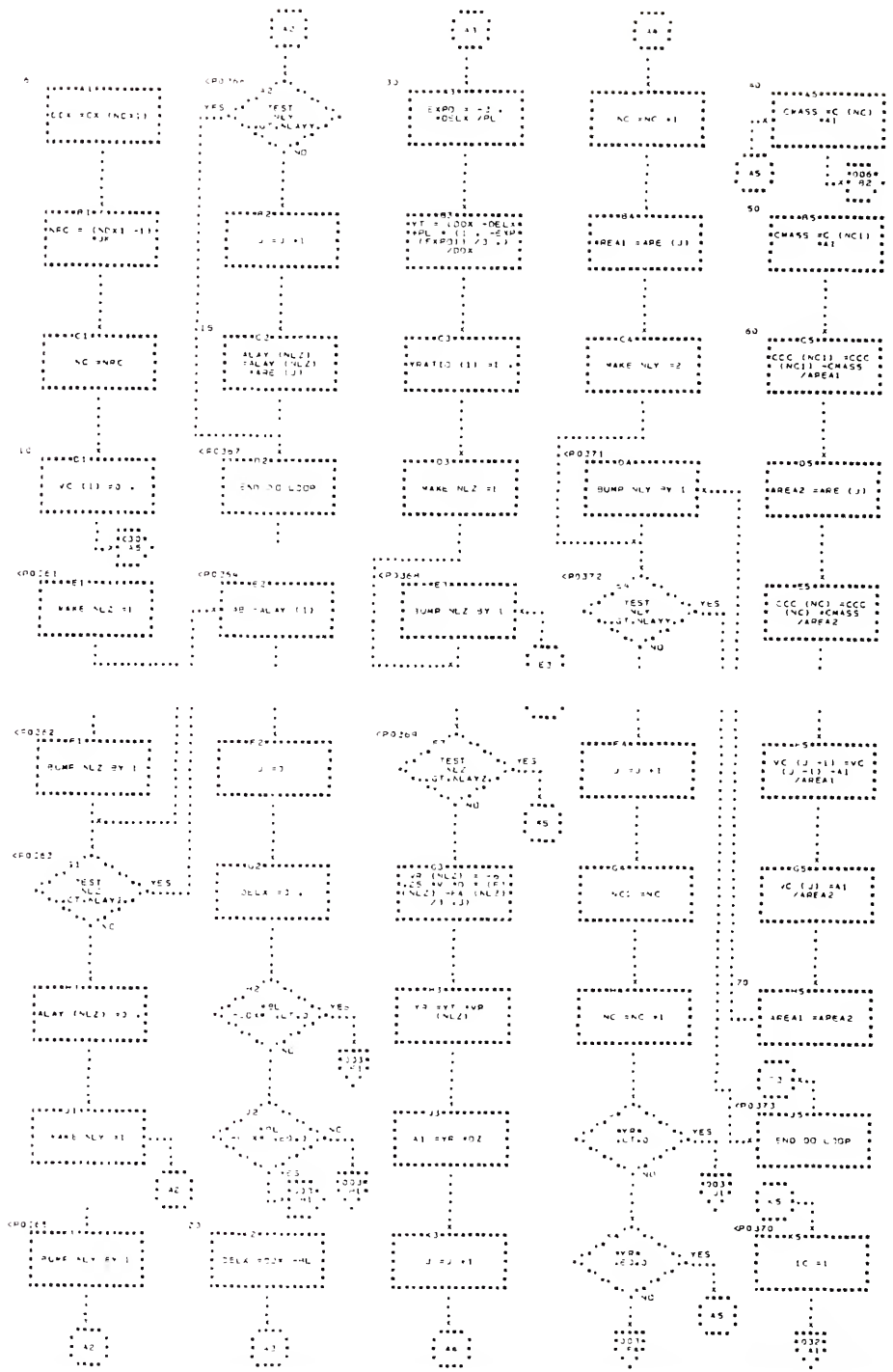
This appendix contains a flow chart produced using a utility program of the Northeast Regional Data Center, Gainesville, Florida, for the program, CANNET3D, a program designed to simulate mass transport in low energy tidal canal networks using a method of second moments.

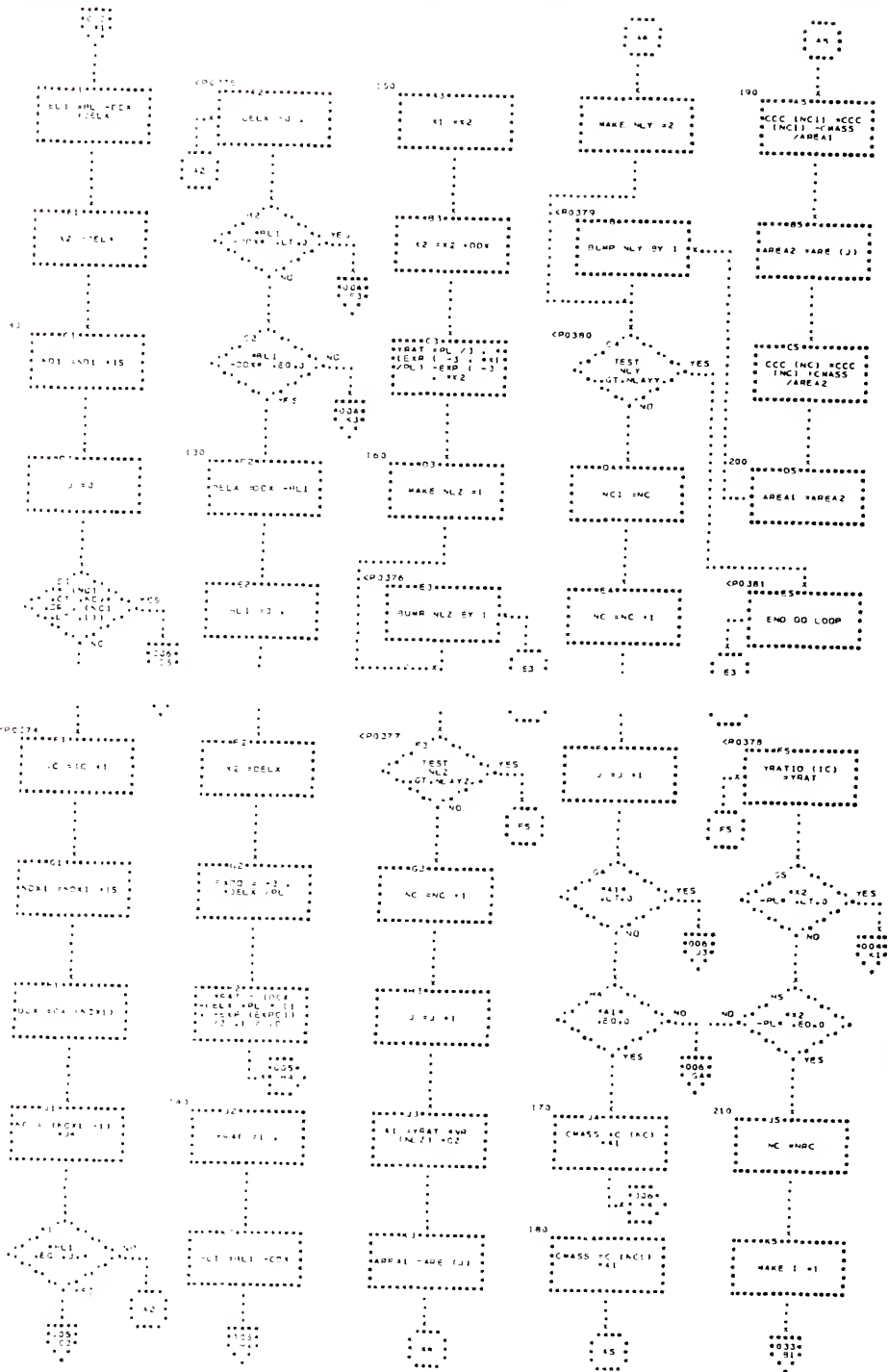


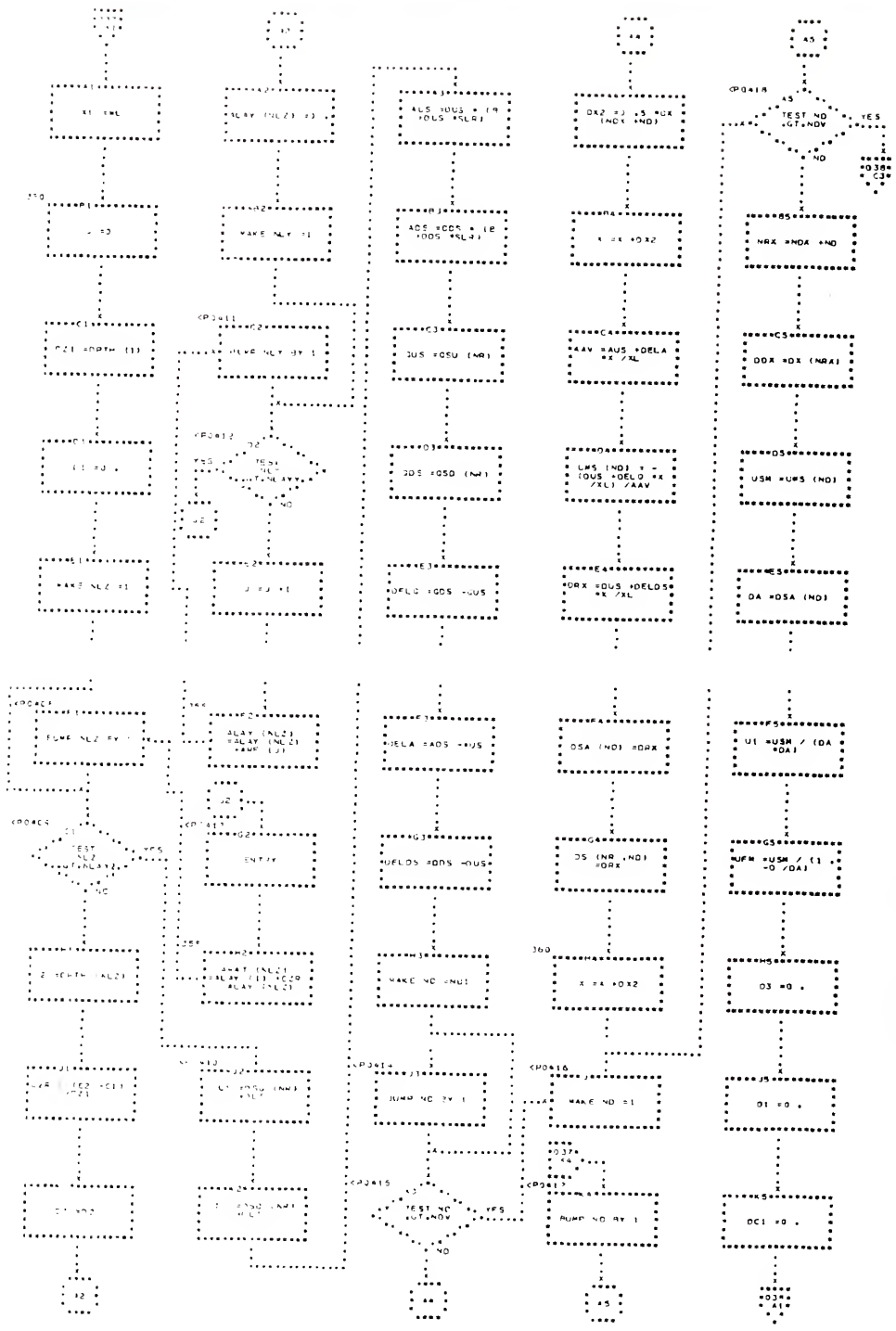












APPENDIX C
PROGRAM LISTING

This appendix contains a listing of the computer program, CANNET3D, a program designed to simulate mass transport in low energy tidal canal networks using a method of second moments.

07 MAY 1978

```

$ APA(50)
$ COMMON/DL12/ MPL, CMAX, VMAX, DXMIN, DXSC
$ DIMENSION OPT4(50), OPT5(50), DXJN(50), XM(6),
$ DYJN(50), DOJN(50), XTAV(6), TAU(5), SUBNEW(5), TEXT(20),
$ DECA(2000), VOLNEW(5), AREA(50,36), DEP(50,6),
$ WS(25), WANG(25), AA(50), CTE(5), OXZ(50), DVX(10), VV1(10), SUMA(6),
$ WFUNC(6), VOLJ(50), CC(2000), FFX(2000), VL(6), XX(10), DELAC(50),
$ PRX(2000), CCJ(1000), QIV(50), CIV(50), VJ(1000), VSUM(10),
$ VU(50,36), VD(50,36), VL(50,36), VR(50,36),
$ VV(50,36), VVD(50,36), VVL(50,36), VVR(50,36)
$ FORMAT(615)
5001 FORMAT(F10,0,I5,F10,0,2I5)
5002 FORMAT(8F10,0)
5003 FORMAT(5X,5I5/8F10,0)
5004 FORMAT(4I5,2F10,0)
5005 FORMAT(5X,3F10,0,5I5)
5006 FDRMAI(9F8,0)
5007 FORMAT(2I5,2F10,0)
5008 FORMAT(3I5,F10,0)
5009 FCRMAI(20A4)
5000 FORMAT(, NUMBER OF TEST, NTEST= , I2, /
6001 $ , TIDAL PERIOD, T= , F5.2, , HOURS, /
$ , NUMBER OF TIME STEPS BETWEEN OUTPUTS, NPRINT= , I5, /
$ , NUMBER OF TIME STEPS BETWEEN PLOTS, NPLT= , I5, /
$ , TIME INCREMENT, DTH= , F6.4, , HOURS, /
$ , TIDAL AMPLITUDE, AMP= , F5.2, , FEET, /, BACKGROUND, .
$ , CONCENTRATION OF RECEIVING WATERS, CRW= , F5.2, , P, P, M, , /
$ , DIMENSIONLESS LONGITUDINAL DIFFUSION COEFFICIENT, KX= , F6.3, /
$ , DIMENSIONLESS LATERAL DIFFUSION COEFFICIENT, KY= , F6.3, /
$ , DIMENSIONLESS VERTICAL DIFFUSION COEFFICIENT, KZ= , F6.4, /
$ , BACKGROUND DIFFUSION COEFFICIENT, EOE= , F6.4, , SQ. FT. / SEC. , /
$ , VERTICAL MOMENTUM TRANSFER COEFFICIENT, NZ= , F7.5, /
$ , SQ. FT. / SEC. , /, NUMBER OF REACHES, NREACH= , I3, /
$ , NUMBER OF JUNCTIONS, NJUNCE= , I2, /
$ , NUMBER OF LAKES, NLAKE= , I2, /
$ , NUMBER OF TIDAL ENTRANCES, NTE= , I2, /
$ , NUMBER OF LATERAL LAYERS, NLAY= , I1, /
$ , NUMBER OF VERTICAL LAYERS, NLAZY= , I1, /
6002 FORMAT(, , DATA FOR JUNCTION NUMBER , I2, , , /
$ , LONGITUDINAL DISTANCE, DXJN= , F7.2, , FEET, /
$ , LATERAL DISTANCE, DYJN= , F7.2, , FEET, /
$ , MEAN TIDAL DEPTH, DOJN= , F3.2, , FEET, )
6003 FORMAT(, , LATERAL INFLOWS, )
6004 FORMAT(, , REACH , I2, , SECTION , I2, , SECTION CELL , I2,
$ , NETWORK CELL , I3, , QI= , F8.6, , CI= , F7.2, , OPTION= , I1)
6005 FORMAT(, , DECAY DATA, )
6006 FORMAT(, , REACH , I2, , SECTION , I2, , SECTION CELL , I2,

```


07 MAY 1978

RADIAN=PI/180.
OPT67=OPT6+2*OPT7
LAYZ=1./NLAYZ
NZ=0.1*NZ
KX=KX/8.25
KY=KY/8.25

READ IN REACH DATA AND SET UP CELLS

DX(*) - DISTANCE INCREMENT
 NBEGIN(*) - POINTER TO BEGINNING OF REACH
 NDIV(*) - NUMBER OF DIVISIONS ALONG REACH
 NJD(*) - NUMBER OF DOWNSTREAM JUNCTION
 NJU(*) - NUMBER OF UPSTREAM JUNCTION
 NR,NRCH(*) - NUMBER OF REACH
 OPT1 = 0: EQUAL DIVISIONS CALCULATED
 OPT1 = 1: UNEQUAL DIVISIONS READ IN
 OPT1 = -1: OPTION CHANGED FROM UNEQUAL TO EQUAL DIVISIONS
 OPT4 = 0: INITIAL CONCENTRATIONS IN REACH ARE BACKGROUND
 OPT4 = 1: PEAD IN INITIAL CONCENTRATIONS IN REACH
 RANG(*) - REACH ALIGNMENT ANGLE
 RB(*) - REACH BREADTH
 RDECAY(*) - CONSTANT DECAY COEFFICIENT FOR REACH
 RDO(*) - REACH MEAN TIDAL DEPTH
 RL(*) - REACH LENGTH
 RNK(*) - REACH EQUIVALENT SAND ROUGHNESS
 RSL(*) - REACH LEFT BANK INVERSE SIDE SLOPE
 RSR(*) - REACH RIGHT BANK INVERSE SIDE SLOPE

NI=2
 DU 40 NR=1,NREACH
 READ(5,5003)NDV,NJU(NR),NJD(NR),OPT,OPT4(NR),RL(NR),RB(NR),
 RDO(NR),RSL(NR),RSR(NR),RANG(NR),PNK(NR),RDECAY(NR),
 NRCH(NR),NR
 OPT1(NR)=CPT
 NDIV(NR)=NDV
 NBEGIN(NR)=NI-1
 N2=NI+NDV-1
 IF (OPT)10,10,30
 DDX=RL(NR)/NDV
 DO 20 NS=NI,N2
 DX(NS)=DDX
 GO TO 40

30 READ(5,5002)(DX(NS),NS=N1,N2)
 NI=N2+3
 NRCELL=(N2+1)*JK

READ IN JUNCTION DATA

CCCCCCCCCCCCCCCCCCCCCCCCCCCC

C C

07 MAY 1978

00000000000000000000

```

DXJN(*) - LONGITUDINAL LENGTH OF JUNCTION
DYJN(*) - LATERAL LENGTH OF JUNCTION
DJN(*) - MEAN TIDAL DEPTH IN JUNCTION
NRD(*) - NUMBER OF DOWNSTREAM REACH
NRL(*) - NUMBER OF LEFT REACH
NRR(*) - NUMBER OF RIGHT REACH
NRU(*) - NUMBER OF UPSTREAM REACH
OPTS(*) - OPTS=0: INITIAL CONCENTRATION IN JUNCTION IS BACKGROUND
          OPTS=1: READ IN INITIAL CONCENTRATIONS IN JUNCTION
          TIDAL PRISM VOLUMES IN LEFT AND RIGHT BRANCHES
          CONVECTIVE VOLUME OF WIND INTO JUNCTION FROM LEFT AND
          RIGHT BRANCHES
VL(*) , VV(*) -
VVL(*) , VVR(*) -

```

```

NJUNC=NJUNC+1
NLE=NJUNC*MLAKE
NJUNC1=NJUNC+1
IF (NJL.EQ.1) GOTO 52
DO 50 NJ=2,NJL
READ(5,5005) DXJN(NJ),DYJN(NJ),DOJN(NJ),NRU(NJ),NRD(NJ),NRL(NJ)
$ ,NRR(NJ),OPTS(NJ)
IF (NRL(NJ)) 41,41,43
41 DO 42 J=1,JK
   VVL(NJ,J)=0.
42 IF (NRR(NJ)) 44,44,50
44 DO 45 J=1,JK
   VVR(NJ,J)=0.
45 VV(NJ,J)=0.
50 WRITE(6,6002) NJ,DXJN(NJ),DYJN(NJ),DOJN(NJ)
   NJCELL=(NJUNC-1)*JK

```

READ IN TIDAL ENTRANCE DATA

```

CIE(*) - CONCENTRATION AT TIDAL ENTRANCE
TAU(*) - TIDAL ENTRANCE TIME DECAY COEFFICIENT

```

```

52 READ(5,5002) (TAU(NTE),NTE=1,NTE5)
   WRITE(6,6024)
   DO 55 NTE=1,NTE5
   WRITE(6,6025) NTE,TAU(NTE)
   CIE(NTE)=CRW
   TAU(NTE)=EXP(-3.*DTF/TAU(NTE))
55

```

READ IN AND LOCATE LATERAL INFLOWS

```

CIC(*) - CCNSTANT LATERAL INFLOW CONCENTRATION
NC - NUMBER OF CROSS-SECTIONAL CELL IN REACH

```

000000

000000

07 MAY 1978

```

NDX          - NUMBER OF SECTION
NQI(*)      - NUMBER OF CELL CONTAINING LATERAL INFLOW
NRQI        - NUMBER OF REACH CONTAINING LATERAL INFLOW
NR          - NUMBER OF CANAL
OPT2(*)     - OPT2= 0: CONSTANT LATERAL INFLOW
              - OPT2= 1: VARIABLE LATERAL INFLOW
              - OPT2=-1: END OF DATA
CCI(*)      - CONSTANT LATERAL INFLOW RATE

```

```

WRITE(6,6003)
  IQIC=0
  IQIVT=0
  NQ=0

```

```

70  NG=NG+1
    READ(5,5034) OPT,NR,NDX,NC,CQI,CCI
    OPT2(NQ)=OPT
    IF (OPT,LT,0) GOTO 100
    NCELL=(NBEGIN(NR)+NDX-1)*JK+NC
    NRQI(NQ)=NR
    NQI(NQ)=NCELL

```

```

80  WRITE(6,6004)NR,NDX,NC,NCELL,CQI,CCI,OPT
    IF (OPT) 100,80,90
    IQIC=IQIC+1
    CQC(IQIC)=CCI
    CIC(IQIC)=CCI

```

```

90  GOTO 70
    IQIVT=IQIVT+1
100 GOTO 70
    NQI(NQ)=5999
    NRQI(NQ)=9999

```

READ IN AND LOCATE DECAY DATA

```

DECAY(*)    - DECAY COEFFICIENT
NC          - NUMBER OF CROSS-SECTIONAL CELL IN REACH
NOE(*)      - NUMBER OF CELL CONTAINING DECAY TERM
NDX        - NUMBER OF SECTION
NR         - NUMBER OF REACH
            - NR=-1: END OF DATA

```

```

ND=1
WRITE(6,6005)
DO 110 NC=1,NRCELL
  DECAY(NC)=0
110 READ(5,5008) NR,NDX,NC,DEC
  IF (OPT) 140,130,13
130 NCELL=(NBEGIN(NR)+NDX-1)*JK+NC
  DECAY(NCELL)=DEC

```

CCCCCCCC

CCCCCCCC

07 MAY 1978

```

WRITE(6,6006) NR,NDX,NC,NCELL,DEC
ND=ND+1
GOTO 120

```

CCCCC

```

READ IN AND LOCATE BENDS
BENDR(*,*)- RADIUS OF BEND
BENDL(*,*)- CENTER-LINE LENGTH OF BEND
F1(*),F4(*)- ROZOVSKI'S FUNCTIONS

```

```

140 WRITE(6,6018)
IB=0
DO 142 NR=1,NREACH
NOV=NDIV(NR)
CO 142 ND=1,NOV
BENDR(NR,ND)=0.
144 IF(NR) 146,146,145
BENDR(NR,NDX)=BR
BENDL(NR,NDX)=BL
IB=IB+1

```

```

WRITE(6,6019) NR,NDX,BR,BL
GOTO 144
146 IF(IB.EG.0) GOTO 149
FT1=0.
FT3=0.

```

```

DO 148 NLZ=1,NLAYZ
P=Z-1.
FT2=0.
IS=1

```

```

DO 147 I=1,5
FT2=FT2+P**((I+1)/(I+1)**I)*IS
IS=-IS
FT2=2.*FT2+1.28987*P
F1(NLZ)=2.*(FT2-FT1)*NLAYZ
FT1=FT2
FT4=Z*(-2.8845+Z*(4.6818-1.7297*Z))
F4(NLZ)=NLAYZ*(FT4-FT3)
FT3=FT4

```

148

CCCCC

SET UP INITIAL SALINE CONDITIONS

```

DSM - ELEVATION OF INTERFACE BELOW MEAN SEA LEVEL
RHCF - DENSITY OF FRESHWATER
RHCS - DENSITY OF SALTWATER
DSL1(*) - ELEVATION OF INTERFACE AT LOW TIDE
XS(*,*) - DISTANCE MOVED BY DENSITY CURRENT

```

07 MAY 1978

```

C      U4TE      -      VALUE OF U4 AT TIDAL ENTRANCE
149 IF(OPT8) 160,160,150
150 READ(5,5002) DSM,RHOF,RHOS,U4TE
    WRITE(6,6020) DSM,RHOF,RHOS,U4TE
    DSMLT=DSM*AMP
    RII=G*(1.-RHOF/RHOS)
    DO 155 NR=1,NREACH
      DSU(NR)=0
      DSD(NR)=0
      SALTH=RDO(NR)-DSMLT
      AM(NR)=SALTH*LT*Q, SALTH=0
      DSLT(NR)=SALTH*(RB(NR)+0.5*SALTH*(PSL(NR)+RSR(NR)))
155 DO 165 ND=1,50
160 DO 165 NLZ=1,NLAYZ
165 XS(ND,NLZ)=0
C      ORDER REACHES FROM UPSTREAM TO TIDAL ENTRANCES
C      CALL ORDER
C      SET UP BUFFER CELLS AT ENDS OF REACHES
DO 63 NR=1,NREACH
  INDJ=INDJND(NR)
  NJNU=NJU(NR)
  NDX=NBEGIN(NR)
  IF(NJNU-1) 56,56,57
  DX(NDX)=CX(NDX+1)
56   GOTO 58
57   DX(NDX)=DXJN(NJNU)/NLAY
58   NDX=NDX+NDIV(NR)
60   GOTO (60,61,61,62), INDJ
60   DX(NDX+1)=DXJN(NJN(NR))/NLAY
61   GOTO 63
61   DX(NDX+1)=DYJN(NJN(NR))/NLAY
62   GOTO 63
62   CX(NDX+1)=DX(NDX)
63 CONTINUE
C      WRITE CANAL DATA
C      WRITE(6,6023)
C      NI=2
C      DO 170 NR=1,NREACH
C      WRITE (6,6007)NR
C      NDV=NDIV(NR)

```

07 MAY 1978

```

WRITE (6,6008)NDV,NJU(NR),NJD(NR),RL(NR),RB(NR),RDO(NR),
$ RSL(NR),RSR(NR),RANG(NR),RNK(NR),RDECAY(NR)
RNK(NR)=25*.7/RNK(NR)/E
N2=N1-1+NDV
WRITE (6,6009)OPT1(NR)
WRITE (6,6010)(DX(NS),NS=N1,N2)
N1=N2+3

```

170

CCCCCCCC

INITIALIZE ARRAYS IN REACHES

```

C(*) - CONCENTRATION
F(*) - CENTER OF MASS
R(*) - WIDTH OF DISTRIBUTION
VEL(*) - LONGITUDINAL VELOCITY

```

```

NI=JK1
DO 230 NR=1,NREACH
N2=N1-1+NDIV(NR)*JK
IF (OPT4(NR))180,180,200
180 DO 190 NC=N1,N2
190 C(NC)=CRW
GO TO 210
200 READ(5,5006)(C(NC),NC=N1,N2)
210 DO 220 NC=N1,N2
FX(NC)=0.
RX(NC)=1.
VEL(NC)=0.
N1=N2+JKK1

```

220
230

CCCCC

INITIALIZE ARRAYS IN JUNCTIONS

```

CJ(*) - CONCENTRATION IN JUNCTION

```

```

IF(NJL.EQ.1)GOTO 295
NI=1
DO 290 NJ=2,NJL
OPT=OPT5(NJ)
DO 285 NLY=1,NLAY
DO 285 NLZ=1,NLAY
N2=N1-1+NLAY
IF (OPT) 240,240,260
240 DO 250 NJC=N1,N2
250 CJ(NJC)=CRW
GOTO 285
260 READ(5,5006)(CJ(NJC),NJC=N1,N2)
285 N1=N2+1
290 CONTINUE

```

240
250

260
285
290

C

07 MAY 1978

```

WS(I)=WSP*1.46667
IF(NIW.LT.NW) NIW=IW
IF((IW-NW)/500.490.490
NIW=NIW
IW=0
WSX=0.
WSY=C.0J01
CC 510 NNW=I.NIW
WSX=WSX+WS(NNW)*SIN(WANG(NNW))
WSY=WSY+WS(NNW)*COS(WANG(NNW))
WSX=WSX/NIW
WSY=WSY/NIW
WS2=SQR(WSX*WSX+WSY*WSY)
ANG2=ATAN(WSX/WSY)
IF(WSY) 501.511.511
501 IF(WSX) 502.503.504
502 ANG2=ANG2-PI
GOTO 511
503 ANG2=ANG1
GOTO 511
ANG2=ANG2*PI
504 ANG2=ANG2+PI
511 IWC=IWC+1
WSC=WS1+IWC*(WS2-WS1)/INTERP
WANGC=ANG1+IWC*(ANG2-ANG1)/INTERP
IF(IWC-INTERP) 513.512.512
IWC=0
IW=IW+1
WS1=WS2
ANG1=ANG2
DELDP=DELD
DELD=COSINE-COSP
SET INITIAL SALINE CONDITIONS
DTE - ELEVATION OF INTERFACE FROM LOW TIDE VALUE AT TIDAL ENT.
DSL(* ) - LOW TIDE ELEVATIONS OF INTERFACE
DSTE - ELEVATION OF INTERFACE AT TIDAL ENTRANCE
DSD(* ) - ELEVATION OF INTERFACE AT DOWNSTREAM SECTION OF REACH
DSU(* ) - ELEVATION OF INTERFACE AT UPSTREAM SECTION OF REACH
QSD(* ) - VOLUME TRANSPORT THROUGH DOWNSTREAM SECTION OF REACH
QSU(* ) - VOLUME TRANSPORT THROUGH UPSTREAM SECTION OF REACH
DSTE=0.
IF(OPT8) 524.524.514
514 IF((DELD.CE.O.)*AND.(DELDP.LE.O.)) GOTO 515
515 CC 516 NR=1,NREACH

```

CCCCCCCC

07 MAY 1978

```

C      IF(NLAKE) 541,541,537
537 00 540 NL=NJUNCI,NJL
      NR=NRD(INL)
      NDX=NBEGIN(NR)-1
      DO 535 J=1,JK
        NC=NC+1
        C(NC)=CJ(NL)
        FX(NC)=0.
        RX(NC)=1.
540 CONTINUE
C      SET CONSTANTS AND INITIALIZE COUNTERS FOR TIME STEP
C      IQIC - CONSTANT LATERAL INFLOW COUNTER
C      IGIV - VARIABLE LATERAL INFLOW COUNTER
C      NG - LATERAL INFLOW COUNTER
C      NCTE - TIDAL ENTRANCE COUNTER
541  IQIC=0
      IGIV=0
      NC=0
      NCOI=NQI(1)
      NCTE=0
      DO 842 NNR=1,NREACH
C      CONSTANTS FOR REACH
C      NR=NRCH(NNR)
C      NDV=NDIV(NR)
C      RLX=RL(NR)
C      D=RCO(NR)
C      D=DO+CCSINE
C      SL=RSL(NR)
C      SR=RSR(NR)
C      RNK1=RNK(NR)
C      B=RB(NR)
C      A=D*(B+.5*D*(SL+SR))
C      AP=AA(NR)
C      AA(NR)=A
C      DELA=A-AP
C      NJNU=NJU(NR)
C      NJND=NJD(NR)
C      INCJ=INDJND(NR)
      IF(NJNU-1) 542,542,543
      V=0.
542  GOTO 544

```


07 MAY 1978

```

552      QT=QT+DELG
        JC=0
        SUMD=0.
DO 553  NLZ=1,NLAYZ
        SUMA(NLZ)=0.
        QLAY=QL(NLZ)
        DA=DELA*GLAY/QT
        SUMD=SUMD+DELD*QLAY/QT
        DPTH(NLZ)=DEP(NR,NLZ)+SUMD
DO 552  (NR,NLZ)=DPTH(NLZ)
        552  NLY=1,NLAYY
        JC=JC+1
        APC=AREA(NR,JC)
        AC=APC+DA*QXZ(JC)/QLAY
        SUMA(NLZ)=SUMA(NLZ)+AC
        DELAC(JC)=AC-APC
        ARE(JC)=AC
        AREA(NR,JC)=AC
        APA(JC)=APC/AC
        JC=0
        SUMATL=SUMA(NLAYZ)
DO 554  NLZ=1,NLAYZ
        XW(NLZ)=K*WIND*WFUNC(NLZ)*SUMATL/(SUMA(NLZ)*NZ)
DO 554  NLY=1,NLAYY
        JC=JC+1
        VVD(NJNU,JC)=(XW(NLZ)+XS(NDV,NLZ))*APE(JC)
        VD(NJNU,JC)=-V*GXZ(JC)/QT
554  CALL MEAND
        SALINE WEDGE
        IF(DSTE.GT.0.) CALL WEDGE
        SIMULATION PROCEEDS THROUGH SEGMENTS OF REACH NR
DO 730  ND=1,NDV
        NDX=NDX+1
        DOX=CX(NDX)
        D1=0.
        D2=0.
        JC=0
        SECONDARY CURRENT
        IF(BENDR(NR,ND).GT.0.) CALL HELIX
        LATERAL INFLOW

```

C C C

C C C

C C C

07 MAY 1978

```

610 I=1,J,K
IF(NC+I-NCQI) G1C,570,610
NC=NG+1
NCQI=NGI(NQ)
IF(OPT2(NQ)) S80,S80,590
IGIC=IGIC+1
CGI=QIC(IGIC)*DTH
CCI=CIC(IGIC)
GOTO 600
IQIV=IQIV+1
LOC=LOCV(IQIV)
CGI=QIV(LCC)*DTH
CCI=CIV(LCC)
V=V-CGI*DDX
C(NC+I)=C(NC+I)+CGI*CCI/(ARE(JC+I))
600
610 CONTINUE

```

SIMULATION PROCEEDS THROUGH CROSS-SECTIONAL CELLS OF SEGMENT ND

```

XT - - DISTANCE MOVED DUE TO TIDE
XW(*) - - DISTANCE MOVED DUE TO WIND
XS(*,*) - - DISTANCE MOVED DUE TO DENSITY CURRENT

```

```

D0 726 NLZ=1,NLAYZ
D3=DEPTH(NLZ)
D0 725 NLY=1,NLAYY
JC=JC+1
NC=NC+1
APPA=APA(JC)
CN=C(NC)*APPA
FNX=EX(NC)
RNA=RX(NC)*APPA
XT=- (V+(.5*FNX) *DDX*DELA)*QXZ(JC)/(QT*ARE(JC))+0.001
X=XW(NLZ)*XT+XS(ND,NLZ)/APPA
VELOC=X/DTS
VEL(NC)=VELOC
CI=C(NC)

```

LONGITUDINAL DIFFUSION VELOCITY

```

EX - - LONGITUDINAL DISPERSION COEFFICIENT
XD - - DISTANCE MOVED DUE TO DISPERSION VELOCITY

```

```

IF((ND,EO,1),OR,(ND,EG,NDV)) GOTO 620
NC1=NC-JK
EX=KX*D*ABS(VELOC+VEL(NC1))*0.5+EO
C2=C(NC1)
DXAV=0.5*(DDX+DX(NDX-1))

```

C C C C C C C

C C C C C C C

07 MAY 1978

XD=-2.*DTS*EX*(C1-C2)/(DXAV*(C1+C2+0.00001))
X=X+XD

LATERAL DIFFUSIONAL MASS TRANSFER

EY - LATERAL DISPERSION COEFFICIENT

620 IF(NLY.EQ.1) GOTD 630

NCY=NC-1
EY=KY*D*ABS(VELOC+VEL(NCY))*0.5+E0
DY=0.5*(ARE(JC)+ARE(JC-1))*NLAYZ/D
DMY=DTS*EY*(C1-C(NCY))/(DY*DY)
CCC(NC)=CCC(NC)-DMTY
CCC(NCY)=CCC(NCY)+DMTY

VERTICAL DIFFUSIONAL MASS TRANSFER

EZ - VERTICAL DISPERSION COEFFICIENT

RI - RICHARDSON NUMBER

630 IF(NLZ.EQ.1) GOTD 640

NCZ=NC-NLAYY
DZ=DPH(NLZ-1)
DI=0.5*(DI+D2)
D2=0.5*(D2+D3)
DZ=D23-D12
DS9=D*D7/5.
DUDZ=(X-XX(NLY))/(DTS*DZ)
EZ=KZ*DS9*ABS(DUDZ)+E0

IF(DSTE) 636,636,632

632 DSALT=DS(NR,ND)
IF((D21-DSALT)*(D12-DSALT)) 634,636,636

634 RI=RI/(CZ*DUEZ*DUDZ)

IF(RI.GT.10) RI=10.

EZ=EZ*SQRT(1.-0.1*RI)

DMTZ=DTS*EZ*(C1-C(NCZ))/(DZ*DZ)

CCC(NC)=CCC(NC)-DMTZ

CCC(NCZ)=CCC(NCZ)+DMTZ

XX(NLY)=X

LONGITUDINAL TRANSFER BETWEEN CELLS, CONSERVING MOMENTS

IS=ABS(X)/X

FNX=FNX+X/DDX

P=(IS*FNX+.5*RNX-.5)/RNX

IP=P+P-1

IF(IP)700,720,720

CC(NC)=CC(NC)+CN

700

CCCC

CCCCC

CCCC

07 MAY 1978

```

720      FFX(NC)=FFX(NC)+FNX*CN
        RRX(NC)=RRX(NC)+CN*(RNK*RNK+12.*FNX*FNX)
        P1=1.-P
        FCN=PI*CN
        PRNX=PI*RNK
        CC(NC)=CC(NC)+PCN
        FC=5*(1.-PRNX)*IS
        FFX(NC)=FFX(NC)+FC*PCN
        RRX(NC)=RRX(NC)+FCN*(PRNX*PRNX+12.*FC*FC)
        DDXI=DX(NDX+IS)
        PDX=PC*DCX/DDXI
        PCN=PDXX*CN
        PRNX=PDXX*RNK
        NCI=NC+JK*IS
        CC(NCI)=CC(NCI)+PCN
        FC=5*(PRNX-1)*IS
        FFX(NCI)=FFX(NCI)+FC*PCN
        RRX(NCI)=RRX(NCI)+FCN*(PRNX*PRNX+12.*FC*FC)
725      CONTINUE
726      O1=O2
733      V=V+DDX*DELA
        VOLJ(NJND)=VOLJ(NJND)+V
        J=0
731      GO TO (731,733,735,737). INDJ
732      CO 732 NLZ=1,NLAYZ
733      DO 732 NLY=1,NLAY
        J=J+1
732      VU(NJND,J)=(XW(NLZ)+XS(1,NLZ))*ARE(J)
733      CO 734 NLZ=1,NLAYZ
734      DO 734 NLY=1,NLAY
        J=J+1
733      VV(NJND,J)=(XW(NLZ)+XS(1,NLZ))*ARE(J)
734      GO TO 737
735      DO 736 NLZ=1,NLAYZ
736      DO 736 NLY=1,NLAY
        J=J+1
735      VV(NJND,J)=(XW(NLZ)+XS(1,NLZ))*ARE(J)
736      VR(NJND,J)=-V*QXZ(J)/QT
        FLOW INTO RECEIVING WATERS
737      IF (INDJ-4) 780,740,740
740      NCTE=NCTE+1
        VOL=0.

```

C
C
C

07 MAY 1978

```

GCM=0,
DO 770 J=1,JK
  NC=NC+1
  IF(VEL(NC-JK)) 760,760,750
  IF(CN) 752,752,751
  FN=FFX(NC)/CN
  RT=RRX(NC)/CN-12.*FN*FN
  IF(RT) 752,752,754
  R=1.
  CN=CRW
  GOTC 756
  R=SQRT(RT)
  VCL=VOL+R
  GCM=GCM+CN
  GOTD 770
  NCI=NC-JK
  CN=CC(NC)
  IF(CN-CRW) 762,762,764
  CC(NC)=CRW
  CCC(NC)=0.
  FFX(NC)=0.
  RRX(NC)=CRW
  GOTD 77C
  FN=FFX(NC)/CN
  RTERM=RRX(NC)/CN-12.*FN*FN
  IF(RTERM.LT.C.) WRITE(5,6017)
  R=1.-SQRT(RTERM)
  CNTE=CTE(NC)*R
  CC(NC)=CN+CNTE
  FC=.5*(1.-R)
  FFX(NC)=FFX(NC)+FC*CNTE
  RRX(NC)=RRX(NC)+CNTE*(R*R+12.*FC*FC)
770 CONTINUE
  VOLNEW(NC)=VOL/NLAY
  SUBNEW(NC)=GCM/NLAY
780 IF(NJNU-1) 785,800,842
C
C
C TRANSFER ACROSS NULL POINT
785 NRN=-NJNU
  NRX=NBEGIN(NRN)
  NDX=NDX-NDV
  NCN=NRX*JK+1
  NC=(NDX-1)*JK
  DXR=DX(NCX)/DX(NRX)
  J=0
  DO 790 NLZ=1,NLAY

```

07 MAY 1978

```

NCN=NCN+NLAYY
DO 790 NLY=1,NLAYY
  J=J+1
  MNC=NCN-NLY
  CC(NNC)=CC(NNC)+CC(NC+J)*DXR*ARE(J)/AREA(NRN,J)
790   GOT0 842

```

C
C
C

INDUCED VERTICAL FLOW AT DEAD-ENDS

```

800   MDX=NDX-NCV
      DDX=DX(NDX+1)
      NC=NDX*JK
      VDE=0.1
      CDE=0.
DO 815 NLZ=1,NLAYZ
  XWZ=XW(NLZ)+XS(1,NLZ)
IF(XWZ) 805 815 815
  JC=(NLZ-1)*NLAYY
  NRC=NC+JC
DO 810 NLY=1,NLAYY
  NRC=NRC+1
  FF(NRC)=0.
  RR(NRC)=CC(NRC)
  VOL=-XWZ*ARE(JC+NLY)
  VDE=VDE+VCL
  CDE=CDE+C(NRC)*VCL
810   CONTINUE
      CF=CCE/VDE
DO 840 NLZ=1,NLAYZ
  XWZ=XW(NLZ)+XS(1,NLZ)
IF(XWZ) 840 840 820
  JC=(NLZ-1)*NLAYY
  NRC=NC+JC
DO 830 NLY=1,NLAYY
  NRC=NRC+1
  CC(NRC)=CC(NRC)+CF*XWZ/DDX
840   CONTINUE
842   CONTINUE

```

C
C
C

FLOW IN AND FROM JUNCTION

```

IF(NJUNC.EQ.1) GOT0 1015
DO 1010 NJ=2,NJUNC
  NRUU=NRU(NJ)
  NRDC=NRD(NJ)
  NRLF=NRL(NJ)
  NRRR=RRR(NJ)
  DO=DOJN(NJ)

```

07 MAY 1978

```

O=DO+COSINE
DXJ=DXJN(NJ)
DYX=DXJ/NLAYY
DYJ=DYJN(NJ)
DYY=DYJ/NLAYY
VOLC=DXX*DYX*D/MLAYZ
NJB=(NJ-2)*JJK
JC=0
JY1=0
00 922 NLZ=1,NLAYZ
NJC=NJB
JY=NLZ*NLAYY+1
DELSX=0.
VTUS=0.
VTDS=0.
00 845 NLY=1,NLAYY
JC=JC+1
VUS=VU(NJ,JC)
VTUS=VTUS+VUS+VL(NJ,JC)+VR(NJ,JC)
VTDS=VTDS+VD(NJ,JC)
VLD=(VUS-VD(NJ,JC))/VOLC
DVX(NLY)=VUD
DELSX=DELSX+VUD
VVI(NLY)=VUS/VOLC
IF (DELSX.EQ.0.) DELSX=0.001
DELVLC=(VTDS-VTUS)/(NLAYY*NLAYY)
APPA=1.+DELVLC/VOLC
00 850 NLY=1,NLAYY
00 847 NLY=1,NLAYY
NJC=NJC+1
CCJ(NJC)=CJ(NJC)*APPA
NJC=NJC+JKLAY
NJC=NJB
APPA1=APPA-1.
00 920 NL=1,NLAYY
JY=JY-1
JY1=JY1+1
VLB=VL(NJ,JY)
DVI=(VLB+VR(NJ,JY1))/VOLC+NLAYY*APPA1
V2=VLB/VOLC
VVLB=VVL(NJ,JY)
DVIY=(VVLB+VVR(NJ,JY1))/NLAYY
00 910 NLY=1,NLAYY
JJC=(NLZ-1)*NLAYY+NLY
NJC=NJC+1
V1=VVI(NLY)
V3=V1+DVI*DVX(NLY)/DELSX
VVI(NLY)=V3

```

07 MAY 1978

```

V4=V1+V2+APPA1-V3
VVL5=VVU(NJ,JJC)
DVX=(VVUS-VVD(NJ,JJC))/NLAY
V3=V3+(VVUS-NL*DVX)/VOLC
V4=V4+(VVLB-NLY*DVVY)/VOLC
VJ(NJC)=1.+(DVVX+DVVY)/VOLC
NJCX=NJC+JK
NJCY=NJC+1

```

```

IF(NL.EQ.NLAY) GOTO 885
IF(V3) 860,860,870
CVOL=V3*CJ(NJCX)

```

860

GOTO 880

CVOL=V3*CJ(NJC)

CCJ(NJC)=CCJ(NJC)-CVOL

CCJ(NJC)=CCJ(NJC)+CVOL

IF(NLY.EQ.NLAY) GOTO 910

IF(V4) 890,890,900

CVCL=V4*CJ(NJCY)

GOTO 905

CVCL=V4*CJ(NJC)

CCJ(NJC)=CCJ(NJC)-CVOL

CCJ(NJC)=CCJ(NJC)+CVOL

V2=V4

NJC=NJC+JKLAY

NJB=NJB+NLAY

910

920

922

C C C

FLOW TO AND FROM UPSTREAM REACH

```

N1=(NJ-2)*JJK+1
NDX=NBEGIN(NRUU)+NDIV(NRUU)
NC=(NDX-1)*JK
JC=0

```

DO 940 NLZ=1,NLAY

N2=N1-I+NLAY

DO 935 NJX=N1,N2

JC=JC+1

NC=NC+1

NC1=NC+JK

ARA=AREA(NRUU,JC)

VOLU=-VVU(NJ,JC)-VVU(NJ,JC)

VOLU=930,935,925

P=VOLU/(ARA*DX(NDX))

CN=P*CJ(NJX)

CCJ(NJX)=CCJ(NJX)-CJ(NJX)*VOLU/VOLC

CC(NC)=CC(NC)+CN

FP=S*(1.-P)

FFX(NC)=FFX(NC)+CN*FP

RRX(NC)=RRX(NC)+CN*(P*P+1.*FP*FP)

925

07 MAY 1978

```

GOTO 935
CCJ(NJX)=CCJ(NJX)+CC(NC1)*DXX*ARA/VOLC
930 CONTINUE
935 NI=N2+1
940

```

C C

FLOW TO AND FROM DOWNSTREAM REACH

```

NI=(NJ-1)*JJK-JK+1
NDX=NBEGIN(NRDD)
NC=NDX*JK
JC=0
DO 960 NLZ=1,NLAYZ
N2=NI-1,NLAYY
DO 950 NJX=N1,N2
JC=JC+1
NC=NC+1
NC1=NC-JK
ARA=AREA(NRDD,JC)
VOLD=-VD(NJ,JC)-VVD(NJ,JC)
IF (VOLD) 942,950,945
P=-VOLD/(ARA*CX(NDX*1))
CN=P*CCJ(NJX)
CCJ(NJX)=CCJ(NJX)+CJ(NJX)*VOLD/VOLC
CC(NC)=CC(NC)+CN
FP=.5*(P+1)
FFX(NC)=FFX(NC)+CN*FP
RRX(NC)=RRX(NC)+CN*(P*P+12)*FP*FP)
GOTO 950
CCJ(NJX)=CCJ(NJX)+CC(NC1)*DXX*ARA/VOLC
945 CONTINUE
950 NI=N2+1
960

```

C C

FLOW TO AND FROM LEFT BRANCH

```

IF (NRLL,EG,0) GOTO I000
NDX=NBEGIN(NRLL)*NDIV(NRLL)
NC=(NDX-1)*JK
NBA=(NJ-1)*JJK+1
NJE=NB
JC=0
DO 998 NLZ=1,NLAYZ
DO 995 NLY=1,NLAYY
JC=JC+1
NJE=NJE+JK
NC=NC+1
NC1=NC+JK
ARA=AREA(NRLL,JC)
VOLL=-VL(NJ,JC)-VVL(NJ,JC)

```

C C

07 MAY 1978

```

970 IF (VOLL) 980,995,970
    P=VOLL/(ARA*DX(NDX))
    CN=P*CCJ(NJY)
    CCJ(NJY)=CCJ(NJY)-CJ(NJY)*VOLL/VOLC
    CC(NC)=CC(NC)+CN
    FP=S*(1-P)
    FFX(NC)=FFX(NC)+CN*FP
    RRX(NC)=RRX(NC)+CN*(P*P+12.*FP*FP)
980 CCJ(NJY)=CCJ(NJY)+CC(NC1)*DYY*ARA/VOLC
995 GOTO 995
998 CONTINUE
    NJY=NB+NLAYY*NLZ
    C
    C
    C
    FLOW TO AND FROM RIGHT BRANCH
1000 IF (NRRR*EO.C) GOTO 1004
    NBN=(NJ-2)*JJK-JK+1
    NJY=NB
    NDX=NBEGIN(NRRR)*NDIV(NRRR)
    NC=(NDX-1)*JK
    JC=0
    DO 1002 NLZ=1,NLAYZ
    DO 1001 NLY=1,NLAYY
        JC=JC+1
        NJY=NJY+JK
        NC=NC+1
        NC1=NC+JK
        ARA=AREA(NRRR,JC)
        VOLR=-VR(NJ,JC)-VVR(NJ,JC)
        P=VOLR/ARA*DX(NDX)
        CN=P*CCJ(NJY)
        CCJ(NJY)=CCJ(NJY)-CJ(NJY)*VOLR/VOLC
        CC(NC)=CC(NC)+CN
        FP=S*(1-P)
        FFX(NC)=FFX(NC)+CN*FP
        RRX(NC)=RRX(NC)+CN*(P*P+12.*FP*FP)
991 GOTO 1001
    CONTINUE
    NJY=NB+NLAYY*NLZ
    C
    C
    C
    BALANCE VOLUMES IN JUNCTION
1004 NJC=(NJ-2)*JJK
    DO 1010 NL=1,NLAYY
    DO 1008 NLZ=2,NLAYZ
    DO 1008 NLY=1,NLAYY

```

07 MAY 1978

```

NJC=NJC+1
NJC1=NJC+NLAYY
VVL=VJ(NJC)-1.
IF(VDL) 1005,1005,1006
CVVL=CJ(NJC1)*VVL
GOTO 1007
1005
1006 CVVL=CJ(NJC)*VVL
1007 CCJ(NJC)=CCJ(NJC)-CVVL
1008 CCJ(NJC1)=CCJ(NJC1)+CVVL
1010 VJ(NJC1)=VJ(NJC1)+VVL
NJC=NJC+NLAYY
C
C FLOOD FLOW FROM TIDAL ENTRANCES
C
1015 DO 1020 NTE=1,NTES
CONC=(1.-VOLNEW(NTE))*CTE(NTE)+SUBNEW(NTE)
1020 CTE(NTE)=CRW+(CCNC-CRW)*TAU(NTE)
N1=JK1
DO 1105 NR=1,NREACH
RDEC=PDECAY(NR)
N2=N1-1+NCIV(NR)*JK
1021 IF(NJUC(NR)-1) 1021,1021,1023
N3=N1-1+JK
DO 1022 NC=N1,N3
CN=CC(NC)
C(NC)=CRW+(CN+CCC(NC)-CRW)*(1.-DTH*(PDEC+DECAY(NC)))
1022 FX(NC)=0.
RX(NC)=1.
N1=N3+1
1023 DO 1100 NC=N1,N2
CN=CC(NC)
CN=CRW+(CN+CCC(NC)-CRW)*(1.-DTH*(PDEC+DECAY(NC)))
1030 IF(CNN) 1040,1040,1040,1030
C(NC)=CNN
1040 IF(CN) 1050,1050,1050,1060
C(NC)=CRW
1050 FX(NC)=0.
RX(NC)=1.
GOTO 1100
1060 FN=FFX(NC)/CN
RT=RX(NC)/CN-12.*FN*FN
1070 IF(RT) 1050,1050,1070
RX(NC)=SCRT(RT)
FX(NC)=FN
1100 CONTINUE
1105 NI=N2+JKK1
IF(NJUNC,EC,1) GOTO 1115
DC 1110 NJC=1,NJCELL

```

07 MAY 1978

```
      CJN=CCJ(NJC)
      IF (CJN.LT.0.) CJN=0.
      CJ(NJC)=CJN
1110  IF(NP.EG.NPRINT) CALL WRITIT
1115  IF(NPL.EG.NPLOT) CALL SHOWIT
2000  CONTINUE
9999  CALL WRITIT
      STOP
      CONTINUE
      END
```


07 MAY 1978

```

230 CICB(IQ) = CIC(IQ)
240 N=0
    NC=0
    NV=0
    DO 280 NNR=1,NREACH
        NVTOT=0
        NR=NRCH(NNR)
        CO 280 IQ=1,NQ
            OPT=CPT2B(IQ)
            IF(OPT,EQ,1) NVTOT=NVTOT+1
            IF(NR-NRCI(IQ)) 280,250,280
    250 N=N+1
        NOI(N)=NOIB(IQ)
        OPT2(N)=CPT
    IF(OPT) 280,260,27)
    260 NC=NC+1
        NCTOT=IG-NVTOT
        QIC(NC)=QICB(NCTOT)
        CIC(NC)=CICB(NCTOT)
    GO TO 280
    NV=NV+1
    LCCV(NV) = NVTOT
280 CONTINUE
    RETURN
    END

```

07 MAY 1578

```

SUBROUTINE MEAND
  COMMON/BL4/ DPTH(6),DM(50,30),DB,AREAB(50,6),DMIN
  COMMON/BL5/ ARE(50),SL,SR,B,V,D,DX(500),DTS,DDX,NBEGIN(50)
  COMMON/BL9/ AREACH,JK,NJUNC,NLAY,NLAYZ,NR,ND,NDV,NDIV(50),NDX,
  $ INDJ,NJNL,NJND

```

CC
CC
CC
CC
CC

THIS SUBROUTINE CALCULATES THE MEAN DEPTH ASSOCIATED WITH EACH CELL

ARE(*) - CROSS-SECTIONAL AREA OF CELL IN REACH
DM(*,*) - MEAN DEPTH OF FLOW ASSOCIATED WITH CELL IN REACH

```

2 IF (ABS(CE-OPTH(NLAYZ))-DMIN) 2,6,6

```

```

  DO 4 NLZ=1,NLAYZ
    DPTH(NLZ)=DB*NLZ/NLAYZ
  DO 4 NLY=1,NLAY

```

```

  4 JC=JC+1
    ARE(JC)=AREAB(NR,NLZ)
  6 JC=0
    JC=0

```

```

  DP=0.
  SRSR=SQRT(SR)
  DO 170 NLZ=1,NLAYZ
    D=DPTH(NLZ)
    DL=D-DP
    DP=0

```

```

  SLDL=SL*DL
  AL=.5*SLDL*DL
  AR=.5*SR*DL*DL
  Y1=J.

```

```

  B1=D*SL
  B2=B1+B
  DELA=0.

```

```

  DO 10 NLY=1,NLAY
    NC=NC+1
    DELA=DELA+ARE(NC)
    AM=DELA-AL-AR
    W=AM/DL

```

```

  10 DO 170 NLY=1,NLAY
    JC=JC+1
    A=ARE(JC)

```

```

  20 IF (A-AL) 20,20,30
    AL=AL-A

```

```

    Y2=SQRT(2.*A/SL+Y1*Y1)
    DM(NR,JC)=A/(Y2-Y1)

```

```

  30 GOTO 170
    AA=A-AL
    AL=AL-A

```

07 MAY 1978

```

40 IF(AA-AM-1.) 40.40.50
   Y2=SLDL+AA/DL
   GOTO 60
50 AAA=AA-AM
   IF(AAA.GT.AR) AAA=AR
   Y2=SLDL+MSR*CL-SRSR*SQRT(2.*(AR-AAA))
60 IF(Y1-B1) 70.110.110
70 IF(Y2-B1) 160.160.30
80 IF(Y2-B2-.5) 9J.50.100
90 DM(NR.JC)=$((Y2-B1)*D+.5*(B1-Y1)*(D+Y1/SL))/(Y2-Y1)
   GOTO 170
100 $ DM(NR.JC)=(B*D+.5*(B1-Y1)*(D+Y1/SL)+(Y2-B2)*(D-.5*(Y2-B2)/SR))/
   (Y2-Y1)
   GOTO 170
110 IF(Y1-B2) 120.150.150
120 IF(Y2-B2) 130.130.140
130 DM(NR.JC)=0
   GOTO 170
140 IF(SR.EQ.0.) GOTO 130
   DM(NR.JC)=$((B2-Y1)*D+(Y2-B2)*(D-.5*(Y2-B2)/SR))/(Y2-Y1)
   GOTO 170
150 DM(NR.JC)=D+(E2-.5*(Y1+Y2))/SR
   GOTO 170
160 DM(NR.JC)=.5*(Y1+Y2)/SL
170 Y1=Y2
   RETURN
   END

```

07 MAY 1978

```

SUBROUTINE WRITIT
COMMON/BL5/ ARE(50),SL,SR,B,V,D,DX(500),DTS,DDX,NBEGIN(50)
COMMON/BL7/ FX(2000),RX(2000),VEL(2000),CJ(1000),NT,DTH,NP
COMMON/BL8/ C(2000),COSINE,CCC(2000),A,WSC,WANGC
COMMON/BL9/ NREACH,JK,NJUNC,NLAYZ,NLAYZ,NP,ND,NDV,NDIV(50),NDX,
$ INDJ,NJNU,NJND
6000 FORMAT(/,TIME',F7.2',HOURS: TIDAL DIFFERENCE =',F6.3,' FEET',/
$ WIND SPEED =',F4.1,' FT/SEC: WIND DIRECTION =',F4.0,' DEGREES,/)
6001 FORMAT(,REACH NUMBER',I2,')
6002 FORMAT(IX,I5(F8.3))
6003 FORMAT(, JUNCTION NUMBER',I2,')
6004 FORMAT(IX,9C(,))
6005 FORMAT(,X',F7.1,/,C/,I5(F8.3))
6006 FORMAT(8X,/,VEL/,I5(F8.3))

```

```

C THIS SUBROUTINE WRITES OUT THE RESULTS EVERY NPRINT STEPS AND AT THE
C END OF THE SIMULATION
C

```

```

NP=0
TIME=NT*DTH
WANGLE=WANGC*180./3.141593+180.
WRITE(6,6000) TIME,COSINE,WSC,WANGLE
NI=JK+1
DO 20 NR=1,NREACH
NDX=NBEGIN(NR)
X=0.
NDV=NDIV(NR)
WRITE(6,6001) NR
DO 10 ND=1,NDV
N2=NI-1+JK
NDX=NDX+1
DX2=0.5*CX(NDX)
X=X+DX2
WRITE(6,6005) X,C(NC),NC=NI,N2)
WRITE(6,6006) (VEL(NC),NC=NI,N2)
X=X+DX2
10 NI=N2+1
20 IF (NJUNC.EQ.1) GOTO 40
NI=1
DO 30 NJ=2,NJUNC
WRITE(6,6003) NJ
CC 30 NLY=1,NLAYZ
DO 30 NLY=1,NLAYZ
N2=NI-1+NLAYZ
WRITE(6,6002) (CJ(NJC),NJC=NI,N2)
30 NI=N2+1
40 WRITE(6,6004)

```

07 MAY 1978

RETURN
END

07 MAY 1978

```

SUBROUTINE FELIX
COMMON/BL5/ ARE(50),SL,SR,B,V,D,DX(500),DTS,DDX,NBEGIN(50)
COMMON/BL8/ C(2000),COSINE,CCC(2000),A,MSC,WANGC
COMMON/BL9/ NREACH,JK,NJUNC,NLAY,NLAYZ,NR,ND,NDV,NDIV(50),NDX,
$ INDJ,NJNU,NJNO
COMMON/BL10/ BENCHR(50,50),BENDL(50,50),F1(6),F4(6)
COMMON/BL11/ YRATIC(20),ALAY(6),VR(6)

```

THIS SUBROUTINE CALCULATES THE RADIAL FLOW BETWEEN CELLS DUE TO BENDS
BASED ON ROZOVSKII'S THEORY

NOTE: BR<0 INDICATES BEND TO RIGHT
BR>0 INDICATES BEND TO LEFT

LATERAL TRANSFER IN CELLS AT CROWN OF BEND

```

J=0
BL=BENDL(NR,ND)
BR=BENDR(NR,ND)
PL=102,*C
DZ=D/NLAYZ
NLAY1=NLAYY-1
NLAYZ1=NLAYZ-1
IS=-ABS(V)/V
DO 10 I=1,JK
  BL2=0.5*(BL-DCX)-DX(NDX-IS)
  NDX1=NDX
  NDI=ND
  2 IF (BL2) 6,6,4
  4 NDX1=NDX1-IS
  NCI=NDI-IS
  BL2=BL2-DCX(NDX1-IS)
  GOTO 2
  6 DDX=DX(NCX1)
  NRC=(NDX1-1)*JK
  NCR=NC
  VC(I)=0.
  10 DO 15 NLZ=1,NLAYZ
    ALAY(NLZ)=0.
    DO 15 NLY=1,NLAY
      J=J+1
      15 ALAY(NLZ)=ALAY(NLZ)+ARE(J)
      AB=ALAY(1)
      J=0
      DELX=0.
      IF (BL-DDX) 20,30,30
      20 DELX=DDX-EL
      30 EXP0=-3.*DELX/PL

```

CCCCCCCC

07 MAY 1978

```

YT=(CDX-DELX*PL*(1.-EXP(EXPO))/3.)/DDX
YRATIC(1)=1.
DO 70 NLZ=1,NLAYZ
  YR(NLZ)=-6.25*V*D*(F1(NLZ)-F4(NLZ))/3.3)*AB/(A*BF*ALAY(NLZ))
  YR=YT*VR(NLZ)
  A1=YR*DZ
  J=J+1
  NC=NC+1
  AREA1=ARE(J)
  DC 70 NLY=2,NLAY
  J=J+1
  NC1=NC
  NC=NC+1
  IF(YR) 40,40,50
  CMASS=C(NC)*A1
  CMASS=C(NC1)*A1
  CCC(NC1)=CCC(NC1)-CMASS/AREA1
  AREA2=ARE(J)
  CCC(NC)=CCC(NC)+CMASS/AREA2
  VC(J-1)=VC(J-1)-A1/AREA1
  VC(J)=A1/AREA2
  AREA1=AREA2

```

```

40
50
60
70
C
C
C

```

LATERAL TRANSFER IN ADJACENT SEGMENTS IN DIRECTION OF FLOW

```

IC=1
BL1=BL-DDX*DELX
X2=DELX
ND1=ND1+IS
J=0
IF((ND1*GT*NDV).OR.(ND1.LT.1)) GOTO 210
IC=IC+1
NDX1=NDX1+IS
DDX=DX(NDX1)
NC=(NDX1-1)*JK
IF(BL1.EQ.0.) GOTO 150
DELX=0.
IF(BL1-DDX) 130,13,140
BL1=0.
X2=DELX
EXPC=-J.*CELX/PL
YRAT=(DDX-DELX*PL*(1.-EXP(EXPO))/3.)/(DDX*YT)
GOTO 160
YRAT=1.
BL1=BL1-DDX
GOTO 160

```

```

130
140
160

```


07 MAY 1978

```

260      GOTO 270
270      CMASS=C(NC)*VRB*YRAT
280      CCC(NC)=CCC(NC)-CMASS/ARE(J)
      CCC(NCZ)=CCC(NCZ)+CMASS/ARE(J+NLAY)
      J=J+1
      NC=NC+2
      NCI=NC-1
      VLB=VLB+VC(J)*ARE(J)
      IF (VLB) 290,290,300
290      CMASS=C(NC)*VLB*YRAT
      GOTO 310
300      CMASS=C(NCI)*VLB*YRAT
310      CCC(NC)=CCC(NC)+CMASS/ARE(J+1)
      CCC(NCI)=CCC(NCI)-CMASS/ARE(J)
      NCI=NC
      NC=NC+1
      J=J+2
      VRB=VRB+VC(J)*ARE(J)
      IF (VRB) 320,320,330
320      CMASS=C(NCI)*VRB*YRAT
      GOTO 340
330      CMASS=C(NC)*VRB*YRAT
340      CCC(NC)=CCC(NC)-CMASS/ARE(J)
      CCC(NCI)=CCC(NCI)+CMASS/ARE(J-1)
350      NC=NC+JK*(IS-1)
999      RETURN
      END

```

```

SUBROUTINE WEDGE
COMMON/BL3/ NRJ(50),NRD(50),NRL(50),NRR(50)
COMMON/BL4/ DPTH(6),DM(50,36),DB,AREAB(50,6),DMIN
COMMON/BL5/ ARZ(50),SL,SR,B,V,DX(500),DTS,DDX,NBEGIN(50)
COMMON/BL7/ FX(2000),RX(2000),VEL(2000),CJ(1000),NT,DTH,NP
COMMON/BL8/ C(2000),COSINE,CCC(2000),A,WSC,WANGC
COMMON/BL9/ NREACH,JK,NJUNC,NLAY,NLAYZ,NR,ND,NDV,NDIV(50),NDX,
  INDJ,NJNU,NJND
COMMON/BL11/ DSLT(50),XS(50,6),QSU(50),QSD(50),DSU(50),DSD(50),
  INDS(50),UR4(50),DELD,SRATIO,RLX,DS(50,50),FL(50),AM(50),
  APA(50)
DIMENSION VV(50,6),UMS(50),NUR(3),DSA(50),ALAY(6),ARAT(6)

```

```

C THIS SUBROUTINE CALCULATES THE VELOCITY FIELD ASSOCIATED WITH THE
C MOVEMENT OF A SALINE WEDGE IN A REACH
C

```

```

  DLT=DSL(NR)
  CO 10 ND=1,NDV
  DSA(ND)=0.001
  UMS(ND)=0.
  DS(NR,ND)=DLT
  CO 10 NLZ=1,NLAYZ
  XS(ND,NLZ)=0.
  NDV2=NDV*2.
  CO 15 ND=1,NCV2
  CO 15 NLZ=1,NLAYZ
  VV(NC,NLZ)=0.
  10 IF(QSU(NR)+QSD(NR)) 20,959,20
  NRXX=NDX
  NDV1=NDV-1
  ND1=1
  X=0.
  XL=RLX
  SLR=0.5*(SL+SR)

```

```

EBB TIDE CONDITIONS

```

```

  30 IF(DELD) 30,30,80
  DU1=DSU(NR)
  DU2=DU1*SRATIO
  DSC(NR)=DU2
  DU1=DU1+DLT
  DU2=DU2+DLT
  DD1=DSD(NR)
  DD2=DD1*SRATIO
  DSD(NR)=DD2
  CC1=CC1+DLT

```

```

C
C

```

07 MAY 1978

```

DD2=DD2+DLT
AU1=DU1*(B+DU1*SLR)
AU2=CU2*(B+DU2*SLR)
AD1=DD1*(B+DD1*SLR)
AD2=DD2*(B+DD2*SLR)
AAS=0.5*(AU1+AU2)
AADS=0.5*(AD1+AD2)
DELAU=AU1-AU2
DEPAD=AD1-AD2
WL=RLX*FL(NR)
IF(WL.LT.RLX) XL=WL
QQ=-0.5*XL*(DELAU+DEPAD)+QSU(NR)
QSC(NR)=QQ
IF(INDJ-4) 40.50,50
NRDD=NRD(NJND)
QSU(NRQD)=QSU(NRQD)+Q0
50 IF(WL-RLX) 320.350,350

```

FLOOD TIDE CONDITIONS

```

80 QDS=QSD(NR)
DDS=DSD(NR)
U4=UR4(NR)
AMD=AM(NR)
FL(NR)=1.
I=INDS(NR)
WL=2.*U4*DDS
GOTO (120,280,310), I
90 IF(WL-RLX) 320.320,100
100 IF(NJNU-1) 270.270,110
110 INDS(NR)=1
120 QUS=QDS*(1.-RLX/WL)
DSU(NR)=QUS
DT=QUS+DLT
AUS=DT*(B+DT*SLR)-AM(NP)
QUS=AUS*U4*DDS
QSU(NR)=QUS
IR=0
NRUU=NRU(NJNU)
IF(INDS(NRUU)-3) 140.120,130
130 GUS=QUS-QSD(NRUU)
GOTO 150
140 IR=IR+1
NUR(IF)=NRUU
150 NRLL=NRU(NJNU)
IF(NRLL) 190.190,150
160 IF(INDS(NRLL)-3) 150.170,170
170 QUS=QUS-QSD(NRLL)

```

C
C
C

```

180   GOTO 190
      IR=IR+1
      NUR(IR)=NRLL
190   NRRR=NR(NJNU)
      IF(NRRR) 230,230,230
200   IF(NRRR) 230,230,230
210   GUS=GUS-CSD(NRRR)
      GOTO 230
220   IR=IR+1
      NUR(IR)=NRRR
230   IF(IR) 280,280,240
240   ASUM=0.
250   ASUM=ASUM+AM(NUR(I))
      DD 25C I=1,IF
      DD 260 I=1,IR
      NRX=NUR(I)
      DSC(NRX)=GUS
      UR4(NRX)=UA*AMD/AM(NRX)
      QSD(NRX)=GUS*AM(NRX)/ASUM
      GOTO 350
260   INDS(NR)=2
      DUS=(WL/RLX-1.)*DDS
270   IF(DDC-DUS) 290,290,350
280   DSL(NR)=DDS-0.031
      GOTO 350
290   INDS(NR)=3
      DUS=DSU(NR)
300   D1=DUS+DLT
310   D2=DDS+DLT
      DELV=(D2-D1)*(B+(D1+D2)*SLR)*RLX
      QSD(NR)=GSU(NR)+DELV
      C
      C
      C
      CALCULATE DISTANCE MOVED BY MASS IN EACH CELL OF REACH
320   GOTO 350
      FL(NR)=WL/RLX
      RLX1=RLX-WL
      DD X=0.
330   NRX=NRX+1
      X=X+CDX
      DD X=0.5*DX(NRX)
      GOTO 999
      X=X+DDX
340   IF(X-RLX1) 330,330,340
      X=X-DDX-RLX1
      ND I=NRX-NDX
      XL=WL
350   J=0

```

07 MAY 1978

```

DZ1=DEPTH(1)
D1=0.
356 NLZ=1,NLAYZ
DZ=DEPTH(NLZ)
DZR=(DZ-D1)/DZ1
D1=DZ
ALAY(NLZ)=0.
355 NLY=1,NLAYY
J=J+1
ALAY(NLZ)=ALAY(NLZ)+ARE(J)
ARAT(NLZ)=ALAY(1)*DZR/ALAY(NLZ)
DUS=DSU(NR)+DLT
DUS=DSU(NR)+DLT
AUS=DUS*(B+DUS*SLR)
ADS=CDS*(B+DUS*SLR)
GUS=GSU(NR)
GDS=GSD(NR)
DELO=QDS-GUS
DELA=ADS-AUS
DELOS=QDS-DUS
360 ND=NC1*NDV
DX2=0.5*CX(NDX+ND)
X=X+DX2
AAV=AUS+CELA*X/XL
UMS(ND)=-((GUS+DELO*X/XL)/AAV
DRX=CUS+DELOS*X/XL
DSA(NC)=CRX
DS(NR,ND)=DRX
X=X+CX2
360 D0 420 ND=1,NDV
NRX=NDX+NC
DDX=DX(NRX)
USM=LMS(ND)
DA=DSA(ND)
UI=USM/(CA*DA)
UFM=USM/(1.-O/DA)
D3=0.
D1=0.
DC1=0.
C0 420 NLZ=1,NLAYZ
DZ=DEPTH(NLZ)
DZ=DZ-D1
IF (D1-DA) 370,400,400
IF (D2-DA) 380,380,390
DC2=DZ-D2*DZ
XMS=U1*(CC2-DC1)*ARAT(NLZ)/DZ
GOTO 410
390 D3=DZ-D2-DA

```

07 MAY 1978

```

DC2=DA*DA*DA
XMS=(U1*(DC2-DC1)+UFM*DJ)*ARAT(NLZ)/DZ
GOTO 410
DJ=J+1
XMS=UFM*ARAT(NLZ)
XS(ND,NLZ)=XMS
VV(NRX-1,NLZ)=VV(NRX-1,NLZ)-XMS/DX(NRX-1)
VV(NRX,NLZ)=VV(NRX,NLZ)+XMS/DX(NRX)
DJ=DC2
DC1=DC2

```

C
C
C

COMPUTE UPWARD INDUCED FLOW

```

NRC=(NDX+1)*JK
DO 510 ND=1,NDVI
NRX=NCX+ND
J=0
VOL=0.
CO 500 NLZ=2,NLAYZ
VOL=VOL+VV(NRX,NLZ-1)*ALAY(NLZ-1)
IF(VOL) 460,495,480
CO 470 NLY=1,NLAY
J=J+1
JZ=J+NLAY
NRC=NRC+1
NRCZ=NRC+NLAY
CMASS=C(NRCZ)*VOL*APA(JZ)
CCC(NRCZ)=CCC(NRCZ)+CMASS/ALAY(NLZ)
CCC(NRC)=CCC(NRC)-CMASS/ALAY(NLZ-1)
GOTO 500
CO 490 NLY=1,NLAY
J=J+1
JZ=J+NLAY
NRC=NRC+1
NRCZ=NRC+NLAY
CMASS=C(NRC)*VOL*APA(J)
CCC(NRC)=CCC(NRC)-CMASS/ALAY(NLZ-1)
CCC(NRCZ)=CCC(NRCZ)+CMASS/ALAY(NLZ)
GOTO 500
495 NRC=NRC+NLAY
500 CONTINUE
510 NRC=NRC+NLAY
999 RETURN
END

```


07 MAY 1978

```

HEAD(1)=0.
10 DO 10 I=2,6
   HEAD(I)=(I-1)*DEL C
   DELV=0.5*VMAX
   HEAD(7)=-VMAX
   HEAD(8)=-DEL V
   HEAD(9)=0.
   HEAD(10)=DEL V
   HEAD(11)=VMAX
   WRITE(6,6003) HEAD
   CMX=0.32*CMAX
   VMX=0.05*VMAX
   DXM=0.5*DXMIN
   IXSC=DXSC/DXM+0.5
   WRITE(6,6004)
   NDV=NDIV(NR)
   IX1=1
   IXC=0
   ISC=0
   X=0.
   DO 90 ND=1,NDV
     NRX=NRX+1
     DX2=0.5*DX(NRX)
     X=X+DX2
     IX2=X/DXM-0.5
     IF(IX2.LT.IX1) GOTO 25
     DO 20 I=IX1,IX2
       ISC=ISC+1
     IF(ISC-IXSC) 12,14,14
     WRITE(6,6005)
     GOTO 20
   14   ISC=0
       IXC=IXC+1
       IX=IXC*DXSC
       WRITE(6,6011) IX
     20 CONTINUE
     25   IX1=IX2+2
       CCH(1)=CCH2
       VCH(21)=CH2
     30   DO 30 I=2,51
       CCH(I)=CH1
     40   DO 40 I=1,20
       VCH(I)=CH1
     50   DO 50 I=22,41
       VCH(I)=CH1
       CS=0.
       VS=0.
     DC 70 NLZ=1,NLAYZ

```

07 MAY 1978

```

CCZ=0.
VVZ=0.
LC(NLZ)=NLZ
LV(NLZ)=NLZ
DO 60 NLY=I,NLAY
   NC=NC+1
   CN=C(NC)
   VN=VEL(NC)
   CS=CS+CN
   VS=VS+VN
   CCZ=CCZ+CN
60   VVZ=VVZ+VN
70   IC(NLZ)=CCZ/(NLAY*VMX)+0.5
   IV(NLZ)=VVZ/(NLAY*VMX)+21.5
   IC(NLAYZ)=CS/(JK*CMX)+0.5
   IV(NLAYZ)=VS/(JK*VMX)+21.5
   LC(NLAYZ)=7
   LV(NLAYZ)=7
DO 80 NLZ=1,NLAYZ
   CCH(IC(NLZ)+1)=CHSET(LC(NLZ))
   VCH(IV(NLZ))=CHSET(LV(NLZ))
   ISC=ISC+1
82   IF(ISC-IXSC) 82,84,84
   WRITE(6,6005) X,CCH,VCH
GOTO 90
84   ISC=0
   IXC=IXC+1
   IX=IXC*DXSC
   WRITE(6,6012) X,CCH,IX,VCH
90   X=X+DX2
   IX2=X/DXM+0.5
   CO 100 I=IX1,IX2
   ISC=ISC+1
92   IF(ISC-IXSC) 92,94,94
   WRITE(6,6005)
GOTO 100
94   ISC=0
   IXC=IXC+1
   IX=IXC*DXSC
   WRITE(6,6011) IX
CONTINUE
   DZ=(RCO(NR)+COSINE)/NLAY
DO 110 NLZ=1,NLAY
   D=D+DZ
110  WRITE(6,6008) CHSET(NLZ),NLZ,D
      WRITE(6,6009) CHSET(7)

```

07 MAY 1578

NRX=NRX+2
NC=NC+2*JK
WRITE(6,6000)
RETURN
END

120

APPENDIX D

COMPUTER RESULTS FOR 57 ACRES OCTOBER STUDY CASE

This appendix contains the output produced by CANNET3D, a program designed to simulate mass transport in low energy tidal canal networks, for the October, 1977, study of the 57 Acres system.

565-CANNET3D-GO - -FT06F001

NUMBER OF TEST,NTEST= 1

57 ACRES CANAL SITE, JUPITER, FLORIDA
SIMULATION OF OCTOBER 1977 FIELD STUDY

NUMBER OF TIME INCREMENTS,NDT= 584
TIDAL PERIOD,T= 12.42 HOURS
NUMBER OF TIME STEPS BETWEEN OUTPUTS,NPRINT= 80
NUMBER OF TIME STEPS BETWEEN PLOTS,NPLOT= 292
TIME INCREMENT,DT= 0.0625 HOURS
TIDAL AMPLITUDE,AMP= 1.15 FEET
BACKGROUND CONCENTRATION OF RECEIVING WATERS,CRW= 0.20 P.P.M.
DIMENSIONLESS LONGITUDINAL DIFFUSION COEFFICIENT,KX= 0.100
DIMENSIONLESS LATERAL DIFFUSION COEFFICIENT,KY= 0.100
DIMENSIONLESS VERTICAL DIFFUSION COEFFICIENT,KZ= 0.0005
BACKGROUND DIFFUSION COEFFICIENT,EU= 0.0005 SQ.FT./SEC.
VERTICAL MOMENTUM TRANSFER COEFFICIENT,NZ= 0.00200 SQ.FT./SEC.
NUMBER OF REACHES,NREACH= 5
NUMBER OF JUNCTIONS,NJUNC= 2
NUMBER OF LAKES,NLAKE= 0
NUMBER OF TIDAL ENTRANCES,NTE= 1
NUMBER OF LATERAL LAYERS,NLAY= 1
NUMBER OF VERTICAL LAYERS,NLAYZ= 3

DATA FOR JUNCTION NUMBER 2:
LONGITUDINAL DISTANCE,CXJN= 350.00 FEET
LATERAL DISTANCE,DYJN= 130.00 FEET
MEAN TIDAL DEPTH,COJN= 8.00 FEET

DATA FOR JUNCTION NUMBER 3:
LONGITUDINAL DISTANCE,CXJN= 130.00 FEET
LATERAL DISTANCE,DYJN= 130.00 FEET
MEAN TIDAL DEPTH,COJN= 7.00 FEET

TIDAL ENTRANCE DATA:
TIME DECAY COEFFICIENT FOR TIDAL ENTRANCE 1 = 6.210 HOURS

LATERAL INFLOWS:

DECAY DATA:

BEND DATA:

DATA FOR REACH NUMBER 1:
 NUMBER OF DIVISIONS ALCNG REACH,NDIV= 42
 UPSTREAM JUNCTION,NJU= 1
 DOWNSTREAM JUNCTION,NJD= 2
 LENGTH,RL= 4200.0 FEET
 BREADTH,RB= 65.0 FEET
 MEAN TIDAL DEPTH,RCD= 8.00 FEET
 LEFT BANK INVERSE SIDE SLOPE,RSL= 3.00
 RIGHT BANK INVERSE SIDE SLOPE,RSR= 3.00
 REACH ALIGNMENT ANGLE,ANGLE,RANG= 240.0 DEGREES
 EQUIVALENT SAND ROUGHNESS,RNKS= 15.00 FEET
 CONSTANT DECAY COEFFICIENT FOR REACH,RDECAY= 0.0 /HOUR
 LONGITUDINAL SPATIAL INCREMENTS,DX (DPTI= 0):
 100.00 100.00 100.00 100.00 100.00 100.00 100.00 100.00 100.00 100.00 100.00 100.00 100.00
 100.00 100.00 100.00 100.00 100.00 100.00 100.00 100.00 100.00 100.00 100.00 100.00 100.00
 100.00 100.00 100.00 100.00 100.00 100.00 100.00 100.00 100.00 100.00 100.00 100.00 100.00

DATA FOR REACH NUMBER 2:
 NUMBER OF DIVISIONS ALCNG REACH,NDIV= 13
 UPSTREAM JUNCTION,NJU= 1
 DOWNSTREAM JUNCTION,NJD= 3
 LENGTH,RL= 1300.0 FEET
 BREADTH,RB= 50.0 FEET
 MEAN TIDAL DEPTH,RCD= 6.20 FEET
 LEFT BANK INVERSE SIDE SLOPE,RSL= 3.00
 RIGHT BANK INVERSE SIDE SLOPE,RSR= 3.00
 REACH ALIGNMENT ANGLE,ANGLE,RANG= 340.0 DEGREES
 EQUIVALENT SAND ROUGHNESS,RNKS= 15.00 FEET
 CONSTANT DECAY COEFFICIENT FOR REACH,RDECAY= 0.0 /HOUR
 LONGITUDINAL SPATIAL INCREMENTS,DX (DPTI= 0):
 100.00 100.00 100.00 100.00 100.00 100.00 100.00 100.00 100.00 100.00 100.00 100.00 100.00

DATA FOR REACH NUMBER 3:
 NUMBER OF DIVISIONS ALCNG REACH,NDIV= 7
 UPSTREAM JUNCTION,NJU= 1
 DOWNSTREAM JUNCTION,NJD= 3
 LENGTH,RL= 700.0 FEET
 BREADTH,RB= 50.0 FEET
 MEAN TIDAL DEPTH,RCD= 6.30 FEET
 LEFT BANK INVERSE SIDE SLOPE,RSL= 3.00
 RIGHT BANK INVERSE SIDE SLOPE,RSR= 3.00

CONCENTRATIONS IN P.P.M, AND LONGITUDINAL VELOCITIES IN FT/SEC. 8)

DIGITIZED TIDAL DATA

DIGITIZED WIND SPEED AND ANGLE AVERAGED OVER 6.00 HOURS (INTERPOLATION FACTOR=

0.0 FT/SEC: TIDAL DIFFERENCE= -1.150 FEET

REACH NUMBER 1:

X= 50.0/C

/VEL

0.200

0.0

2.000

0.0

0.0

0.200

0.0

2.500

0.0

0.0

0.200

0.0

3.000

0.0

0.0

0.200

0.0

4.000

0.0

0.0

0.200

0.0

2.100

0.0

0.0

0.200

0.0

2.600

0.0

0.0

0.200

0.0

4.000

0.0

0.0

0.200

0.0

4.000

0.0

0.0

0.200

0.0

0.0

0.200

0.0

5.500

0.0

0.0

0.200

0.0

10.000

0.0

0.0

0.200

0.0

10.000

0.0

0.0

0.200

0.0

10.000

0.0

0.0

0.200

0.0

10.000

0.0

0.0

0.200

0.0

3.000

0.0

0.0

0.200

0.0

1.400

0.0

0.0

0.200

0.0

1.500

0.0

0.0

0.200

0.0

1.700

0.0

0.0

0.200

0.0

1.400

0.0

0.0

0.200

0.0

1.400

0.0

0.0

0.200

0.0

1.400

0.0

0.0

0.200

0.0

1.400

0.0

0.0

0.200

0.0

1.400

0.0

0.0

0.200

0.0

1.400

0.0

0.0

0.200

0.0

1.400

0.0

0.0

0.200

0.0

1.400

0.0

0.0

0.200

0.0

1.400

0.0

0.0

0.200

0.0

1.400

0.0

0.0

0.200

0.0

1.400

0.0

0.0

0.200

0.0

1.400

0.0

0.0

0.200

0.0

1.400

0.0

0.0

0.200

0.0

1.400

0.0

0.0

0.200

0.0

1.400

0.0

0.0

0.200

0.0

1.400

0.0

0.0

0.200

0.0

1.400

0.0

0.0

0.200

0.0

1.400

0.0

0.0

0.200

0.0

1.400

0.0

0.0

0.200

0.0

1.400

0.0

0.0

0.200

0.0

1.400

0.0

0.0

0.200

0.0

1.400

0.0

0.0

0.200

0.0

1.400

0.0

0.0

0.200

0.0

1.400

0.0

0.0

0.200

0.0

1.400

0.0

0.0

0.200

0.0

1.400

0.0

0.0

0.200

0.0

1.400

0.0

0.0

0.200

0.0

1.400

0.0

0.0

0.200

0.0

1.400

0.0

0.0

0.200

0.0

1.400

0.0

0.0

0.200

0.0

1.400

0.0

0.0

0.200

0.0

1.400

0.0

0.0

0.200

0.0

1.400

0.0

0.0

0.200

0.0

1.400

0.0

0.0

0.200

0.0

1.400

0.0

0.0

0.200

0.0

1.400

0.0

0.0

0.200

0.0

1.400

0.0

0.0

0.200

0.0

1.400

0.0

0.0

0.200

0.0

1.400

0.0

X= 2050.0/C/ /VEL	0.200	0.200	0.200	1.400
X= 2150.0/C/ /VEL	0.0	0.0	0.0	1.400
X= 2250.0/C/ /VEL	0.0	0.0	0.0	1.400
X= 2350.0/C/ /VEL	0.0	0.0	0.0	1.400
X= 2450.0/C/ /VEL	0.0	0.0	0.0	1.400
X= 2550.0/C/ /VEL	0.0	0.0	0.0	1.400
X= 2650.0/C/ /VEL	0.0	0.0	0.0	1.400
X= 2750.0/C/ /VEL	0.0	0.0	0.0	1.400
X= 2850.0/C/ /VEL	0.200	0.200	0.200	1.400
X= 2950.0/C/ /VEL	0.0	0.0	0.0	1.400
X= 3050.0/C/ /VEL	0.0	0.0	0.0	1.400
X= 3150.0/C/ /VEL	0.0	0.0	0.0	1.400
X= 3250.0/C/ /VEL	0.0	0.0	0.0	1.400
X= 3350.0/C/ /VEL	0.0	0.0	0.0	1.400
X= 3450.0/C/ /VEL	0.0	0.0	0.0	1.400
X= 3550.0/C/ /VEL	0.0	0.0	0.0	1.400
X= 3650.0/C/ /VEL	0.0	0.0	0.0	1.400
X= 3750.0/C/ /VEL	0.0	0.0	0.0	1.400
X= 3850.0/C/ /VEL	0.0	0.0	0.0	1.400
X= 3950.0/C/ /VEL	0.0	0.0	0.0	1.400
X= 4050.0/C/ /VEL	0.0	0.0	0.0	1.400
X= 4150.0/C/ /VEL	0.0	0.0	0.0	0.800
REACH NUMBER	2:			
X= 50.0/C/ /VEL	0.200	0.200	0.200	0.0
X= 150.0/C/ /VEL	0.0	0.0	0.0	0.200

X=	/VEL/	0.0	0.0	0.0	0.0
X=	250.0/C/	0.200	0.200	0.200	0.200
X=	/VEL/	0.0	0.0	0.0	0.0
X=	350.0/C/	0.200	0.200	0.200	0.200
X=	/VEL/	0.0	0.0	0.0	0.0
X=	450.0/C/	0.200	0.200	0.200	0.200
X=	/VEL/	0.0	0.0	0.0	0.0
X=	550.0/C/	0.200	0.200	0.200	0.200
X=	/VEL/	0.0	0.0	0.0	0.0
X=	650.0/C/	0.200	0.200	0.200	0.200
X=	/VEL/	0.0	0.0	0.0	0.0
X=	750.0/C/	0.200	0.200	0.200	0.200
X=	/VEL/	0.0	0.0	0.0	0.0
X=	850.0/C/	0.200	0.200	0.200	0.200
X=	/VEL/	0.0	0.0	0.0	0.0
X=	950.0/C/	0.200	0.200	0.200	0.200
X=	/VEL/	0.0	0.0	0.0	0.0
X=	1050.0/C/	0.200	0.200	0.200	0.200
X=	/VEL/	0.0	0.0	0.0	0.0
X=	1150.0/C/	0.200	0.200	0.200	0.200
X=	/VEL/	0.0	0.0	0.0	0.0
X=	1250.0/C/	0.200	0.200	0.200	0.200
X=	/VEL/	0.0	0.0	0.0	0.0
REACH NUMBER		3.			
X=	50.0/C/	0.200	0.200	0.200	0.200
X=	/VEL/	0.0	0.0	0.0	0.0
X=	150.0/C/	0.200	0.200	0.200	0.200
X=	/VEL/	0.0	0.0	0.0	0.0
X=	250.0/C/	0.200	0.200	0.200	0.200
X=	/VEL/	0.0	0.0	0.0	0.0
X=	350.0/C/	0.200	0.200	0.200	0.200
X=	/VEL/	0.0	0.0	0.0	0.0
X=	450.0/C/	0.200	0.200	0.200	0.200
X=	/VEL/	0.0	0.0	0.0	0.0
X=	550.0/C/	0.200	0.200	0.200	0.200
X=	/VEL/	0.0	0.0	0.0	0.0
X=	650.0/C/	0.200	0.200	0.200	0.200
X=	/VEL/	0.0	0.0	0.0	0.0
REACH NUMBER		4.			
X=	50.0/C/	0.200	0.200	0.200	0.200
X=	/VEL/	0.0	0.0	0.0	0.0
X=	150.0/C/	0.200	0.200	0.200	0.200
X=	/VEL/	0.0	0.0	0.0	0.0
X=	250.0/C/	0.200	0.200	0.200	0.200
X=	/VEL/	0.0	0.0	0.0	0.0
X=	350.0/C/	0.200	0.200	0.200	0.200
X=	/VEL/	0.0	0.0	0.0	0.0
X=	450.0/C/	0.200	0.200	0.200	0.200

X=	550.0/C/	/VEL/	0.0	0.0	0.0
X=	550.0/C/	/VEL/	0.200	0.200	0.200
X=	650.0/C/	/VEL/	0.0	0.0	0.0
X=	650.0/C/	/VEL/	0.200	0.200	0.200
X=	750.0/C/	/VEL/	0.0	0.0	0.0
X=	750.0/C/	/VEL/	0.200	0.200	0.200
X=	850.0/C/	/VEL/	0.0	0.0	0.0
X=	850.0/C/	/VEL/	0.200	0.200	0.200
REACH NUMBER 5:					
X=	83.3/C/	/VEL/	0.0	0.0	0.0
X=	83.3/C/	/VEL/	0.200	0.200	0.200
X=	250.0/C/	/VEL/	0.0	0.0	0.0
X=	250.0/C/	/VEL/	0.200	0.200	0.200
X=	416.7/C/	/VEL/	0.0	0.0	0.0
X=	416.7/C/	/VEL/	0.200	0.200	0.200
X=	583.3/C/	/VEL/	0.0	0.0	0.0
X=	583.3/C/	/VEL/	0.200	0.200	0.200
X=	750.0/C/	/VEL/	0.0	0.0	0.0
X=	750.0/C/	/VEL/	0.200	0.200	0.200
X=	916.7/C/	/VEL/	0.0	0.0	0.0
X=	916.7/C/	/VEL/	0.200	0.200	0.200
X=	1083.3/C/	/VEL/	0.0	0.0	0.0
X=	1083.3/C/	/VEL/	0.200	0.200	0.200
X=	1250.0/C/	/VEL/	0.0	0.0	0.0
X=	1250.0/C/	/VEL/	0.200	0.200	0.200
X=	1416.7/C/	/VEL/	0.0	0.0	0.0
X=	1416.7/C/	/VEL/	0.200	0.200	0.200
X=	1583.3/C/	/VEL/	0.0	0.0	0.0
X=	1583.3/C/	/VEL/	0.200	0.200	0.200
X=	1750.0/C/	/VEL/	0.0	0.0	0.0
X=	1750.0/C/	/VEL/	0.200	0.200	0.200
X=	1916.7/C/	/VEL/	0.0	0.0	0.0
X=	1916.7/C/	/VEL/	0.200	0.200	0.200
X=	2083.3/C/	/VEL/	0.0	0.0	0.0
X=	2083.3/C/	/VEL/	0.200	0.200	0.200
X=	2250.0/C/	/VEL/	0.0	0.0	0.0
X=	2250.0/C/	/VEL/	0.200	0.200	0.200
X=	2416.7/C/	/VEL/	0.0	0.0	0.0
X=	2416.7/C/	/VEL/	0.200	0.200	0.200
JUNCTION NUMBER 2:					
	0.200				
	0.200				
JUNCTION NUMBER 3:					
	0.200				
	0.200				

X= 2250.0/C	/VEL	0.006	0.032	0.039
X= 2350.0/C	/VEL	0.462	0.578	0.759
X= 2450.0/C	/VEL	0.006	0.034	0.041
X= 2550.0/C	/VEL	0.463	0.578	0.758
X= 2650.0/C	/VEL	0.007	0.037	0.043
X= 2750.0/C	/VEL	0.463	0.577	0.758
X= 2850.0/C	/VEL	0.007	0.038	0.044
X= 2950.0/C	/VEL	0.463	0.577	0.758
X= 3050.0/C	/VEL	0.007	0.038	0.046
X= 3150.0/C	/VEL	0.464	0.578	0.757
X= 3250.0/C	/VEL	0.007	0.041	0.048
X= 3350.0/C	/VEL	0.464	0.578	0.758
X= 3450.0/C	/VEL	0.008	0.043	0.050
X= 3550.0/C	/VEL	0.456	0.570	0.761
X= 3650.0/C	/VEL	0.008	0.044	0.052
X= 3750.0/C	/VEL	0.432	0.536	0.744
X= 3850.0/C	/VEL	0.008	0.046	0.053
X= 3950.0/C	/VEL	0.387	0.682	0.682
X= 4050.0/C	/VEL	0.309	0.464	0.557
X= 4150.0/C	/VEL	0.331	0.047	0.057
X= 4250.0/C	/VEL	0.009	0.363	0.374
X= 4350.0/C	/VEL	0.267	0.048	0.059
X= 4450.0/C	/VEL	0.009	0.050	0.061
X= 4550.0/C	/VEL	0.259	0.242	0.213
X= 4650.0/C	/VEL	0.009	0.051	0.063
X= 4750.0/C	/VEL	0.240	0.229	0.210
X= 4850.0/C	/VEL	0.010	0.053	0.064
X= 4950.0/C	/VEL	0.225	0.219	0.207
X= 5050.0/C	/VEL	0.010	0.054	0.066
X= 5150.0/C	/VEL	0.213	0.211	0.204
X= 5250.0/C	/VEL	0.010	0.056	0.068
X= 5350.0/C	/VEL	0.206	0.206	0.202
X= 5450.0/C	/VEL	0.010	0.057	0.070
X= 5550.0/C	/VEL	0.202	0.202	0.201
X= 5650.0/C	/VEL	0.011	0.059	0.072
X= 5750.0/C	/VEL	0.200	0.201	0.200
X= 5850.0/C	/VEL	0.011	0.060	0.073
X= 5950.0/C	/VEL	0.200	0.200	0.200
REACH NUMBER	/VEL	0.011	0.062	0.075
X= 50.0/C	/VEL	0.200	0.200	0.201
X= 150.0/C	/VEL	0.200	0.200	0.201
X= 250.0/C	/VEL	0.000	0.003	0.003
X= 350.0/C	/VEL	0.200	0.200	0.200
X= 450.0/C	/VEL	0.000	0.005	0.006

2:

X= 350.0/C/	0.200	0.200	0.200
/VEL/	0.001	0.007	0.200
X= 450.0/C/	0.200	0.200	0.008
/VEL/	0.001	0.009	0.200
X= 550.0/C/	0.200	0.200	0.011
/VEL/	0.001	0.011	0.200
X= 650.0/C/	0.200	0.200	0.013
/VEL/	0.001	0.013	0.200
X= 750.0/C/	0.200	0.200	0.015
/VEL/	0.001	0.014	0.200
X= 850.0/C/	0.200	0.200	0.018
/VEL/	0.001	0.016	0.200
X= 950.0/C/	0.200	0.200	0.020
/VEL/	0.001	0.018	0.200
X= 1050.0/C/	0.200	0.200	0.023
/VEL/	0.001	0.020	0.200
X= 1150.0/C/	0.200	0.200	0.025
/VEL/	0.001	0.022	0.200
X= 1250.0/C/	0.200	0.200	0.028
/VEL/	0.001	0.024	0.200
REACH NUMBER	3:	0.024	0.030
X= 50.0/C/	0.200	0.201	0.200
/VEL/	-0.000	0.001	0.001
X= 150.0/C/	0.200	0.200	0.200
/VEL/	-0.000	0.003	0.004
X= 250.0/C/	0.200	0.200	0.200
/VEL/	0.000	0.005	0.006
X= 350.0/C/	0.200	0.200	0.200
/VEL/	0.000	0.006	0.009
X= 450.0/C/	0.200	0.006	0.011
/VEL/	0.000	0.008	0.011
X= 550.0/C/	0.200	0.200	0.200
/VEL/	0.000	0.010	0.013
X= 650.0/C/	0.200	0.200	0.200
/VEL/	0.001	0.012	0.016
REACH NUMBER	4:	0.012	0.016
X= 50.0/C/	0.200	0.200	0.200
/VEL/	0.005	0.029	0.036
X= 150.0/C/	0.200	0.200	0.200
/VEL/	0.005	0.030	0.037
X= 250.0/C/	0.200	0.200	0.200
/VEL/	0.005	0.032	0.039
X= 350.0/C/	0.200	0.200	0.200
/VEL/	0.005	0.033	0.041
X= 450.0/C/	0.200	0.199	0.199
/VEL/	0.006	0.035	0.043
X= 550.0/C/	0.200	0.200	0.200
/VEL/	0.006	0.037	0.045

WIND SPEED= 5.0 FT/SEC: WIND DIRECTION= 332. DEGREES

WIND REACH	WIND SPEED	WIND DIRECTION	WIND DIRECTION
NUMBER	FT/SEC	DEGREES	DEGREES
X= 50.0/C/	0.789	0.837	0.878
/VEL/	0.000	0.001	0.001
X= 150.0/C/	0.501	0.525	0.553
/VEL/	0.000	0.002	0.003
X= 250.0/C/	1.357	1.099	1.121
/VEL/	0.001	0.004	0.004
X= 350.0/C/	1.166	1.330	1.330
/VEL/	0.001	0.005	0.006
X= 450.0/C/	1.025	1.170	1.279
/VEL/	0.001	0.006	0.007
X= 550.0/C/	1.034	1.047	1.091
/VEL/	0.001	0.008	0.009
X= 650.0/C/	1.219	1.129	1.101
/VEL/	0.002	0.009	0.011
X= 750.0/C/	1.564	1.380	1.315
/VEL/	0.002	0.011	0.012
X= 850.0/C/	2.069	1.717	1.583
/VEL/	0.002	0.012	0.014
X= 950.0/C/	2.341	2.137	1.934
/VEL/	0.002	0.014	0.016
X= 1050.0/C/	2.528	2.637	2.459
/VEL/	0.003	0.015	0.017
X= 1150.0/C/	3.071	3.080	3.049
/VEL/	0.003	0.016	0.019
X= 1250.0/C/	2.872	3.260	3.450
/VEL/	0.003	0.018	0.021
X= 1350.0/C/	2.425	3.162	3.551
/VEL/	0.003	0.019	0.022
X= 1450.0/C/	2.010	2.926	3.452
/VEL/	0.004	0.021	0.024
X= 1550.0/C/	1.602	2.604	3.228
/VEL/	0.004	0.022	0.026
X= 1650.0/C/	1.215	2.154	2.810
/VEL/	0.004	0.024	0.027
X= 1750.0/C/	0.890	1.597	2.164
/VEL/	0.005	0.025	0.029
X= 1850.0/C/	0.658	1.081	1.456
/VEL/	0.005	0.026	0.031
X= 1950.0/C/	0.609	0.750	0.923
/VEL/	0.005	0.028	0.032
X= 2050.0/C/	0.588	0.624	0.670
/VEL/	0.005	0.029	0.034
X= 2150.0/C/	0.587	0.615	0.629
/VEL/	0.006	0.031	0.036
X= 2250.0/C/	0.524	0.623	0.652
/VEL/	0.006	0.032	0.037

X = 2350.07C /	0.580	0.616	0.651
/VEL /	0.006	0.034	0.039
X = 2450.07C /	0.578	0.606	0.634
/VEL /	0.006	0.035	0.041
X = 2550.07C /	0.577	0.601	0.623
/VEL /	0.007	0.036	0.042
X = 2650.07C /	0.577	0.601	0.621
/VEL /	0.007	0.038	0.044
X = 2750.07C /	0.578	0.601	0.622
/VEL /	0.007	0.039	0.046
X = 2850.07C /	0.579	0.601	0.623
/VEL /	0.007	0.041	0.047
X = 2950.07C /	0.578	0.601	0.622
/VEL /	0.008	0.042	0.045
X = 3050.07C /	0.578	0.601	0.622
/VEL /	0.008	0.044	0.051
X = 3150.07C /	0.578	0.601	0.622
/VEL /	0.008	0.045	0.052
X = 3250.07C /	0.575	0.601	0.622
/VEL /	0.008	0.046	0.054
X = 3350.07C /	0.568	0.599	0.621
/VEL /	0.009	0.048	0.056
X = 3450.07C /	0.565	0.595	0.620
/VEL /	0.009	0.049	0.057
X = 3550.07C /	0.536	0.589	0.619
/VEL /	0.009	0.589	0.619
X = 3650.07C /	0.516	0.581	0.615
/VEL /	0.009	0.582	0.611
X = 3750.07C /	0.496	0.571	0.611
/VEL /	0.010	0.053	0.062
X = 3850.07C /	0.475	0.559	0.606
/VEL /	0.010	0.055	0.064
X = 3950.07C /	0.455	0.547	0.599
/VEL /	0.010	0.056	0.065
X = 4050.07C /	0.434	0.534	0.592
/VEL /	0.010	0.058	0.067
X = 4150.07C /	0.413	0.520	0.584
/VEL /	0.011	0.059	0.069
REACH NUMBER	2 :		
X = 50.07C /	0.209	0.210	0.209
/VEL /	0.009	0.011	-0.017
X = 150.07C /	0.204	0.205	0.202
/VEL /	0.009	0.013	-0.014
X = 250.07C /	0.200	0.200	0.199
/VEL /	0.009	0.015	-0.012
X = 350.07C /	0.200	0.200	0.201
/VEL /	0.009	0.018	-0.009
X = 450.07C /	0.200	0.200	0.200

X =	/VEL/	0.009	0.020	-0.007
X =	550.0/C/	0.200	0.200	0.200
X =	/VEL/	0.009	0.022	0.004
X =	650.0/C/	0.200	0.200	0.200
X =	/VEL/	0.010	0.024	0.001
X =	750.0/C/	0.200	0.200	0.200
X =	/VEL/	0.010	0.026	0.001
X =	850.0/C/	0.200	0.200	0.200
X =	/VEL/	0.010	0.029	0.004
X =	950.0/C/	0.200	0.200	0.200
X =	/VEL/	0.010	0.031	0.006
X =	1050.0/C/	0.200	0.200	0.200
X =	/VEL/	0.010	0.033	0.009
X =	1150.0/C/	0.200	0.200	0.200
X =	/VEL/	0.010	0.035	0.012
X =	1250.0/C/	0.200	0.200	0.200
X =	/VEL/	0.010	0.038	0.014
REACH NUMBER 3:				
X =	50.0/C/	0.206	0.206	0.207
X =	/VEL/	-0.004	-0.004	0.010
X =	150.0/C/	0.201	0.203	0.204
X =	/VEL/	-0.004	-0.002	0.013
X =	250.0/C/	0.200	0.200	0.199
X =	/VEL/	-0.004	0.000	0.000
X =	350.0/C/	0.200	0.200	0.200
X =	/VEL/	-0.004	0.003	0.015
X =	450.0/C/	0.200	0.200	0.200
X =	/VEL/	-0.004	0.005	0.020
X =	550.0/C/	0.200	0.200	0.200
X =	/VEL/	-0.004	0.007	0.023
X =	650.0/C/	0.200	0.200	0.200
X =	/VEL/	-0.003	0.009	0.025
REACH NUMBER 4:				
X =	50.0/C/	0.200	0.200	0.200
X =	/VEL/	-0.000	0.023	0.041
X =	150.0/C/	0.200	0.200	0.200
X =	/VEL/	-0.000	0.024	0.043
X =	250.0/C/	0.200	0.200	0.200
X =	/VEL/	0.003	0.026	0.045
X =	350.0/C/	0.200	0.200	0.200
X =	/VEL/	0.000	0.027	0.047
X =	450.0/C/	0.200	0.200	0.200
X =	/VEL/	0.001	0.029	0.048
X =	550.0/C/	0.200	0.200	0.200
X =	/VEL/	0.001	0.030	0.050
X =	650.0/C/	0.200	0.200	0.200
X =	/VEL/	0.001	0.032	0.052
X =	750.0/C/	0.200	0.200	0.200

X=	850.0/C	/VEL/	0.001	0.033	0.054
X=	200	/VEL/	0.200	0.200	0.200
REACH	NUMBER	S:	0.002	0.035	0.056
X=	83.3/C	/VEL/	0.260	0.355	0.414
X=	250.0/C	/VEL/	0.014	0.066	0.071
X=	416.7/C	/VEL/	0.014	0.333	0.391
X=	583.3/C	/VEL/	0.244	0.068	0.073
X=	750.0/C	/VEL/	0.015	0.311	0.365
X=	916.7/C	/VEL/	0.229	0.071	0.076
X=	1083.3/C	/VEL/	0.015	0.334	0.334
X=	1250.0/C	/VEL/	0.217	0.073	0.079
X=	1416.7/C	/VEL/	0.016	0.259	0.298
X=	1583.3/C	/VEL/	0.209	0.075	0.082
X=	1750.0/C	/VEL/	0.016	0.235	0.263
X=	1916.7/C	/VEL/	0.204	0.078	0.084
X=	2083.3/C	/VEL/	0.016	0.217	0.234
X=	2250.0/C	/VEL/	0.202	0.080	0.087
X=	2416.7/C	/VEL/	0.201	0.207	0.215
X=	2583.3/C	/VEL/	0.017	0.082	0.090
X=	2750.0/C	/VEL/	0.200	0.203	0.206
X=	2916.7/C	/VEL/	0.018	0.085	0.093
X=	3083.3/C	/VEL/	0.200	0.202	0.203
X=	3250.0/C	/VEL/	0.018	0.087	0.095
X=	3416.7/C	/VEL/	0.200	0.201	0.202
X=	3583.3/C	/VEL/	0.018	0.090	0.098
X=	3750.0/C	/VEL/	0.200	0.201	0.201
X=	3916.7/C	/VEL/	0.019	0.092	0.101
X=	4083.3/C	/VEL/	0.200	0.200	0.200
X=	4250.0/C	/VEL/	0.019	0.094	0.103
X=	4416.7/C	/VEL/	0.200	0.200	0.200
X=	4583.3/C	/VEL/	0.019	0.097	0.106
X=	4750.0/C	/VEL/	0.200	0.200	0.200
X=	4916.7/C	/VEL/	0.020	0.099	0.109
X=	5083.3/C	/VEL/	0.200	0.200	0.200
X=	5250.0/C	/VEL/	0.020	0.100	0.109

JUNCTION NUMBER 2:
0.228
0.370

JUNCTION NUMBER 3:
0.426
0.200
0.200
0.200

TIME 15:00 HOURS: TICAL DIFFERENCE= 0.100 FEET
WIND SPEED= 11.4 FT/SEC: WIND DIRECTION= 6. DEGREES
REACH NUMBER 1:
X= 50.0/C/ 1.015 0.976 0.914

X=	150.0/C	/VEL	-0.036	-0.026	0.039
X=	250.0/C	/VEL	1.152	1.161	0.905
X=	350.0/C	/VEL	-0.036	-0.028	0.036
X=	450.0/C	/VEL	1.102	1.039	0.903
X=	550.0/C	/VEL	-0.037	-0.031	0.033
X=	650.0/C	/VEL	1.121	1.170	1.190
X=	750.0/C	/VEL	-0.037	-0.033	0.030
X=	850.0/C	/VEL	1.188	1.290	1.169
X=	950.0/C	/VEL	-0.038	-0.036	0.027
X=	1050.0/C	/VEL	1.861	2.064	1.256
X=	1150.0/C	/VEL	-0.038	-0.038	0.024
X=	1250.0/C	/VEL	2.417	2.664	1.742
X=	1350.0/C	/VEL	-0.038	-0.040	0.021
X=	1450.0/C	/VEL	2.857	3.033	2.412
X=	1550.0/C	/VEL	-0.039	-0.043	0.018
X=	1650.0/C	/VEL	3.034	2.971	3.070
X=	1750.0/C	/VEL	-0.039	-0.045	0.015
X=	1850.0/C	/VEL	2.826	2.582	3.149
X=	1950.0/C	/VEL	-0.040	-0.048	0.012
X=	2050.0/C	/VEL	2.478	1.561	2.799
X=	2150.0/C	/VEL	-0.040	-0.050	0.009
X=	2250.0/C	/VEL	1.972	1.380	2.148
X=	2350.0/C	/VEL	-0.041	-0.052	0.006
X=	2450.0/C	/VEL	1.510	1.308	1.266
X=	150.0/C	/VEL	-0.041	-0.055	0.003
X=	140.0/C	/VEL	1.142	0.804	0.822
X=	130.0/C	/VEL	-0.042	-0.057	0.000
X=	120.0/C	/VEL	0.876	0.685	0.691
X=	110.0/C	/VEL	-0.042	-0.060	-0.003
X=	100.0/C	/VEL	0.708	0.631	0.643
X=	90.0/C	/VEL	-0.042	-0.062	-0.005
X=	80.0/C	/VEL	0.628	0.609	0.614
X=	70.0/C	/VEL	-0.043	-0.065	-0.008
X=	60.0/C	/VEL	0.605	0.603	0.606
X=	50.0/C	/VEL	-0.043	-0.067	-0.011
X=	40.0/C	/VEL	0.602	0.602	0.605
X=	30.0/C	/VEL	-0.044	-0.070	-0.014
X=	20.0/C	/VEL	0.601	0.601	0.604
X=	10.0/C	/VEL	-0.044	-0.072	-0.017
X=	2050.0/C	/VEL	0.598	0.598	0.603
X=	2150.0/C	/VEL	-0.045	-0.074	-0.020
X=	2250.0/C	/VEL	0.596	0.593	0.601
X=	2350.0/C	/VEL	-0.045	-0.077	-0.023
X=	2450.0/C	/VEL	0.594	0.586	0.594
X=	2350.0/C	/VEL	-0.046	-0.079	-0.026
X=	2250.0/C	/VEL	0.590	0.575	0.585
X=	2150.0/C	/VEL	-0.046	-0.082	-0.029
X=	2450.0/C	/VEL	0.584	0.544	0.542

X=	/VEL/	-	0.046	-	0.084	-	0.032
X=	2550.C/C	0.571	0.505	0.526	0.505	0.526	0.505
X=	2650.0/C	-0.047	-0.087	-0.047	-0.087	-0.047	-0.087
X=	2750.0/C	0.555	0.478	0.555	0.478	0.555	0.478
X=	2850.0/C	-0.047	-0.089	-0.047	-0.089	-0.047	-0.089
X=	2950.0/C	0.537	0.456	0.537	0.456	0.537	0.456
X=	3050.0/C	-0.048	-0.091	-0.048	-0.091	-0.048	-0.091
X=	3150.0/C	0.518	0.433	0.518	0.433	0.518	0.433
X=	3250.0/C	-0.049	-0.094	-0.049	-0.094	-0.049	-0.094
X=	3350.0/C	0.497	0.407	0.497	0.407	0.497	0.407
X=	3450.0/C	-0.049	-0.096	-0.049	-0.096	-0.049	-0.096
X=	3550.0/C	0.473	0.381	0.473	0.381	0.473	0.381
X=	3650.0/C	-0.049	-0.099	-0.049	-0.099	-0.049	-0.099
X=	3750.0/C	0.449	0.354	0.449	0.354	0.449	0.354
X=	3850.0/C	-0.050	-0.101	-0.050	-0.101	-0.050	-0.101
X=	3950.0/C	0.425	0.329	0.425	0.329	0.425	0.329
X=	4050.0/C	-0.050	-0.104	-0.050	-0.104	-0.050	-0.104
X=	4150.0/C	0.400	0.306	0.400	0.306	0.400	0.306
X=	REACH NUMBER	-	-	-	-	-	-
X=	50.0/C	0.050	0.106	0.050	0.106	0.050	0.106
X=	150.0/C	-0.051	-0.108	-0.051	-0.108	-0.051	-0.108
X=	250.0/C	0.355	0.266	0.355	0.266	0.355	0.266
X=	350.0/C	-0.051	-0.111	-0.051	-0.111	-0.051	-0.111
X=	450.0/C	0.323	0.252	0.323	0.252	0.323	0.252
X=	550.0/C	-0.052	-0.113	-0.052	-0.113	-0.052	-0.113
X=	650.0/C	0.280	0.242	0.280	0.242	0.280	0.242
X=	750.0/C	-0.052	-0.116	-0.052	-0.116	-0.052	-0.116
X=	850.0/C	0.258	0.234	0.258	0.234	0.258	0.234
X=	950.0/C	-0.053	-0.118	-0.053	-0.118	-0.053	-0.118
X=	1050.0/C	0.255	0.227	0.255	0.227	0.255	0.227
X=	1150.0/C	-0.053	-0.121	-0.053	-0.121	-0.053	-0.121
X=	1250.0/C	0.252	0.222	0.252	0.222	0.252	0.222
X=	1350.0/C	-0.054	-0.123	-0.054	-0.123	-0.054	-0.123
X=	1450.0/C	0.246	0.217	0.246	0.217	0.246	0.217
X=	1550.0/C	-0.054	-0.126	-0.054	-0.126	-0.054	-0.126
X=	1650.0/C	0.201	0.201	0.201	0.201	0.201	0.201
X=	1750.0/C	0.112	0.368	0.112	0.368	0.112	0.368
X=	1850.0/C	0.201	0.201	0.201	0.201	0.201	0.201
X=	1950.0/C	0.111	0.065	0.111	0.065	0.111	0.065
X=	2050.0/C	0.201	0.201	0.201	0.201	0.201	0.201
X=	2150.0/C	0.111	0.062	0.111	0.062	0.111	0.062
X=	2250.0/C	0.201	0.201	0.201	0.201	0.201	0.201
X=	2350.0/C	0.111	0.059	0.111	0.059	0.111	0.059
X=	2450.0/C	0.202	0.202	0.202	0.202	0.202	0.202
X=	2550.0/C	0.111	0.056	0.111	0.056	0.111	0.056
X=	2650.0/C	0.202	0.202	0.202	0.202	0.202	0.202
X=	2750.0/C	0.111	0.053	0.111	0.053	0.111	0.053

X=	650.0/C/ /VEL/	0.203	0.202	0.204
X=	750.0/C/ /VEL/	0.110	0.050	-0.137
X=	850.0/C/ /VEL/	0.203	0.202	0.221
X=	950.0/C/ /VEL/	0.110	0.047	-0.141
X=	1050.0/C/ /VEL/	0.201	0.203	0.234
X=	1150.0/C/ /VEL/	0.110	0.043	-0.145
X=	1250.0/C/ /VEL/	0.202	0.205	0.244
REACH NUMBER	3 :	0.109	0.040	-0.149
X=	50.0/C/ /VEL/	0.204	0.204	0.204
X=	150.0/C/ /VEL/	-0.004	-0.004	0.201
X=	250.0/C/ /VEL/	0.004	-0.007	0.201
X=	350.0/C/ /VEL/	0.004	0.200	-0.002
X=	450.0/C/ /VEL/	0.200	-0.010	-0.006
X=	550.0/C/ /VEL/	0.005	0.200	0.200
X=	650.0/C/ /VEL/	0.200	-0.013	-0.010
X=	750.0/C/ /VEL/	0.005	0.200	0.200
X=	850.0/C/ /VEL/	0.205	-0.016	-0.013
REACH NUMBER	4 :	0.005	0.200	0.199
X=	50.0/C/ /VEL/	0.246	0.298	0.324
X=	150.0/C/ /VEL/	-0.011	-0.049	-0.054
X=	250.0/C/ /VEL/	0.262	0.293	0.300
X=	350.0/C/ /VEL/	0.012	-0.052	-0.057
X=	450.0/C/ /VEL/	0.272	0.283	0.273
X=	550.0/C/ /VEL/	0.012	-0.055	-0.060
X=	650.0/C/ /VEL/	0.277	0.271	0.249
X=	750.0/C/ /VEL/	0.278	-0.057	-0.063
X=	850.0/C/ /VEL/	0.013	0.259	0.233
X=	950.0/C/ /VEL/	0.280	-0.060	-0.066
X=	1050.0/C/ /VEL/	-0.013	0.250	0.226
X=	1150.0/C/ /VEL/	0.273	-0.062	-0.065
X=	1250.0/C/ /VEL/	-0.014	0.240	0.218
X=	1350.0/C/ /VEL/	0.259	-0.065	-0.072
X=	1450.0/C/ /VEL/	0.214	0.228	0.210
X=	1550.0/C/ /VEL/	0.250	-0.067	-0.075
X=	1650.0/C/ /VEL/	-0.015	0.219	0.205
X=	1750.0/C/ /VEL/	0.246	-0.070	-0.078

```

REACH NUMBER 5:
X= 83.3/C/ 0.246 0.219 0.202
   /VEL/ 0.083 -0.037 -0.251
X= 250.0/C/ 0.247 0.214 -0.201
   /VEL/ 0.082 -0.041 -0.255
X= 416.7/C/ 0.239 0.209 -0.201
   /VEL/ 0.082 -0.045 -0.260
X= 583.3/C/ 0.237 0.206 -0.200
   /VEL/ 0.081 -0.049 -0.265
X= 750.0/C/ 0.217 0.203 -0.200
   /VEL/ 0.080 -0.053 -0.270
X= 916.7/C/ 0.210 0.202 -0.200
   /VEL/ 0.079 -0.057 -0.275
X= 1083.3/C/ 0.205 0.201 -0.200
   /VEL/ 0.079 -0.061 -0.280
X= 1250.0/C/ 0.202 0.200 -0.200
   /VEL/ 0.078 -0.065 -0.285
X= 1416.7/C/ 0.201 0.200 -0.200
   /VEL/ 0.077 -0.069 -0.290
X= 1583.3/C/ 0.200 0.200 -0.200
   /VEL/ 0.076 -0.073 -0.294
X= 1750.0/C/ 0.200 0.200 -0.200
   /VEL/ 0.076 -0.077 -0.299
X= 1916.7/C/ 0.200 0.200 -0.200
   /VEL/ 0.075 -0.081 -0.304
X= 2083.3/C/ 0.200 0.200 -0.200
   /VEL/ 0.074 -0.085 -0.309
X= 2250.0/C/ 0.200 0.200 -0.200
   /VEL/ 0.073 -0.085 -0.314
X= 2416.7/C/ 0.200 0.200 -0.200
   /VEL/ 0.073 -0.089 -0.319
JUNCTION NUMBER 2:
0.242
0.213
0.204

```

```

JUNCTION NUMBER 3:
0.203
0.241
0.276

```

WIND PROFILE NUMBER 1: THE FLOW STATE OF SIMULATION IS 10.25 HOURS
 INITIAL DISTANCE - 3.000 FEET; WIND SPEED 12.5 FT/SEC; WIND DIRECTION - 9. DEGREES

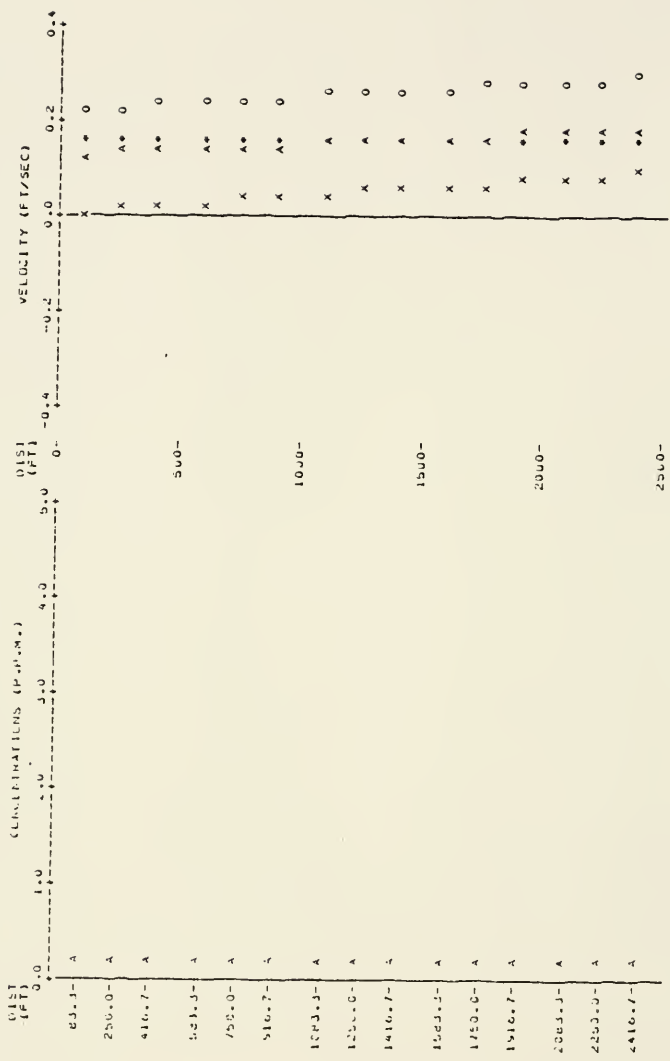


PLUTE FOR TRACE GASES 2 1/2 HRS FROM START OF SIMULATION IS 12:00 HOURS
 TIME DIFFERENCE = 0.050 FEET; WIND SPEED = 12.5 FT/SEC; WIND DIRECTION = 8. DEGREES



0 = LAYER (USE 1.0 FT)
 O = LAYER (USE 1.5 FT)
 A = LAYER (USE 2.5 FT)
 A = AVERAGE OVER LAYERS

ALTS FOR EACH RUN: 5 : TIME FROM START OF SIMULATION IS 10.25 HOURS
 : TICAL DIFFERENCE -0.050 FEET: WIND SPEED 12.5 FT/SEC: WIND DIRECTION= 8. DEGREES



* = LAYER 1 (Z= 1.3 FT)
 0 = LAYER 2 (Z= 4.0 FT)
 X = LAYER 3 (Z= 0.5 FT)
 A = AVERAGE OVER LAYERS

TIME 20.00 HOURS: TIDAL DIFFERENCE = -0.900 FEET
 WIND SPEED= 11.1 FT/SEC: WIND DIRECTION= 0. DEGREES
 REACH NUMBER 1:
 X= 50.0/C// 2.340 2.022 2.026
 /VEL// -0.018 -0.013 0.027
 X= 150.0/C// 2.458 2.170 1.928
 /VEL// -0.017 -0.010 0.030
 X= 250.0/C// 2.287 2.127 1.881
 /VEL// -0.017 -0.027 0.033
 X= 350.0/C// 2.013 2.009 1.784
 /VEL// -0.016 -0.005 0.037
 X= 450.0/C// 1.719 1.843 1.694
 /VEL// -0.016 -0.002 0.040
 X= 550.0/C// 1.457 1.693 1.615
 /VEL// -0.015 0.001 0.044
 X= 650.0/C// 1.251 1.522 1.552
 /VEL// -0.015 0.004 0.047
 X= 750.0/C// 1.057 1.368 1.501
 /VEL// -0.014 0.007 0.050
 X= 850.0/C// 0.856 1.270 1.463
 /VEL// -0.014 0.010 0.054
 X= 950.0/C// 0.636 1.199 1.430
 /VEL// -0.013 0.013 0.057
 X= 1050.0/C// 0.894 1.142 1.396
 /VEL// -0.013 0.015 0.061
 X= 1150.0/C// 0.864 1.105 1.358
 /VEL// -0.012 0.018 0.064
 X= 1250.0/C// 0.843 1.086 1.323
 /VEL// -0.012 0.021 0.068
 X= 1350.0/C// 0.822 1.070 1.302
 /VEL// -0.011 0.024 0.071
 X= 1450.0/C// 0.802 1.059 1.279
 /VEL// -0.011 0.027 0.074
 X= 1550.0/C// 0.782 1.048 1.229
 /VEL// -0.010 0.030 0.078
 X= 1650.0/C// 0.760 1.034 1.235
 /VEL// -0.010 0.033 0.081
 X= 1750.0/C// 0.732 1.021 1.224
 /VEL// -0.009 0.035 0.085
 X= 1850.0/C// 0.702 1.010 1.220
 /VEL// -0.008 0.038 0.088
 X= 1950.0/C// 0.668 0.997 1.209
 /VEL// -0.008 0.041 0.091
 X= 2050.0/C// 0.632 0.972 1.459
 /VEL// -0.007 0.044 0.095
 X= 2150.0/C// 0.554 0.929 1.530

X=	2250.0/C/	/VEL/	-0.007	0.047	0.098
X=	2350.0/C/	/VEL/	0.556	0.867	1.547
X=	2450.0/C/	/VEL/	-0.519	0.050	0.102
X=	2550.0/C/	/VEL/	-0.006	0.790	1.487
X=	2650.0/C/	/VEL/	0.485	0.052	0.105
X=	2750.0/C/	/VEL/	-0.005	0.709	1.353
X=	2850.0/C/	/VEL/	0.456	0.055	0.108
X=	2950.0/C/	/VEL/	-0.005	0.633	1.168
X=	3050.0/C/	/VEL/	0.430	0.058	0.112
X=	3150.0/C/	/VEL/	-0.004	0.570	0.566
X=	3250.0/C/	/VEL/	0.407	0.061	0.115
X=	3350.0/C/	/VEL/	-0.004	0.523	0.784
X=	3450.0/C/	/VEL/	0.387	0.064	0.119
X=	3550.0/C/	/VEL/	-0.003	0.492	0.654
X=	3650.0/C/	/VEL/	0.364	0.067	0.122
X=	3750.0/C/	/VEL/	-0.003	0.471	0.585
X=	3850.0/C/	/VEL/	0.341	0.070	0.126
X=	3950.0/C/	/VEL/	-0.002	0.452	0.558
X=	4050.0/C/	/VEL/	0.323	0.072	0.129
X=	4150.0/C/	/VEL/	-0.002	0.435	0.545
X=	4250.0/C/	/VEL/	0.310	0.075	0.132
X=	4350.0/C/	/VEL/	-0.001	0.418	0.532
X=	4450.0/C/	/VEL/	0.289	0.078	0.136
X=	4550.0/C/	/VEL/	-0.001	0.403	0.519
X=	4650.0/C/	/VEL/	0.287	0.081	0.139
X=	4750.0/C/	/VEL/	-0.000	0.388	0.508
X=	4850.0/C/	/VEL/	0.277	0.084	0.143
X=	4950.0/C/	/VEL/	0.000	0.374	0.497
X=	5050.0/C/	/VEL/	0.266	0.087	0.146
X=	5150.0/C/	/VEL/	0.001	0.360	0.485
X=	5250.0/C/	/VEL/	0.257	0.090	0.149
X=	5350.0/C/	/VEL/	0.001	0.346	0.473
X=	5450.0/C/	/VEL/	0.248	0.092	0.153
X=	5550.0/C/	/VEL/	0.002	0.332	0.460
X=	5650.0/C/	/VEL/	0.241	0.095	0.156
X=	5750.0/C/	/VEL/	0.002	0.319	0.447
X=	5850.0/C/	/VEL/	0.235	0.098	0.160
X=	5950.0/C/	/VEL/	0.003	0.307	0.433
X=	6050.0/C/	/VEL/	0.233	0.101	0.163
X=	6150.0/C/	/VEL/	0.003	0.295	0.418
REACH NUMBER	:		2:	0.104	0.167
X=	50.0/C/	/VEL/	0.228	0.228	0.228
X=	150.0/C/	/VEL/	0.087	0.070	-0.114
X=	250.0/C/	/VEL/	0.087	0.229	0.226
X=	350.0/C/	/VEL/	0.087	0.074	-0.109
X=	450.0/C/	/VEL/	0.087	0.229	0.226
X=	550.0/C/	/VEL/	0.087	0.078	-0.105

X = 350.0/C/	0.233	0.229	0.225
/VEL/	0.087	0.082	-0.100
X = 450.0/C/	0.230	0.229	-0.100
/VEL/	0.087	0.086	-0.105
X = 550.0/C/	0.230	0.228	0.223
/VEL/	0.088	0.089	-0.090
X = 650.0/C/	0.231	0.228	0.223
/VEL/	0.088	0.093	-0.085
X = 750.0/C/	0.231	0.228	0.222
/VEL/	0.088	0.097	-0.081
X = 850.0/C/	0.231	0.227	0.220
/VEL/	0.088	0.101	-0.079
X = 950.0/C/	0.230	0.226	0.219
/VEL/	0.089	0.105	-0.071
X = 1050.0/C/	0.238	0.225	0.217
/VEL/	0.089	0.109	-0.069
X = 1150.0/C/	0.226	0.223	0.215
/VEL/	0.089	0.113	-0.062
X = 1250.0/C/	0.223	0.221	0.213
/VEL/	0.089	0.117	-0.057
REACH NUMBER	3:		
X = 50.0/C/	0.204	0.202	0.205
/VEL/	-0.067	-0.063	0.011
X = 150.0/C/	0.199	0.203	0.203
/VEL/	-0.066	0.000	0.016
X = 250.0/C/	0.200	0.200	0.200
/VEL/	-0.066	0.004	0.021
X = 350.0/C/	0.200	0.200	0.200
/VEL/	-0.066	0.008	0.025
X = 450.0/C/	0.200	0.200	0.200
/VEL/	-0.066	0.012	0.030
X = 550.0/C/	0.207	0.202	0.200
/VEL/	-0.065	0.016	0.035
X = 650.0/C/	0.212	0.205	0.201
/VEL/	-0.065	0.019	0.039
REACH NUMBER	4:		
X = 50.0/C/	0.228	0.216	0.212
/VEL/	0.002	0.050	0.075
X = 150.0/C/	0.249	0.220	0.213
/VEL/	0.003	0.053	0.079
X = 250.0/C/	0.255	0.227	0.216
/VEL/	0.003	0.056	0.083
X = 350.0/C/	0.261	0.233	0.220
/VEL/	0.004	0.059	0.086
X = 450.0/C/	0.264	0.242	0.224
/VEL/	0.004	0.062	0.090
X = 550.0/C/	0.263	0.257	0.231
/VEL/	0.005	0.065	0.093

X=	650.0/C/ /VEL/	0.258 0.005	0.267 0.068	0.246 0.097
X=	750.0/C/ /VEL/	0.249 0.006	0.267 0.071	0.265 0.101
X=	850.0/C/ /VEL/	0.006	0.241 0.074	0.274 0.104
REACH NUMBER 5:				
X=	83.3/C/ /VEL/	0.239 0.052	0.274 0.183	0.270 0.056
X=	250.0/C/ /VEL/	0.233 0.093	0.259 0.188	0.217 0.062
X=	416.7/C/ /VEL/	0.226 0.094	0.245 0.193	0.216 0.067
X=	583.3/C/ /VEL/	0.219 0.214	0.234 0.197	0.212 0.073
X=	750.0/C/ /VEL/	0.096 0.211	0.225 0.202	0.210 0.079
X=	916.7/C/ /VEL/	0.096 0.209	0.207 0.213	0.208 0.084
X=	1083.3/C/ /VEL/	0.057 0.208	0.212 0.210	0.090 0.206
X=	1250.0/C/ /VEL/	0.058 0.207	0.216 0.208	0.096 0.206
X=	1416.7/C/ /VEL/	0.099 0.208	0.221 0.207	0.101 0.206
X=	1583.3/C/ /VEL/	0.100 0.209	0.226 0.207	0.107 0.206
X=	1750.0/C/ /VEL/	0.101 0.211	0.230 0.207	0.113 0.206
X=	1916.7/C/ /VEL/	0.102 0.214	0.235 0.208	0.118 0.207
X=	2083.3/C/ /VEL/	0.102 0.210	0.240 0.209	0.124 0.207
X=	2250.0/C/ /VEL/	0.103 0.218	0.245 0.210	0.129 0.207
X=	2416.7/C/ /VEL/	0.104	0.249	0.207
JUNCTION NUMBER 2:				
		0.242		
		0.265		
		0.333		
JUNCTION NUMBER 3:				
		0.214		
		0.211		

TIME 25.00 HOURS: TIDAL DIFFERENCE= -1.100 FEET

4.0 FT/SEC: WIND DIRECTION= 42, DEGREES

WIND SPEED= REACH NUMBER	1:	2:	3:	4:	5:	6:	7:	8:	9:	10:	11:	12:	13:	14:	15:	16:	17:	18:	19:	20:	21:	22:	23:	24:	25:	26:	27:	28:	29:	30:	31:	32:	33:	34:	35:	36:	37:	38:	39:	40:	41:	42:	43:	44:	45:	46:	47:	48:	49:	50:																																																																																																																																																																																																																																																																																																																																																																																																																																																																																																																																																																										
X= 50.0/C/ /VEL	2.197	-0.007	2.183	-0.007	2.170	-0.007	2.156	-0.007	2.142	-0.007	2.128	-0.007	2.114	-0.007	2.100	-0.007	2.086	-0.007	2.072	-0.007	2.058	-0.007	2.044	-0.007	2.030	-0.007	2.016	-0.007	2.002	-0.007	1.988	-0.007	1.974	-0.007	1.960	-0.007	1.946	-0.007	1.932	-0.007	1.918	-0.007	1.904	-0.007	1.890	-0.007	1.876	-0.007	1.862	-0.007	1.848	-0.007	1.834	-0.007	1.820	-0.007	1.806	-0.007	1.792	-0.007	1.778	-0.007	1.764	-0.007	1.750	-0.007	1.736	-0.007	1.722	-0.007	1.708	-0.007	1.694	-0.007	1.680	-0.007	1.666	-0.007	1.652	-0.007	1.638	-0.007	1.624	-0.007	1.610	-0.007	1.596	-0.007	1.582	-0.007	1.568	-0.007	1.554	-0.007	1.540	-0.007	1.526	-0.007	1.512	-0.007	1.498	-0.007	1.484	-0.007	1.470	-0.007	1.456	-0.007	1.442	-0.007	1.428	-0.007	1.414	-0.007	1.400	-0.007	1.386	-0.007	1.372	-0.007	1.358	-0.007	1.344	-0.007	1.330	-0.007	1.316	-0.007	1.302	-0.007	1.288	-0.007	1.274	-0.007	1.260	-0.007	1.246	-0.007	1.232	-0.007	1.218	-0.007	1.204	-0.007	1.190	-0.007	1.176	-0.007	1.162	-0.007	1.148	-0.007	1.134	-0.007	1.120	-0.007	1.106	-0.007	1.092	-0.007	1.078	-0.007	1.064	-0.007	1.050	-0.007	1.036	-0.007	1.022	-0.007	1.008	-0.007	0.994	-0.007	0.980	-0.007	0.966	-0.007	0.952	-0.007	0.938	-0.007	0.924	-0.007	0.910	-0.007	0.896	-0.007	0.882	-0.007	0.868	-0.007	0.854	-0.007	0.840	-0.007	0.826	-0.007	0.812	-0.007	0.798	-0.007	0.784	-0.007	0.770	-0.007	0.756	-0.007	0.742	-0.007	0.728	-0.007	0.714	-0.007	0.700	-0.007	0.686	-0.007	0.672	-0.007	0.658	-0.007	0.644	-0.007	0.630	-0.007	0.616	-0.007	0.602	-0.007	0.588	-0.007	0.574	-0.007	0.560	-0.007	0.546	-0.007	0.532	-0.007	0.518	-0.007	0.504	-0.007	0.490	-0.007	0.476	-0.007	0.462	-0.007	0.448	-0.007	0.434	-0.007	0.420	-0.007	0.406	-0.007	0.392	-0.007	0.378	-0.007	0.364	-0.007	0.350	-0.007	0.336	-0.007	0.322	-0.007	0.308	-0.007	0.294	-0.007	0.280	-0.007	0.266	-0.007	0.252	-0.007	0.238	-0.007	0.224	-0.007	0.210	-0.007	0.196	-0.007	0.182	-0.007	0.168	-0.007	0.154	-0.007	0.140	-0.007	0.126	-0.007	0.112	-0.007	0.098	-0.007	0.084	-0.007	0.070	-0.007	0.056	-0.007	0.042	-0.007	0.028	-0.007	0.014	-0.007	0.000	-0.007	-0.014	-0.007	-0.028	-0.007	-0.042	-0.007	-0.056	-0.007	-0.070	-0.007	-0.084	-0.007	-0.098	-0.007	-0.112	-0.007	-0.126	-0.007	-0.140	-0.007	-0.154	-0.007	-0.168	-0.007	-0.182	-0.007	-0.196	-0.007	-0.210	-0.007	-0.224	-0.007	-0.238	-0.007	-0.252	-0.007	-0.266	-0.007	-0.280	-0.007	-0.294	-0.007	-0.308	-0.007	-0.322	-0.007	-0.336	-0.007	-0.350	-0.007	-0.364	-0.007	-0.378	-0.007	-0.392	-0.007	-0.406	-0.007	-0.420	-0.007	-0.434	-0.007	-0.448	-0.007	-0.462	-0.007	-0.476	-0.007	-0.490	-0.007	-0.504	-0.007	-0.518	-0.007	-0.532	-0.007	-0.546	-0.007	-0.560	-0.007	-0.574	-0.007	-0.588	-0.007	-0.602	-0.007	-0.616	-0.007	-0.630	-0.007	-0.644	-0.007	-0.658	-0.007	-0.672	-0.007	-0.686	-0.007	-0.700	-0.007	-0.714	-0.007	-0.728	-0.007	-0.742	-0.007	-0.756	-0.007	-0.770	-0.007	-0.784	-0.007	-0.798	-0.007	-0.812	-0.007	-0.826	-0.007	-0.840	-0.007	-0.854	-0.007	-0.868	-0.007	-0.882	-0.007	-0.896	-0.007	-0.910	-0.007	-0.924	-0.007	-0.938	-0.007	-0.952	-0.007	-0.966	-0.007	-0.980	-0.007	-0.994	-0.007	-1.008	-0.007	-1.022	-0.007	-1.036	-0.007	-1.050	-0.007	-1.064	-0.007	-1.078	-0.007	-1.092	-0.007	-1.106	-0.007	-1.120	-0.007	-1.134	-0.007	-1.148	-0.007	-1.162	-0.007	-1.176	-0.007	-1.190	-0.007	-1.204	-0.007	-1.218	-0.007	-1.232	-0.007	-1.246	-0.007	-1.260	-0.007	-1.274	-0.007	-1.288	-0.007	-1.302	-0.007	-1.316	-0.007	-1.330	-0.007	-1.344	-0.007	-1.358	-0.007	-1.372	-0.007	-1.386	-0.007	-1.400	-0.007	-1.414	-0.007	-1.428	-0.007	-1.442	-0.007	-1.456	-0.007	-1.470	-0.007	-1.484	-0.007	-1.498	-0.007	-1.512	-0.007	-1.526	-0.007	-1.540	-0.007	-1.554	-0.007	-1.568	-0.007	-1.582	-0.007	-1.596	-0.007	-1.610	-0.007	-1.624	-0.007	-1.638	-0.007	-1.652	-0.007	-1.666	-0.007	-1.680	-0.007	-1.694	-0.007	-1.708	-0.007	-1.722	-0.007	-1.736	-0.007	-1.750	-0.007	-1.764	-0.007	-1.778	-0.007	-1.792	-0.007	-1.806	-0.007	-1.820	-0.007	-1.834	-0.007	-1.848	-0.007	-1.862	-0.007	-1.876	-0.007	-1.890	-0.007	-1.904	-0.007	-1.918	-0.007	-1.932	-0.007	-1.946	-0.007	-1.960	-0.007	-1.974	-0.007	-1.988	-0.007	-1.999	-0.007	-2.000	-0.007

X= 2350.07C/ VEL/	0.856	0.923	0.988
X= 2450.07C/ VEL/	-0.023	-0.096	-0.098
X= 2550.07C/ VEL/	-0.870	-0.890	-0.953
X= 2650.07C/ VEL/	-0.024	-0.059	-0.102
X= 2750.07C/ VEL/	-0.850	-0.839	-0.893
X= 2850.07C/ VEL/	-0.024	-0.103	-0.107
X= 2950.07C/ VEL/	-0.824	-0.774	-0.814
X= 3050.07C/ VEL/	-0.025	-0.107	-0.111
X= 3150.07C/ VEL/	-0.782	-0.702	-0.725
X= 3250.07C/ VEL/	-0.026	-0.111	-0.116
X= 3350.07C/ VEL/	-0.731	-0.628	-0.637
X= 3450.07C/ VEL/	-0.027	-0.115	-0.121
X= 3550.07C/ VEL/	-0.673	-0.561	-0.559
X= 3650.07C/ VEL/	-0.027	-0.119	-0.125
X= 3750.07C/ VEL/	-0.615	-0.506	-0.500
X= 3850.07C/ VEL/	-0.028	-0.122	-0.130
X= 3950.07C/ VEL/	-0.560	-0.466	-0.461
X= 4050.07C/ VEL/	-0.029	-0.126	-0.134
X= 4150.07C/ VEL/	-0.511	-0.439	-0.440
X= 4250.07C/ VEL/	-0.029	-0.130	-0.139
X= 4350.07C/ VEL/	-0.471	-0.416	-0.419
X= 4450.07C/ VEL/	-0.030	-0.134	-0.143
X= 4550.07C/ VEL/	-0.438	-0.379	-0.366
X= 4650.07C/ VEL/	-0.031	-0.138	-0.148
X= 4750.07C/ VEL/	-0.412	-0.355	-0.347
X= 4850.07C/ VEL/	-0.031	-0.142	-0.152
X= 4950.07C/ VEL/	-0.351	-0.347	-0.343
X= 5050.07C/ VEL/	-0.032	-0.145	-0.157
X= 5150.07C/ VEL/	-0.375	-0.339	-0.338
X= 5250.07C/ VEL/	-0.033	-0.149	-0.162
X= 5350.07C/ VEL/	-0.362	-0.332	-0.332
X= 5450.07C/ VEL/	-0.034	-0.153	-0.166
X= 5550.07C/ VEL/	-0.347	-0.325	-0.326
X= 5650.07C/ VEL/	-0.034	-0.157	-0.171
X= 5750.07C/ VEL/	-0.312	-0.319	-0.319
X= 5850.07C/ VEL/	-0.035	-0.161	-0.175
X= 5950.07C/ VEL/	-0.294	-0.316	-0.311
REACH NUMBER	2.	-0.165	-0.180
X= 50.07C/ VEL/	0.001	0.227	0.227
X= 150.07C/ VEL/	0.001	-0.002	-0.005
X= 250.07C/ VEL/	0.001	0.227	0.227
X= 350.07C/ VEL/	0.000	-0.007	-0.011
X= 450.07C/ VEL/	0.000	0.227	0.227
X= 550.07C/ VEL/	0.000	-0.012	-0.018
X= 650.07C/ VEL/	0.000	0.227	0.227
X= 750.07C/ VEL/	0.000	-0.018	-0.024
X= 850.07C/ VEL/	0.000	0.227	0.227
X= 950.07C/ VEL/	0.000	-0.018	-0.024
X= 1050.07C/ VEL/	0.000	0.227	0.227
X= 1150.07C/ VEL/	0.000	-0.018	-0.024
X= 1250.07C/ VEL/	0.000	0.227	0.227
X= 1350.07C/ VEL/	0.000	-0.018	-0.024
X= 1450.07C/ VEL/	0.000	0.227	0.227
X= 1550.07C/ VEL/	0.000	-0.018	-0.024
X= 1650.07C/ VEL/	0.000	0.227	0.227
X= 1750.07C/ VEL/	0.000	-0.018	-0.024
X= 1850.07C/ VEL/	0.000	0.227	0.227
X= 1950.07C/ VEL/	0.000	-0.018	-0.024
X= 2050.07C/ VEL/	0.000	0.227	0.227
X= 2150.07C/ VEL/	0.000	-0.018	-0.024
X= 2250.07C/ VEL/	0.000	0.227	0.227
X= 2350.07C/ VEL/	0.000	-0.018	-0.024
X= 2450.07C/ VEL/	0.000	0.227	0.227
X= 2550.07C/ VEL/	0.000	-0.018	-0.024
X= 2650.07C/ VEL/	0.000	0.227	0.227
X= 2750.07C/ VEL/	0.000	-0.018	-0.024
X= 2850.07C/ VEL/	0.000	0.227	0.227
X= 2950.07C/ VEL/	0.000	-0.018	-0.024
X= 3050.07C/ VEL/	0.000	0.227	0.227
X= 3150.07C/ VEL/	0.000	-0.018	-0.024
X= 3250.07C/ VEL/	0.000	0.227	0.227
X= 3350.07C/ VEL/	0.000	-0.018	-0.024
X= 3450.07C/ VEL/	0.000	0.227	0.227
X= 3550.07C/ VEL/	0.000	-0.018	-0.024
X= 3650.07C/ VEL/	0.000	0.227	0.227
X= 3750.07C/ VEL/	0.000	-0.018	-0.024
X= 3850.07C/ VEL/	0.000	0.227	0.227
X= 3950.07C/ VEL/	0.000	-0.018	-0.024
X= 4050.07C/ VEL/	0.000	0.227	0.227
X= 4150.07C/ VEL/	0.000	-0.018	-0.024
X= 4250.07C/ VEL/	0.000	0.227	0.227
X= 4350.07C/ VEL/	0.000	-0.018	-0.024
X= 4450.07C/ VEL/	0.000	0.227	0.227
X= 4550.07C/ VEL/	0.000	-0.018	-0.024
X= 4650.07C/ VEL/	0.000	0.227	0.227
X= 4750.07C/ VEL/	0.000	-0.018	-0.024
X= 4850.07C/ VEL/	0.000	0.227	0.227
X= 4950.07C/ VEL/	0.000	-0.018	-0.024
X= 5050.07C/ VEL/	0.000	0.227	0.227
X= 5150.07C/ VEL/	0.000	-0.018	-0.024
X= 5250.07C/ VEL/	0.000	0.227	0.227
X= 5350.07C/ VEL/	0.000	-0.018	-0.024
X= 5450.07C/ VEL/	0.000	0.227	0.227
X= 5550.07C/ VEL/	0.000	-0.018	-0.024
X= 5650.07C/ VEL/	0.000	0.227	0.227
X= 5750.07C/ VEL/	0.000	-0.018	-0.024
X= 5850.07C/ VEL/	0.000	0.227	0.227
X= 5950.07C/ VEL/	0.000	-0.018	-0.024
X= 6050.07C/ VEL/	0.000	0.227	0.227
X= 6150.07C/ VEL/	0.000	-0.018	-0.024
X= 6250.07C/ VEL/	0.000	0.227	0.227
X= 6350.07C/ VEL/	0.000	-0.018	-0.024
X= 6450.07C/ VEL/	0.000	0.227	0.227
X= 6550.07C/ VEL/	0.000	-0.018	-0.024
X= 6650.07C/ VEL/	0.000	0.227	0.227
X= 6750.07C/ VEL/	0.000	-0.018	-0.024
X= 6850.07C/ VEL/	0.000	0.227	0.227
X= 6950.07C/ VEL/	0.000	-0.018	-0.024
X= 7050.07C/ VEL/	0.000	0.227	0.227
X= 7150.07C/ VEL/	0.000	-0.018	-0.024
X= 7250.07C/ VEL/	0.000	0.227	0.227
X= 7350.07C/ VEL/	0.000	-0.018	-0.024
X= 7450.07C/ VEL/	0.000	0.227	0.227
X= 7550.07C/ VEL/	0.000	-0.018	-0.024
X= 7650.07C/ VEL/	0.000	0.227	0.227
X= 7750.07C/ VEL/	0.000	-0.018	-0.024
X= 7850.07C/ VEL/	0.000	0.227	0.227
X= 7950.07C/ VEL/	0.000	-0.018	-0.024
X= 8050.07C/ VEL/	0.000	0.227	0.227
X= 8150.07C/ VEL/	0.000	-0.018	-0.024
X= 8250.07C/ VEL/	0.000	0.227	0.227
X= 8350.07C/ VEL/	0.000	-0.018	-0.024
X= 8450.07C/ VEL/	0.000	0.227	0.227
X= 8550.07C/ VEL/	0.000	-0.018	-0.024
X= 8650.07C/ VEL/	0.000	0.227	0.227
X= 8750.07C/ VEL/	0.000	-0.018	-0.024
X= 8850.07C/ VEL/	0.000	0.227	0.227
X= 8950.07C/ VEL/	0.000	-0.018	-0.024
X= 9050.07C/ VEL/	0.000	0.227	0.227
X= 9150.07C/ VEL/	0.000	-0.018	-0.024
X= 9250.07C/ VEL/	0.000	0.227	0.227
X= 9350.07C/ VEL/	0.000	-0.018	-0.024
X= 9450.07C/ VEL/	0.000	0.227	0.227
X= 9550.07C/ VEL/	0.000	-0.018	-0.024
X= 9650.07C/ VEL/	0.000	0.227	0.227
X= 9750.07C/ VEL/	0.000	-0.018	-0.024
X= 9850.07C/ VEL/	0.000	0.227	0.227
X= 9950.07C/ VEL/	0.000	-0.018	-0.024
X= 10050.07C/ VEL/	0.000	0.227	0.227

X =	/VEL/	-0.000	-0.023	-0.031
X =	550.0/C/	0.227	0.227	0.227
X =	/VEL/	-0.001	0.028	-0.037
X =	650.0/C/	0.227	0.226	0.226
X =	/VEL/	-0.001	0.034	-0.044
X =	750.0/C/	0.227	0.226	0.225
X =	/VEL/	-0.001	0.035	-0.050
X =	850.0/C/	0.226	0.225	0.223
X =	/VEL/	-0.002	0.044	-0.056
X =	950.0/C/	0.225	0.222	0.219
X =	/VEL/	-0.002	0.050	-0.063
X =	1050.0/C/	0.224	0.220	0.217
X =	/VEL/	-0.002	0.055	-0.069
X =	1150.0/C/	0.222	0.219	0.218
X =	/VEL/	-0.002	0.060	-0.076
X =	1250.0/C/	0.221	0.220	0.219
X =	/VEL/	-0.003	0.066	-0.082
REACT NUMBER 3:				
X =	50.0/C/	0.202	0.202	0.202
X =	/VEL/	0.000	-0.002	-0.004
X =	150.0/C/	0.202	0.202	0.202
X =	/VEL/	0.000	-0.007	-0.010
X =	250.0/C/	0.201	0.201	0.201
X =	/VEL/	-0.000	-0.013	-0.017
X =	350.0/C/	0.200	0.200	0.200
X =	/VEL/	-0.001	-0.018	-0.023
X =	450.0/C/	0.200	0.202	0.204
X =	/VEL/	-0.001	-0.023	-0.029
X =	550.0/C/	0.204	0.211	0.213
X =	/VEL/	-0.001	-0.028	-0.036
X =	650.0/C/	0.212	0.218	0.218
X =	/VEL/	-0.002	-0.033	-0.042
REACT NUMBER 4:				
X =	50.0/C/	0.223	0.226	0.226
X =	/VEL/	-0.012	-0.074	-0.090
X =	150.0/C/	0.226	0.226	0.226
X =	/VEL/	-0.012	-0.078	-0.094
X =	250.0/C/	0.229	0.230	0.238
X =	/VEL/	-0.013	-0.082	-0.099
X =	350.0/C/	0.233	0.253	0.296
X =	/VEL/	-0.014	-0.086	-0.104
X =	450.0/C/	0.241	0.299	0.335
X =	/VEL/	-0.014	-0.090	-0.109
X =	550.0/C/	0.257	0.316	0.336
X =	/VEL/	-0.015	-0.094	-0.114
X =	650.0/C/	0.264	0.317	0.330
X =	/VEL/	-0.016	-0.098	-0.118
X =	750.0/C/	0.279	0.318	0.323

X=	850.0/C/	/VEL/	-0.016	-0.102	-0.123
	/VEL/	/VEL/	0.296	0.317	0.313
	REACH NUMBER		-0.017	-0.106	-0.128
X=	83.3/C/	5:			
	/VEL/		0.303	0.280	0.253
X=	250.0/C/		0.026	-0.166	-0.213
	/VEL/		0.295	0.260	0.237
X=	416.7/C/		-0.026	-0.172	-0.221
	/VEL/		0.284	0.245	0.227
X=	583.3/C/		-0.027	-0.178	-0.229
	/VEL/		0.273	0.235	0.221
X=	750.0/C/		-0.029	-0.185	-0.236
	/VEL/		0.260	0.227	0.216
X=	916.7/C/		-0.030	-0.191	-0.244
	/VEL/		0.245	0.220	0.210
X=	1083.3/C/		-0.031	-0.198	-0.251
	/VEL/		0.233	0.214	0.204
X=	1250.0/C/		-0.032	-0.204	-0.259
	/VEL/		0.224	0.208	0.201
X=	1416.7/C/		-0.033	-0.210	-0.266
	/VEL/		0.218	0.204	0.201
X=	1583.3/C/		-0.034	-0.217	-0.274
	/VEL/		0.213	0.203	0.200
X=	1750.0/C/		-0.036	-0.223	-0.281
	/VEL/		0.210	0.202	0.200
X=	1916.7/C/		-0.037	-0.229	-0.289
	/VEL/		0.208	0.201	0.200
X=	2083.3/C/		-0.038	-0.236	-0.296
	/VEL/		0.205	0.200	0.200
X=	2250.0/C/		-0.039	-0.242	-0.304
	/VEL/		0.201	0.200	0.200
X=	2416.7/C/		-0.040	-0.248	-0.312
	/VEL/		0.200	0.200	0.200
	JUNCTION NUMBER 2:		-0.042	-0.255	-0.319
	0.292				
	0.314				
	0.304				
	JUNCTION NUMBER 3:				
	0.221				
	0.221				
	0.220				

TIME 30.00 HOURS: TIDAL DIFFERENCE= -0.050 FEET

WIND SPEED 10.7 FT/SEC: WIND DIRECTION 92. DEGREES

REACH NUMBER 1: 1.329 1.520 1.485

X= 50.0/C/

X=	150.0/C//	/VEL//	-0.070	-0.049	0.083
X=	150.0/C//	/VEL//	1.245	1.450	1.518
X=	250.0/C//	/VEL//	-0.070	-0.047	0.085
X=	250.0/C//	/VEL//	1.201	1.417	1.571
X=	350.0/C//	/VEL//	-0.070	-0.046	0.087
X=	350.0/C//	/VEL//	1.163	1.385	1.625
X=	450.0/C//	/VEL//	-0.070	-0.044	0.089
X=	450.0/C//	/VEL//	1.130	1.352	1.677
X=	550.0/C//	/VEL//	-0.069	-0.043	0.090
X=	550.0/C//	/VEL//	1.102	1.318	1.730
X=	650.0/C//	/VEL//	-0.069	-0.041	0.092
X=	650.0/C//	/VEL//	1.077	1.283	1.753
X=	750.0/C//	/VEL//	-0.069	-0.040	0.094
X=	750.0/C//	/VEL//	1.053	1.247	1.769
X=	850.0/C//	/VEL//	-0.069	-0.039	0.096
X=	850.0/C//	/VEL//	1.030	1.208	1.764
X=	950.0/C//	/VEL//	-0.068	-0.037	0.098
X=	950.0/C//	/VEL//	1.009	1.167	1.734
X=	1050.0/C//	/VEL//	-0.068	-0.036	0.099
X=	1050.0/C//	/VEL//	0.989	1.126	1.682
X=	1150.0/C//	/VEL//	-0.068	-0.034	0.101
X=	1150.0/C//	/VEL//	0.969	1.088	1.607
X=	1250.0/C//	/VEL//	-0.067	-0.033	0.103
X=	1250.0/C//	/VEL//	0.946	1.051	1.506
X=	1350.0/C//	/VEL//	-0.067	-0.031	0.105
X=	1350.0/C//	/VEL//	0.914	1.016	1.390
X=	1450.0/C//	/VEL//	-0.067	-0.030	0.107
X=	1450.0/C//	/VEL//	0.873	0.978	1.281
X=	1550.0/C//	/VEL//	-0.067	-0.028	0.109
X=	1550.0/C//	/VEL//	0.823	0.937	1.196
X=	1650.0/C//	/VEL//	-0.066	-0.027	0.110
X=	1650.0/C//	/VEL//	0.765	0.891	1.132
X=	1750.0/C//	/VEL//	-0.066	-0.025	0.112
X=	1750.0/C//	/VEL//	0.706	0.840	1.085
X=	1850.0/C//	/VEL//	-0.066	-0.024	0.114
X=	1850.0/C//	/VEL//	0.648	0.789	1.046
X=	1950.0/C//	/VEL//	-0.066	-0.022	0.116
X=	1950.0/C//	/VEL//	0.593	0.739	1.012
X=	2050.0/C//	/VEL//	-0.065	-0.021	0.118
X=	2050.0/C//	/VEL//	0.542	0.691	0.980
X=	2150.0/C//	/VEL//	-0.065	-0.019	0.119
X=	2150.0/C//	/VEL//	0.487	0.644	0.950
X=	2250.0/C//	/VEL//	-0.065	-0.018	0.121
X=	2250.0/C//	/VEL//	0.459	0.600	0.921
X=	2350.0/C//	/VEL//	-0.064	-0.016	0.123
X=	2350.0/C//	/VEL//	0.428	0.561	0.893
X=	2450.0/C//	/VEL//	-0.064	-0.015	0.125
X=	2450.0/C//	/VEL//	0.402	0.526	0.863

X=	2550.0/C/	/VEL/	-0.064	-0.013	0.127
X=	2550.0/C/	/VEL/	0.381	0.494	0.830
X=	2650.0/C/	/VEL/	-0.064	-0.012	0.128
X=	2650.0/C/	/VEL/	0.364	0.464	0.799
X=	2750.0/C/	/VEL/	-0.063	-0.010	0.130
X=	2750.0/C/	/VEL/	0.349	0.437	0.769
X=	2850.0/C/	/VEL/	-0.063	-0.009	0.132
X=	2850.0/C/	/VEL/	0.335	0.411	0.734
X=	2950.0/C/	/VEL/	-0.063	-0.007	0.134
X=	2950.0/C/	/VEL/	0.319	0.387	0.688
X=	3050.0/C/	/VEL/	-0.063	-0.006	0.136
X=	3050.0/C/	/VEL/	0.305	0.364	0.631
X=	3150.0/C/	/VEL/	-0.062	-0.004	0.138
X=	3150.0/C/	/VEL/	0.294	0.342	0.568
X=	3250.0/C/	/VEL/	-0.062	-0.003	0.139
X=	3250.0/C/	/VEL/	0.288	0.324	0.507
X=	3350.0/C/	/VEL/	-0.062	-0.001	0.141
X=	3350.0/C/	/VEL/	0.284	0.313	0.455
X=	3450.0/C/	/VEL/	-0.062	0.000	0.143
X=	3450.0/C/	/VEL/	0.281	0.301	0.416
X=	3550.0/C/	/VEL/	-0.061	0.002	0.145
X=	3550.0/C/	/VEL/	0.280	0.293	0.388
X=	3650.0/C/	/VEL/	-0.061	0.003	0.147
X=	3650.0/C/	/VEL/	0.279	0.287	0.363
X=	3750.0/C/	/VEL/	-0.061	0.005	0.148
X=	3750.0/C/	/VEL/	0.278	0.282	0.340
X=	3850.0/C/	/VEL/	-0.060	0.006	0.150
X=	3850.0/C/	/VEL/	0.278	0.277	0.326
X=	3950.0/C/	/VEL/	-0.060	0.008	0.152
X=	3950.0/C/	/VEL/	0.277	0.317	0.317
X=	4050.0/C/	/VEL/	-0.060	0.009	0.154
X=	4050.0/C/	/VEL/	0.276	0.269	0.309
X=	4150.0/C/	/VEL/	-0.060	0.011	0.156
X=	4150.0/C/	/VEL/	0.274	0.266	0.301
REACH NUMBER	2:	/VEL/	-0.059	0.012	0.158
X=	50.0/C/	/VEL/	0.227	0.227	0.227
X=	100.0/C/	/VEL/	-0.011	-0.006	0.013
X=	150.0/C/	/VEL/	0.227	0.227	0.227
X=	200.0/C/	/VEL/	-0.011	-0.004	0.015
X=	250.0/C/	/VEL/	0.227	0.227	0.227
X=	300.0/C/	/VEL/	-0.011	-0.002	0.017
X=	350.0/C/	/VEL/	0.227	0.229	0.227
X=	400.0/C/	/VEL/	-0.010	-0.000	0.020
X=	450.0/C/	/VEL/	0.226	0.225	0.227
X=	500.0/C/	/VEL/	-0.010	-0.002	0.022
X=	550.0/C/	/VEL/	0.225	0.226	0.226
X=	600.0/C/	/VEL/	-0.010	-0.004	0.025

X= 650.07C/	0.223	0.224	0.225
/VEL/	-0.010	0.005	0.027
X= 750.07C/	0.222	0.222	0.223
/VEL/	-0.010	0.007	0.029
X= 850.07C/	0.221	0.221	0.221
/VEL/	-0.010	0.009	0.032
X= 950.07C/	0.222	0.221	0.220
/VEL/	-0.010	0.011	0.034
X= 1050.07C/	0.227	0.224	0.221
/VEL/	-0.010	0.013	0.037
X= 1150.07C/	0.240	0.235	0.226
/VEL/	-0.010	0.015	0.039
X= 1250.07C/	0.236	0.247	0.242
/VEL/	-0.009	0.017	0.041
REACH NUMBER	3		
X= 50.07C/	0.257	0.257	0.256
/VEL/	0.156	0.073	-0.110
X= 150.07C/	0.257	0.256	0.252
/VEL/	0.106	0.072	-0.108
X= 250.07C/	0.256	0.253	0.249
/VEL/	0.107	0.073	-0.109
X= 350.07C/	0.250	0.245	0.247
/VEL/	0.107	0.075	-0.105
X= 450.07C/	0.241	0.236	0.247
/VEL/	0.107	0.077	-0.101
X= 550.07C/	0.230	0.230	0.248
/VEL/	0.107	0.079	-0.098
X= 650.07C/	0.231	0.228	0.249
/VEL/	0.107	0.081	-0.096
REACH NUMBER	4		
X= 50.07C/	0.224	0.241	0.239
/VEL/	0.103	0.097	-0.076
X= 150.07C/	0.225	0.240	0.237
/VEL/	0.103	0.098	-0.074
X= 250.07C/	0.227	0.241	0.235
/VEL/	0.103	0.100	-0.072
X= 350.07C/	0.229	0.242	0.234
/VEL/	0.104	0.101	-0.071
X= 450.07C/	0.231	0.247	0.235
/VEL/	0.104	0.103	-0.069
X= 550.07C/	0.232	0.242	0.233
/VEL/	0.104	0.105	-0.067
X= 650.07C/	0.234	0.241	0.235
/VEL/	0.104	0.106	-0.065
X= 750.07C/	0.236	0.244	0.242
/VEL/	0.105	0.108	-0.063
X= 850.07C/	0.239	0.249	0.235
/VEL/	0.105	0.109	-0.061

```

REACH NUMBER 5:
X= 83.3/C/ 0.270 0.247
   /VEL/ 0.028 0.062
X= 250.0/C/ 0.249 0.218
   /VEL/ 0.028 0.065
X= 416.7/C/ 0.238 0.211
   /VEL/ 0.028 0.068
X= 583.3/C/ 0.231 0.209
   /VEL/ 0.029 0.071
X= 750.0/C/ 0.224 0.207
   /VEL/ 0.029 0.074
X= 916.7/C/ 0.217 0.205
   /VEL/ 0.030 0.077
X= 1083.3/C/ 0.212 0.203
   /VEL/ 0.208 0.092
X= 1250.0/C/ 0.208 0.206
   /VEL/ 0.031 0.095
X= 1416.7/C/ 0.206 0.204
   /VEL/ 0.031 0.097
X= 1583.3/C/ 0.204 0.203
   /VEL/ 0.032 0.089
X= 1750.0/C/ 0.203 0.202
   /VEL/ 0.032 0.092
X= 1916.7/C/ 0.202 0.201
   /VEL/ 0.033 0.095
X= 2083.3/C/ 0.201 0.200
   /VEL/ 0.033 0.098
X= 2250.0/C/ 0.200 0.200
   /VEL/ 0.033 0.101
X= 2416.7/C/ 0.200 0.200
   /VEL/ 0.034 0.112
JUNCTION NUMBER 2:
0.271
0.254
0.267
JUNCTION NUMBER 3:
0.223
0.241
0.249

```

```

TIME 35.00 HOURS: TIDAL DIFFERENCE= -2.050 FEET
WIND SPEED= 12.3 FT/SEC: WIND DIRECTION= 89, DEGREES
REACH NUMBER 1:
X= 50.0/C/ 1.167 1.195 1.187
   /VEL/ -0.071 -0.070 0.128
X= 150.0/C/ 1.148 1.189 1.190
   /VEL/ -0.071 -0.069 0.130

```

X=	250.0/C/ /VEL/	1.129	1.183	1.194
X=	350.0/C/ /VEL/	-0.071	-0.067	0.132
X=	450.0/C/ /VEL/	0.070	0.066	0.133
X=	550.0/C/ /VEL/	0.084	0.116	0.138
X=	650.0/C/ /VEL/	0.058	0.065	0.135
X=	750.0/C/ /VEL/	-0.070	-0.063	0.137
X=	850.0/C/ /VEL/	0.031	0.142	0.196
X=	950.0/C/ /VEL/	-0.069	-0.062	0.138
X=	1050.0/C/ /VEL/	0.004	0.129	0.194
X=	1150.0/C/ /VEL/	-0.069	-0.056	0.140
X=	1250.0/C/ /VEL/	0.069	0.114	0.190
X=	1350.0/C/ /VEL/	-0.069	-0.050	0.142
X=	1450.0/C/ /VEL/	0.050	0.110	0.186
X=	1550.0/C/ /VEL/	-0.068	-0.058	0.143
X=	1650.0/C/ /VEL/	0.068	0.085	0.180
X=	1750.0/C/ /VEL/	-0.068	-0.056	0.145
X=	1850.0/C/ /VEL/	0.067	0.070	0.174
X=	1950.0/C/ /VEL/	-0.067	-0.055	0.147
X=	2050.0/C/ /VEL/	0.067	0.054	0.167
X=	2150.0/C/ /VEL/	-0.067	-0.053	0.148
X=	2250.0/C/ /VEL/	0.067	0.039	0.159
X=	2350.0/C/ /VEL/	-0.067	-0.052	0.150
X=	2450.0/C/ /VEL/	0.066	0.024	0.150
X=	2550.0/C/ /VEL/	-0.066	-0.050	0.152
X=	2650.0/C/ /VEL/	0.066	0.009	0.141
X=	2750.0/C/ /VEL/	-0.066	-0.049	0.153
X=	2850.0/C/ /VEL/	0.066	0.094	0.131
X=	2950.0/C/ /VEL/	-0.066	-0.048	0.125
X=	3050.0/C/ /VEL/	0.066	0.079	0.121
X=	3150.0/C/ /VEL/	-0.066	-0.046	0.156
X=	3250.0/C/ /VEL/	0.066	0.045	0.158
X=	3350.0/C/ /VEL/	-0.066	-0.045	0.158
X=	3450.0/C/ /VEL/	0.066	0.047	0.099
X=	3550.0/C/ /VEL/	-0.066	-0.043	0.160
X=	3650.0/C/ /VEL/	0.066	0.031	0.088
X=	3750.0/C/ /VEL/	-0.066	-0.042	0.161
X=	3850.0/C/ /VEL/	0.066	0.015	0.076
X=	3950.0/C/ /VEL/	-0.066	-0.040	0.163
X=	4050.0/C/ /VEL/	0.065	0.089	0.064
X=	4150.0/C/ /VEL/	-0.065	-0.039	0.165
X=	4250.0/C/ /VEL/	0.065	0.083	0.051
X=	4350.0/C/ /VEL/	-0.065	-0.038	0.166
X=	4450.0/C/ /VEL/	0.065	0.067	0.038
X=	4550.0/C/ /VEL/	-0.065	-0.036	0.168
X=	4650.0/C/ /VEL/	0.065	0.085	0.024
X=	4750.0/C/ /VEL/	-0.065	-0.035	0.170

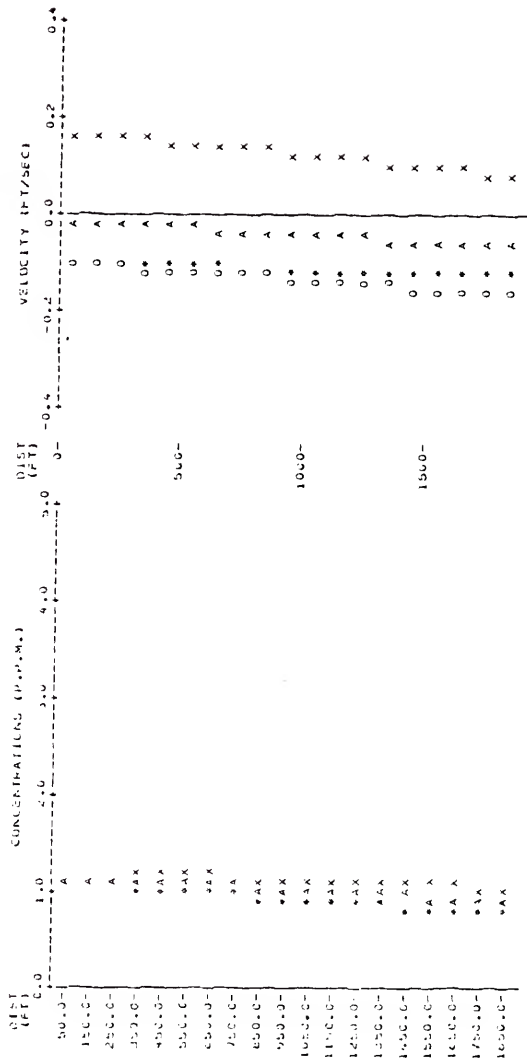
X= 2650.0/C/	0.611	0.835	1.011
/VEL/	-0.064	-0.033	0.171
X= 2750.0/C/	0.595	0.818	0.997
/VEL/	-0.064	-0.032	0.173
X= 2850.0/C/	0.580	0.801	0.982
/VEL/	-0.064	-0.030	0.175
X= 2950.0/C/	0.565	0.784	0.967
/VEL/	-0.064	-0.029	0.176
X= 3050.0/C/	0.550	0.767	0.952
/VEL/	-0.063	-0.028	0.178
X= 3150.0/C/	0.535	0.750	0.937
/VEL/	-0.063	-0.026	0.180
X= 3250.0/C/	0.520	0.733	0.921
/VEL/	-0.063	-0.025	0.181
X= 3350.0/C/	0.505	0.715	0.904
/VEL/	-0.062	-0.023	0.183
X= 3450.0/C/	0.489	0.696	0.887
/VEL/	-0.062	-0.022	0.185
X= 3550.0/C/	0.472	0.677	0.870
/VEL/	-0.062	-0.020	0.186
X= 3650.0/C/	0.457	0.658	0.851
/VEL/	-0.062	-0.019	0.188
X= 3750.0/C/	0.440	0.637	0.832
/VEL/	-0.061	-0.018	0.190
X= 3850.0/C/	0.403	0.616	0.812
/VEL/	-0.061	-0.016	0.191
X= 3950.0/C/	0.371	0.592	0.791
/VEL/	-0.061	-0.015	0.193
X= 4050.0/C/	0.333	0.569	0.770
/VEL/	-0.061	-0.013	0.195
X= 4150.0/C/	0.291	0.517	0.746
/VEL/	-0.060	-0.012	0.196
REACT NUMBER	2:		
X= 50.0/C/	0.227	0.227	0.227
/VEL/	-0.005	-0.005	0.012
X= 150.0/C/	0.227	0.227	0.227
/VEL/	-0.005	-0.003	0.015
X= 250.0/C/	0.227	0.230	0.228
/VEL/	-0.005	-0.000	0.017
X= 350.0/C/	0.226	0.224	0.226
/VEL/	-0.005	0.002	0.020
X= 450.0/C/	0.227	0.227	0.226
/VEL/	-0.005	0.004	0.022
X= 550.0/C/	0.226	0.227	0.227
/VEL/	-0.004	0.006	0.025
X= 650.0/C/	0.225	0.226	0.226
/VEL/	-0.004	0.009	0.028
X= 750.0/C/	0.225	0.225	0.225

X=	850.0/C/ /VEL/	-0.004	0.011	0.030
X=	850.0/C/ /VEL/	0.234	0.225	0.225
X=	550.0/C/ /VEL/	-0.004	0.017	0.033
X=	550.0/C/ /VEL/	0.224	0.224	0.235
X=	1050.0/C/ /VEL/	-0.004	0.015	0.035
X=	1050.0/C/ /VEL/	0.225	0.225	0.225
X=	1150.0/C/ /VEL/	-0.004	0.017	0.038
X=	1150.0/C/ /VEL/	0.225	0.225	0.225
X=	1250.0/C/ /VEL/	-0.004	0.020	0.041
X=	1250.0/C/ /VEL/	0.230	0.226	0.225
REACH NUMBER	3:	0.004	0.022	0.043
X=	50.0/C/ /VEL/	0.239	0.239	0.239
X=	150.0/C/ /VEL/	0.073	0.085	-0.149
X=	250.0/C/ /VEL/	0.239	0.239	0.238
X=	350.0/C/ /VEL/	0.073	0.085	-0.146
X=	450.0/C/ /VEL/	0.240	0.087	0.238
X=	550.0/C/ /VEL/	0.074	0.239	-0.144
X=	650.0/C/ /VEL/	0.241	0.085	-0.141
REACH NUMBER	4:	0.074	0.239	0.240
X=	50.0/C/ /VEL/	0.241	0.091	-0.139
X=	150.0/C/ /VEL/	0.241	0.240	0.243
X=	250.0/C/ /VEL/	0.074	0.093	-0.136
X=	350.0/C/ /VEL/	0.241	0.241	0.248
X=	450.0/C/ /VEL/	0.074	0.096	-0.134
REACH NUMBER	5:	0.074	0.243	0.276
X=	50.0/C/ /VEL/	0.241	0.112	-0.118
X=	150.0/C/ /VEL/	0.088	0.248	0.293
X=	250.0/C/ /VEL/	0.241	0.113	-0.116
X=	350.0/C/ /VEL/	0.088	0.254	0.319
X=	450.0/C/ /VEL/	0.242	0.115	-0.114
X=	550.0/C/ /VEL/	0.088	0.263	0.353
X=	650.0/C/ /VEL/	0.244	0.116	-0.112
REACH NUMBER	6:	0.246	0.275	0.395
X=	50.0/C/ /VEL/	0.089	0.118	-0.111
X=	150.0/C/ /VEL/	0.249	0.291	0.451
X=	250.0/C/ /VEL/	0.089	0.119	-0.109
X=	350.0/C/ /VEL/	0.254	0.311	0.518
X=	450.0/C/ /VEL/	0.089	0.121	-0.107
X=	550.0/C/ /VEL/	0.260	0.337	0.590
X=	650.0/C/ /VEL/	0.089	0.122	-0.105
REACH NUMBER	7:	0.268	0.367	0.662
X=	83.3/C/ /VEL/	0.090	0.124	-0.104
X=	83.3/C/ /VEL/	0.294	0.414	0.619
X=	83.3/C/ /VEL/	0.030	0.083	0.040

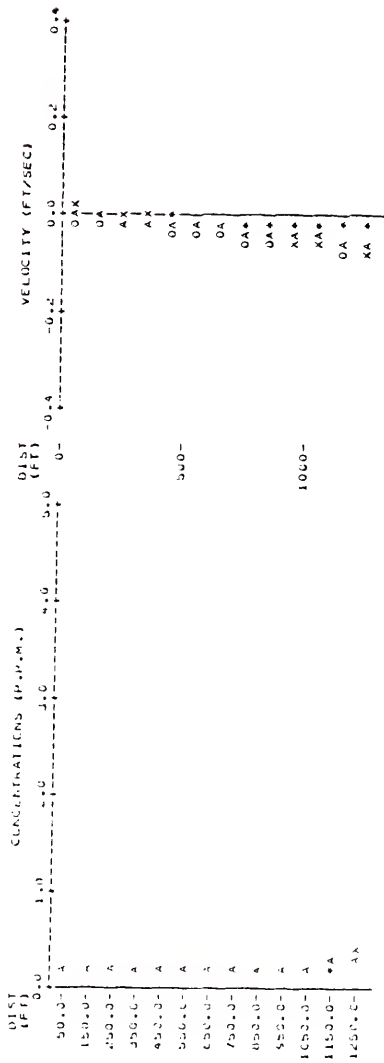
X=	250.0/C/ /VEL/	0.322	0.415	0.532
X=	416.77C/ /VEL/	0.031	0.085	0.043
X=	583.37C/ /VEL/	0.329	0.407	0.490
X=	750.07C/ /VEL/	0.329	0.387	0.046
X=	750.07C/ /VEL/	0.322	0.395	0.458
X=	916.77C/ /VEL/	0.324	0.390	0.049
X=	1083.37C/ /VEL/	0.032	0.382	0.432
X=	1250.07C/ /VEL/	0.312	0.392	0.051
X=	1416.77C/ /VEL/	0.033	0.368	0.407
X=	1583.37C/ /VEL/	0.297	0.094	0.054
X=	1750.07C/ /VEL/	0.033	0.350	0.378
X=	1916.77C/ /VEL/	0.282	0.397	0.057
X=	2083.37C/ /VEL/	0.033	0.328	0.346
X=	2250.07C/ /VEL/	0.269	0.306	0.060
X=	2416.77C/ /VEL/	0.034	0.102	0.315
X=	2416.77C/ /VEL/	0.257	0.287	0.292
X=	2416.77C/ /VEL/	0.034	0.104	0.065
X=	2416.77C/ /VEL/	0.248	0.272	0.277
X=	2416.77C/ /VEL/	0.035	0.106	0.068
X=	2416.77C/ /VEL/	0.240	0.262	0.268
X=	2416.77C/ /VEL/	0.035	0.109	0.071
X=	2416.77C/ /VEL/	0.234	0.254	0.260
X=	2416.77C/ /VEL/	0.036	0.111	0.073
X=	2416.77C/ /VEL/	0.228	0.247	0.252
X=	2416.77C/ /VEL/	0.036	0.113	0.076
X=	2416.77C/ /VEL/	0.222	0.239	0.243
X=	2416.77C/ /VEL/	0.036	0.116	0.079

JUNCTION NUMBER 2:
0.268
0.407
0.713
JUNCTION NUMBER 3:
0.241
0.241
0.253

PLATE FOR EACH NUMBER 1 LINE FROM DIAMETER SIMULATION IS -64.00 HOURS
 TIDAL DIFFERENCE = -1.650 FEET; WIND SPEED = 13.3 FT/SEC; WIND DIRECTION = 89. DEGREES

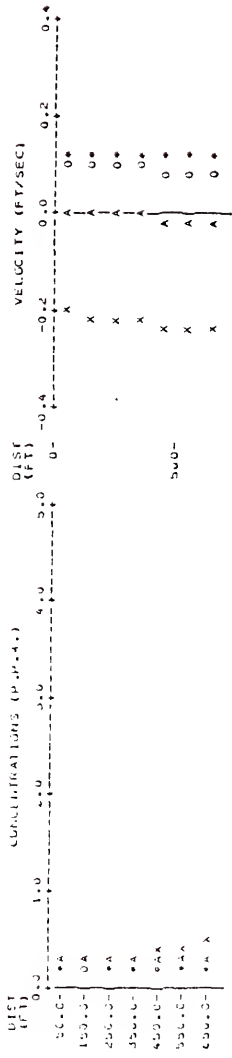


PLOTS FOR EACH NUMBER * : TIME FROM START OF SIMULATION IS 46.20 HOURS
 : TIAL DIFFERENCE = 1.00 FEET: WIND SPEED = 13.7 FT/SEC: WIND DIRECTION = 89. DEGREES



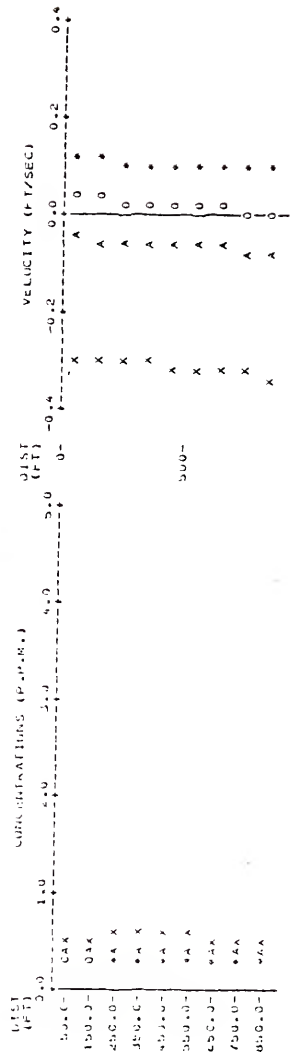
0 = LAYER 0 (Z = 0.5 FT)
 1 = LAYER 1 (Z = 2.5 FT)
 2 = LAYER 2 (Z = 3.5 FT)
 X = LAYER 3 (Z = 3.5 FT)
 A = AVERAGE OVER LAYERS

PLOTS FOR BEACH NUMBER 3 : TIME FROM START OF SIMULATION IS 36.60 HOURS
 : TIDAL DIFFERENCE = 1.000 FEET : WIND SPEED = 13.9 FT/SEC : WIND DIRECTION = 89. DEGREES



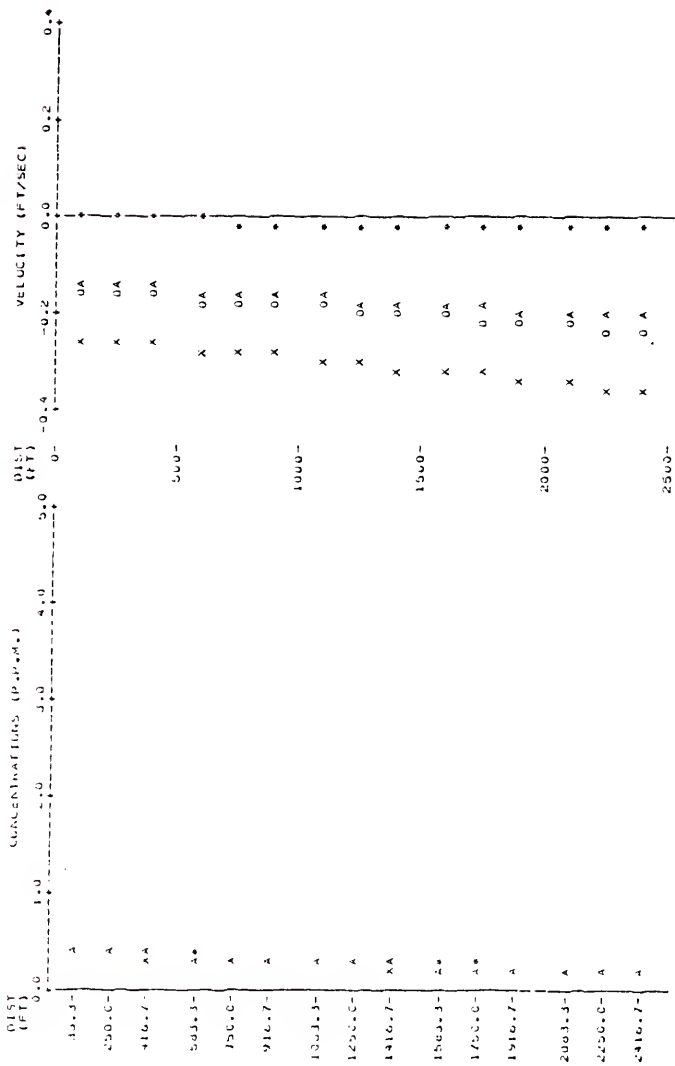
0 = LAYER 1 (Z = 0.0 FT)
 1 = LAYER 2 (Z = 1.0 FT)
 X = LAYER 3 (Z = 3.0 FT)
 A = AVERAGE OVER LAYERS

PLOTS FOR BEACH NUMBER 4 : LINE FROM STAKE IN SIMULATION IS 50.000 HOURS
 TIDAL DIFFERENCE = 1.050 FEET WIND SPEED = 13.9 FT/SEC WIND DIRECTION = 89. DEGREES



0 = LAYER 0 (Z = 1.0 FT)
 1 = LAYER 1 (Z = 2.0 FT)
 2 = LAYER 2 (Z = 3.0 FT)
 A = AVERAGE OVER LAYERS

PLOTS FOR EACH NUMBER : TIME FROM START OF OBSERVATION IS 06:20 HOURS
 : LOCAL CORRECTION = -11000 FEET; WIND SPEED = 1329 FT/SEC; WIND DIRECTION = 89. DEGREES



0 = LAYER 1 (Z = 1.1 FT)
 1 = LAYER 2 (Z = 1.2 FT)
 X = LAYER 3 (Z = 5.3 FT)
 A = AVERAGE OVER LAYERS

TIME 36.50 HOURS: TIDAL DIFFERENCE= -1.650 FEET
WIND SPEED= 13.9 FT/SEC: WIND DIRECTION= 89, DEGREES
REACH NUMBER 1:

X= 50.0/C	1.146	1.138
/VEL	-0.092	0.168
X= 150.0/C	1.135	1.143
/VEL	-0.102	0.163
X= 250.0/C	1.126	1.148
/VEL	-0.107	0.159
X= 350.0/C	1.116	1.151
/VEL	-0.107	0.154
X= 450.0/C	1.104	1.153
/VEL	-0.114	0.149
X= 550.0/C	1.092	1.152
/VEL	-0.118	0.145
X= 650.0/C	1.079	1.150
/VEL	-0.122	0.140
X= 750.0/C	1.066	1.146
/VEL	-0.126	0.136
X= 850.0/C	1.052	1.140
/VEL	-0.130	0.131
X= 950.0/C	1.039	1.134
/VEL	-0.134	0.126
X= 1050.0/C	1.024	1.126
/VEL	-0.138	0.122
X= 1150.0/C	1.010	1.116
/VEL	-0.142	0.117
X= 1250.0/C	0.995	1.107
/VEL	-0.146	0.113
X= 1350.0/C	0.980	1.096
/VEL	-0.150	0.108
X= 1450.0/C	0.964	1.085
/VEL	-0.153	0.103
X= 1550.0/C	0.948	1.073
/VEL	-0.157	0.099
X= 1650.0/C	0.933	1.060
/VEL	-0.161	0.094
X= 1750.0/C	0.917	1.047
/VEL	-0.165	0.090
X= 1850.0/C	0.901	1.034
/VEL	-0.169	0.085
X= 1950.0/C	0.885	1.020
/VEL	-0.173	0.080
X= 2050.0/C	0.869	1.006
/VEL	-0.177	0.076
X= 2150.0/C	0.853	0.991

X= 2250.0/C/	/VEL/	-0.120	-0.181	0.071
X= 2350.0/C/	/VEL/	-0.121	-0.186	0.077
X= 2450.0/C/	/VEL/	-0.122	-0.185	0.066
X= 2550.0/C/	/VEL/	-0.122	-0.189	0.062
X= 2650.0/C/	/VEL/	-0.122	-0.193	0.062
X= 2750.0/C/	/VEL/	-0.123	-0.197	0.057
X= 2850.0/C/	/VEL/	-0.124	-0.197	0.053
X= 2950.0/C/	/VEL/	-0.124	-0.201	0.053
X= 3050.0/C/	/VEL/	-0.125	-0.205	0.048
X= 3150.0/C/	/VEL/	-0.125	-0.205	0.048
X= 3250.0/C/	/VEL/	-0.125	-0.205	0.043
X= 3350.0/C/	/VEL/	-0.126	-0.209	0.043
X= 3450.0/C/	/VEL/	-0.126	-0.212	0.039
X= 3550.0/C/	/VEL/	-0.127	-0.212	0.039
X= 3650.0/C/	/VEL/	-0.127	-0.216	0.034
X= 3750.0/C/	/VEL/	-0.127	-0.220	0.034
X= 3850.0/C/	/VEL/	-0.128	-0.224	0.025
X= 3950.0/C/	/VEL/	-0.128	-0.224	0.025
X= 4050.0/C/	/VEL/	-0.129	-0.228	0.020
X= 4150.0/C/	/VEL/	-0.130	-0.228	0.020
X= 4250.0/C/	/VEL/	-0.130	-0.232	0.016
X= 4350.0/C/	/VEL/	-0.130	-0.232	0.016
X= 4450.0/C/	/VEL/	-0.131	-0.236	0.011
X= 4550.0/C/	/VEL/	-0.131	-0.236	0.011
X= 4650.0/C/	/VEL/	-0.132	-0.240	0.007
X= 4750.0/C/	/VEL/	-0.132	-0.244	0.007
X= 4850.0/C/	/VEL/	-0.133	-0.244	0.002
X= 4950.0/C/	/VEL/	-0.133	-0.248	0.002
X= 5050.0/C/	/VEL/	-0.133	-0.252	0.003
X= 5150.0/C/	/VEL/	-0.134	-0.252	0.003
X= 5250.0/C/	/VEL/	-0.134	-0.256	0.007
X= 5350.0/C/	/VEL/	-0.135	-0.256	0.007
REACH NUMBER	2:	-0.135	-0.260	0.012
X= 5450.0/C/	/VEL/	-0.008	0.227	0.016
X= 5550.0/C/	/VEL/	-0.008	0.227	0.016
X= 5650.0/C/	/VEL/	-0.009	0.227	0.021
X= 5750.0/C/	/VEL/	-0.009	0.227	0.021
X= 5850.0/C/	/VEL/	-0.009	0.227	0.027
X= 5950.0/C/	/VEL/	-0.009	0.227	0.027
X= 6050.0/C/	/VEL/	-0.009	0.227	0.027
X= 6150.0/C/	/VEL/	-0.009	0.227	0.027
X= 6250.0/C/	/VEL/	-0.009	0.227	0.027
X= 6350.0/C/	/VEL/	-0.009	0.227	0.027
X= 6450.0/C/	/VEL/	-0.009	0.227	0.027
X= 6550.0/C/	/VEL/	-0.009	0.227	0.027
X= 6650.0/C/	/VEL/	-0.009	0.227	0.027
X= 6750.0/C/	/VEL/	-0.009	0.227	0.027
X= 6850.0/C/	/VEL/	-0.009	0.227	0.027
X= 6950.0/C/	/VEL/	-0.009	0.227	0.027
X= 7050.0/C/	/VEL/	-0.009	0.227	0.027
X= 7150.0/C/	/VEL/	-0.009	0.227	0.027
X= 7250.0/C/	/VEL/	-0.009	0.227	0.027
X= 7350.0/C/	/VEL/	-0.009	0.227	0.027
X= 7450.0/C/	/VEL/	-0.009	0.227	0.027
X= 7550.0/C/	/VEL/	-0.009	0.227	0.027
X= 7650.0/C/	/VEL/	-0.009	0.227	0.027
X= 7750.0/C/	/VEL/	-0.009	0.227	0.027
X= 7850.0/C/	/VEL/	-0.009	0.227	0.027
X= 7950.0/C/	/VEL/	-0.009	0.227	0.027
X= 8050.0/C/	/VEL/	-0.009	0.227	0.027
X= 8150.0/C/	/VEL/	-0.009	0.227	0.027
X= 8250.0/C/	/VEL/	-0.009	0.227	0.027
X= 8350.0/C/	/VEL/	-0.009	0.227	0.027
X= 8450.0/C/	/VEL/	-0.009	0.227	0.027
X= 8550.0/C/	/VEL/	-0.009	0.227	0.027
X= 8650.0/C/	/VEL/	-0.009	0.227	0.027
X= 8750.0/C/	/VEL/	-0.009	0.227	0.027
X= 8850.0/C/	/VEL/	-0.009	0.227	0.027
X= 8950.0/C/	/VEL/	-0.009	0.227	0.027
X= 9050.0/C/	/VEL/	-0.009	0.227	0.027
X= 9150.0/C/	/VEL/	-0.009	0.227	0.027
X= 9250.0/C/	/VEL/	-0.009	0.227	0.027
X= 9350.0/C/	/VEL/	-0.009	0.227	0.027
X= 9450.0/C/	/VEL/	-0.009	0.227	0.027
X= 9550.0/C/	/VEL/	-0.009	0.227	0.027
X= 9650.0/C/	/VEL/	-0.009	0.227	0.027
X= 9750.0/C/	/VEL/	-0.009	0.227	0.027
X= 9850.0/C/	/VEL/	-0.009	0.227	0.027
X= 9950.0/C/	/VEL/	-0.009	0.227	0.027
X= 10050.0/C/	/VEL/	-0.009	0.227	0.027

X= 350.0/C/	0.227	0.226	0.226
/VEL/	-0.009	-0.028	-0.009
X= 450.0/C/	0.227	0.227	0.227
/VEL/	-0.010	-0.034	-0.016
X= 550.0/C/	0.226	0.226	0.226
/VEL/	-0.010	-0.040	-0.023
X= 650.0/C/	0.225	0.225	0.225
/VEL/	-0.010	-0.046	-0.030
X= 750.0/C/	0.225	0.225	0.225
/VEL/	-0.011	-0.051	-0.037
X= 850.0/C/	0.224	0.225	0.224
/VEL/	-0.011	-0.057	-0.044
X= 950.0/C/	0.224	0.224	0.225
/VEL/	-0.012	-0.063	-0.051
X= 1050.0/C/	0.225	0.225	0.223
/VEL/	-0.012	-0.069	-0.057
X= 1150.0/C/	0.231	0.274	0.297
/VEL/	-0.012	-0.075	-0.065
X= 1250.0/C/	0.258	0.331	0.420
/VEL/	-0.013	-0.080	-0.071
REACH NUMBER	3:		
X= 50.0/C/	0.249	0.251	0.260
/VEL/	0.115	0.109	-0.205
X= 150.0/C/	0.245	0.249	0.276
/VEL/	0.115	0.104	-0.211
X= 250.0/C/	0.242	0.251	0.298
/VEL/	0.114	0.098	-0.218
X= 350.0/C/	0.241	0.257	0.328
/VEL/	0.114	0.092	-0.225
X= 450.0/C/	0.243	0.268	0.367
/VEL/	0.113	0.087	-0.232
X= 550.0/C/	0.246	0.283	0.411
/VEL/	0.113	0.081	-0.238
X= 650.0/C/	0.250	0.301	0.454
/VEL/	0.113	0.076	-0.245
REACH NUMBER	4:		
X= 50.0/C/	0.266	0.344	0.521
/VEL/	0.111	0.038	-0.291
X= 150.0/C/	0.264	0.348	0.537
/VEL/	0.110	0.034	-0.296
X= 250.0/C/	0.265	0.366	0.552
/VEL/	0.110	0.029	-0.301
X= 350.0/C/	0.269	0.385	0.562
/VEL/	0.109	0.025	-0.306
X= 450.0/C/	0.276	0.404	0.559
/VEL/	0.108	0.021	-0.311
X= 550.0/C/	0.284	0.422	0.552
/VEL/	0.108	0.017	-0.316

X = 650,0/C/	0.293	0.438	0.544
/VEL/	0.107	0.013	-0.321
X = 750,0/C/	0.304	0.453	0.534
/VEL/	0.106	0.009	-0.325
X = 850,0/C/	0.316	0.466	0.522
/VEL/	0.106	0.004	-0.330
REACH NUMBER	5:		
X = 83,3/C/	0.355	0.397	0.399
/VEL/	-0.005	-0.151	-0.251
X = 250,0/C/	0.367	0.384	0.376
/VEL/	-0.007	-0.157	-0.259
X = 416,7/C/	0.365	0.368	0.349
/VEL/	-0.008	-0.164	-0.267
X = 583,3/C/	0.357	0.348	0.321
/VEL/	-0.009	-0.170	-0.274
X = 750,0/C/	0.346	0.325	0.297
/VEL/	-0.010	-0.177	-0.282
X = 916,7/C/	0.331	0.302	0.279
/VEL/	-0.011	-0.183	-0.289
X = 1083,3/C/	0.312	0.283	0.267
/VEL/	-0.013	-0.190	-0.297
X = 1256,0/C/	0.294	0.269	0.258
/VEL/	-0.014	-0.196	-0.305
X = 1416,7/C/	0.277	0.258	0.241
/VEL/	-0.015	-0.203	-0.312
X = 1583,3/C/	0.264	0.247	0.216
/VEL/	-0.016	-0.209	-0.320
X = 1750,0/C/	0.253	0.233	0.207
/VEL/	-0.018	-0.216	-0.328
X = 1916,7/C/	0.244	0.217	0.203
/VEL/	-0.019	-0.222	-0.335
X = 2083,3/C/	0.235	0.204	0.201
/VEL/	-0.020	-0.229	-0.343
X = 2250,0/C/	0.227	0.202	0.200
/VEL/	-0.021	-0.235	-0.351
X = 2416,7/C/	0.220	0.200	0.200
/VEL/	-0.022	-0.242	-0.358
JUNCTION NUMBER	2:		
0,304			
0,455			
0,510			
0,269			
0,363			
0,451			

JUNCTION NUMBER 3:

0,451

REFERENCES

- Abbott, M. E., Bahl-Madsen, E. J., Hinstrup, P. I., Lee, A., Viir, M. E., and Verwey, A., 1975. "River and Estuary Modeling with the Siva System," Symposium on Modeling Techniques, Modeling '75, Second Annual Symposium of the Waterways, Harbors and Coastal Engineering Division, ASCE, Vol. 1, Sept. 1975, pp. 740-763.
- Awies, W. F., 1969. Numerical Methods for Partial Differential Equations. Barnes and Noble, New York, NY, 1969.
- Aris, R., 1956. "On the Dispersion of a Solute in a Fluid Flowing Through a Tube," Proceedings, Royal Society of London, Series A, Vol. 239, No. 1200, Apr. 1956, pp. 61-77.
- Bella, D. A., and Robbins, W. L., 1968. "Difference Modeling of Stream Pollution," Journal of the Sanitary Engineering Division, ASCE, Vol. 94, SA5, Oct. 1968, pp. 995-1011.
- Blumberg, A. F., 1977. "Numerical Model of Estuarine Circulation," Journal of the Hydraulics Division, ASCE, Vol. 103, HY3, March 1977, pp. 295-311.
- Book, D. L., Boris, J. P., and Orin, K., 1975. "Flux-Corrected Transport II: Generalizations of the Method," Journal of Computational Physics, Vol. 19, No. 3, July 1975, pp. 248-283.
- Boris, J. P., and Book, D. L., 1973. "Flux Corrected Transport I. SHATA, A Fluid Transport Algorithm That Works," Journal of Computational Physics, Vol. 17, No. 1, Jan. 1973, pp. 38-69.
- Boris, J. P., and Book, D. L., 1976. "Flux Corrected Transport III. Minimal Error Flux Algorithms," Journal of Computational Physics, Vol. 20, No. 4, Apr. 1976, pp. 399-431.
- Powder, K. F., and Hamilton, E., 1975. "Some Experiments With a Numerical Model of Circulation and Mixing in a Tidal Estuary," Estuarine and Coastal Marine Science, Vol. 3, 1975, pp. 281-301.
- Bretschneider, C. L., 1966. "Engineering Aspects of Hurricane Surge," Ch. 5, Estuary and Coastal Hydrodynamics, A. T. Ippen, ed., McGraw-Hill Book Co., New York, NY, 1966.
- Grundreit, E., and Paines, W. J., 1964. "The Production and Diffusion of Vorticity in Duct Flow," Journal of Fluid Mechanics, Vol. 19, July 1964, pp. 375-391.
- Callaway, R. J., Pyra, E. J., and Dittworth, C. R., 1969. "Mathematical Model of the Columbia River from the Pacific Ocean to Bonneville Dam. [Part I - Theory, Program Notes and Programs,]" NTIS No. PB-207-422, USDI, 1969. Pacific Northwest Water Lab., LWA, Corvallis, OR, Nov. 1969.

Callaway, R. J., and Byram, K. V., 1970. "Mathematical Model of the Columbia River From the Pacific Ocean to Bonneville Dam. Part II - Input - Output and Initial Verification Procedures," NTIS No. PB-202-423, Pacific Northwest Water Laboratory, EPA, Corvallis, OR, Dec. 1970.

Carter, L. J., 1974. The Florida Experience, Land and Water Policy In a Growth State, Published for Resources for the Future, Inc., by Johns Hopkins Univ. Press, Baltimore, MD, 1974.

Chiu, C. L., and Lee, T.-S., 1971. "Method of Calculating Secondary Flow," Water Resources Research, Vol. 7, No. 4, Aug. 1971, pp. 834-844.

Christensen, B. A., 1975. Personal Communication, April 1975.

Christensen, B. A. and Snyder, R. M., 1978. "Establishment of Residential Waterfront Property by Construction of Canal Systems in Coastal Wetlands. Problems and Solutions," Paper 1301, Coastal Zone 78 Conference, San Francisco, CA, March 1978.

Christodoulou, G. C., Connor, J. J., and Pearce, B. R., 1976. "Mathematical Modeling of Dispersion in Stratified Waters," Report MITSG 76-14, M.I.T., Cambridge, MA, Nov. 1976.

Cooper, C. K., and Pearce, B. R., 1977. "A Three-Dimensional Numerical Model to Calculate Currents in Coastal Water Utilizing a Depth Varying Vertical Eddy Viscosity," M.S. Thesis and Report 226, Parsons Laboratory, M.I.T., Cambridge, MA, Aug. 1977.

Council on Environmental Quality, 1970. First Annual Report presented to Congress, Aug. 1970, p.v.

Dlubac, J. J., 1976. "Vertical Dispersion in Open Channel Flow," High Honors Thesis, Hydraulic Lab., Dept. of Civil Engr., Univ. of Fla., Gainesville, FL, Dec. 1976.

Egan, B. A., and Mahoney, J. R., 1972. "Numerical Modeling of Advection and Diffusion of Urban Area Source Pollutants," Journal of Applied Meteorology, No. 11, March 1972, pp. 312-322.

Elder, J. W., 1959. "The Dispersion of Marked Fluid in Turbulent Shear Flow," Journal of Fluid Mechanics, Vol. 5, Part 4, May 1959, pp. 544-560.

Environmental Protection Agency, 1975. "Finger-Fill Canal Studies, Florida and North Carolina," Report EPA 904/9-76-017, Surveillance and Analysis Section, EPA, Athens, GA, May 1975.

Feigner, K. D., and Harris, H. S., 1970. "Documentation Report - FWQA Dynamic Estuary Model," NTIS No. PB-197-103, Federal Water Quality Administration, U.S. Dept. of Interior, Washington, D.C., July 1970.

Fischer, H. B., 1967. "The Mechanics of Dispersion in Natural Streams," Journal of the Hydraulics Division, ASCE, Vol. 93, HY6, Nov. 1967, pp. 187-216.

Fischer, H. B., 1969. "The Effect of Bends on Dispersion in Streams," Water Resources Research, Vol. 5, No. 2, Apr. 1969, pp. 496-506.

Gentry, R. A., Martin, R. E., and Daly, B. J., 1966. "An Eulerian Differencing Method for Unsteady Compressible Flow Problems," Journal of Computational Physics, Vol. 1, No. 1, Aug. 1966, pp. 87-118.

Goldstein, S., 1938. Modern Developments in Fluid Mechanics, Clarendon Press, Oxford, England, 1938.

Graham, D. S., 1977. "A Review and Evaluation of Selected Numerical Models for Coastal Zone Water Management," Proceedings of Seminar on Freshwater and the Florida Coast, Southwest Florida Water Management District, Report 1977-1 and Florida Sea Grant Report 22, Oct. 1977, pp. 41-78.

Grimsrud, G. P., Finnemore, E. J., and Owen, H. J., 1976. "Evaluation of Water Quality Models - A Management Guide for Planners," EPA, NTIS No. PB-256 412, Systems Control, Inc., July 1976.

Harleman, D. R. F., 1966. "Diffusion Processes in Stratified Flow," Ch. 12, Estuary and Coastal Hydrodynamics, A. T. Ippen, ed., McGraw Hill Book Co., New York, NY, June 1966.

Harleman, D. R. F., 1971. "One-Dimensional Models," Ch. 3, Estuarine Modeling: An Assessment, George H. Ward, and William H. Esprey, Jr. eds., Tracor, Inc., Austin, TX, Feb. 1971.

Harleman, D. R. F., and Lee, C. H., 1969. "The Computation of Tides and Currents in Estuaries and Canals," Tech. Bul. No. 16, Committee on Tidal Hydraulics, Corps of Engineers, U. S. Army, Sept. 1969.

Heaps, N. S., 1972. "On the Numerical Solution of the Three-Dimensional Hydrodynamic Equations for Tides and Storm Surges," Nem. Soc. R. Sci., Liege, Belgium, Vol. 6, No. 2, 1972, pp. 143-180.

Heaps, N. S., 1974. "Development of a Three-Dimensional Model of the Irish Sea," Rapp. P-V Reun. Cons. Int. Explor. Mer, Dec. 1974, pp. 147-162.

Hellstrom, B., 1941. "Wind Effects on Lakes and Rivers," Proceedings of the Royal Swedish Institute for Engineering Research, No. 158, 1941.

Hess, K. W., and White, F. M., 1974. "A Numerical Model of Narragansett Bay," Marine Tech. Report 20, Univ. of Rhode Island, Kingston, RI, 1974.

Holley, E. R., and Harleman, D. R. F., 1965. "Dispersion of Pollutants in Estuary Type Flows," Report 74, Hydrodynamics Laboratory, M.I.T., prepared for U.S. Dept. of HEW, Cambridge, MA, Jan. 1965.

Horowitz, J., and Bazel, L., 1977. "An Analysis of Planning for Advanced Wastewater Treatment (AWT)," Draft Final Report, prepared for U.S. EPA, Vertex Corporation, McLean, VA, July 1977.

Ikeda, S., and Kikkawa, H., 1976. "Secondary Circulation in Straight Channels," Report of Department of Foundation Engineering, Faculty of Engineering, Saitama University, Urawa, Saitama, Japan, Vol. 6, 1976, pp. 1-13.

International Business Machines Corporation, 1974. IBM System/360 and System/370, FORTRAN IV Language, 11th ed., GC28-6516-10, IBM Corporation, New York, NY, May, 1974.

Jobson, H. E., and Sayre, W. W., 1983-1966. "Predicting Concentration Profiles in Open Channels," Journal of the Hydraulics Division, ASCE, Vol. 96, HY10, 1970, pp. 1983-1996.

Keulegan, G. H., 1951. "Wind Tides in Small Closed Channels," Journal of the National Bureau of Standards, Vol. 46, No. 5, 1951, pp. 358-381.

Keulegan, G. H., 1958. "The Motion of Saline Fronts in Still Water," Report 5831, National Bureau of Standards, Apr. 1958.

King, I. P., Norton, W. R., and Orlob, G. T., 1973. "A Finite Element Solution for Two-Dimensional Density Stratified Flow," Report WRE 11360, prepared for OWRR, U. S. Dept. of Interior, Water Resources Engineers, Inc., Walnut Creek, CA, March 1973.

Langer, J. L., Pyatt, E. E., and Shubinski, R. P., 1971. "Storm Water Management Model," Vols. 1-4, NTIS Nos. PB-203-291, PB-203-292, U. S. EPA, Washington, D.C., July 1971.

Langley, T. B., 1976. "The Effect of a Boat Basin on the Dispersive Pollutant Transport in a Dead-End Canal," M.S. Thesis, Hydraulic Laboratory, Dept. of Civil Engr., Univ. of Fla., Gainesville, FL, Aug. 1976.

✓ Lee, J. K., 1977. "An Explicit One-Dimensional Finite-Difference Model of Pollutant Transport in Tidal Finger Canal Networks," M.S. Thesis, Hydraulic Lab., Dept. of Civil Engr., Univ. of Fla., Gainesville, FL, March 1977.

Leendertse, J. J., and Liu, S. K., 1975. "Modeling of Three-Dimensional Flows in Estuaries," Vol. 1, Symposium on Modeling Techniques, San Francisco, CA, ASCE, Sept. 1975, pp. 625-642.

Leimkuhler, W., Connor, J., Wang, J., Christodoulou, G., and Sungren, S., 1975. "Two-Dimensional Finite-Element Dispersion Model," Vol. II, Symposium on Modeling Techniques, San Francisco, CA, ASCE, Sept. 1975, pp. 1467-1486.

Lighthill, M. J., and Whitham, G. B., 1955. "On Kinematic Waves: I-Flood Movement in Long Rivers," Proceedings of the Royal Society, Series A, Vol. 229, No. 1178, May 1955, p. 281.

Lombardo, P. S., 1973. "Critical Review of Currently Available Water Quality Models," NTIS No. PB-222-265, Report for OWRR by Hydrocomp, Inc., Palo Alto, CA, July 1973.

Madsen, O. S., 1977. "A Realistic Model of the Wind-Induced Ekman Boundary Layer," Journal of Physical Oceanography, Vol. 7, Issue No. 2, March 1977, pp. 248-255.

McKeehan, D. S., 1975. "Water Motion in Closed-End Canals," M.S. Thesis, Rosenstiel School of Marine and Atmospheric Science, Univ. of Miami, FL, Sept. 1975.

Metcalf and Eddy, Inc., University of Florida, and Water Resources Engineers, Inc., 1971. "Storm Water Management Model," Water Pollution Control Research Series 11024D0C07/71, for EPA, July 1971.

Milne, W. E., 1970. Numerical Solution of Differential Equations, Dover Publications, New York, N.Y., 1970.

Molenkamp, C. R., 1968. "Accuracy of Finite-Difference Methods Applied to the Advection Equation," Journal of Applied Meteorology, Vol. 7, April 1968, pp. 160-167.

Morris, F. W. IV, 1978. "Hydraulic Measurements, Data Analysis, and Rational Design Procedures for Residential Tidal Canal Networks," Ph.D. Dissertation, Hydraulic Lab., Dept. of Civil Engr., Univ. of Fla., Gainesville, FL, June 1978.

Morris, F. W. IV, and Christensen, B. A., 1976a. "Hydrodynamics and Environmental Design Criteria for Residential Canals. A Discussion of Current Research Activities," Hydraulic Lab., Dept. of Civil Engr., Univ. of Fla., Gainesville, FL, 1976.

Morris, F. W. IV, and Christensen, B. A., 1976b. "Hydrodynamics and Flushing Characteristics of Residential Canals in Palm Beach County: A Discussion of Current Research Activities," Hydraulic Lab., Dept. of Civil Engr., Univ. of Fla., Gainesville, FL, 1976.

Morris, F. W. IV, Walton, R., and Christensen, B. A., 1977a. "Evaluation of a Hybrid Computer Model of Pollutant Flushing in Tidal Canals," Report to Florida, Project No. R/OE-4, Hydraulic Lab., Dept. of Civil Engr., Univ. of Fla., Gainesville, FL, Feb. 1977.

Morris, F. W. IV, Walton, R., Dlubac, J. J., and Christensen, B. A., 1977b. "Hydrodynamic Factors Involved in Finger Canal and Borrow Lake Flushing in Florida's Coastal Zone - II," Interim Report to Florida Sea Grant, Project No. R/OE-4, Hydraulic Lab., Dept. of Civil Engr., Univ. of Fla., Gainesville, FL, March 1977.

Morris, F. W. IV, Walton, R., and Christensen, B. A., 1978. "Hydrodynamic Factors Involved in Finger Canal and Borrow Lake Flushing in Florida's Coastal Zone," Report HY-7801, Final Report to Florida Sea Grant, Hydraulic Laboratory, Department of Civil Engineering, University of Fla., Gainesville, FL, March 1978.

Munk, W. H., and Anderson, E. R., 1948. "Note on the Theory of the Thermocline," Journal of Marine Research, Vol. 7, No. 3, 1948, pp. 276-295.

- Nikuradse, J., 1933. "Stromungsgesetz in Rauhen Rohren, " Verein Deutscher Ingenieure, Forschungsheft 361, (1933); or NACE TM 1292, (Nov. 1950), as referenced in "Friction Factors in Open Channels," Journal of the Hydraulics Division, ASCE, Vol. 89, HY2, March 1963.
- N.O.A.A., 1974. Tide Tables, High and Low Water Prediction 1975, East Coast of North and South America, Washington, D.C., 1974.
- Noh, W. F., and Protter, M. H., 1963. "Difference Methods and Equations of Hydrodynamics," Journal of Mathematics and Mechanics, Vol. 12, No. 2, March/April 1963, pp. 149-191.
- Obukhov, A.M., 1971. "Turbulence in an Atmosphere with a Non-uniform Temperature," Boundary-Layer Meteorology, Vol. 2, No. 1, 1971, pp. 7-29.
- Okubo, A., 1971. "Horizontal and Vertical Mixing in the Sea," from Impingement of Man on the Oceans, D. H. Wood, ed., J. Wiley and Sons, New York, NY, 1971.
- Parr, A. D., and Christensen, B. A., 1977. "An Effective Method for Increasing Dispersion Rates in Residential Canals in the Coastal Zone," Proceedings 25th Annual Speciality Conference, Hydraulics of the Coastal Zone, ASCE, Texas A & M, College Station, TX, Aug. 1977.
- Pedersen, L. B., and Prahm, L. P., 1973. "A Method for Numerical Solution of the Advection Equation," Tellus, Vol. 26, 1973, pp. 594-602.
- Pritchard, D. W., 1956. "The Dynamic Structure of a Coastal Plain Estuary," Journal of Marine Research, Vol. 15, pp. 33-42, 1956.
- Pritchard, D. W., 1971. "Hydrodynamic Models," Ch. 2, Estuarine Modeling: An Assessment, George H. Ward, and William H. Espey, Jr. eds., Tracor, Inc., Austin, TX, Feb. 1971.
- Richardson, L. F., 1926. "Atmospheric Diffusion Shown on a Distance-Neighbour Graph," Proceedings of the Royal Society, Series A, Vol. 110, 1926.
- Roache, P. J., 1972. Computational Fluid Dynamics, Hermosa Publishers, Albuquerque, NM, 1972.
- Roberts, K. V., and Weiss, N. O., 1966. "Convective Difference Schemes," Mathematics of Computation, Vol. 20, No. 94, April 1966, pp. 272-299.
- Rozovskii, I. L., 1957. Flow of Water in Bends of Open Channels, Academy of Sciences of the Ukrainian S.S.R., Translated from Russian, Published for the National Science Foundation, Washington, D.C., and the U.S. Dept. of the Interior by the Israel Program for Scientific Translations, 1957.
- Saville, T., Jr., 1953. "Wind Setup and Waves in Shallow Water," Beach Erosion Board Technical Memorandum, No. 27, 1953.

- Savonius, S. J., 1931. The Wing-Rotor, Savonius and Company, Helsingfors, Finland, 1931.
- Schiller, E. J., and Sayre, W. W., 1973. "Vertical Mixing of Heated Effluents in Open-Channel Flow," Ph.D. Dissertation, Report No. 148, Institute of Hydraulic Research, Univ. of Iowa, Iowa City, IA, 1973.
- Smith, G. D., 1975. Numerical Solution of Partial Differential Equations, Oxford Mathematical Handbooks, Oxford University Press, First Published 1965, Reprint, 1975.
- Snyder, R. M., 1976. "Residential Canals and the Environment," Snyder Oceanography Services, Jupiter, FL, Oct. 1976.
- Snyder, R. M., 1977. "The Marine Ecosystem from an Engineering Viewpoint," Proceedings of Seminar on Freshwater and the Florida Coast, South West Florida Water Management District Report No. 1977-1, and Florida Sea Grant Report No. 22, October 1977, pp. 107-128.
- Sorondo, V. J., and Baldwin, H. E., 1977. "Efficient Parallel Computation for Modeling Diffusion in Open Channels," Proceedings of Summer Computer Simulation Conference, Society for Computer Simulation, Chicago, IL, 1977.
- Spaulding, M., 1976. "Numerical Modeling of Pollutant Transport Using a Lagrangian Marker Particle Technique," NASA Technical Memorandum X-73970, Langley Research Center, Hampton, VA, Aug. 1976.
- Stone, H. L., and Brian, P. L. T., 1963. "Numerical Solution of Convective Transport Problem," Journal American Institute of Chemical Engineering, Vol. 9, No. 5, September 1963, pp. 681-688.
- Swenty, B. J., 1977. "Vertical Dispersion in Open Channels with Large Side Wall Roughness Elements," M. S. Thesis, Hydraulic Lab., Dept. of Civil Engr., Univ. of Fla., Gainesville, FL, 1977.
- Taylor, Sir G. I., 1953. "Dispersion of Soluble Matter in Solvent Flowing Slowly Through a Tube," Proceedings of the Royal Society, Series A, Vol. 186, 1953, pp. 186-203.
- Taylor, Sir G. I., 1954. "The Dispersion of Matter in Turbulent Flow Through a Pipe," Proceedings of the Royal Society of London, Series A, Vol. 223, No. 1155, May 1954, pp. 446-468.
- van Dorn, W. G., 1953. "Wind Stress on an Artificial Pond," Journal of Marine Research, Vol. 12, No. 3, 1953, pp. 219-275.
- Vanoni, V. A., 1946. "Transportation of Suspended Sediment by Water," Transactions of ASCE, Vol. 111, Paper No. 2267, 1946, pp. 67-102.
- von Neumann, J., and Richtmyer, R. D., 1950. "A Method for the Numerical Calculation of Hydrodynamic Shocks," Journal of Applied Physics, Vol. 21, March 1950, pp. 232-237.

Vreugdenhil, C. B., 1973. "Computational Methods for Channel Flows," Publication No. 100, Committee for Hydrological Research TNO, Delft Hydraulics Lab., The Netherlands, 1973.

Walton, R., 1976a. "Mathematical Modeling of Pollution Transport in Floridian Canals," IAHR Symposium on Unsteady Flow in Open Channels, University of Newcastle-Upon-Tyne, in association with BHRA, April 1976.

Walton, R., 1976b. "Pollution Transport in Canal Networks with Small Tidal Ranges Using a Characteristic Finite-Difference Technique," A.G.U. Annual Fall Meeting, American Geophysical Union, San Francisco, CA, Dec. 1976.

Walton, R. and Price, R. K., 1975. "Influence of Lateral Flow Over a Flood Plain on Flood Waves," Report INT 140, Hydraulics Research Station, Wallingford, England, March 1975.

Walton, R., Morris, F. W., IV and Christensen, B. A., 1975. "A Fluvio Hydrographic Survey of Frenchman's Creek, Jupiter, Florida," Report to Snyder Oceanography Services, Inc., Jupiter, Florida, Hydraulic Lab., Dept. of Civil Engr., Univ. of Fla., Gainesville, FL, Oct. 1975.

Walton, R., Morris, F. W. IV, Evans, A. J., Jr., and Christensen, B. A., 1975. "A Fluvio-Hydrographic Survey of 57 Acres," Report for Royal American Realty Co., Lake Park, Florida, Hydraulic Lab., Dept. of Civil Engr., Univ. of Fla., Gainesville, FL, Dec. 1975.

Walton, R., and Christensen, B. A., 1977. "Evaluation of Pollution Transport in a One-Dimensional Canal Network Using a Method of Characteristics," First International Conference on Mathematical Modeling, St. Louis, Aug. 1977.

Wang, J. D., and Connor, J. J., 1975. "Mathematical Modeling of Near Coastal Circulation," Ph.D. Dissertation, and Report No. 200, Parsons Lab., M.I.T., Cambridge, MA, 1975.

Wolman, M. G., and Brush, L. M., 1961. "Factors Controlling the Size and Shape of Stream Channels in Coarse Noncohesive Sands," Geological Survey Professional Paper 282-G, 1961.

Wu, J., 1969. "Wind Stress and Surface Roughness at the Air-Sea Interface," Journal of Geophysical Research, Vol. 74, Jan. 1969, pp. 444-445.

Yotsukura, N., Fischer, H. B., and Sayre, W. W., 1970. "Measurement of Mixing Characteristics of the Missouri River Between Sioux City, Iowa, and Plattsmouth, Nebraska," USGS Water-Supply Paper 1899-G, U. S. Gvnt. Printing Office, Washington, D.C., 1970.

Zeidler, R. B., 1976. "Coastal Dispersion of Pollutants," Journal of the Waterways, Harbors and Coastal Engineering Division, ASCE, Vol. 102, WW2, May 1976, pp. 235-254.

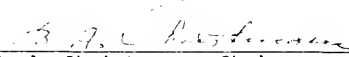
BIOGRAPHICAL SKETCH

Raymond Walton was born in London, England, in 1951. He graduated from Blackpool Grammar School, England, in 1968, and went on to receive his B.Sc. with honors in Mathematics from University College London in 1971. From 1971 to 1972, he studied engineering hydrology at the University of Newcastle-Upon-Tyne, England, under a National Environmental Research Council grant, and graduated with a M.Sc.

During 1973 and 1974, he spent eighteen months as a Scientific Officer at the Hydraulics Research Station, Wallingford, England, working in particular on numerical flood routing models. Since September, 1974, he has studied hydraulics and hydrology at the University of Florida. As a Graduate Research Associate in the Hydraulic Laboratory of the Department of Civil Engineering, he has worked on numerical modeling of solute transport in tidal canal networks.

He is a member of the American Society of Civil Engineers, the American Geophysical Union, Omicron Delta Kappa, Tau Beta Pi, and Epsilon Lambda Chi.

I certify that I have read this study and that in my opinion it conforms to acceptable standards of scholarly presentation and is fully adequate, in scope and quality, as a dissertation for the degree of Doctor of Philosophy.



B. A. Christensen, Chairman
Professor of Civil Engineering

I certify that I have read this study and that in my opinion it conforms to acceptable standards of scholarly presentation and is fully adequate, in scope and quality, as a dissertation for the degree of Doctor of Philosophy.



Wayne C. Huber
Associate Professor of Environmental
Engineering Sciences

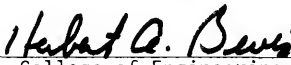
I certify that I have read this study and that in my opinion it conforms to acceptable standards of scholarly presentation and is fully adequate, in scope and quality, as a dissertation for the degree of Doctor of Philosophy.



Z. R. Pop-Stojanovic
Professor of Mathematics

This dissertation was submitted to the Graduate Faculty of the College of Engineering and to the Graduate Council, and was accepted as partial fulfillment of the requirements for the degree of Doctor of Philosophy.

June 1978



Herbert A. Lewis
Dean, College of Engineering

Dean, Graduate School

UNIVERSITY OF FLORIDA



3 1262 08666 284 7